

Induction of the Activation of Immunity Against Opioids and
Mycobacterium tuberculosis by a Chimeric Vaccine

Doctoral Thesis

by

SIDHANTA NANDA

(Regd. No. 2018BMZ0001)



DEPARTMENT OF BIOMEDICAL ENGINEERING

INDIAN INSTITUTE OF TECHNOLOGY ROPAR

JUNE, 2023

Induction of the Activation of Immunity Against Opioids and
Mycobacterium tuberculosis by a Chimeric Vaccine

A Thesis Submitted
In Partial Fulfillment of the Requirements
For the Degree of

DOCTOR OF PHILOSOPHY

by

SIDHANTA NANDA

(Regd. No. 2018BMZ0001)



DEPARTMENT OF BIOMEDICAL ENGINEERING
INDIAN INSTITUTE OF TECHNOLOGY ROPAR
JUNE, 2023

Sidhanta Nanda: Induction of the Activation of Immunity Against Opioids and *Mycobacterium tuberculosis* by a Chimeric Vaccine.

Copyright© 2023, Indian Institute of Technology Ropar

All Rights Reserved

DEDICATED SOLEY TO
MAA, NANI & BHAI

DECLARATION OF ORIGINALITY

I, at this moment, declare that the work presented in the thesis entitled “INDUCTION OF THE ACTIVATION OF IMMUNITY AGAINST OPIOIDS AND *MYCOBACTERIUM TUBERCULOSIS* BY A CHIMERIC VACCINE” has been solely authored by me. It presents the results of my independent investigation/research conducted from July 31st, 2018, to June 6th, 2023, under the supervision of Prof. Javed Naim Agrewala, Professor, Department of Biomedical Engineering, IIT Ropar. To the best of my knowledge, it is an original work, both in terms of research contents and narrative, and has not been submitted or accepted elsewhere, in part or whole, for the award of any degree, diploma, fellowship, associateship or similar title of any university or institutions. Further due credit has been attributed to the relevant state-of-the-art collaborations with appropriate citations and acknowledgements in line with the established ethical norms and practices. I also declare that any idea/data/facts/figures/source stated in my thesis has not been fabricated/falsified/ misrepresented. All the principles of academic honesty and integrity have been followed. The Institute reserves the right to withdraw the thesis from the archive and revoke the associated degree conferred if the idea is unoriginal, manufactured, or plagiarised. Additionally, the Institute reserves the right to appraise all concerned sections of society for their information and necessary actions. If accepted, I now consent for my thesis to be available online in the institute’s open-access repository, inter-library loan, and the title & abstract to be made available to outside organisations.

Signature

Sidhanta Nanda
Name: Sidhanta Nanda

Entry Number: 2018BMZ0001

Program: Ph.D.

Department: Biomedical Engineering

Indian Institute of Technology Ropar

Rupnagar, Punjab 140001

Date: 06.09.2023

ACKNOWLEDGMENTS

I would like to express my deepest gratitude to my PhD mentor Prof Javed N. Agrewala, for his invaluable guidance and mentorship throughout my doctoral journey. From the moment he admitted me into his laboratory, I was captivated by his exceptional qualities, which left an indelible mark on my personal and professional development. Right from the beginning, I was struck by my mentor's unwavering commitment to moral righteousness and self-discipline. His dedication to maintaining a well-ordered laboratory environment set a high standard for everyone in the lab. Under his mentorship, I learned the importance of ethical conduct in research and imbibed these principles in my everyday life. Through his exemplary actions, I gained a deep appreciation for the significance of integrity and accountability in scientific pursuits. One of the most enriching aspects of working with my mentor was the opportunity to learn how to conduct research meticulously and systematically. Our morning interactions were an invaluable source of knowledge as he patiently shared his insights and experiences regarding the execution and planning of experiments. Through weekly laboratory meetings, journal clubs, and thought-provoking brainstorming sessions, I was exposed to cutting-edge discoveries and emerging research trends. I am eternally grateful for my mentor's continuous guidance and training, which played a pivotal role in shaping my scientific talent. His belief in my abilities encouraged me to explore my aptitude for science and instilled the confidence to think independently. His mentorship went beyond imparting technical skills; he nurtured my critical thinking abilities and encouraged me to ask thought-provoking questions, fostering a deep appreciation for pursuing knowledge. Without his guidance, I would not have had the privilege of experiencing the transformative power of scientific research. I am indebted to him for his unwavering dedication and for believing in my potential when I doubted myself.

I express my heartfelt gratitude to Prof R Ahuja, Director, and Prof SK Das, the former Director, for providing the necessary infrastructure and facilities that enabled me to pursue my PhD at IIT Ropar.

I am immensely grateful to the members of my Doctoral Committee, Dr Srivatsava Naidu for his support and help whenever I needed it; Dr Yashveer Singh for his guidance in conjugational chemistry and nanotechnology experiments; Dr Durba Pal and Dr Jitendra Prasad for their constructive comments and suggestions.

I would like to extend my sincere appreciation to Dr Sanyog Jain from NIPER-Mohali and Prof M Owais from Aligarh Muslim University, Aligarh, for their support in providing animals and laboratory facilities, which were crucial for the successful execution of animal experiments. I am thankful to Dr Sharvan Sehrawat from IISER-Mohali for offering TLR-2 knockout mice. Furthermore, I express my gratitude to Dr Abhishek Ghosh and Prof D Basu from PGIMER, Chandigarh, for providing patient samples and ensuring timely ethical clearance. Dr Vijender Bhalla from CSIR-IMTECH deserves special mention for his assistance in antibody affinity experiments. I would like to extend my gratitude to Dr Srinivashan and Mr Yamin from the Animal House, NIPER-Mohali, for their diligent efforts in maintaining and providing animals for my research.

I am thankful to Dr Ritika Gautam from the Indian Institute of Technology Kanpur, Dr Anupam Bandyopadhyay, Dr Narinder Singh, Dr Rajendra Srivastav from the Indian Institute of Technology Ropar for their valuable comments and suggestions.

I am grateful to Prof Rafi Ahmad, Prof Clare, and Dr Sukant Nayak for their support in enabling me to attend the Nature's Next Gen Immunology Conference 2020 in Israel.

I am grateful to my seniors, Dr Gurpreet, Dr Kanti, Dr Sanpreet, Dr Deep, and my esteemed colleague Mr Adeel, who have provided me with knowledge, experimental skills, laboratory organisation guidance, and valuable writing advice during my PhD. I also thank my fellow juniors Nilesh, Kritika, Shivani, Rahul, Taruna, Junaid, Shivank, and Affan for their unwavering support. Moreover, my colleagues Dr Sheetanshu, Dr Leena, Dr Nahida, Dr Ajinkya, Dr Kushagra, Mr Rishav, Mr Rohan, Miss Shana, and Mr Samauddhin have been of great assistance and wonderful friends throughout my time in the laboratory and institute.

I want to express my heartfelt gratitude to Mrs Swojanya, Mr Dinesh, Mr Ravinder, Mr Akshpreet, Mr Haque, Mr Jitendra, Mr Dharmendra, Mrs Punam, Mr Harpreet, Mr Sushil and Mr Sunil for their administrative assistance and procurement of chemicals and reagents, which greatly contributed to the smooth execution of my experiments. I am also thankful to the staff of Administration, Finance and Accounts, Store and Purchase, Staff Club, ESD, Library, IT, Canteen, Horticulture, Hostel, and Mess for their support. I am incredibly grateful to Mr Balwinder for his kind and caring nature, eagerness to learn, and pleasant personality, which made me feel like a family member. His help was always invaluable to me.

I extend my heartfelt gratitude to Prof. Javed Sir and Mam for their parental love, care, and affection throughout my tenure. They have always been like family, and I am deeply grateful for their support.

I am thankful to all those who contributed to the experiments, supplied the necessary chemicals, and facilitated outsourced investigations. A special thanks go to the Central Bureau of Narcotics for providing morphine. I am grateful to the Department of Science and Technology (DST-INSPIRE) for granting me the fellowship that enabled me to complete my PhD successfully.

I express my sincerest gratitude and appreciation to all the individuals who have provided me with assistance and support during my journey to obtain my doctorate. Direct and indirect contributions have been invaluable, and I could not have accomplished this feat without them.

Finally, I extend my sincerest gratitude to my Maa, Mummy, Papa, Bhai and Nani for making countless sacrifices and providing unwavering support, positivity, and determination throughout my pursuit of this PhD. Without their contributions, none of this would have been possible.

Sidhanta

CERTIFICATE

This is to certify that the thesis entitled "*Induction of the activation of immunity against opiods and Mycobacterium tuberculosis by a chimeric vaccine.*", submitted by Mr Sidhanta Nanda (2018BMZ0001) for the award of the degree of Doctor of Philosophy of the Indian Institute of Technology Ropar, is a record of bonafide research work carried out under my guidance and supervision. To the best of my knowledge and belief, the work presented in this thesis is original. It has not been submitted, either in part or whole, for the award of any other degree, diploma, fellowship, associateship or similar title of any university or institution.

The thesis has reached the standard of fulfilling the requirements of the regulations relating to the degree.



Signature of the Supervisor
Prof. Javed Naim Agrewala
Department of Biomedical Engineering
Indian Institute of Technology Ropar
Rupnagar, Punjab 140001
Date: 06.09.2023

LAY SUMMARY

Drug addiction is a significant issue that not only impacts individuals but also poses a threat to public safety. Opioid substitution therapy (OST) is employed as a treatment for opioid addiction; however, it carries the risk of creating dependency on the treatment drug for patients. Researchers actively seek alternatives to OST, such as vaccines, to address these concerns. This study explored the potential of a nanotechnology-based vaccine expressing morphine and an immune-booster Pam3Cys (TLR-2 agonist) on the nanoparticles generated from the Acr1 antigen of *Mycobacterium tuberculosis*. The chimeric vaccine is designed to elicit immunity against morphine and tuberculosis (TB).

The vaccine demonstrated the ability to enhance the proliferation of B cells and T cells. The vaccinated animals produced high-affinity anti-morphine antibodies, eliminating morphine from their bloodstream and brain. Furthermore, the vaccine downregulated opioid receptors, thereby preventing morphine from binding to these receptors and neutralising its effects. Additionally, the vaccine triggered the production of central memory B cells and T cells. Memory cells provide long-term protection against diseases.

In the future, this vaccine holds promising potential as a prophylactic measure to protect against opioid dependency.

ABSTRACT

Drug addiction has dire consequences for individuals and significantly threatens public well-being. Presently, opioid substitution therapy (OST) relies on buprenorphine, a morphine agonist, to address opioid dependency. However, a risk exists of patients developing dependence on the treatment drug. Naloxone is employed in OST as a carrier for buprenorphine. While naloxone competes with opioids for binding, it can result in various adverse effects, including cardiovascular complications, brain tissue damage, and neurological disorders.

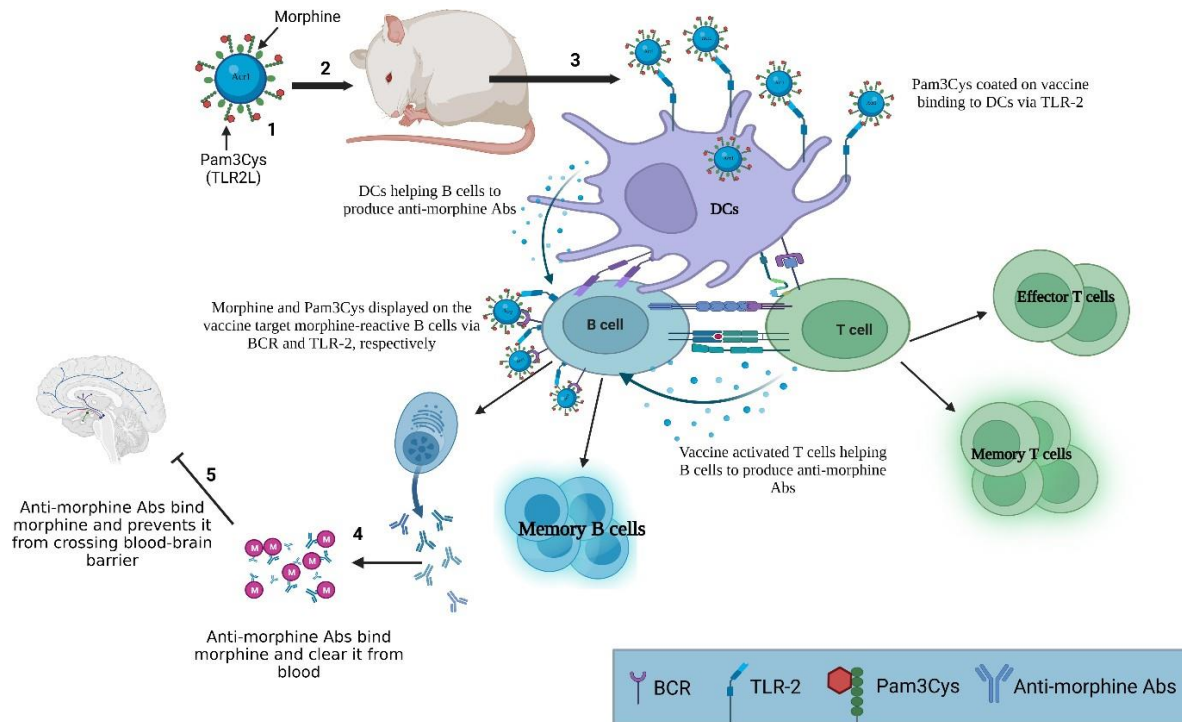
Numerous studies have indicated a higher prevalence of tuberculosis (TB) infection among individuals struggling with drug addiction. Opioids contribute to immunosuppression, rendering individuals more susceptible to TB. Hence, it is crucial to explore alternative therapies for opioid addiction. Vaccines have played a vital role in eradicating debilitating diseases like poliomyelitis, smallpox, and measles. Similarly, vaccines can serve as a powerful tool in mitigating the effects of opioids.

We utilised nanotechnology and created a novel vaccine displaying morphine and Pam3Cys (TLR-2 agonist) on the surface of Acr1 nanoparticles (MAPNV). Acr1, an immunodominant antigen of *Mycobacterium tuberculosis* (*Mtb*), holds potential as a vaccine candidate against TB.

The MAPNV vaccine demonstrated self-adjuvant properties and stimulated the proliferation and differentiation of morphine-specific B cells and Acr1-reactive CD4 T cells. Vaccination induced the production of high-affinity anti-morphine antibodies, which effectively eliminated morphine from the bloodstream and brain of the animals. Additionally, a downregulation in the expression of addiction-associated OPRM and dopamine genes was observed. This suggests the vaccine may prevent morphine from binding to opioid receptors and reduce its addictive effects. Moreover, a significant increase in the pool of memory CD4 T cells and B cells indicates the long-lasting impact of the vaccine. Generating morphine-reactive B cells and Acr1-specific CD4 T cells further highlights the vaccine's potential to confer immunity against morphine and *Mtb*.

In the future, MAPNV holds promise to protect against morphine addiction and TB infection.

GRAPHICAL ABSTRACT



LIST OF PUBLICATIONS

1. Kumar Das D[#], Zafar MA[#], **Nanda S[#]**, Singh S, Lamba T, Bashir H, Singh P, Maurya SK, Nadeem S, Sehrawat S, Bhalla V, Agrewala JN. Targeting dendritic cells with TLR-2 ligand-coated nanoparticles loaded with *Mycobacterium tuberculosis* epitope induces antituberculosis immunity. **J Biol Chem**. 2022 Dec;298(12):102596 (equal contributions).
2. Arora L, Patra D, Roy S, **Nanda S**, Singh N, Verma AK, Chakraborti A, Dasgupta S, Pal D. Hypoxia-induced miR-210-3p expression in lung adenocarcinoma potentiates tumour development by regulating CCL2-mediated monocyte infiltration. **Mol Oncol**. 2022 Jun 3. 10.1002/1878-0261.13260.
3. Mihooliya KN, Nandal J, Kumari A, **Nanda S**, Verma H, Sahoo DK; Studies on efficient production of a novel lasparaginase by a newly isolated *Pseudomonas resinovorans* IGS-131 and its heterologous expression in *Escherichia coli*; **Biotech**. 2020 Apr; 10(4):148.
4. Kaur G, Singh S, **Nanda S**, Zafar MA, Malik JA, Arshi MU, Lamba T, Agrewala JN. Fiction and Facts about BCG Imparting Trained Immunity against COVID-19. **Vaccines** 2022, 10, 1006.
5. Chowdhury A, Chatterjee S, Kushwaha A, **Nanda S**, Dhilip Kumar TJ, Bandyopadhyay A; Sulfonyl Diazaborine ‘Click’ Chemistry Enables Rapid and Efficient Bioorthogonal Labeling; **Chem Eur J**. 2023, e202300393, 10.1002/chem.202300393.
6. **Nanda S**, Zafar MA, Singh S, Gautam R, Ghosh A, Basu D, Agrewala JN; Chronic administration of morphine provokes the generation of anti-morphine antibodies and immunosuppression in individuals with opioid use disorder. **IJMR** (communicated).
7. Pasricha K, Prajapati S, **Nanda S**, Lamba T, Zafar MA, Tripathi NM, Bandyopadhyay A, Agrewala JN, Cross-reactive T cell and B cell epitopes of mycobacteria and SARS-CoV-2: a possible reason for a higher rate of protection of TB-endemic population against COVID-19. **J Trans Med** (communicated).
8. Ahmad Malik JA, **Nanda S**, Zafar MA, Sehrawat S, Agrewala JN; Influence of chronic administration of morphine and its withdrawal on the behaviour of zebrafish, **J Biosciences** (in press).

CONFERENCES

International

1. Presented 'Induction of the Activation of Immunity against Opioids and *Mycobacterium tuberculosis* by Chimeric Vaccine' at the 'Nature's Conference Next Gen Immunology 2020', Weizmann Institute of Science, Israel.

National

1. Poster presentation at National Seminar on "Biotechnology for Sustainable Utilization of Bioresources (BSUB- 2018)". North Orissa University, Odisha (12-20 October)
2. Poster presentation at UK-India International workshop on "Advance Biomaterials and Biosensors (ABB-2018)" by British Council and Newton Bhabha fund. IIT Ropar (8-12 November)
3. Poster presentation at IMMUNOCON-2019. D.A.E Convention Center, Mumbai (14-16 November)
4. Poster presentation in Pan-IIT research scholar conclave, 2019. IIT Delhi (20-22 December)
5. Invited speaker for the technical session for NGS in Immunology in SPARC INDO-US workshop 2020, IIT Ropar (6-8 June)
6. Poster presentation at IMMUNOCON-2022. PGIMER, Chandigarh (24-26 November).

PATENT

1. Development of a novel Acr1 nano vaccine displaying on the surface morphine and TLR-2 ligand to impart enduring immunity against morphine addiction and tuberculosis infection. (Applied)

TABLE OF CONTENTS

LIST OF FIGURES AND TABLES

ABBREVIATIONS

CHAPTER 1: INTRODUCTION

1.1. Background	01
1.2. Context	07
1.3. Purpose	08
1.4. <i>Significance, Scope and Definitions</i>	11

CHAPTER 2: LITERATURE REVIEW

2.1. Opioid addiction is a serious and growing public health issue worldwide	13
2.2. Opioid addiction represents a global menace	13
2.3. Limitation of current anti-opioid therapy	15
2.4. The development of anti-opioid vaccines is an ongoing field of research	15
2.5. The Acr1 protein has been studied as a potential drug target for treating tuberculosis (TB)	21
2.6. TLR agonists have emerged as a novel adjuvant in immunological research	26
2.7. Nanoparticles; emerging option for developing immunological vaccine	29
2.8. Generation of anti-hapten antibodies through chronic use of morphine	32

CHAPTER 3: MATERIALS AND METHODS

3.1. Purification of Acr1 protein	36
3.2. Synthesis of Acr1 nanoparticles (AN)	37
3.3. Synthesis of morphine-Acr1-Pam3Cys nanoparticles vaccine (MAPNV)	37
3.4. Testing particulation efficiency	37
3.5. Particle size distribution and zeta potential measurement	38

3.6. Particle morphology demonstrated by scanning electron microscopy (SEM)	38
3.7. Investigation of redispersion ability of MAPNV	38
3.8. Analysis of MAPNV using Fourier Transform Infrared (FTIR) Spectroscopy	39
3.9. Surface scanning analysis of MAPNV	39
3.10. Evaluating the efficiency of morphine conjugation on the surface of MAPNV	39
3.11. Evaluating the efficiency of Pam3Cy (P3C) conjugation on the surface of MAPNV	40
3.12. Colourimetric analysis for detecting conjugation of Pam3Cys on the MAPNV	40
3.13. Determination of morphine immobilisation on the surface of MAPNV by flow cytometer	41
3.14. Enzyme-linked immunosorbent assay (ELISA) for detecting morphine on the MAPNV	41
3.15. Time-dependent stability of nanoparticles using dynamic light scattering	41
3.16. UV-Visible spectroscopy study revealed the stability of MAPNV	42
3.17. Determination of pH-dependent stability of the MAPNV	42
3.18. Synthesis of morphine-protein conjugates	42
3.19. Western blotting to detect the conjugation of morphine with BSA	43
3.20. Demonstration of the cytotoxicity of MAPNV	43
3.21. Evaluation of MAPNV-induced lymphoproliferation	44
3.22. The detection of morphine reactive B cells in the animals immunised with MAPVN	44
3.23. MAPNV-FITC phagocytosis by macrophages	44
3.24. Evaluation of adjuvant property of MAPNV	44
3.25. Demonstration of the immunostimulatory efficacy of the MAPNV in mice exposed to morphine	45
3.26. Demonstration of MAPNV-FITC phagocytoses through TLR-2	45
3.27. The examination of the prophylactic efficacy of MAPNV vaccine	46
3.28. Testing of the therapeutic efficiency of MAPNV vaccine	46
3.29. Investigation of the proliferation of CD4 T and B cells obtained from	46

the vaccinated animals.	
3.30. Enumeration of morphine reactive B cells in the MAPNV vaccinated animals	47
3.31. Measuring anti-morphine Abs in the MAPNV vaccinated animals	47
3.32. Estimation of IgG and IgM subtype of anti-morphine Abs on MAPNV immunization	47
3.33. Estimation of morphine in the brain and serum on immunisation with MAPNV	48
3.34. Isolation of RNA from the brain and splenocytes on inoculation of MAPNV	48
3.35. Synthesis of cDNA from the RNA	49
3.36. RT-qPCR to determine the cytokines gene expression level in the MAPNV vaccinated animals	49
3.37. Examining the effects of vaccination on the behaviour of animals	50
3.38. Evaluation of affinity of the anti-morphine Abs	50
3.39. Estimation of anti-morphine Abs levels in the serum of chronic morphine abusers	50
3.40. Demonstration of the level of anti-morphine Abs	51
3.41. Estimation of free morphine in the serum of chronic morphine users	51
3.42. Neutralisation of morphine by anti-morphine Abs	52
3.43. Isolation of RNA from the serum of chronic morphine users	52
3.44. Preparation of the cDNA	53
3.45. Statistical analysis	53

CHAPTER 4: RESULTS

4.1. The <i>Mycobacterium tuberculosis</i> (<i>Mtb</i>) Acr1 protein nanoparticles (AN) coated with morphine and Pam3Cys exhibited polydispersity and positive zeta potentials	55
4.2. Particulation efficiency of Acr1 nanoparticles (AN)	57
4.3. Scanning electron microscopy (SEM) showed that MAPNVs are highly ordered and crystalline with minimal aggregation	58
4.4. The freeze-drying demonstrated a decrease in the MAPNV	58

4.5. Fourier transform infrared (FTIR) spectra of MAPNV	59
4.6. The conjugation of morphine and Pam3Cys on the surface of MAPNV	60
4.7. The concentration of morphine in the nanoparticles suggested effective conjugation of morphine on the surface of MAPNV	61
4.8. The presence of Pam3Cys on the surface of MAPNV	62
4.9. The binding of morphine on the surface of MAPNV	64
4.10. The hydrodynamic size of MAPNV was stable at 4 °C for 180 days	66
4.11. The detection of morphine in the morphine-BSA conjugate by immunoblotting	70
4.12. MAPNV is not cytotoxic for the cells	71
4.13. MAPNV has self-adjuvant properties and stimulates B cells to release anti-morphine Abs that clear the morphine from the brain and blood	73
4.14. Immunisation with MAPNV does not require any exogenous adjuvant and induces optimum proliferation, differentiation and generation of CD4 T cells memory cells	81
4.15. MAPNV effectively activated macrophage function suppressed due to regular exposure to morphine	86
4.16. MAPNV induced the activation of B cells and T cells in the mice exposed to morphine	89
4.17. DC endocytose MAPNV predominantly through the TLR-2 pathway	91
4.18. MAPNV vaccination downregulates the expression of OPRM and dopamine genes	94
4.19. MAPNV exhibited therapeutic efficacy and induced the proliferation of B cells and secretion of anti-morphine Abs that neutralised the presence of morphine in the blood and brain	95

4.20. MAPNV exhibited therapeutic efficacy and induced the proliferation, differentiation and generation of memory CD4 T cells	100
4.21. Immunotherapy with MAPNV downregulates the expression of addiction-associated OPRM and dopamine genes	106
4.22. Immunotherapy with MAPNV downregulates the addiction behaviour in the vaccinated animals	108
4.23. The presence of anti-morphine Abs in the serum of patients with Opioid Use Disorder (OUD)	111
4.24. The presence of morphine in the serum of the OUD patients	115
4.25. Anti-morphine Abs binds morphine	116
4.26. Morphine supports the expression of FoxP-3	118
4.27. The patients with OUD showed a weaker generation of Abs against the Acr1 protein of <i>Mtb</i>	119
CHAPTER 5: DISCUSSIONS	122
CHAPTER 6: SUMMARY	134
CHAPTER 7: BIBLIOGRAPHY	137

LIST OF FIGURES

CHAPTER 1

- Fig. 01. Global estimation of the drug users
- Fig. 02. World TB occurrence
- Fig. 03. Different measures of harm associated with the drugs
- Fig. 04. Significance of the study in terms of reducing opioid addictions

CHAPTER 2

- Fig. 01. Prevalence of opioid addiction across countries
- Fig. 02. Design and synthesis of a morphine-6-succinyl-bovine serum albumin hapten for vaccine
- Fig. 03. B cell-based platform for generating a-opioid hybridomas against opioids
- Fig. 04. Schematic representation showing the synthesis of the hydrolytically stable hapten linked to a poly (lactic-co-glycolic acid) (PLGA) nanoparticle with CpG oligonucleotides (CpG ODN) as a Th1 adjuvant
- Fig. 05. Simplified schematic diagram of heroin conjugate conjugates immunological pathway and mechanism of action.
- Fig. 06. Optimized curve of morphine hapten concentration displaying fluorescence intensity
- Fig. 07. BCG-liposomes alpha-crystalline protein 1 (Acr1L) provides significantly better protection than BCG
- Fig. 08. Immunization with L91 protects guinea pigs against *Mycobacterium tuberculosis*
- Fig. 09. Binding of Pam3Cys with TLR1-TLR2 complex
- Fig. 10. E91NP3 vaccination reduces Mtb burden in the lungs
- Fig. 11. A graphical representation of the mechanisms by which nanoparticles alter the induction of immune responses

CHAPTER 4

- Fig. 01. The *Mycobacterium tuberculosis* (Mtb) Acr1 protein nanoparticles (AN) coated with morphine and Pam3Cys exhibited polydispersity and positive zeta potentials
- Fig. 02. Particulation efficiency of Acr1 nanoparticles (AN)
- Fig. 03. Scanning electron microscopy (SEM) showed that MAPNVs are highly ordered and crystalline with minimal aggregation

- Fig. 04. The freeze-drying demonstrated a decrease in the MAPNV
- Fig. 05. Fourier transform infrared (FTIR) spectra of MAPNV
- Fig. 06. The conjugation of morphine and Pam3Cys on the surface of MAPNV
- Fig. 07. The concentration of morphine in the nanoparticles suggested effective conjugation of morphine on the surface of MAPNV
- Fig. 08. The presence of Pam3Cys on the surface of MAPNV
- Fig. 09. The binding of morphine on the surface of MAPNV
- Fig. 10. The hydrodynamic size of MAPNV was stable at 4 °C for 180 days
- Fig. 11. The detection of morphine in the morphine-BSA conjugate by immunoblotting
- Fig. 12. MAPNV is not cytotoxic for the cells
- Fig. 13. MAPNV has self-adjuvant properties and stimulates B cells to release anti-morphine Abs that clears the morphine from the brain and blood
- Fig. 14. Immunisation with MAPNV does not require any exogenous adjuvant and induces optimum proliferation, differentiation and generation of CD4 T cells memory cells
- Fig. 15. MAPNV effectively activated macrophage function suppressed due to regular exposure to morphine
- Fig. 16. MAPNV induced the activation of B cells and T cells in the mice exposed to morphine
- Fig. 17. DC endocytose MAPNV primarily through the TLR-2 pathway
- Fig. 18. MAPNV vaccination downregulates the expression of OPRM and dopamine genes
- Fig. 19. MAPNV exhibited therapeutic efficacy and induced the proliferation of B cells and secretion of anti-morphine Abs that neutralised the presence of morphine in the blood and brain
- Fig. 20. MAPNV exhibited therapeutic efficacy and induced the proliferation, differentiation and generation of memory CD4 T cells
- Fig. 21. Immunotherapy with MAPNV downregulates the expression of addiction-associated OPRM and dopamine genes
- Fig. 22. Immunotherapy with MAPNV downregulates the analgesic behaviour in the vaccinated animals
- Fig. 23. The presence of anti-morphine Abs in the serum of patients with Opioid Use Disorder (OUD)
- Fig. 24. The presence of morphine in the serum of the OUD patients
- Fig. 25. The binding efficiency of anti-morphine Abs to morphine

Fig. 26 Morphine supports the expression of FoxP-3

Fig. 27. The patients with OUD showed a weaker generation of Abs against the Acr1 protein of *Mtb*

LIST OF TABLES

CHAPTER 1

Table 1. List of common opioids and their characteristics.

ABBREVIATIONS

Ab	Antibody
ACK	Ammonium chloride lysis buffer
Acr1	alpha-crystallin-related protein 1
Acr1-Nps	Acr1 nanoparticles
Acr1-M-P3C	Acr1-morphine-Pam3Cys nanoparticles.
Ag	Antigen
AIDS	Acquired Immune Deficiency Syndrome
AN	Acr1 nanoparticles
ANOVA	Analysis of variance
APC	Antigen-presenting cells
APN	Acr1-Pam3Cys nanoparticles
BCG	Bacillus/Bacille/Bacilli Calmette-Guerin
bioP₃C	biotinylated Pam3Cys
BMDC	Bone marrow-derived dendritic cell
BSA	Bovine serum albumin
CCR	Chemokine receptor
CD	Cluster of differentiation
CNT	Carbon nanotubes
CTL	Cytotoxic T lymphocytes
d	day
DAMP	Damage associated molecular pattern
DCs	Dendritic cells
ddH₂O	Double distilled water

DNA	Deoxyribonucleic acid
DOTS	Directly observed treatment and short-course drug therapy
EE	Entrapment efficiency
FBS	Fetal bovine serum
Fc	Fraction crystallisable
Fig	Figure
GM-CSF	Granulocyte-macrophage colony-stimulating factor
h	Hour/s
HIV	Human Immunodeficiency virus
HLA	Human Leukocyte Antigen
HSP	Heat shock protein
IFA	Incomplete Freund's adjuvant
IFN-γ	Interferon- γ
IKK	I κ B kinase
IL	Interleukin
MFI	Integrated mean/median fluorescence intensity
iNOS	Inducible nitric oxide synthase
KLH	Keyhole limpet hemocyanin
LPS	Lipopolysaccharide
mAbs	Monoclonal antibodies
MAN	Morphine-Acr1 nanoparticles
MAPNV	Morphine-Acr1-Pam3Cys nanoparticle vaccine
MDP	Muramyl dipeptide
MFI	Mean fluorescent intensity

MHC	Major histocompatibility complex
<i>Mtb</i>	<i>Mycobacterium tuberculosis</i>
NF-κB	Nuclear factor kappa B
NO	Nitric oxide
NP	Nanoparticle
OD	Optical density
P3C	Pam3Cys
PAMPs	Pathogen-associated molecular patterns
PBS	Phosphate buffered saline
PBST	1X PBS + 0.1% Tween-20
PCL	Poly(ε-caprolactone)
PDI	Poly dispersity index
pH	Negative logarithm of hydrogen ion concentration
PRRs	Pattern recognition receptors
PVDF	Polyvinylidene difluoride
Pam2Cys/Pam2CSK4/P3C	S-[2,3-bis(palmitoyloxy)-propyl]-(R)-cysteinyl-(lysyl)3-lysine
Pam3Cys/Pam3CSK4/P3C	N-palmitoyl-S-[2,3-bis(palmitoyloxy)-propyl]-(R)-cysteinyl-(lysyl)3-lysine
r	Recombinant
R&D	Research and Development
rpm	Rotations per minute
RPMI	Roswell Park Memorial Institute
RR-TB	Rifampicin-resistant tuberculosis
s.c.	Subcutaneous
SD	Standard deviation

SN	Supernatants
SPPS	solid-phase peptide synthesis
TB	Tuberculosis
TCR	T cell receptor
TDR	Totally drugs resistant
The	T helper
TLR	Toll-Like Receptor
TNFα	Tumor necrosis factor-alpha
TPP	Pentasodium tripolyphosphate hexahydrate
TRAF	TNF receptor-associated factor 6
Treg	Regulatory T cells
UN	United Nations
Vol.	Volume
WHO	World Health Organization

Symbols

α	Alpha
β	Beta
γ	Gamma
κ	Kappa
\pm	Plus-minus
μ	Micro
\leq	Less than or equal to
\geq	More than or similar to
ζ	Zeta

Units of measurement

%	Percentage
$\times g$	Centrifugal force equal to gravitational force
μg	Microgram
μl	Microlitre
$\mu Cal \cdot s^{-1}$	Micro calories per second
$^{\circ}C$	Degrees Celsius
h	Hour(s)
kDa	kilo Dalton
kHz	kilo Hertz
M	Molar
mg	Milligrams

min	Minutes
ml	Milliliter
mM	Millimolar
mV	Millivolts
ng	Nanogram
nM	Nanomolar
nm	Nanometer
N/m	Newton per meter
OD	Optical density
V	Volts

Techniques

DLS	Dynamic light scattering
DSC	Differential scanning calorimetry
ELISA	Enzyme-linked immunosorbent assay
FACS	Fluorescence assisted cell sorting
FE-SEM	Field emission scanning electron microscopy
FMT	Fluorescence molecular tomography
FT-IR	Fourier-transform infrared spectroscopy
TEM	Transmission electron microscopy
TGA	Thermogravimetric analysis
ITC	Isothermal titration calorimetry

Chemicals

CaCl₂	Calcium chloride
DMSO	Dimethylsulphoxide
EDC	N-(3-Dimethylaminopropyl)-N'-ethyl carbodiimide hydrochloride
H₂SO₄	Sulphuric acid
H₂O₂	Hydrogen peroxide
HCl	Hydrochloric acid
HRP	Horseradish peroxidase
KBr	Potassium bromide
KCl	Potassium chloride
KH₂PO₄	Potassium dihydrogen phosphate
KHCO₃	Potassium bicarbonate
MES	2-(N-morpholino)ethane sulfonic acid
MgCl₂	Magnesium chloride
Na₂CO₃	Sodium carbonate
Na₂HPO₄	Disodium hydrogen phosphate
NaCl	Sodium chloride
NaHCO₃	Sodium bicarbonate
NaN₃	Sodium azide
NaOH	Sodium hydroxide
NHS	N-Hydroxysuccinimide
NH₄Cl	Ammonium chloride
OPD	Ortho phenylenediamine
PEG	Poly(ethylene glycol)

PLA	Poly(lactide)
PLGA	Poly(lactic-co-glycolic acid)
PMMA	Poly(methyl methacrylate)
PMSF	Phenylmethanesulfonyl fluoride
PPD	Purified Protein Derivative
SDS	Sodium dodecyl sulphate
TMB	Tetramethylbenzidine
β-ME/2-ME	β- or 2- mercaptoethanol

1.1 *Background.* Drug addiction, also known as substance use disorder, is a persistent condition wherein individuals exhibit compulsive substance abuse despite the detrimental and hazardous effects. Various factors contribute to drug addiction, such as self-medication for emotional distress, peer pressure, and the pursuit of enhanced physical or mental performance. Addiction inflicts physical, psychological, and social harm, including the development of physical dependence, which manifests as withdrawal symptoms upon drug discontinuation. Treatment for drug addiction typically entails psychotherapy, medication, and lifestyle adjustments.

Opioid Use Disorder (OUD) represents a prominent substance use condition characterised by a chronic and recurring pattern of compulsive opioid consumption, disregarding the detrimental consequences. Symptoms associated with this disorder encompass an intense desire for opioids, difficulty in controlling usage, persistent engagement in drug use despite risks or harm, withdrawal symptoms, tolerance, and occasionally physical dependence.

GLOBAL ESTIMATES OF THE NUMBERS OF DRUG USERS IN MILLIONS (2020)

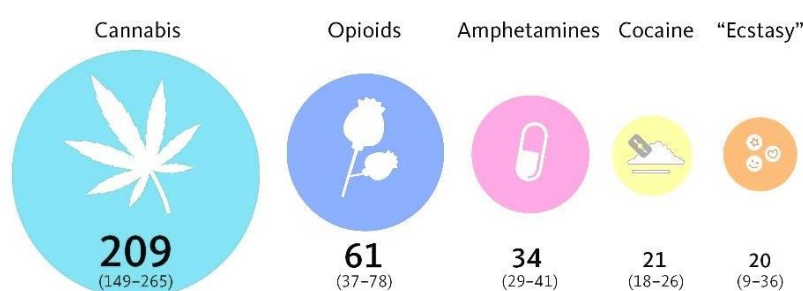


Fig. 1. Global estimation of the drug users (Figure adapted from World Drug Report 2022, UNODC).

The World Drug Report 2022 reveals that opioid use disorder affects approximately 61 million individuals across 130 countries (*World Drug Report 2022*). Drug use-related deaths account for around 0.5 million fatalities globally. Opioids are responsible for over 70% of these deaths, with over 30% resulting from overdoses. In 2021, the World Health Organization (WHO) reported nearly 0.1 million deaths caused explicitly by opioid overdoses. Non-fatal opioid overdoses occur significantly more frequently than fatal cases (*World Health Report 2022*).

CHAPTER 1

INTRODUCTION

There are ten commonly used types of opioids for OUD globally. These include 1. Morphine, 2. Hydrocodone, 3. Oxycodone, 4. Codeine, 5. Fentanyl, 6. Methadone, 7. Buprenorphine, 8. Naloxone, 9. Tramadol, and 10. Hydromorphone. Among them, morphine is widely recognised as the primary alkaloid in all opioids, serving as the precursor compound. Its potent analgesic properties make it particularly susceptible to abuse (*UNODC reports on opioids, 2021*).

Table 1. Types of opioids.

	Natural	Semi-synthetic	Synthetic
Source	Naturally occurring	Derived from natural opioids	Synthesised independently
Chemical Structure	Typical	Similar	Dissimilar
Examples	Morphine Codeine	Hydromorphone Oxymorphone Hydrocodone Oxycodone Heroin	Methadone Fentanyl Meperidine Tramadol

Morphine, a potent opioid analgesic, is widely utilised to manage moderate to severe pain. Its mechanism of action involves binding to opioid receptors in the brain, spinal cord, and gastrointestinal tract. This binding inhibits the transmission of pain signals to the brain, resulting in robust pain relief. However, prolonged use of morphine can lead to addiction, necessitating higher doses to achieve the same pain-relieving effects. Furthermore, morphine impacts the respiratory and cardiovascular systems, causing respiratory depression, decreased heart rate, and lowered blood pressure (*Stephen et al. 2017*). It also influences the body's endocrine system, leading to elevated cortisol levels and pain suppression. Additionally, morphine can elevate dopamine levels, potentially inducing feelings of euphoria.

Morphine significantly affects the immune system, increasing the vulnerability to infections by compromising its ability to protect the body against pathogens. Studies have shown that morphine inhibits the generation of antibodies, reducing antibody levels in the bloodstream. Moreover, it hampers the production of antibodies in response to vaccines (*Kleinschmidt et al. 2013*). Additionally, morphine impairs the function of T cells by diminishing the production of cytokines that aid in their immune activities. It reduces the number of circulating T cells,

impairing their effectiveness in combating infections (*Pergolizzi et al. 2019*). Furthermore, morphine diminishes the expression of specific B cell receptors, limiting their capacity to recognise and respond to foreign antigens. The function of macrophages is impaired by morphine (*Henrickson et al. 2015*). It reduces the production of pro-inflammatory cytokines like TNF- α , IL-1 β , and IL-6 and decreases the expression of toll-like receptors (TLRs) and other cell surface molecules crucial for macrophage activation. Moreover, morphine impairs macrophages' chemotaxis and phagocytic activity, decreasing inflammation. Additionally, morphine curtails nitric oxide production, an essential mediator of inflammation, and reduces the generation of reactive oxygen species that can cause cellular and tissue damage.

Morphine exerts detrimental effects on dendritic cells (DCs), impairing their responsiveness to antigenic stimulation (*Mukherjee et al. 2016*). It diminishes their migration capacity, reducing their ability to encounter environmental antigens. Moreover, morphine hampers antigen presentation, limiting the body's capacity to mount a robust immune response. Additionally, morphine binds to dendritic cell receptors and induces hyperpolarisation, disrupting their normal functioning. The release of neurotransmitters by dendritic cells is also inhibited by morphine, leading to decreased neuronal excitability. Collectively, these effects contribute to compromised immune system functioning, rendering the body more susceptible to infections and illnesses.

The immune-suppressive nature of morphine paves the way for opportunistic infections. Individuals under the influence of morphine face an elevated risk of developing skin, lung, and urinary tract diseases (*Hussain et al. 2018*). Furthermore, opioid users are more prone to experiencing complications from existing infections due to the impact of opioids on the body's immune defence mechanisms. Morphine significantly heightens the risk of tuberculosis (TB) infection. Long-term use of morphine has been found to impair the ability of macrophages to combat *Mycobacterium tuberculosis* (*Mtb*). Additionally, morphine usage increases the susceptibility to pneumonia due to the compromised immune system (*Gurnaney et al. 2014*).

Estimated TB incidence rates, 2020

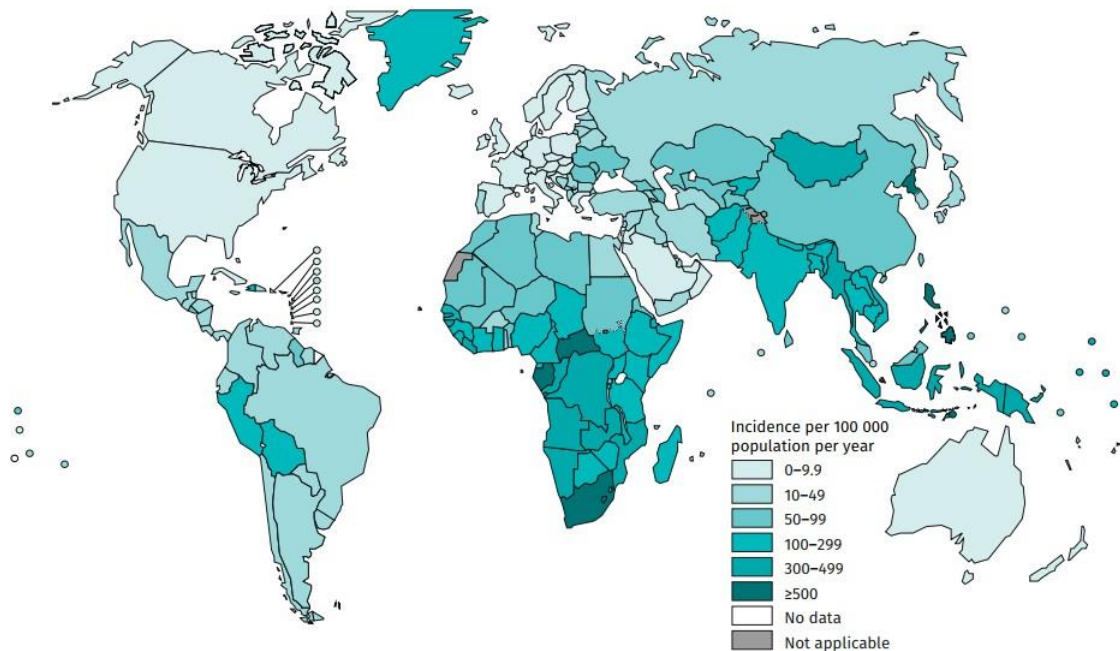


Fig. 2. World TB occurrence (Source World TB Report 2021). India is a TB-endemic country, with an estimated 2.8 million cases in 2019. The country has been classified as a high TB burden country by the World Health Organization (WHO), with 27% of the global estimated TB burden and accounts for about 40% of TB deaths worldwide. TB poses a significant public health concern and ranks as a leading cause of death in TB-endemic regions (*Global Tuberculosis Report. 2019*). The latent phase of TB infection occurs when an individual is infected with the bacteria but does not exhibit any signs or symptoms of active TB. During this phase, the person is not contagious and does not experience any health issues. However, without treatment, the latent infection can, at any time, progress to active TB. It is crucial to treat latent TB infection to reduce the risk of developing active TB. In India, latent TB infection (LTBI) is widespread, particularly among high-risk populations residing in densely populated urban areas, individuals with HIV/AIDS, and those with close contact with active TB cases. The immune-suppressive nature of morphine impacts the immunity against *Mtb*, exacerbating latent phase infections and promoting the transition to active TB.

Opioid substitution therapy (OST) is an evidence-based treatment for opioid use disorder that effectively addresses both the physical and psychological symptoms of opioid addiction. It has been proven to decrease opioid use and criminal activities, enhance the quality of life, reduce the risk of overdose and mortality, improve treatment retention, and lower the incidence of

HIV and other blood-borne diseases related to intravenous drug use. OST involves prescribing opioid medications like methadone or buprenorphine as a substitute for illicit opioids such as heroin, morphine, or fentanyl. By supporting individuals in abstinence from forbidden opioids, reducing criminal behaviour, and promoting physical and mental well-being, OST facilitates their engagement in treatment. Numerous studies have demonstrated that OST is one of the most effective approaches for treating opioid addiction, as it reduces mortality rates, improves the quality of life, and diminishes drug use.

Many opioid agonists used to treat OUD impair the immune system's function. Buprenorphine is an opioid agonist, and opioids have been known to cause a decrease in immunity. Studies have shown that opioid use can cause a reduction in white blood cells, leading to an increased risk of infection (*Hauptman et al. 2014*). Buprenorphine has the potential for dependence or addiction, although the risks are significantly lower than other opioids. Prolonged or high-dose drug usage can lead to dependence, manifesting in cravings, tolerance, and withdrawal symptoms. However, it is not effective in controlling addiction in patients. Additionally, its immune-suppressive nature increases the likelihood of contracting infectious diseases.

A vaccine is a biological substance that induces active acquired immunity against a specific disease. Typically, a vaccine contains a substance that resembles a disease-causing microorganism or its component. The vaccine is often derived from weakened or inactivated forms of the microbe, its toxins, or surface proteins. The vaccine stimulates the body's immune system to recognise the substance as a threat, eliminate it, and subsequently recognise and destroy any future encounter with a related microorganism (*National Institute of Allergy and Infectious Diseases, 2019*). Vaccines can serve as prophylactic measures, preventing or reducing the impact of future infections. They can also have therapeutic applications, such as cancer vaccines currently under investigation. Vaccines have been crucial in eradicating smallpox, polio, measles, mumps, and rubella (*Henderson et al. 2017*). They have significantly reduced the occurrence of infectious diseases like whooping cough, diphtheria, and tetanus. Vaccines are widely regarded as one of the most successful interventions in public health.

An anti-narcotics vaccine is a specific type used to diminish or eliminate an individual's cravings for drugs, particularly opioids. This vaccine is designed to activate the body's immune system, prompting the production of antibodies that recognise and clear the narcotics from the bloodstream. By doing so, the antibodies prevent the narcotics from crossing the blood-brain

barrier and exerting their desired effects. Additionally, the vaccine triggers an immune response against drugs, helping reduce cravings and relapse risk. The primary distinction between an anti-narcotics vaccine and Opioid Substitution Therapy (OST) lies in their purpose. In contrast, an anti-narcotics vaccine has a prophylactic effect and prevents the influence of substance abuse, whereas OST treats the disease after its occurrence. OST provides short-term relief for individuals who are not yet prepared to make the necessary lifestyle changes to overcome addiction or for those who are already dependent on opioids. It aims to diminish cravings and dependency. In contrast, a vaccine-based approach holds more significant potential for long-term treatment by preventing the user from experiencing the drug's effects altogether, thus thwarting addiction. This approach offers more sustained protection against relapse, particularly for individuals who have not yet developed a dependence. Ultimately, an anti-narcotics vaccine may prove more effective than OST in assisting individuals in overcoming addiction.

A recent study demonstrated that the anti-heroin vaccine prevented the effects of heroin when administered to four non-human primates (*McDonald et al. 2020*). The primates did not exhibit withdrawal symptoms upon receiving the vaccine. These findings suggest the potential role of vaccines, which can address the issue of heroin abuse and addiction and reduce the risk of overdose and associated fatalities. In another study, a vaccine against heroin yielded mixed results. The vaccine candidate employed a small fragment of heroin as the antigen, accompanied by an adjuvant comprising aluminium hydroxide and polyoxyethylene sorbitan monolaurate. In preclinical studies conducted on mice, the vaccine candidate produced better antibodies against heroin than the control group. Although the vaccine candidate did not exhibit the desired level of effectiveness, it represents a promising step forward in developing a clinically viable heroin vaccine (*Manson et al. 2019*). Although the use of vaccines to treat substance abuse is relatively new, they have been gaining momentum in recent years as a potentially viable treatment for addiction.

1.2 *Context.* Opioid receptors are widely distributed throughout the body, including the cells of the immune system viz T cells, B cells, dendritic cells, macrophages, etc. Opioid receptors are found on the surface of these cells that interact with opioids. When opioids bind to these receptors on immune cells, they can modulate immune responses and affect the function and activity of these cells (*Stolbach et al. 2008*). For example, opioid receptors on T cells and B

cells can influence their proliferation, activation, and cytokine production. In contrast, opioid receptors on dendritic cells can affect antigen presentation and immune cell communication. The presence of opioid receptors on immune cells allows opioids to exert immunomodulatory effects and influence immune responses.

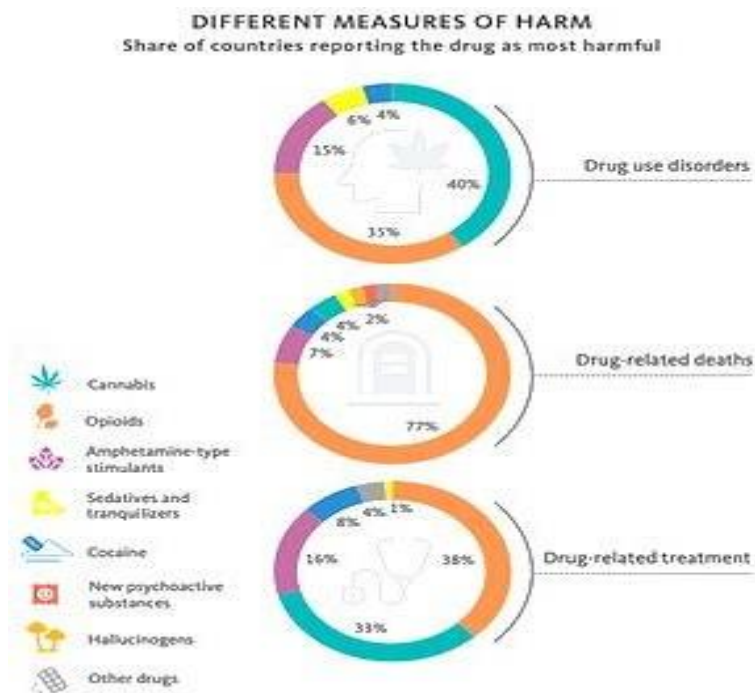


Fig. 3. Different measures of harm associated with the drugs (Source World Drug Report 2022).

Morphine, in particular, has been identified as having potent immunosuppressive effects. It has been observed to reduce the production of cytokines, T-cells, and white blood cells and dampen inflammatory responses. This immunosuppression compromises the production of antibodies crucial for defending against infections, thus increasing the risk of developing diseases (Ceccarelli *et al.* 2020). Developing an anti-opioid vaccine can potentially mitigate fatal overdoses resulting from morphine use. Such a vaccine would stimulate the production of antibodies in the body that can bind to and neutralise morphine when they enter the bloodstream. By preventing morphine from reaching the brain and activating its rewarding effects, the vaccine reduces the risk of overdose. The antibodies can bind to opioid molecules,

providing enhanced protection against opioid overdose. Anti-morphine vaccines offer a significant advantage by reducing the consumption of morphine among individuals struggling with its addiction, eliminating the need for regular medication or therapy. Vaccines offer long-lasting protection, and the effect lasts for several months.

Currently, there are various proposed anti-narcotics vaccines; however, their effectiveness is limited due to their inability to neutralise opioids in the bloodstream, generate enduring immunity against opioids, counteract opioid-induced immunosuppression in addicts, exhibit broad specificity across different opioids, demonstrate low-affinity antibodies towards opioid, and ineffective in completely treating opioid addictions (*Cunningham et al. 2019*). The development of an opioid vaccine is a complex undertaking with many uncertainties. Research indicates that conjugate-based vaccines elicit antibodies with a short active duration and may necessitate booster shots. Additionally, the vaccine's efficacy varies among different opioids. Moreover, it remains unclear how effective the vaccine would be in real-world scenarios, as individuals might still be exposed to high opioid doses and could be tempted to take higher doses if they perceive themselves as protected. These questions remain unanswered. As a solution to this challenge, we propose the development of a nanoparticle-based vaccine targeting morphine to generate high affinity, neutralising and enduring antibodies against morphine. Nano-technology has revolutionised vaccine development and administration by targeting antigens, improving effectiveness, safety, stability, and cost-effectiveness.

1.3 Purpose. Anti-opioid vaccines represent a promising prophylactic and therapeutic strategy for addressing substance abuse, offering the potential for long-term protection against relapse. These vaccines target morphine and stimulate the immune system to produce antibodies that bind to the morphine. Thus, preventing morphine from entering the brain and exerting its effects. This strategy can potentially reduce the risk of relapse and facilitate a more sustained recovery process. Morphine, a naturally occurring alkaloid derived from the opium poppy plant, is a key player in opioid addiction. By binding to opioid receptors in the brain, morphine reduces pain signals and induces feelings of relaxation and euphoria (*U.S. National Library of Medicine, 2019*). However, due to its slower onset, longer duration of action, and potential for respiratory depression and fatal outcomes in high doses, morphine is associated with a higher risk of dependence and addiction. Moreover, as morphine is a primary alkaloid in almost all opioids, a vaccine targeting morphine may prove more effective than one targeting other

opioids. Such a vaccine could mitigate the risk of overdose, adverse effects, and addiction by obstructing the reward effects of opioids (*Tseng et al. 2021*). Consequently, developing a morphine-targeted vaccine represents a viable strategy for combatting the opioid epidemic.

Opioid administration exerts a profound immunosuppressive effect on the immune system, increasing vulnerability to opportunistic infections (*Gelkopf et al. 2009*). Such a situation creates a fertile ground for the activation of latent *Mtb* infection, further exacerbating the problem. Hence, we thought to generate a chimeric vaccine to address the problem of both drug addiction and TB infection. Acr1 is a member of the Acyl-CoA synthetase family and represents a promising target for therapeutic intervention against *Mtb*. Several studies have unequivocally established the pivotal role of Acr1 in generating protective immunity against *Mtb* (*Jia et al. 2022; Lew et al. 2020; Gowthaman et al. 2011; Siddiqui et al. 2015; Rai et al. 2017; Das et al. 2022*). Therefore, Acr1 emerges as a highly favourable candidate for developing vaccines against TB.

Nanoparticle-based vaccines hold tremendous promise in the quest for more efficacious immunological interventions. Notably, nanoparticles offer an array of advantages over conventional vaccine delivery methods. These advantages encompass enhanced antigen specificity, safeguarding against antigen degradation, targeted delivery to specific immune cells, and sustained release of antigens (*Mandal et al. 2018*). To capitalise on these merits, we have engineered a novel vaccine delivery system utilising Acr1 protein-based nanoparticles expressing morphine and TLR-2 ligand Pam3Cys on its surface. This innovative approach aims to provoke an immune response against morphine, generating high-affinity antibodies against morphine that confer protection against its abuse. With unwavering optimism, we anticipate this pioneering strategy will be a powerful platform for developing a highly effective vaccine. Further, the efficacy of vaccines was significantly augmented through the judicious use of TLR-2 ligand as an adjuvant to modulate the immune system by targetting dendritic cells. Furthermore, this approach activated adaptive immunity and the innate immune system through TLR-mediated signalling of antigen-presenting cells (APCs). Moreover, harnessing the power of TLR ligands can shorten the amount of antigen required for vaccine effectiveness, thereby mitigating the economic burden and adverse effects associated with traditional vaccines. Hence, TLR ligands are indispensable in enhancing vaccine efficacy by invigorating the immune system and reducing the requisite antigen dosage for optimal efficacy. In this regard,

we have adeptly utilised Pam3Cys, a potent TLR-2 ligand, to amplify the vaccine's immunogenicity and confer upon it a self-adjuvating property. Notably, TLR-2 receptors are abundantly expressed on the surface of DCs, rendering them an ideal target for vaccine delivery. It is worth highlighting that dendritic cells, as the sole APCs in the immune system capable of activating naive T cells, assume a pivotal role in orchestrating robust immune responses.

Based on this, we aimed to understand the potential of this vaccine in combating the influence of morphine and advancing the field of immunotherapy. With this, we aimed to evaluate the potential of the newly developed vaccine for its ability to reduce or eliminate the deleterious effects of morphine effectively and for the treatment of opioid addiction. We have developed an innovative vaccine utilising Acr1 protein-based nanoparticles. These nanoparticles are engineered to present both morphine and the TLR-2 ligand Pam3Cys on their surface to achieve the following objectives: -

- I. Preparation and characterisation of a vaccine consisting of Acr1 nanoparticles that display morphine and Pam3Cys on their surface.
- II. Investigation of the adjuvant properties of the vaccine through the activation of DCs, B cells, and macrophages mediated by Pam3Cys.
- III. Study the endocytosis of the vaccine expressing Pam3Cys, specifically through the TLR-2 pathway.
- IV. Evaluation of the nanoparticles expressing morphine in terms of their ability to activate, proliferate, and differentiate morphine-specific B cells.
- V. To monitor the generation of long-term memory B cells specific to morphine and the secretion of high-affinity anti-morphine antibodies.
- VI. Demonstration of the activation, proliferation, and differentiation of Acr1 reactive T cells and the subsequent secretion of anti-Acr1 antibodies.
- VII. Assessment of the therapeutic and prophylactic efficacy of the vaccine in mitigating the effects of morphine using a murine model.

1.4 Significance, Scope and Definitions. The chimeric vaccine developed in this study holds substantial significance and has a broad scope, as it addresses multiple challenges associated with opioid addiction and TB. Firstly, the vaccine has demonstrated its ability to mitigate cravings and reduce opioid usage, providing a potential solution for individuals struggling with

opioid addiction. Additionally, it offers protection against TB for drug abusers, who are particularly vulnerable to opportunistic infections.

The vaccine administration in the murine system has shown promising results, eliciting the production of high-affinity anti-morphine antibodies. These antibodies effectively neutralise the presence of morphine in the bloodstream, inhibiting its access to the brain and its addictive effects. Moreover, the vaccine stimulates the activation of Acr1 reactive CD4 T cells and B cells' secretion of anti-Acr1 antibodies. This immune response holds excellent potential for combating morphine addiction and *Mtb* infection.

In summary, this study establishes the considerable potential of the vaccine as a remedial measure. It not only addresses the challenges associated with morphine addiction by reducing desire and usage but also protects against TB. This research opens up new possibilities for developing effective interventions to combat addiction and infectious diseases simultaneously.

2.1 Opioid addiction is a serious and growing public health issue worldwide. Over 62 million people are estimated to suffer from opioid addiction, which rises yearly. The use of opioids, whether for medical purposes or recreation, can lead to the development of a chronic disorder characterised by compulsive drug use, cravings, and continued use despite negative consequences. Developing opioid addiction involves biological, psychological, and sociocultural factors. It is believed that a combination of genetic predisposition, environmental influences, and personal choices contribute to the onset of addiction. Biologically, opioid addiction is associated with brain reward system changes. Opioids stimulate the brain's reward system, causing the release of neurotransmitters like dopamine and serotonin, which produce feelings of pleasure and reward. With repeated opioid use, the brain's reward system can become disrupted, leading to compulsive drug-seeking behaviour and intense cravings. Psychologically, opioid addiction is often linked to feelings of anxiety, depression, and stress. Individuals with opioid addiction may use drugs to cope with negative emotions or challenging situations. Socio-culturally, opioid addiction is associated with poverty, unemployment, limited education, and lack of access to primary healthcare and social support. Moreover, social stigma and discrimination against individuals with opioid addiction further compound the problem. Given the complexity of opioid addiction, effective treatment should address all these factors. Treatment typically involves a combination of medications, such as buprenorphine and naltrexone, and psychosocial interventions, like cognitive-behavioural therapy and contingency management.

2.2 Opioid addiction represents a global menace. Opioid addiction embodies a threat with intricate dimensions, encompassing over-prescription, poverty, limited access to mental health and addiction treatment services, and societal stigma. The extent and complexity of the opioid crisis emphasise the need for a comprehensive and holistic approach to tackling the issue. This review examines the opioid crisis from a public health perspective, focusing on its epidemiology, risk factors, and evidence-based interventions for prevention and treatment. The World Health Organization (WHO) estimates that over 62 million people globally are dependent on opioids, although this figure is likely an underestimation of the true prevalence of opioid addiction. Opioid addiction is a significant public health problem in numerous countries. In the United States, the opioid crisis has been referred to as an epidemic.

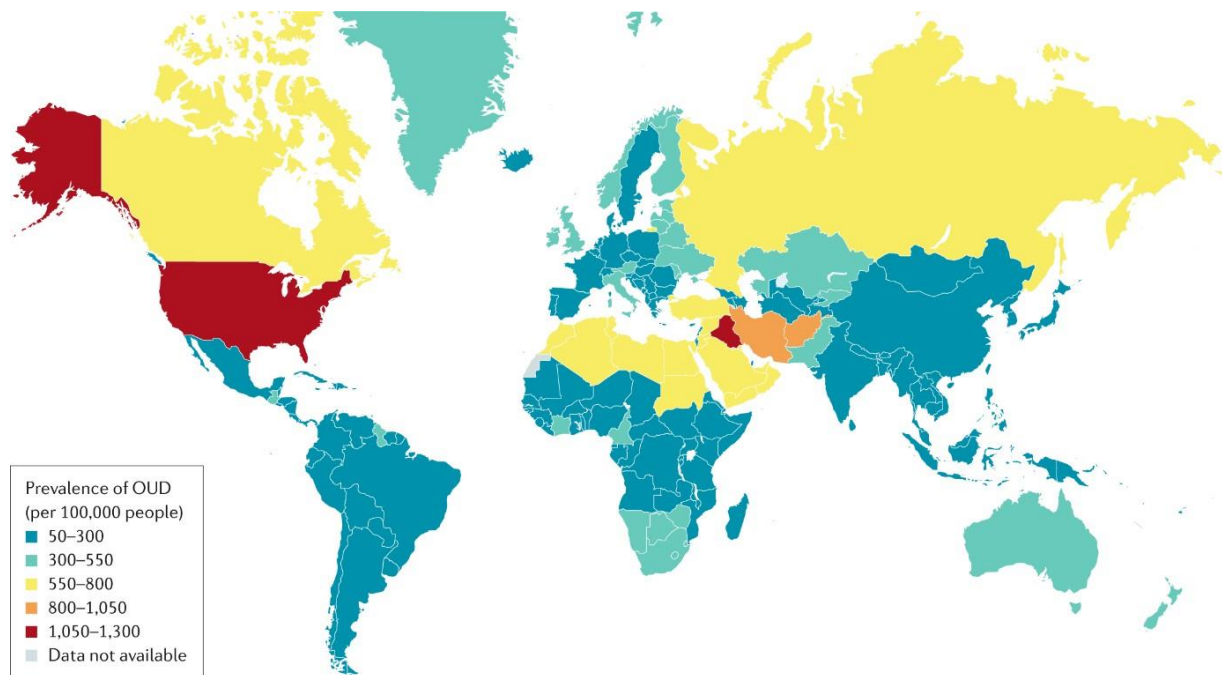


Fig. 1. Prevalence of opioid addiction across countries. Darker shades indicate higher prevalence rates, with the darkest shades representing a rate of more than 30% of the population affected. The lightest shades represent 0-4% of the population affected. (Adapted from John et al., 2020).

The prevalence of opioid addiction varies across countries, with the highest rates reported in the United States of America and Canada (Fig. 1). The Netherlands has the highest prevalence in Europe, followed by Norway and Germany. In Asia, China and India have the highest prevalence, while in Africa, Nigeria and South Africa report the highest rates. Risk factors associated with opioid addiction differ by country. In the United States, poverty, mental health issues, and access to opioids are among the risk factors. In Europe, poverty, access to opioids, and injection drug use contribute to the problem. In Asia, poverty, access to opioids, and limited treatment availability are significant risk factors. In Africa, poverty, access to opioids, and inadequate treatment access play a role. The public health consequences of opioid addiction are diverse. Common effects include increased rates of overdose deaths, TB, HIV and hepatitis C infections, and crime. In the United States, the opioid crisis has led to a rise in opioid-related overdose deaths. In Europe, the crisis is associated with increased HIV and hepatitis C infections among people who inject drugs. In Asia, it has been linked to higher levels of crime

and violence. In Africa, the crisis is associated with increased rates of HIV and hepatitis C infections (*World Drug Report 2022*).

2.3 Limitation of current anti-opioid therapy. Opioid Substitution Therapy (OST) is an evidence-based treatment for opioid use disorder that has been proven to reduce opioid dependence and criminal activity, improve quality of life, and decrease the risk of overdose and death. OST involves prescribing opioid medications like methadone or buprenorphine as substitutes for illicit opioids such as heroin, morphine, or fentanyl. Multiple studies have demonstrated the effectiveness of OST in reducing mortality rates, improving quality of life, and decreasing drug use. Buprenorphine, an opioid agonist commonly used in OST, is an effective treatment for opioid addiction. However, concerns exist regarding its potential for dependence, addiction, and an increased risk of infection due to its immune-suppressive properties. Several studies have indicated buprenorphine can lower white blood cell counts, increasing disease risk. Furthermore, buprenorphine alone may not be sufficient to address addiction in patients and can lead to dependence or addiction if taken in high doses or for prolonged periods. Overall, OST is a highly effective treatment for opioid addiction, with ample evidence demonstrating its ability to reduce mortality rates, improve quality of life, and decrease drug use. However, healthcare providers should carefully monitor patients receiving buprenorphine, adjusting dosages as necessary. Patients should be informed about the potential risks associated with the medication and closely monitored for signs of dependence or addiction.

2.4 The development of anti-opioid vaccines is an ongoing field of research. Vaccines are being explored as potential treatments for addiction to opioids, cocaine, and other addictive substances. The goal is to develop vaccines that can reduce cravings and prevent relapse. Several promising vaccine candidates have been developed and have undergone clinical trials. For example, a vaccine for cocaine addiction has been created and is currently in phase I clinical trials. This vaccine works by introducing a protein that binds to opioids in the body, eliminating their ability to produce dopaminergic effects. Additionally, vaccines are being developed to target addiction to opioids, methamphetamine, and other substances of abuse. Researchers are investigating the possibility of using combination vaccines to address addiction to multiple substances.

CHAPTER 2

REVIEW OF LITERATURE

In recent years, the development of vaccines has emerged as a promising strategy to combat the growing problem of opioid addiction. In this regard, Akbarzadeh et al. undertook the important task of designing a hapten as an immunogen for a vaccine against morphine addiction (Akbarzadeh et al. 1999). The study focused on developing the morphine-6-succinyl-bovine serum albumin (M6S-BSA) conjugate for vaccine development. This conjugate was created by synthesising the hapten, morphine-6-succinyl, and linking it to bovine serum albumin (BSA) (Fig. 2). The hapten synthesis involved a series of chemical reactions, including anhydrous morphine with succinic anhydride in the presence of benzene, followed by a reaction with an activated ester and a coupling agent. The immunogenicity of this conjugate was evaluated in mice, and the results demonstrated that M6S-BSA could induce an anti-morphine immune response. The M6S-BSA conjugate proved an effective immunogen, eliciting a strong immune response.

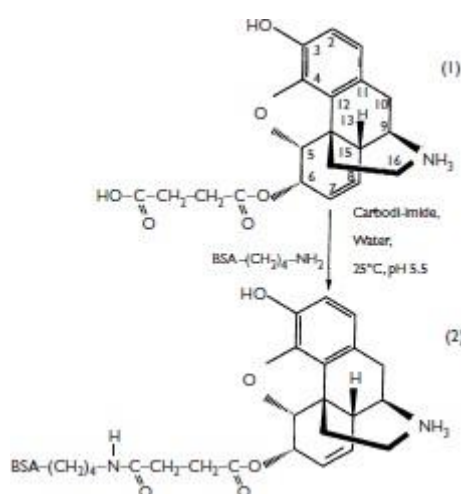


Fig. 2. Design and synthesis of morphine-6-succinyl-bovine serum albumin hapten for vaccine development against morphine addiction (Adapted from Akbarzadeh et al. 1999).

Recently, studies have highlighted the use of monoclonal antibodies in eliminating morphine dependence. It has been reported that specific and high-affinity monoclonal antibodies against morphine could eliminate morphine dependency (Baehr et al. 2020). The study revealed that the monoclonal antibodies exhibited a high affinity for morphine, with an average binding constant of 1×10^{-7} M, and displayed strong specificity, showing no cross-reactivity to other opioids (Fig. 3).

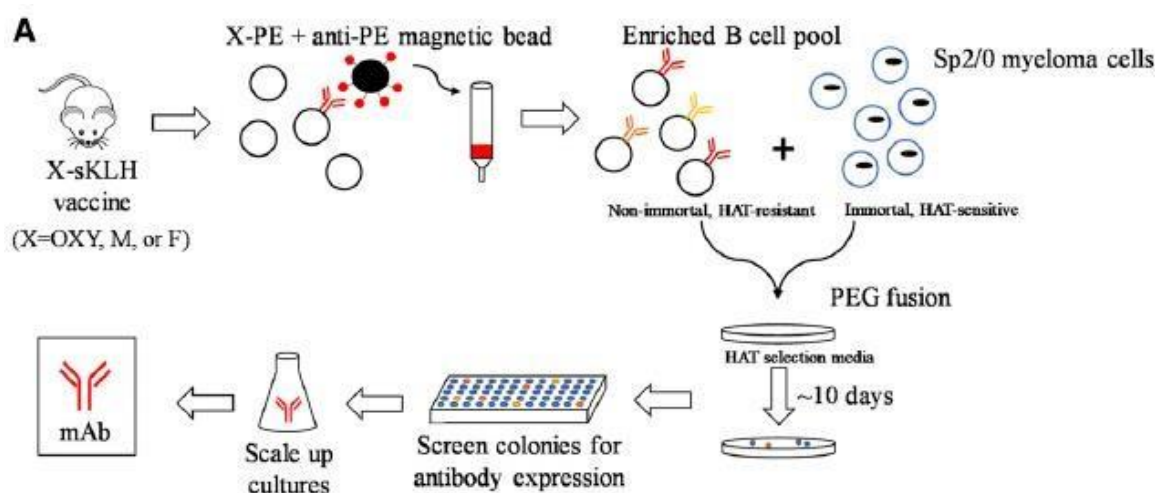


Fig. 3. B cell-based platform for generating hybridomas against opioids. Workflow for hybridoma generation. Antigen-specific cells from immunised mice were selected by magnetic enrichment for polyethene glycol (PEG) fusion with Sp2/0 myeloma cells; hypoxanthine aminopterin-thymidine (HAT)-resistant colonies were transferred to plates and screened for expression of anti-opioid antibodies by ELISA (Adapted from Baehr et al. 2020).

Heroin addiction poses a significant public health challenge, causing numerous individuals physical, psychological, and social harm. A promising approach to address this issue involves the development of a bivalent vaccine capable of preventing relapse to heroin and morphine. In 2006, Benito Anton conducted research to evaluate the effectiveness of such a vaccine in rodents. The study revealed that the vaccine successfully triggered an immune response to heroin and morphine, preventing the drugs' psychoactive effects from reaching the brain (Anton et al. 2006). Qian et al. developed a bivalent morphine/heroin vaccine with a novel hapten design and assessed its efficacy in rats. The study demonstrated that the vaccine effectively reduced the behavioural effects of morphine and heroin, indicating its potential as a treatment option for opioid addiction in humans. The unique design of the hapten used in the vaccine, which exhibited greater specificity to the opioid receptor than previous hapten, likely contributed to its enhanced effectiveness in attenuating the behavioural effects of these drugs.

In recent years, there has been an increasing interest in developing new vaccine strategies to combat the escalating problem of heroin addiction. In 2011, Neil Stowe conducted a study

investigating a novel vaccine strategy to induce protective immunity against heroin. This approach utilised a rabies virus-based vaccine to trigger an immune response against the drug. The study tested the vaccine in a mouse model of heroin addiction and observed a significant reduction in heroin-seeking behaviour. A subsequent clinical trial evaluated the vaccine's efficacy in humans, revealing a substantial increase in antibody titre against heroin in the vaccinated individuals. Moreover, these individuals reported a decrease in heroin-seeking behaviour, highlighting the promise of the rabies virus-based vaccine strategy in inducing protective immunity against heroin.

Bremer et al. investigated the impact of a hydrolytically stable hapten (heroin) and a Th1 adjuvant [CpG oligonucleotides (CpG ODN)] on the performance of a heroin vaccine (Bremer et al. 2012). The findings revealed that the combination of a hydrolytically stable hapten (heroin linked to PLGA) and a Th1 adjuvant significantly enhanced the vaccine's efficacy compared to the control group (Fig. 4). Moreover, the results indicated that the combined use of the two substances elicited a more robust immune response than alone. The hydrolytically stable hapten significantly increased the antibody titre of the heroin vaccine compared to the control, suggesting its enhanced ability to bind to heroin molecules and induce a strong immune response. Combining the hapten with the Th1 adjuvant produced a synergistic effect, resulting in a higher antibody titre than expected.

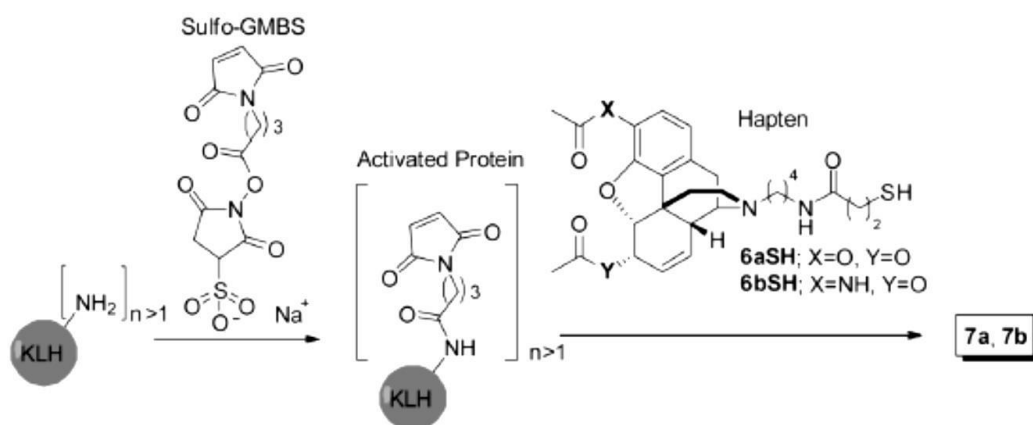


Fig. 4. Schematic representation showing the synthesis of the hydrolytically stable hapten linked to a poly (lactic-co-glycolic acid) (PLGA) nanoparticle with CpG oligonucleotides (CpG ODN) as a Th1 adjuvant (Adapted from Bremer et al. 2012).

The efficacy of a heroin vaccine was tested using intramuscular injection with an additional TLR-9 agonist. The results demonstrated that the vaccine was more effective when administered intramuscularly with a TLR-9 agonist. Further, the vaccine reduced heroin self-administration in rats by 50%. However, adding the TLR-9 agonist reduced heroin self-administration by up to 60%. These findings suggest that including TLR-9 agonists can significantly improve the vaccine's efficacy when administered via intramuscular injection. The study revealed that the vaccine effectiveness was dose-dependent, with higher doses resulting in a reduction of up to 80% in heroin self-administration (*Bremer et al. 2014*). Further, the group reported the development of a clinically viable heroin vaccine. The study on mice demonstrated that the vaccine successfully induced an immune response against heroin, showing promise in preventing heroin addiction (Fig. 5) (*Bremer et al. 2017*).

Fig. 5. A simplified schematic diagram of heroin conjugates immunological pathway and mechanism of action. Upon vaccination, the conjugate was taken up by dendritic cells (DCs), processed and displayed on the major histocompatibility complex class II (MHC II) as a haptenated peptide for activation of helper T-cells (Th-cells) via the T-cell receptor (TCR). B-cells, which have encountered the conjugate via their B-cell receptors (BCR) were stimulated by activated Th-cells. Adjuvants alum and CpG ODN enhanced the vaccine response through NLRP3 inflammasome and TLR9 signalling. Memory B-cells and plasma cells produced high affinity anti-6AM IgG antibodies bound to an administered heroin dose (metabolised to 6AM) in the periphery, thus mitigating drug effects in the brain (Adapted from Bremer et al. 2017).

The development of monoclonal antibodies to combat synthetic opioid intoxication has been underway for several years. A study demonstrated that these antibodies can reduce the effects of intoxication (*Malinowski et al. 2019*). The study revealed that antibody-drug conjugates can attach to opioid receptors and block their activity, thus preventing opioids from affecting the body. Furthermore, mouse studies showed that combining the antibody-drug conjugate and an antagonist could decrease the effects of opioids and shorten the recovery time for the animals. The study observed a reduction in the number of opioids crossing the blood-brain barrier and reaching the brain.

Heat shock proteins (HSPs) are stress-induced molecules that play a role in various metabolic pathways and processes. They can serve as carrier-adjuvants for vaccines. Hwang et al. demonstrated that HSP 70 could be used as carrier-adjuvants for an anti-drug vaccine targeting heroin. A novel vaccine candidate combining HSPs and heroin-based antigens was created and administered to mice. The results showed that the vaccine could effectively induce a robust anti-heroin antibody response. Additionally, HSP70 in the vaccine formulation resulted in a higher anti-heroin antibody response (*Hwang et al. 2019*). Further, the group investigated the efficacy of a heroin vaccine across different sexes and strains of mice. The vaccine demonstrated high antibody titre, affinity, and antinociception levels in both sexes and various mouse strains. The study found no significant differences in vaccine effectiveness between sexes or mouse strains (*Hwang et al. 2019*). Cao et al. developed a novel method for determining morphine in human urine using competitive fluorescence immunoassay (CFI). The research aimed to create a CFI for detecting morphine in human urine (*Fig. 6*). Morphine, a potent drug for severe pain, was targeted using a specific antibody and a fluorescent conjugate (*Cao et al. 2019*). The antibody was coupled to solid-phase support (membrane). The solid-phase support was incubated with a solution containing morphine and the fluorescent conjugate. After removing the solution, the solid-phase support was washed to eliminate unbound material. The amount of bound material was then measured using a fluorescent detector.

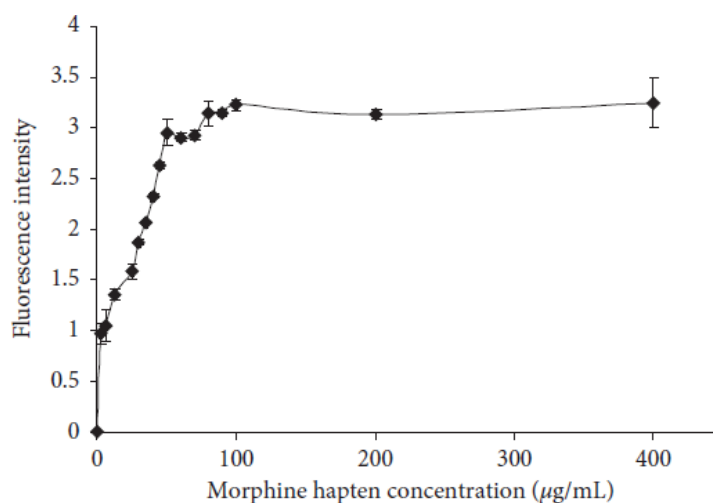


Fig. 6. Optimized curve of morphine hapten concentration displaying the fluorescence intensity (Adapted from Cao et al. 2019).

Méndez et al. evaluated the effectiveness of a morphine/heroin vaccine in reducing opioid and non-opioid drug-induced antinociception in mice (Méndez et al. 2021). The results showed that the vaccine effectively reduced the antinociceptive effects of morphine, heroin, acetaminophen, and ibuprofen. Further, the vaccine reduced the rewarding effects of heroin and morphine. These findings suggested that the vaccine holds promise as a method to reduce opioid-induced antinociception and the seeking of rewarding substances in individuals with substance abuse issues.

2.5 The Acr1 protein has been studied as a potential drug target for treating tuberculosis (TB). Research has shown that Acr1 regulates bacterial cell wall biosynthesis in *Mycobacterium tuberculosis* (*Mtb*), the etiological agent of TB. By inhibiting Acr1 activity, researchers have reduced the viability of *Mtb* and decreased the number of the bacterium in the lungs. Acr1 regulates iron transport and metabolism in *Mtb* and controls its gene expression. The Acr1 plays a crucial role in the survival and pathogenesis of the bacterium. It is a major component of the cell wall of *Mtb*. It contributes to the structural integrity and stability of the cell wall, which is essential for the bacterium's survival under various environmental conditions (Hernandez-Pando et al. 2000). The Acr1 protein is upregulated under stress conditions, such as nutrient limitation, oxidative stress, and exposure to antimicrobial agents. Its expression is believed to help *Mtb* adapt to hostile environments (Manganelli et al. 2002). The Acr1 has been

implicated in immune evasion strategies. It can modulate the host immune response by interfering with macrophage functions, such as phagosome-lysosome fusion, antigen presentation, and cytokine production. This allows *Mtb* to survive and persist within the host (Singh *et al.* 2013). The Acr1 protein has been characterised as a virulence factor of *Mtb*. It contributes to the bacterium's pathogenicity by promoting intracellular survival and replication, inhibiting apoptosis of infected cells, and modulating host immune responses (Dhiman *et al.* 2016). The Acr1 is involved in the interaction between *Mtb* and the host. It can interact with host proteins and cell surface receptors, influencing the outcome of infection and its persistence (Chan *et al.* 1996). These studies highlight the multifaceted importance of the Acr1 protein in the survival and pathogenesis of *Mtb*. It is involved in cell wall stability, stress response, immune evasion, virulence, and host-pathogen interactions. Acr1 provides valuable insights into the mechanisms that *Mtb* employs to persist within the host and contribute to tuberculosis pathogenesis.

The Acr1 protein of *Mtb* is considered an important vaccine candidate for TB. It has demonstrated significant immunogenicity, eliciting an immune response in individuals infected with *Mtb*. Several studies have shown that this antigen can induce both cellular and humoral immune responses, making it a promising candidate for vaccine development (Mustafa *et al.* 2000). The Acr1 protein is highly conserved among different strains of *Mtb*, suggesting that it plays a crucial role in the pathogenesis of TB. Its conservation implies a vaccine targeting this protein could provide broad protection against various *Mtb* strains (Kumar *et al.* 2013). Studies have indicated that vaccination with the Acr1 protein can confer protective immunity against *Mtb* infection. Animal models, such as mice and Guinea pigs, have shown reduced bacterial burden and enhanced control of *Mtb* growth upon vaccination with the Acr1 protein (da Silva, *et al.* 2009). It has been shown that liposomes α -crystalline 1 (Acr1L) enhanced long-lasting protective immunity against *Mtb* in animals previously primed with the BCG vaccine. An increase in the multi-functional CD4 T cells and CD8 T cells expressing high levels of IFN- γ and TNF- α in BCG-primed and Acr1L-boosted animals (BCG-Acr1L) compared to those receiving BCG alone. Additionally, both central and effector memory populations of CD4 and CD8 T cells were significantly expanded. Importantly, BCG-Acr1L demonstrated superior protection to BCG alone, as evidenced by a reduction in bacterial burden and histopathological changes in the lungs (Fig. 7). These findings suggest that BCG-Acr1L could serve as a promising strategy to enhance the effectiveness of BCG vaccination (Siddiqui *et al.* 2015).

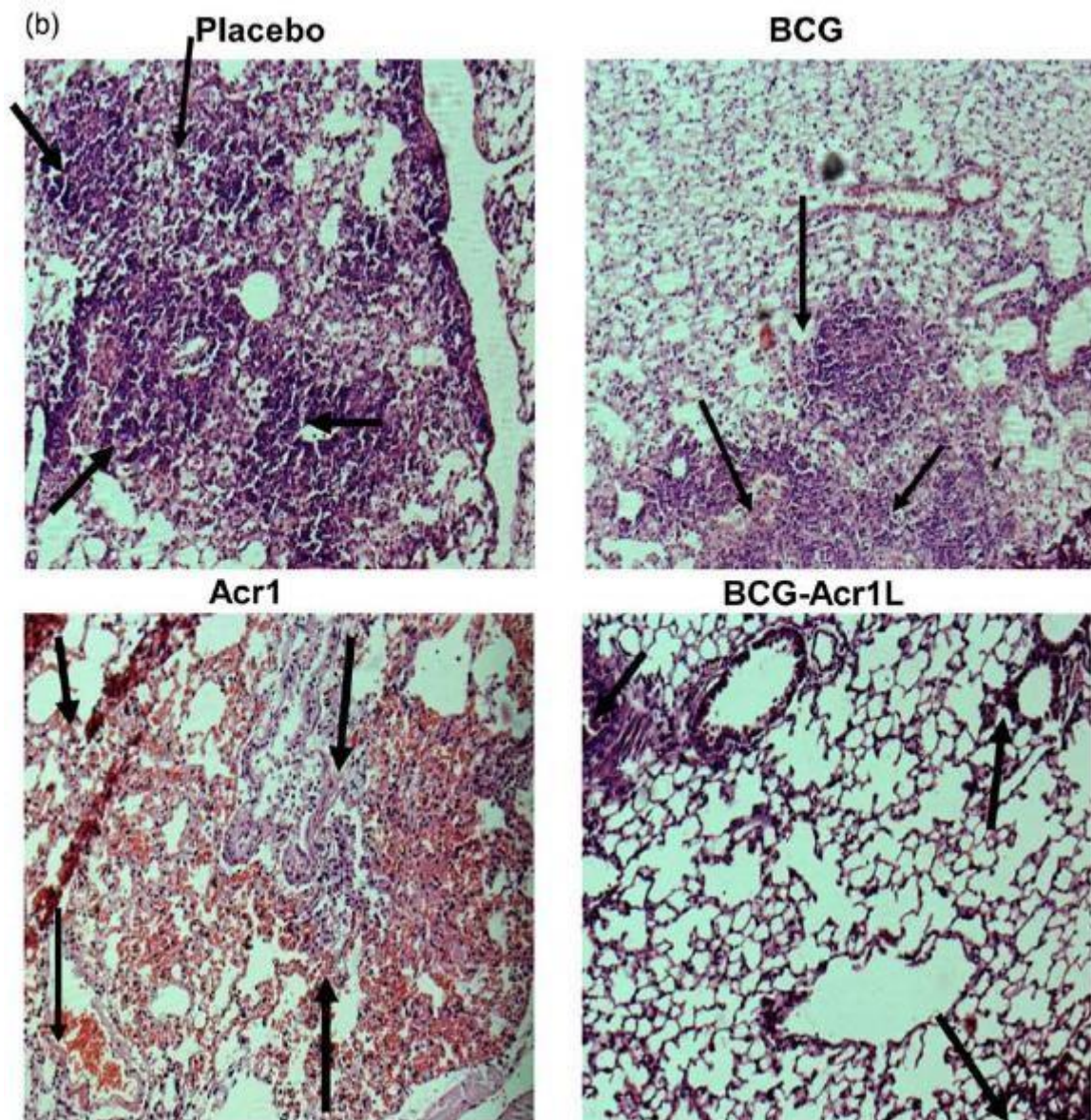


Fig. 7. BCG-liposomes alpha-crystalline protein 1 (Acr1L) provides significantly better protection than BCG. Lungs were fixed in formalin, and sections were stained with haematoxylin and eosin. Photomicrographs (320) display the lung sections. Arrows indicate small or large developing follicular granulomas (Adapted from Siddiqui et al. 2015).

The Acr1 protein contains T-cell epitopes that can trigger specific immune responses. These epitopes are recognised by T cells and play a vital role in the clearance of *Mtb* infection. Identification and characterisation of these epitopes have provided insights into effective vaccines against TB design. The Acr1 protein has been investigated for its adjuvant properties,

capable of enhancing the immune response when combined with other antigens. This suggests that the protein can potentially be used as an adjuvant to improve the efficacy of TB vaccines (Mustafa *et al.* 2000). Gowthaman *et al.* demonstrated that an immunodominant epitope of sequence 91-110 derived from Acr1 of *Mtb* elicited long-lasting Th1 and Th17 immunity. Lipidation of sequence 91-110 epitope of Acr1 (L91) enhanced its immunomodulatory properties and stability, facilitating more efficient targeted delivery to antigen-presenting cells; and in particular, to dendritic cells (DCs). L91 induced a more robust Th1 and Th17 response compared to non-lipidated 91-110 (F91), resulting in increased cytokine production such as IFN- γ , IL-2, IL-17, and TNF- α (Gowthaman *et al.* 2011). Moreover, L91 elicited long-lasting Th1 and Th17 immunity and protected mice and Guinea pigs on exposure to *Mtb* (Fig. 8).

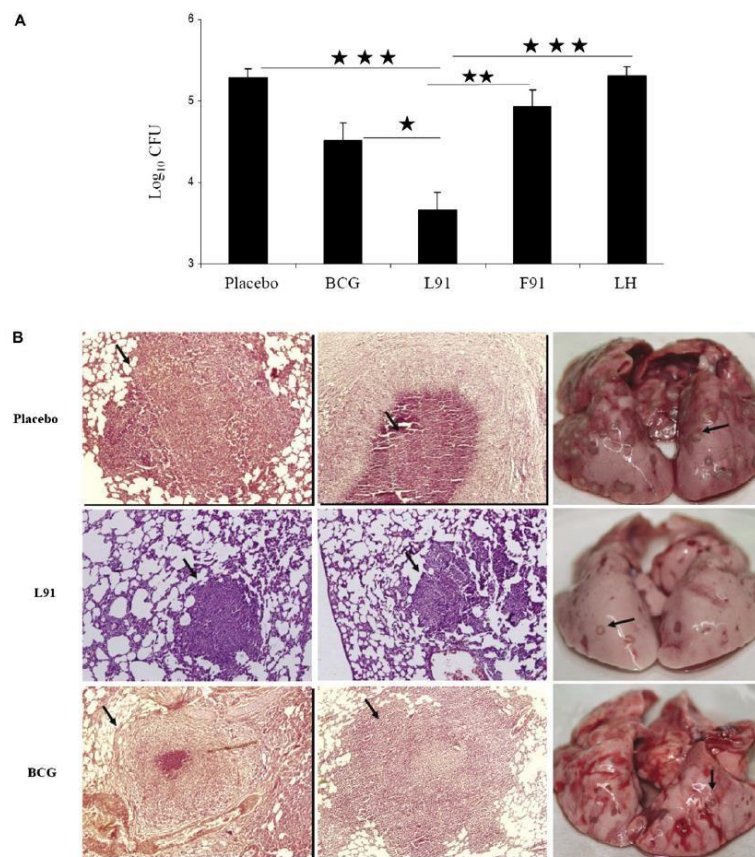


Fig. 8. Immunization with L91 protects Guinea pigs against Mycobacterium tuberculosis. Duncan-Hartley Guinea pigs were immunised with L91 or controls (F91, LH, BCG, and placebo). After 75 days, animals were aerosol challenged with M. tuberculosis. Thirty days after infection, animals were killed. A, Mycobacterial load in the lungs was quantified by inoculating on plates and counting colony-forming units (CFU). Data are mean \pm standard

deviations (log₁₀ value). B, Representative histopathology sections of Guinea pig lungs stained with hematoxylin and eosin. Gross pathology of Guinea pigs' lungs is also shown (col. 3). Arrows indicate granulomas. (Figure adapted from Gowthaman et al. 2011).

Thus, suggesting its potential as a novel therapeutic vaccine against TB. L91 holds a promise as a candidate vaccine against *Mtb* (Rai et al. 2016). In 2017, Amir et al. demonstrated that Acr1 exposure to DCs is crucial in enhancing their functionality maturation. Further, the DCs exhibit upregulation in the expression of MHC and co-stimulatory molecules. Furthermore, the DCs produced predominantly cytokines that help activate and differentiate Th1 cells and Th17 cells viz TNF- α , IFN- γ , IL-12 (Th1 response) and IL-6 and TGF- β , respectively. Consequently, enhancing the immune response is favourable to eliminating *Mtb*.

Rai et al. conducted studies highlighting the significant role of the Acr1 protein in conferring protection against tuberculosis (TB). Acr1, expressed by *Mtb*, is critical in initiating and promoting adaptive immune responses against the pathogen. A novel vaccine formulation was developed to elicit a protective immune response, consisting of a lipidated bi-epitope vaccine to stimulate both CD4 T cell and CD8 T cell immunity against *Mtb*. This vaccine targets two distinct epitopes derived from the Acr1 protein, thereby inducing CD4 T cell and CD8 T cell responses. The vaccine formulation incorporates two specific peptides representing immunodominant epitopes of Acr1, each linked to a lipid moiety that facilitates uptake by antigen-presenting cells (APCs). Following uptake by APCs, the peptides are presented on the surface of APCs in association with MHC class I and II molecules. This presentation enables recognition by CD4 T cells and CD8 T cells, activating effector functions crucial for an effective immune response against *Mtb*, including producing pro-inflammatory cytokines and cytotoxic molecules. Preclinical studies have demonstrated robust CD4 and CD8 T cell responses triggered by the vaccine against *Mtb*. Moreover, the vaccine has shown efficacy in protecting the *Mtb* challenge in animal models, indicating its potential as a promising approach for preventing and treating TB (Rai et al. 2017, 2018). Additionally, Rai et al. demonstrated that L91 effectively enhances the potency of the BCG vaccine, leading to enduring protection against *Mtb*. This innovative vaccination strategy involving BCG priming followed by L91 boosting holds promise as a future prophylactic measure for TB control.

Mubin et al. demonstrated that the Acr1 protein is present in the *Mtb* cell envelope. Acr1 is identified as an *Mtb*-specific outer membrane protein highly expressed during latency but not

in replicating bacterium (*Mubin et al. 2018*). Acr1 modulates the host immune response by interfering with macrophage functions such as phagocytosis, cytokine production, and antigen presentation. By interacting with Toll-like receptor 2 (TLR-2), Acr1 inhibited the activation of macrophages, suppressing the production of pro-inflammatory cytokines (TNF- α , IL-12, and IFN- γ) and promoting the production of anti-inflammatory cytokines (IL-10). This inhibits the activation of other effector cells and suppresses the host's immune response. Acr1 upregulated the expression of MHC-II molecules on macrophages, facilitating the presentation of *Mtb* antigens to T cells. This resulted in T cell activation, leading to increased production of TNF- α , IL-12, and IFN- γ , contributing to the killing of intracellular *Mtb*.

The above-mentioned findings feature Acr1 as an important vaccine candidate against *Mtb*. It shows promising immunogenicity, conservation, protective efficacy, presence of T-cell epitopes, and adjuvant potential.

2.6 TLR agonists have emerged as a novel adjuvant in immunological research. TLRs are a class of pattern recognition receptors (PRRs) that significantly mediate the innate immune response against foreign pathogens. They are transmembrane receptors found on the surface of various APCs like dendritic cells (DCs) and macrophages. TLRs recognise conserved protein molecules of microbes called Pathogen Associated Molecular Patterns (PAMPs), activating the innate immune response and clearance of pathogenic cells (*Mogensen et al. 2006*). Chemically synthesised ligands for TLRs have shown effectiveness and safety, with some advancing to clinical phases. Pam3Cys is a ligand of TLR-2 and is an adjuvant and immunomodulator. Its ability to enhance immune responses, activate TLRs, modulate the immune system, and improve vaccine efficacy is valuable in developing effective vaccines and immunotherapies. Pam3Cys is a synthetic lipopeptide derived from bacterial lipoproteins. It acts as a potent adjuvant, enhancing the immune response to an antigen. When combined with antigens in vaccines, Pam3Cys can stimulate the innate immune system, activating antigen-presenting cells (such as dendritic cells) and enhancing the presentation of antigens to the adaptive immune system.

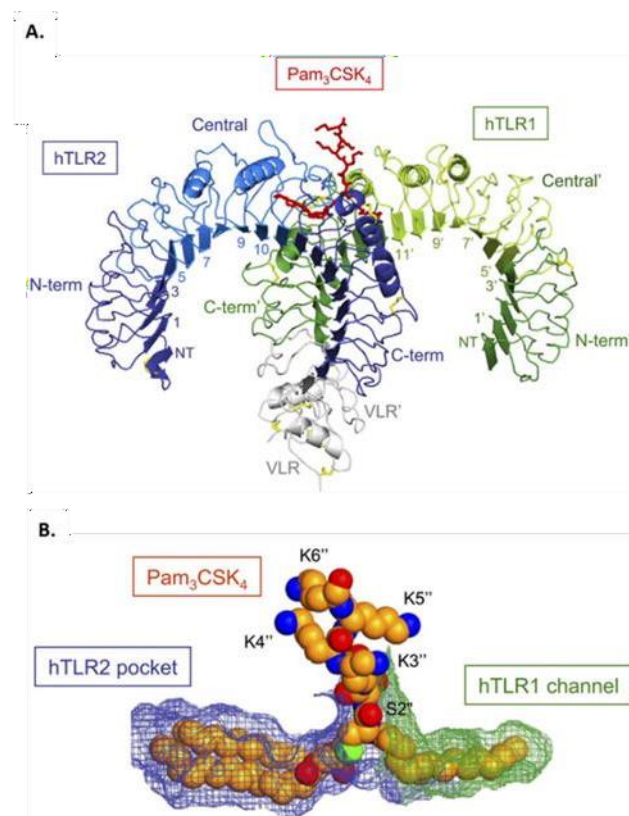


Fig. 9. Binding of Pam3Cys with TLR1-TLR2 complex. The Pam3Cys (Pam3CSK₄) lipopeptide-binding site of the human TLR1-TLR2 complex. (A) Pam3Cys (red) binding over the TLR1 (green)-TLR2 (blue) complex. (B) Two chains of Pam3Cys bind in the pocket of TLR2 (blue), and the third chain binds in the groove of TLR-1 (green) (Figure adapted from Jin et al. 2007).

Pam3Cys activates Toll-like receptor 2 (TLR-2), expressed on various immune cells, including dendritic cells, macrophages, and B cells. TLR-2 recognises and binds to the Pam3Cys, triggering signalling pathways that produce pro-inflammatory cytokines and activate immune cells (*Fig. 9*). This activation enhances the immune response to the antigen (*Kawai and Akira 2010*). Pam3Cys can modulate the immune response by influencing the balance between different subsets of immune cells and their functions. It promotes the development of Th1-type immune responses, characterised by producing pro-inflammatory cytokines such as IFN- γ . This can be beneficial for combating intracellular pathogens and promoting cell-mediated immune responses (*Liu et al. 2014*). Including Pam3Cys in vaccines has improved their efficacy by enhancing the immune response against specific antigens. It can promote the

production of antigen-specific antibodies, enhance antigen-specific T-cell responses, and contribute to the development of immunological memory (*Kasturi et al. 2011*). The immunomodulatory properties of Pam3Cys have been explored for potential therapeutic applications. It has been investigated as an adjuvant in cancer immunotherapy, infectious disease vaccines, and autoimmune disease treatment (*Schwarz et al. 2017*).

TLR-2 recognises components of Gram-positive bacteria such as lipopeptides, peptidoglycan, and lipoteichoic acids. It can form heterodimers like TLR-2/TLR-1 or TLR-2/TLR-6, which recognise synthetic ligands like Pam3Cys or Pam2Cys, respectively. Pam3Cys is a triacylated lipopeptide, while Pam2Cys is a diacylated lipopeptide. The dimerised TLR-2/TLR-1 hetero-complex adopts an 'm'-shaped structure due to the conversion of the C-terminal domains. The three lipid chains of Pam3Cys interact with specific regions in TLR-2 and TLR1, facilitating binding. TLR-2 signalling events involve the recruitment of the MyD88 adaptor protein, leading to the activation of IRAKs, phosphorylation of IRAK-1, activation of TRAF6, and subsequent activation of the TAB2-TAK1-IKK complex (*Medvedev et al. 2016; Qian et al. 2008*). This complex phosphorylates I κ B, resulting in its degradation and release of NF- κ B into the nucleus, leading to the expression of pro-inflammatory genes. TAK1 also activates p38 and JNK, triggering AP-1 transcription factor activation and gene expression (*Pauleau et al. 2008*). Pam3Cys has been extensively studied as a vaccine adjuvant due to its ability to induce the maturation of antigen-presenting cells (APCs) and enhance T cell priming. It has shown potency in inducing a Th1 response, essential for interventions against TB. Additionally, synthetic peptides covalently coupled with Pam3Cys have demonstrated the ability to generate antibodies comparable to those achieved with Freund's complete adjuvant.

In the context of TB, nano-delivery systems targeting DCs with TLR-2 ligand-linked-*Mtb* epitopes have been proposed to induce anti-TB immunity. A recent study by Das et al. investigated the efficacy of a nano-delivery system loaded with Pam3Cys, a TLR-2 ligand, and an immunodominant epitope of the Acr1 antigen of *Mtb* (*Das et al. 2022*). Chitosan nanoparticles loaded with immunodominant epitopes of Acr1 and coated with Pam3Cys successfully induced a protective anti-tuberculosis immune response in mice (Fig. 10). These nanoparticles significantly increased the levels of IFN- γ , IL-12, and TNF- α cytokines compared to the control group.

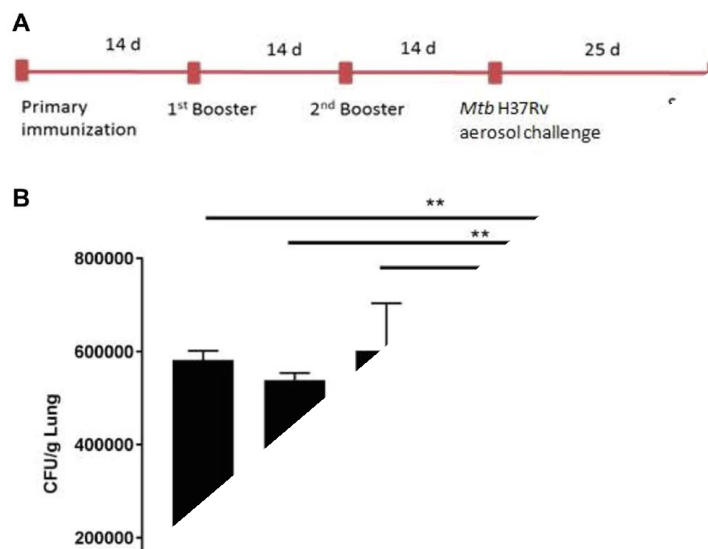


Fig. 10. E91NP3 vaccination reduces the Mtb burden in the lungs. The mice were intranasally immunised with E91NP3. Later, two booster doses were given at an interval of 14 days. Two weeks after the final immunisation, the mice were aerosol-challenged with Mtb-H37Rv. Finally, after 25 days post-infection, the animals were sacrificed to enumerate the Mtb burden in the lungs. A, schematic diagram showing the time points of immunisation, infection, and experimentation. B, the bar graph shows the colony-forming unit count/gram lung tissue for each group of mice (Adapted from Das et al. 2022).

Additionally, they enhanced the production of antigen-specific IgG2a antibodies. These findings highlight the potential of nano-delivery systems loaded with TLR-2 ligands and *Mtb* epitopes for developing anti-TB vaccines.

2.7 Nanoparticles have emerged as a promising option for developing immunological vaccines. These particles can deliver antigens in a targeted and efficient manner, thereby eliciting more potent immune responses than traditional vaccines. Nanoparticles can be formulated without additional adjuvants or components to enhance their immunogenicity, and they can carry multiple antigens within a single injection (Tsioga et al. 2016). As a result, nanoparticles have demonstrated significant potential as effective and efficient tools for developing novel immunological vaccines. The increasing popularity of nanoparticle-based vaccines is attributed

to their superior antigen delivery capabilities compared to conventional vaccines. These vaccines contain a biocompatible polymer that encapsulates an antigenic molecule, such as antigens, epitopes, DNA, etc. (Takash *et al.* 2017; Lippens *et al.* 2013). The antigen is released from the polymer matrix upon administration, triggering an immune response. Nanoparticle-based vaccines offer several advantages over conjugate-centred vaccines. Firstly, they excel more efficiently in delivering antigens to the immune system. The antigen protected within the polymer matrix is shielded from degradation, ensuring its intact delivery to the immune system and consequently leading to a more effective immune response (Baranchuk *et al.* 2005; Mayne *et al.* 2014). Additionally, nanoparticles can be customised for specific applications, enabling the delivery of multiple antigens within a single particle (Fig. 11). The simultaneous administration of various antigens results in a stronger immune response than using a single antigen alone. Moreover, nanoparticles can target specific cells or tissues within the body, facilitating more efficient immune responses (Smith *et al.* 2013)

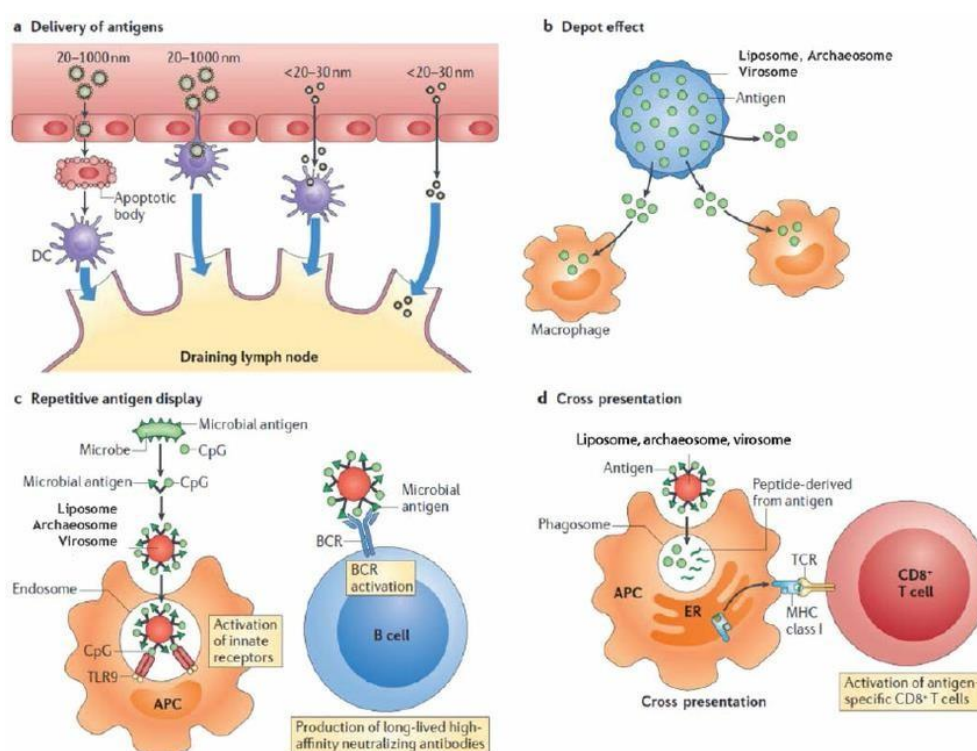


Fig. 11. A graphical representation of the mechanisms by which nanoparticles alter the induction of immune responses. The immunostimulatory activity of nanocarriers such as liposomes, archaeosomes and virosomes depends on diverse mechanisms: antigen delivery, particle size-dependent tissue penetration and access to the lymphatics (a); depot effects, promoting persistence, stability, conformational integrity and gradual release of vaccine

antigens (b); antigen display facilitating B-cell receptor (BCR) coaggregation, triggering and activation (c). Additional mechanisms include Toll-like receptor (TLR)-dependent and TLR-independent signal transduction (not shown); cross-presentation into major histocompatibility type I (MHC-I) pathways caused by nanoparticle-mediated leakage of antigens into the cytosol after phagosome uptake (d); and release of cytokines, chemokines and immunomodulatory molecules that regulate the immune response (not shown). APC, antigen-presenting cell; CpG, cytosine–phosphorothioate–guanine oligodeoxynucleotide; DC, dendritic cell; ER, endoplasmic reticulum; TCR, T-cell receptor. Reproduced and modified with permission (adapted from Smith et al. 2013).

This targeting capability is achieved by the nanoparticle's ability to bind to specific receptors on the target cells, allowing direct delivery of the antigen to the desired cell and ultimately leading to a more robust immune response (Das et al. 2022). Finally, nanoparticle-based vaccines are generally easier to produce compared to conjugate-based vaccines. Their production involves simple methods, such as self-assembly, eliminating the need for complex manufacturing processes (Smith-Reilly 2017).

Nanoparticle-based vaccines offer several advantages over traditional vaccines because they deliver antigens to the immune system with improved efficiency and specificity. These vaccines can enhance antigen potency and specificity, producing more robust and targeted immune responses (Sheikhbahaee et al. 2016). Nanoparticles facilitate antigen uptake and presentation by the immune system, thereby enhancing immune responses (Zhang et al. 2018, Sharma et al. 2018). Additionally, nanoparticles can be loaded with other immunomodulatory molecules, such as adjuvants or ligands, to improve the immune response further. Compared to traditional vaccines, nanoparticle-based vaccines can induce a more potent and specific immune response. In comparison to conjugate-based vaccines, nanoparticle-based vaccines offer several advantages. Notably, nanoparticles provide a larger surface area for antigen presentation, facilitating increased antigen uptake and enhanced immune recognition. Furthermore, nanoparticles can be tailored to target specific cell types, such as antigen-presenting cells, leading to a more targeted immune response. Recent applications of nanoparticle-based vaccines have demonstrated their effectiveness in inducing protective immunity against various vaccines in animal models.

2.8 *Generation of anti-hapten antibodies through chronic use of morphine.* Morphine is an opioid analgesic which is commonly used to manage pain. However, long-term use of morphine can lead to the development of tolerance, reducing its effectiveness. Kim et al. in 2010 discovered the presence of anti-morphine antibodies that potentially contribute to the development of morphine tolerance. Morphine is a large and complex molecule that needs to be broken down into smaller metabolites to exert its pain-relieving effect. However, repeated administration of morphine results in its binding with body proteins viz albumin that, triggers the production of anti-morphine antibodies. These antibodies bind to morphine molecules, preventing their interaction with opioid receptors and reducing pain-relieving effects (*Lamichhane et al. 2021*). Animal studies have shown a correlation between the production of anti-morphine antibodies and the development of morphine tolerance. Rats repeatedly exposed to morphine exhibited increased levels of anti-morphine antibodies, accompanied by a decrease in the pain-relieving effect of morphine, indicating the development of tolerance. Conversely, when rats were given an antibody-blocking drug, the production of anti-morphine antibodies decreased, and the pain-relieving effect of morphine was restored. These findings suggest that anti-morphine antibodies play a crucial role in developing morphine tolerance in rats (*Kim et al. 2010*).

Sajid et al. showed the prevalence of anti-xenobiotic antibodies (AX-Abs) in occupationally exposed individuals to xenobiotics with high cancer risk. The study found that individuals with a low prevalence of AX-Abs had a significantly higher risk of developing cancer than those with a high prevalence of AX-Abs. Specifically, individuals with a low prevalence of AX-Abs were 3.6 times more likely to develop cancer than those with a higher prevalence of AX-Abs. The study revealed that individuals without AX-Abs were more likely to develop cancer than those with AX-Abs. These findings suggest that constant exposure to xenobiotics can result in the binding of these haptenic molecules to body protein. Therefore, making them immunogenic elicits anti-xenobiotics antibodies (*Sajid et al. 2019; Kirchner et al. 2006*).

In a study conducted by Biagini et al. (1990), researchers examined whether workers exposed to opiates at a narcotics manufacturing facility and heroin abusers had antibodies to morphine in their blood. The objective was to determine if these antibodies were present in both the workers and the heroin abusers and if they could indicate opiate exposure (*Biagini et al. 1990*). Serum samples were collected from the workers and the heroin abusers, and a

radioimmunoassay was used to measure the presence of antibodies to morphine (*Cowan et al. 2003*). The results indicated that the workers had significantly higher antibodies to morphine in their serum compared to the heroin abusers. This suggests that the workers had been exposed to more opiates than the heroin abusers. These findings are important as they indicate that workers at a narcotics manufacturing facility are at risk of substantial opiate exposure, potentially leading to an increased risk of developing opioid addiction or other serious health problems. The study's findings also contribute to understanding the prevalence of opioid addiction among individuals exposed to opiates in the workplace. The results support that workers exposed to opiates at a narcotics manufacturing facility may be more likely to develop opioid addiction than others.

Overall, the literature suggests that a nanoparticle-based vaccine may be quite effective in generating long-term anti-morphine antibodies, memory B cells and T cells responses, neutralising morphine in serum, and inhibiting its ability to cross the blood-brain barrier. The vaccine targeted μ -opioid receptor sites and the Acr1 protein using haptens and employing Pam3Cys as a self-adjuvant. Such a vaccine will successfully elicit a long-term memory response, neutralise morphine in serum, and prevent its passage across the blood-brain barrier. Additionally, the vaccine will not induce tolerance to long-term opioid use. It will activate the immune system, such as macrophages and T cells, enhancing the body's ability to combat infections. Hence, the nanoparticle-based vaccine holds great potential for protecting against opioid addiction and TB.

Acr1 binds to TLR-2, providing sufficient adjuvanting properties to MAPNV for generating high-affinity anti-morphine Abs. Anti-morphine Abs will deactivate the effect of morphine, and therefore, the immunosuppressive action of morphine will also be neutralised. MAPNV elicits the generation of the Th1 cell, which is important to defend against Mtb. Hence, MAPNV will offer sufficient protection against Mtb. Consequently, a balance between protection and pathology in the immune response to TB will not be perturbed.

Clinical samples

Blood samples of 22 adult male patients (age 21-40 years) with opioid use disorder (OUD) were collected from the Drug De-addiction and Treatment Centre, Postgraduate Institute of Medical Education and Research, Chandigarh, India, and 22 male healthy controls (age 21-40) from the Indian Institute of Technology, Ropar, India. The study population includes patients with opioid use disorder and a history of chronic heavy morphine use for at least one year. Written informed consent was obtained from all the participants. The study was approved by the Institutional Ethics Committees of the Postgraduate Institute of Medical Education and Research, Indian Institute of Technology (IIT) Ropar. All the experiments were performed per the ethical guidelines of the Biomedical Research on Human Subjects, Central Ethics Committee on Human Research, Indian Council of Medical Research, India.

Animals

Female BALB/c, C57BL/6 and TLR-2^{-/-} mice (aged 6-8 weeks, 22 ± 2 g) were procured from the Animal House Facilities of the National Institute of Pharmaceutical Education and Research (NIPER), Mohali, India, Aligarh Muslim University (AMU), Aligarh, India and Indian Institutes of Science Education and Research (IISER), Mohali, India. The experiments were approved by the Institutional Animal Ethics Committees (IAEC) of the NIPER (IAEC/19/05), AMU (1176/01.4.2022) and IISER (176/20.03.2019). The experiments were performed according to the guidelines issued by the Committee for Control and Supervision of Experiments on Animals (CPCSEA), Ministry of Environment and Forest, Government of India.

Chemicals and reagents

Morphine was purchased from the Opium and Alkaloid Factories (Government of India), New Delhi, India (F.No.9/IMP/Sales/1/2019 - Part-IV/2358) with due clearance and approval from the Central Bureau of Narcotics, Gwalior, India, (0003023), and Food and Drug Administration, Government of Punjab, Kharar, India (Drugs [10] PB. 2019/328).

All the reagents and solvents were purchased from Sigma-Aldrich (St. Louis, MO) or otherwise mentioned. Pam3CSK (tlrl-pms) was purchased from InvivoGen (Paris, France), MES buffer and trehalose from Himedia (Bangalore, India), and sucrose, D-mannitol from SRL (Mumbai, India). N-Hydroxysuccinimide NHS, N-(3-Dimethylaminopropyl), N'-ethylcarbodiimide

(EDC), PEG-3350, propidium iodide, paraformaldehyde, dynasore hydrate, chloroquine diphosphate salt, chlorpromazine hydrochloride, genistein, nystatin, cytochalasin D, rottlerin, 5(6)-carboxyfluorescein diacetate N-succinimidyl ester (CFSE), incomplete Freund's adjuvant from Sigma-Aldrich (Burlington, MO). Fluorochrome conjugated antibodies for flow cytometry CD16/CD32, CD19-PECy7 were procured from BD Biosciences (San Jose, CA), CD4-PE, MHC-11-PerCpCy5.5 from Biolegend (San Diego, CA), CD44 PerCPCyS.5, CD86-PE, CD40 APC from eBiosciences (Waltham, MA). All Abs for ELISA were obtained from BD Pharmingen™ (San Diego, CA). Abs used in Western Blotting were purchased from Invitrogen, Life Technologies (Eugene, OR). The primers for RT-qPCR were bought from Eurofins (Bangalore, India). All tissue culture grade plastic wares were obtained from BD Biosciences (San Jose, CA), Thermo Fisher Scientific (Waltham, MA), Corning™ (Corning, NY), and Sigma Aldrich (St. Louis, MO). RPMI-1640, DMEM and fetal bovine serum (FBS) were procured from GIBCO (Grand Island, NY). Vacutainer tubes were procured from BD Diagnostics (Franklin Lakes, NJ).

3.1 Purification of Acr1 protein. The recombinant Acr1 protein was purified per the protocol mentioned elsewhere (Siddiqui et al., 2011). Briefly, The Acr1-expressing recombinant BL21 cells were grown overnight in LB broth (20 ml) supplemented with ampicillin (100 µg/ml). Later, fresh LB broth (99 ml) was added to the culture (1 ml) and incubated until the OD reached 0.4- 0.6. Later, 1 mM IPTG (100 µl) was added into the cultures and incubated at 37 °C for 4 h. The culture was centrifuged, the pellet was collected and washed with equilibration buffer (50 mM Tris, 250 mM NaCl, 20 mM imidazole) and resuspended in 25 ml of equilibration buffer. It was then sonicated in ice for 15 min with a pulse interval of 10 sec. Ni-NTA beads were packed in a non-absorbent column and washed 10 times the bed volume with deionised water. The beads were equilibrated with an equilibration buffer 10 to 20 times the bed volume. The lysate SN was applied to the column with a minimal flow rate. The column was washed thoroughly with wash buffer (50 mM tris, 250 mM NaCl, 20 mM imidazole) with a minimum flow rate. The protein was eluted in elution buffer (50 mM Tris, 250 mM NaCl, 20 mM imidazole). Dialysis was done overnight against PBS (1 mM, pH 7.4) to remove excess salt and imidazole.

3.2 Synthesis of Acr1 nanoparticles (AN). Acr1 nanoparticles were synthesised, as mentioned elsewhere by Alexandro et al. (2019). Briefly, Acr1 (0.1 g) was mixed with deionised water (Milli-Q type I) (10 ml) and stirred for 30 min at 400 x g at 25±2 °C. A desolvating solution was prepared by mixing acetone (1 ml) with ethanol (1 ml). After 30 min, the desolvating solution was added to the Acr1 solution at a 1 ml/min rate. Immediately glutaraldehyde solution (25%, 0.2 ml) was added. The solution was stirred at 400 x g at 25±2 °C for 1 h, transferred into a 15 ml tube, and centrifuged at 650 x g for 30 min at 4 °C. The SN was collected and stored at 4 °C, while the pellet was dissolved in MES buffer (1:1000 dilution) and stored at 4 °C.

3.3 Synthesis of morphine-Acr1-Pam3Cys nanoparticles vaccine (MAPNV). The MAPNV was synthesised per the protocol mentioned by Alexandro et al. (2019). Momentarily, Acr1 (0.1 g) was dissolved in deionised water (10 ml). The protein solution was stirred for 30 min at 400 x g at 25±2 °C. Morphine (1 mg) and Pam3Cys (1 mg) were dissolved in ethanol (1 ml) and added to the Acr1 solution, and mixed for 15 min. Simultaneously, acetone (1 ml) was mixed with ethanol (1 ml) to create a 1:1 desolating solution. After 30 min, the desolating solution was added to the Acr1 solution at a 1 ml/min rate. Immediately, glutaraldehyde solution (25%, 0.2 ml) was added. The mixture was stirred at 400 x g at 25±2 °C for 1 h. The solution was transferred to a 15 ml falcon tube and centrifuged at 650 x g for 30 min at 4 °C. The SN was collected and stored at 4 °C. The pellet was dissolved in MES buffer (1:1000 dilution) and stored at 4 °C.

3.4 Testing particulation efficiency. The particulation efficiency of Acr1 nanoparticles (AN) was evaluated per the protocol described elsewhere (Liu, 2018). Briefly, the AN were separated by centrifugation (650 x g for 30 min at 4 °C), and the concentration of Acr1 in the SN was estimated by the Bradford method. Briefly, the SN (20 µl) was added to the Bradford reagent (200 µl), and the samples were incubated at 25±2 °C for 10 min. Later, the plate was read at 595 nm in a spectrophotometer Clariostar microplate reader (BMG Labtek, Ortenberg, Germany). The absorbance of each sample was recorded, and the protein concentration was calculated using the Acr1 standard curve. The nanoparticulation efficiency was calculated as follows:

$$\text{Nanoparticulation efficiency (\%)} = \frac{\text{Acr1 concentration before particulation} - \text{Acr1 concentration in the supernatant}}{\text{Acr1 concentration before particulation}} \times 100$$

3.5 Particle size distribution and zeta potential measurement. The size and charge of the synthesised AN and MAPNV were analysed by Nano Sight NS300 (Malvern Analytica Ltd Malvern, UK) per the standard protocol. In short, the nanoparticle pellets were suspended in distilled water (1 ml) and vortexed for 1 min for homogenous distribution. The Nano sight NS300 was set up and calibrated according to the manufacturer's instructions. A 10 µl aliquot of the sample was loaded onto the flow cell. The flow cell was aligned with the laser beam, and the sample was visualised on the computer screen. The particles' size distribution and zeta potential were measured by the analysis software Nano Sight Tracker (Malvern Analytica Ltd, Malvern, UK). Further, the samples were diluted in deionised water (1 ml) and homogenised for 30 min. The samples were loaded in the cuvettes, and the charge on the particles was measured using the Malvern Zetasizer Nano ZS (Malvern Analytica Ltd, Malvern, UK). A blank sample of deionised water was used as a control.

3.6 Particle morphology demonstrated by scanning electron microscopy (SEM). The Acr1 nanoparticles (AN), morphine-Acr1 nanoparticles (MAN) and morphine-Acr1-Pam3Cys nanoparticles (MAPNV) were prepared, and the pellets were collected. The pellets were freeze-dried overnight at -80 °C. The samples were loaded onto copper grids and placed onto the electron microscope stage. The microscope was adjusted to a magnification (20000-23000). A series of images were taken of the samples at various magnifications and orientations and recorded digitally as per the Zeol standard operating procedures. The images were analysed by the software Zeol Image (Zeol pvt ltd, Tokyo, Japan) to measure particle size, shape and surface texture. The AN and MAN were taken as controls.

3.7 Investigation of redispersion ability of MAPNV. The redispersion study was carried out as described by Das et al. (2022). In short, the MAPNV was prepared, and the size of the particles was analysed by Dynamic Light Scattering (DLS). The nanoparticles were freeze-dried. Later,

the nanoparticles were dissolved in deionised water (1 ml). The size of MAPNV was measured using DLS. The redispersion percentage was calculated as follows: -

$$\text{Redispersion (\%)} = \frac{\text{Size before freeze-drying}}{\text{Size after freeze-drying}} \times 100$$

3.8 Analysis of MAPNV using Fourier Transform Infrared (FTIR) spectroscopy. The surface of synthesised nanoparticles was analysed by the Fourier Transform Infrared spectroscopy (Bruker TENSOR 2, Billerica, MA) as per the protocol illustrated by Ahmed et al. (2018). Briefly, Freeze-dried AN and MAPNV were prepared and placed on a sample holder. The FTIR spectrometer was set to the appropriate parameters for the analysis. The sample was scanned spectrum from 4000 cm⁻¹ to 600 cm⁻¹. The absorbance of MAPNV was recorded and compared with AN. The spectra were analysed for differences in the positions of the peaks and intensity between the two samples by Image J software (University of Wisconsin, Madison, WI).

3.9 Surface scanning analysis of MAPNV. The surface of the AN and MAPNV was examined by a Clariostar microplate reader (BMG Labtek, Ortenberg, Germany) using the method described by Sun, Y. et al. (2020). In short, the nanoparticles were suspended in deionised water (1 ml) and were pipetted into the triplicate wells (100 µl/wells) of a 96-well plate. Then, the UV-visible spectrophotometer was set for the number of wavelength scan points 278, excitation wavelength 321.0 – 598.0 nm, step width 1.0 and excitation bandwidth 1.0. The plate was placed in the sample holder, and the surface scan was performed at 200-550 nm wavelengths. The data was analysed using the Labtek data analyser (BMG Labtek, Ortenberg, Germany).

3.10 Evaluating the efficiency of morphine conjugation on the surface of MAPNV. The standard curve was prepared with varying concentrations of morphine (0.1-1.0 mg/ml) in PBS (1 M, pH 7.4) as notified by White et al. (2006). The solutions were mixed thoroughly and allowed to equilibrate for 10 min. The Clariostar microplate reader was set up with a wavelength of 300 nm. The blank solution of PBS (1 M, pH 7.4) was measured in the spectrophotometer, and its absorbance was recorded. The absorbance value of each dilution of morphine standard

solutions was measured. A standard curve was plotted with the concentrations of morphine on the x-axis and absorbance on the y-axis.

The freshly prepared MAPNV was washed thrice with PBS (1 M, pH 7.4). The nanoparticles were suspended in 1 ml PBS (1 M, pH 7.4). The MAPNV was disrupted by ultra-sonication at an amplitude of 60%, frequency of 60 kHz, and time of 30 min. The samples were centrifuged at 650 x g for 30 min at 4 °C, and SNs were pipetted into triplicate wells of a 96-well plate. The reading was taken to detect morphine using a Clariostar microplate reader at a wavelength of 300 nm. The concentration of morphine was calculated by Beer-Lambert law through a curve plotted using different concentrations (0.1-1.0 mg/ml) of standard morphine.

3.11 Evaluating the efficiency of Pam3Cy (P3C) conjugation on the surface of MAPNV. The standard solutions of Pam3Cys (0.1-1.0 mg/ml) solubilised in water: ethanol (1:1 ratio) were prepared, as mentioned by Das et al. (2022). The Clariostar microplate reader was set at a wavelength of 280 nm, and the absorbance of the blank solution (water: ethanol, 1:1 ratio) was noted. The absorbance was recorded, and the standard curve was plotted using different concentrations of Pam3Cys on the x-axis and absorbance on the y-axis.

MAPNV was prepared and washed 3x in PBS. The nanoparticles were suspended in a solution of water/ethanol (1 ml) and disrupted by ultra-sonication (amplitude 60%, frequency 60 kHz, time 30 min). The solution was centrifuged (650 x g for 30 min at 4 °C), and SNs were pipetted into triplicate wells of a 96-well plate. The presence of Pam3Cys in MAPNV was detected at 280 nm by the Clariostar microplate reader, and the concentration was calculated by Beer-Lambert law using a standard curve of Pam3Cys.

3.12 Colourimetric analysis for detecting conjugation of Pam3Cys on the MAPNV. The coating of Pam3Cys on the surface was evaluated by the protocol mentioned by K. C. et al. (2006). In brief, the 96-well plate was coated with cellulose nitrate (0.1 µg/100 µl) by incubating at 37 °C for 1 h. The plate's negatively charged cellulose nitrate surface was incubated with log₂ dilutions of positively charged Acr1-morphine/biotin-P3C at 4 °C overnight. Avidin-HRP was added and incubated at 37 °C. After each incubation, the wells were washed 3x with phosphate buffer (0.1 M, pH 8). The colour was developed using OPD for 20 min, and the reaction was

stopped with 7% H₂SO₄. The absorbance was measured at OD₄₉₂ nm by the Clariostar microplate reader (BMG Labtek, Ortenberg, Germany).

3.13 Determination of morphine immobilisation on the surface of MAPNV by flow cytometer.

The coating of morphine on the surface of MAPNV was determined by Tzeng. et al. (2006). In short, MAPNV was incubated with mouse anti-morphine Abs (1 µg/ml) for 1 h at 25±2 °C. The sample was centrifuged, the SN was discarded, and the pellet was washed 3x with PBST (1 MPBS + Tween 20-0.025%). The pellet was re-suspended in the Alexa Fluro (G) conjugated anti-mouse secondary Abs (1 µg/ml) solution and incubated for 1 h. The nanoparticles were washed 2x and acquired using BD Accuri C6 plus flow cytometer, and analysis was performed using Flowjo software (Franklin Lakes, NJ)

3.14 Enzyme-linked immunosorbent assay (ELISA) for detecting morphine on the MAPNV.

ELISA assay was used to confirm the coating of morphine on the surface of MAPNV, as mentioned by Eggermont, J., & Verbeeck, R. (2002). Briefly, the 96-well ELISA plate was treated with cellulose nitrate (0.1 µg/100 µl) at 37 °C for 2 h. The MAPNV solution (1 µg/ml) was prepared in distilled water (1 ml). MAPNV solution (100 µl) was added to each well and incubated for 2 h at 37 °C. The plate was washed, and 100 µl of the anti-morphine antibodies (1 µg/ml) was added. The plate was incubated at 37 °C for 1 h. The wells were washed three times with PBST. The HRP-conjugated secondary anti-mouse Abs (1 µg/ml, 100 µl) was added to the wells. The plate was incubated at 37 °C for 1 h. The wells were washed 3x with PBST. The substrate buffer was prepared with 5 mg of OPD in 9 ml H₂O and 1 ml H₂O₂. The substrate solution (100 µl) was added to the wells and incubated at 37 °C for 10 min. The reaction was stopped by adding 7% H₂SO₄ (50 µl) to the wells. The absorbance of the solution in the wells was measured at OD₄₉₂ nm using the Clariostar microplate reader (BMG Labtek, Ortenberg, Germany).

3.15 Time-dependent stability of nanoparticles using dynamic light scattering.

The stability of the MAPNV over time was evaluated as per the protocol mentioned in Kesselring, U. (1999). The MAPNV was dissolved in PBS (1 ml). The samples were transferred into a DLS measuring cascade. The hydrodynamic size of the nanoparticles was measured at 0 h. The samples were kept undisturbed in different conditions, such as 4 °C, -20 °C, freeze-dried, and

RT (25 ± 2 °C) for up to 180 days. The samples were reanalysed using DLS to measure their size on days 15, 30, 60, 90, 120, and 180. The particle size distribution was analysed, and the percentage of stable particles over time was determined.

3.16 UV-Visible spectroscopy study revealed the stability of MAPNV. A UV-Vis spectroscopy study was conducted to assess the stability of nanoparticles, as mentioned by Rahman S. et al. (2015). MAPNV (1 mg/ml) was prepared in PBS (1 M, pH 7.4, 1 ml). The samples were transferred into a 96-well plate. The absorbance of the samples was measured at 0 h by a UV-Visible spectrophotometer. The samples were kept undisturbed at 4 °C for 180 days. Later, the samples were reanalysed using the Clariostar microplate reader. The absorbance spectra of the samples were measured. The percentage of particles that remained stable over time was determined.

3.17 Determination of pH-dependent stability of the MAPNV. MAPNV (1 mg/ml) was prepared freshly and dissolved in deionised water, as mentioned by Merkle P. et al. (1999). The sample was transferred into a cuvette. The size and intensity of the nanoparticles were measured over a range of pH values (pH 4-9) over 30 min by DLS. The mean particle size and intensity were calculated for each pH range. Further, the UV-Visible spectrophotometer Clariostar microplate reader (BMG Labtek, Ortenberg, Germany) was used with a spectrum scan (wavelength 320-540 nm) to detect the surface cross-linking status to examine the stability across the different pHs.

3.18 Synthesis of morphine-protein conjugates. Morphine-carrier protein conjugates were prepared using the protocol mentioned by Chen et al. (2017). In brief, morphine (0.1 g) and succinic anhydride (0.1 g) in 2 ml benzene were placed in a 50 ml flask with a condenser and heated for 2 h at 80 °C using a heating mantle. Later, succinic anhydride (0.1 g) was added to the reaction mixture and heated for an extra hour. After cooling to 25 ± 2 °C; the benzene was discarded. The residual benzene was evaporated by air drying. The residue was dissolved in deionised water (10 ml) and adjusted to pH 2 with HCL (1 N). The solution was filtered to remove acid-insoluble material, and the pH was raised to approximately 8 ± 0.5 with NaOH (1 N) and filtered again to remove free morphine. Later the pH was adjusted to 5, resulting in morphine-6-succinate (M-6-S) crystallisation, while the mixture was kept in a refrigerator

overnight. The crystals were harvested by filtration and dried over anhydrous CaCl_2 under decreased pressure. M-6-S (1 mg) was dissolved in 10 ml of distilled water at 37 °C containing BSA (1 mg). The pH of the mixture was adjusted to 5.5, and 1-ethyl-3-(3-dimethyl aminopropyl) carbodiimide (1 mg) was added. The mixture was incubated overnight at 25 ± 2 °C. The reaction mixture was concentrated using a protein concentrator (Pierce™ Protein Concentrator PES, 10K MWCO, Fisher Scientific, Waltham, MA). The same method was used to prepare morphine-Acr1, morphine-KLH, morphine-PhoP and morphine-OVA conjugates.

3.19 Western blotting to detect the conjugation of morphine with BSA. The morphine-BSA (0.1 mg/ml) diluted in Tris-HCL buffer (100 mM, pH 8.5) was heated to 95 °C for 10 min, followed by rapid cooling on ice, as mentioned by Chen et al. (2017). An SDS-PAGE (10 x) buffer was added to the sample and heated to 95 °C for 5 min to denature the proteins. A gradient polyacrylamide gel (4-12%) was prepared, and the sample was loaded into the wells. The gel was placed in an electrophoresis chamber, and the sample and electrophoresis were done at 120 V for 90 min. Later, the gel was removed from the chamber and stained with Coomassie blue stain for 1 h. The gel was washed with a destaining solution for 15 min, and the bands of the BSA in the morphine-BSA conjugate were visualised.

The gel was transferred onto a PVDF membrane using wet phase transfer for 60 min. Later, the membrane was blocked with 5% BSA for 1 h. The membrane was incubated with a mouse anti-morphine Abs overnight at 4 °C. The membrane was washed twice with TBST (10 ml) for 5 min each and incubated with a secondary anti-mouse IgG-HRP Abs for 1 h. The membrane was washed thrice with TBST-20 (10 ml) for 5 min each. The membrane was developed with ECL reagents for 10 min, and the conjugate band was visualised by Chemidoc (Biorad PVT Ltd, Puchheim, Germany).

3.20 Demonstration of the cytotoxicity of MAPNV. The toxicity of the MAPNV on the L929 cells was measured as per the standard operating protocol mentioned in the Alamar blue kit (Thermo-Fisher Scientific, Waltham, MA). The assay was performed in 96-well plates using L929 cells (1×10^6 cells/well) in RPMI-1640-FBS-10% and different concentrations of MAPNV (0-50 µg/ml). After 24, 48, and 72 hours of incubation, Alamar blue reagent (10 µl/well) was added to each well. The plates were incubated for an additional 4 h at 37°C. Later,

the absorbance was read at 570 nm and 600 nm using a Clariostar microplate reader (BMG Labtek, Ortenberg, Germany).

3.21 Evaluation of MAPNV-induced lymphoproliferation. The induction of lymphocytic proliferation by MAPNV was evaluated using the protocol mentioned by Panton et al. (2014). Mice were injected MAPNV (0-20 mg/kg bwt) intraperitoneally on day 0 and day 7. On day 12, the animals were sacrificed, and their spleens were collected. Splenocytes were labelled with CFSE for cell proliferation estimation and incubated with MAPNV (20 µg/ml) for 72 h. The cells were washed and stained with anti-mouse CD19-PE Abs and anti-mouse CD4-APC Abs labelled Abs for B and CD4 T cells. The cells acquired through BD Accuri were analysed by FlowJo software (Franklin Lakes, NJ).

3.22 The detection of morphine reactive B cells in the animals immunised with MAPVN. The generation of morphine reactive B cells due to vaccination of MAPNV was evaluated per the protocol mentioned by Li J et al. (2014). In short, MAPNV (0-20 mg/kg bwt) was injected intraperitoneally into the mice at day 0 and day 7. On day 12, the mice were sacrificed, and the spleens were collected. Splenocytes were challenged *in vitro* with MAPNV (20 µg/kg bwt) for 72 h. Later, the cells (1×10^5) were stained with morphine-FITC conjugate (1 µg/ml) and anti-mouse CD19-PE Abs (1 µg/ml) and analysed to detect morphine-reactive B cells. The cells were acquired by BD Accuri, and analysis was performed by Flowjo software. (Franklin Lakes, NJ).

3.23 MAPNV-FITC uptake by macrophages. The macrophages (RAW 264.7) (50×10^4 cells/well) were incubated with MAPNV (20 µg/ml) in a complete RPMI-1640-FCS (10 %) in a humidified CO₂ incubator at 37 °C for 4 h. The cells were washed thrice with PBS and acquired using BD Accuri, and analysis was performed by Flowjo software. (Franklin Lakes, NJ).

3.24 Evaluation of adjuvant property of MAPNV. The macrophages (RAW 264.7) (50×10^4 cell/swell) were incubated with morphine (10 µg/ml) in complete RPMI-1640-FCS (10%) (to suppress the function of macrophages) in a humidified CO₂ incubator at 37 °C for 24 h to determine the self-adjuvant characteristics of MAPNV as mentioned by T. R et al. (2013).

Later, MAPNV-FITC (20 µg/ml) was added to each well and incubated at 37°C for 4 h. After the incubation period, the medium was removed, and the cells were washed thrice with PBS (5 ml). The cells were detached with trypsin-EDTA (200 µl). The activation of the macrophages was monitored by the uptake of MAPNV-FITC. The data were acquired using BD Accuri, and analysis was performed by Flowjo software. (Franklin Lakes, NJ).

3.25 Demonstration of the immunostimulatory efficacy of the MAPNV in mice exposed to morphine. The immunostimulatory impacts of MAPNV were evaluated by the protocol mentioned in Lu, Z. (2017). The mice were injected with morphine (10 mg/kg bwt) for 7 days. Later, they were inoculated with MAPNV (20 mg/kg bwt) on days 7 and 12. On day 17, the mice were sacrificed, and the splenocytes were stained with CFSE (5 µM). The cells were labelled with CFSE and *in vitro* challenged with MAPNV (20 µg/ml) for 72 h in complete RPMI-1640+FCS (10%). Next, the cells were stained with anti-mouse CD19 Abs for B cells and anti-CD4 for T cells to monitor their proliferation. The cells were acquired using BD Accuri, and analysis was accomplished by Flowjo software (Franklin Lakes, NJ).

3.26 Demonstration of MAPNV-FITC phagocytoses through TLR-2. The importance of TLR-2 in the phagocytosis of MAPNV was evaluated by the method prescribed by Das et al. (2022). The wild-type and TLR-2^{-/-} C57BL/6 female mice (6-8 weeks, 22±2 gm) were injected with morphine (10 mg/kg bwt) for 7 days. On day 8, the mice were sacrificed, and bone marrow cells (BMCs) were collected. The mononuclear cells were then isolated by centrifugation at 400 x g for 10 min and seeded in a 6-well plate (1x10⁶ cells/well) in RPMI-1640+FCS (10%). The cells were stimulated with recombinant mouse IL-4 (20 ng/ml) and GM-CSF (20 ng/ml) and incubated for 6 days. The dendritic cells (DCs) were harvested using trypsin-EDTA (200 µl) and seeded in a 6-well plate (50x10⁴ cells/well). Subsequently, MAPNV-FITC (20 µg/ml) was added into the wells and incubated for 4 h at 37 °C. Later, cells were harvested and stained for CD80, CD86 and CD40 expression using fluorochrome-tagged respective Abs. The cells were acquired using BD Accuri, and analysis was performed by Flowjo software (Franklin Lakes, NJ).

3.27 The examination of the prophylactic efficacy of MAPNV vaccine. The BALB/c mice were vaccinated with MAPNV (20 mg/kg bwt) on day 0 and day 7, and the control groups with

placebo (PBS), morphine (10 mg/kg bwt), MAN (20 mg/kg bwt), MANPV + alum (20 mg/kg bwt) and P3C+MAN+alum (20 mg/kg bwt). Consequently, the mice were injected with morphine (10 mg/kg bwt) from day 12 to 45. On day 46, the mice were sacrificed. The generation of anti-morphine Abs, the proliferation of CD4⁺ T cells and CD19⁺ B cells, long-lasting memory B and T cell generation, morphine neutralisation ability and opioid receptor function tests were monitored.

3.28 Testing of the therapeutic efficiency of MAPNV vaccine. Female BALB/c mice were divided into fourteen groups, with 5 mice/group. The mice were exposed to morphine (10 mg/kg bwt) for 21 days. In between, on days 16 and 18, mice were administered placebo (PBS), morphine (10 mg/kg bwt), M1MAPNV5 (morphine 1 mg/kg bwt + MAPNV 5 mg/kg body weight), M1 MAPNV 10 (morphine 1 mg/kg bwt + MAPNV 10 mg/kg body weight), M1 MAPNV 20 (morphine 1 mg/kg bwt + MAPNV 20 mg/kg body weight), M5 MAPNV 5 (morphine 5 mg/kg bwt + MAPNV 5 mg/kg body weight), M5 MAPNV 10 (morphine 5 mg/kg bwt + MAPNV 10 mg/kg body weight), M5 MAPNV 20 (morphine 5 mg/kg bwt + MAPNV 20 mg/kg body weight), M10 MAPNV 5 (morphine 10 mg/kg bwt + MAPNV 5 mg/kg body weight), M10 MAPNV 10 (morphine 10 mg/kg bwt + MAPNV 10 mg/kg body weight), M10 MAPNV 20 (morphine 10 mg/kg bwt + MAPNV 20 mg/kg body weight), M1APN20 (morphine 1 mg/kg bwt + APN 20 mg/kg body weight), M5APN20 (morphine 5 mg/kg bwt + APN 20 mg/kg body weight), M10APN20 (morphine 10 mg/kg bwt + APN 20 mg/kg body weight). The animals were injected with morphine (1, 5, 10 mg/kg bwt) for 15 days. Later, they were vaccinated on alternative days with 3 doses of MAPNV (5, 10, 20 µg/kg bwt). Later, the mice were sacrificed, and serum, brain and spleens were collected and analysed for B cell and T cell proliferation, long-term memory T cell and B cell generation and opioid receptor expression.

3.29 Investigation of the proliferation of CD4 T and B cells obtained from the vaccinated animals. The immunomodulatory impacts of MAPNV were demonstrated by the protocol mentioned elsewhere in T. R et al. (2013). In short, the single-cell suspension of splenocytes isolated from the vaccinated (prophylactic and therapeutic) and control groups was prepared. The CFSE-labelled splenocytes were cultured with MAPNV (20 µg/ml) for 48 h at 37 °C in a humidified 5% CO₂ incubator. Later, the cells were washed 3X with PBS (2 ml, 1 mM, pH 7.4)

and labelled with fluorochrome labelled anti-CD19 Abs (1 µg/ml) and CD4 Abs (1 µg/ml) Abs and acquired on BD Accuri and analysed by Flowjo software (Franklin Lakes, NJ).

3.30 Examining the presence of memory CD4⁺ T cells on the MAPNV vaccination. The generation of the memory response given MAPNV was demonstrated by the protocol mentioned by Liu, H. et al. (2013). The cells were cultured as mentioned above for the CD4 T and B cell proliferation. After 40 h, the cultures were harvested and stained with fluorochrome labelled anti-mouse CD4, CD44 and CD62L Abs. The cells were acquired through BD Accuri and analysed by Flowjo software. (Franklin Lakes, NJ) for the expression of the CD4⁺CD44^{hi} CD62L^{hi} population.

3.31 Enumeration of morphine reactive B cells in the MAPNV vaccinated animals. The generation of morphine reactive B cells due to vaccination of MAPNV was evaluated per the protocol mentioned by Li J et al. (2014). As mentioned, the spleen was isolated, and a single-cell suspension was prepared and incubated. The cells were harvested and incubated with morphine-FITC conjugate (10 µM/100 µl) and stained with anti-CD19 Abs (1 µg, 10 µl) for 10 mins at 22 °C. After incubation, the cells were washed 2X in PBS. Later, the cells were acquired using BD Accuri, and analysis was performed with Flowjo software. (Franklin Lakes, NJ).

3.32 Measuring anti-morphine Abs in the MAPNV vaccinated animals. The standard ELISA protocol was performed, as mentioned in Vidyarthi et al. (2015). Briefly, the 96-well plates were coated with morphine-KLH conjugates (0.001-1 µM, 100 µl/well). Later, the plates were washed 3X with PBST (Tween 20: 0.025%) and blocked with skimmed milk (5%, 150 µl) for 1 h at 4 °C. After the blocking; the plates were washed 3X with PBST. Serum samples (1:10) from vaccinated animals were added to the different wells. The plates were incubated at 4 °C for 2 h. Later, the secondary anti-mouse IgG+M+A-HRP Abs (0.1 µg/ml, 100 µl) were added, and the plates were incubated for 1 h at 4 °C. The plates were washed 5X with PBST. The colour was developed using a tetramethylbenzidine (TMB) substrate (100 µl), and the absorbance was measured at OD₄₅₀ nm wavelength using a microplate reader (BMG Labtek, Ortenberg, Germany). The serum from placebo (PBS), morphine, MAN, P3C+MAN+Alum and MAPNV + Alum groups were taken as control.

3.33 *Estimation of IgG and IgM subtype of anti-morphine Abs on MAPNV immunisation.* The standard ELISA protocol was performed, as mentioned in Vidyarthi et al. (2015). Momentarily, the 96-well ELISA plate was coated with morphine-KLH conjugate (0.001 μ M, 100 μ l/well) and incubated overnight at 4 °C. The plates were washed 3X with PBST (Tween 20: 0.025%) and blocked with skimmed milk (5%, 150 μ l) for 1 h at 4 °C. After the blocking; the plates were washed 3X with PBST. Serum samples (1:10) from vaccinated animals were added to the different wells. The plates were incubated at 4 °C for 2 h. Later, anti-mouse secondary Abs (IgG) (0.1 μ g/ml, 100 μ l) and anti-mouse secondary Abs (IgM) (0.1 μ g/ml, 100 μ l) were added to separate wells. The reaction was stopped using HCL (1 M, 50 μ l) and incubated for 5 min in the dark at 25 \pm 2 °C. Standard incubation and washing protocols were followed at every step. The absorbance was measured at OD₄₅₀ nm using a Clariostar microplate reader (BMG Labtek, Ortenberg, Germany). The serum from placebo (PBS), morphine, MAN, P3C+MAN+Alum and MAPNV + Alum groups were taken as control.

3.34 *Estimation of morphine in the brain and serum on immunisation with MAPNV.* The quantification of morphine in the serum and brain of the vaccinated and control animals was done per the protocol mentioned by Carneiro et al. (2012) and Matsuda et al. (2012). Firstly, a standard curve was prepared of different concentrations of morphine (0.1-1.0 mg/ml) solubilised in PBS (1 M, pH 7.4). The OD was recorded with a UV-Vis spectrophotometer at a wavelength of OD₃₀₀ nm. The absorbance of the blank solution (PBS, 1 M, pH 7.4) and the different concentrations of morphine (0.01-1 μ M/ml) were recorded and plotted to create a standard curve. The serum samples collected from the animals were pipetted into triplet wells of a 96-well plate. The absorbance of the sample was measured using a UV-Vis spectrophotometer at OD₃₀₀ nm. The concentration of morphine was calculated using the Beer-Lambert law using the standard morphine curve. The values are expressed as μ M. Similarly, the quantification of morphine was done in the brain. Brains from the MAPNV-vaccinated animals were obtained and placed in a homogeniser with PBS (10 mM, pH 7.4) (10 ml) for 10 seconds. Subsequently, it was centrifuged at 10000 x g for 10 min at 4 °C. The sample was transferred into a fresh tube and centrifuged at 10000 x g for 1 h at 4 °C. The SN was discarded, and the pellet was resuspended in PBS (10 ml). This process was repeated two times. Later, NaCl (2M, 1 ml) was added and thoroughly mixed with the samples. The tube was centrifuged at 10000 x g for 1 h at 4 °C. The pellet was resuspended in PBS (10 ml). Later, urea (4 M, 10

ml) was added and mixed with the sample. The sample was centrifuged at 10000 x g for 1 h at 4 °C. SDS (10%) (1 ml) was added to the samples and mixed. The sample was centrifuged at 10000 x g for 1 h at 4 °C. The pellet was resuspended in PBS (10 ml). The solution was dialysed against PBS (1 mM, pH 7.4, 50 ml) for 4 h. The sample was centrifuged at 10000 x g for 1 h at 4 °C. The pellet was resuspended in PBS (10 ml) and stored at -20 °C. The absorbance of the sample was measured using a UV-Vis spectrophotometer at OD₃₀₀ nm. The concentration of morphine was calculated using the Beer-Lambert law using the standard morphine curve. The values are expressed as μM

3.35 Isolation of RNA from the brain and splenocytes on inoculation of MAPNV. RNA was isolated from the brain and splenocytes of the animals as per the standard operating protocol mentioned by the manufacturer (Thermo-Fisher Scientific, Waltham, MA). In short, using a glass homogeniser (Thermo-Fisher Scientific, Waltham, MA), the brain was homogenised in ice in TRIzol reagent (Thermo-Fisher Scientific, Waltham, MA) (1 ml). The homogenate was incubated for 10 min at RT. Chloroform (200 μl) was added to the homogenate, vortexed for 30 seconds, incubated for 10 min at RT and centrifuged at 12000 x g for 15 min at 4 °C. The SN was transferred into a new tube, and isopropanol (500 μl) was gently mixed and incubated for 15 min at RT, and the mixture was centrifuged at 12000 x g for 10 min at 4 °C. The SN was discarded, and the pellet was washed with ethanol (75%, 200 μl) and centrifuged at 12000 x g for 10 min at 4 °C. The pellet was air-dried and dissolved in DEPC-treated water (20 μl), and RNA was quantified using Nano-Drop (Thermo-Fisher Scientific, Waltham, MA) as per the manufacturer's standard operating protocol.

3.36 Synthesis of cDNA from the RNA. The cDNA was prepared using the Reverse Transcription Kit (Thermo-Fisher Scientific, Waltham, MA), as per the manufacturer's protocol. The reagents, RT buffer (2.5 μl), dNTP mix (2.5 μl), random primers (2.5 μl), and reverse transcriptase enzyme (1.0 μl), were added to the RNA (1 μl) isolated from splenocytes and brain separately. The reaction mixture was thoroughly mixed, briefly spun, and incubated at 25 \pm 2 °C for 10 min. Subsequently, enzyme mix (1 μl) was added to the tube and gently mixed. The mixture was incubated at 42 °C for 60 min. Finally, the reverse transcriptase enzyme was inactivated by heating at 85 °C for 5 min, and the cDNA sample was stored at -20 °C until use.

3.37 RT-qPCR to determine the cytokines gene expression level in the MAPNV vaccinated animals. The RT-qPCR analysis was done to evaluate the level of different gene expressions, as mentioned in the standard operating protocol of Sybr Green (Biorad PVT Ltd, Sacramento, California). The RT-qPCR was performed for the cytokine TNF- α , IL-1 β , IL-6, IL-4, and IFN- γ . Firstly, each forward primer (1 μ l) and reverse primer (1 μ l) was added to a clean, nuclease-free DEPC-treated tube. Then nuclease-free DEPC-treated water (4 μ l) was added to the tube. Later, Sybr green (Biorad PVT Ltd, Sacramento, CA) (3 μ l) was added to the tube, and the solution was gently mixed by pipetting. The prepared cDNA (1 μ l) was added to the respective tubes and briefly spun to settle it. Finally, the RT-qPCR was performed according to the program specified, step 0: 50 °C for 25 sec, step 1: 95 °C for 30 sec, step 2: 95 °C for 5 sec, step 3: 60 °C for 30 sec, step 4: 72 °C for 30 sec. Similarly, the RT-qPCR was also performed to evaluate the OPRM and dopamine genes in vaccinated animals' brains.

3.38 Examining the Effects of Vaccination on the Behaviour of Animals. Female BALB/c mice were divided into fourteen groups, with 5 mice/group. The mice were exposed to morphine (10 mg/kg bwt) for 21 days. In between, on days 16 and 18, mice were administered placebo (PBS), morphine (10 mg/kg bwt), MAN (morphine 10 mg/kg bwt + MAN 20 mg/kg body weight), MAPNV (morphine 10 mg/kg bwt + MAPNV 20 mg/kg body weight) and MAPNV + Alum (morphine 10 mg/kg bwt + MAPNV + alum 20 mg/kg body weight). All groups' baseline body weight, food consumption, water intake, and animal movement were recorded every alternative day. The behaviours were then compared before vaccination (day 0) and after vaccination (day 22).

3.39 Estimation of anti-morphine Abs levels in the serum of chronic morphine abusers. The standard ELISA protocol was performed, as mentioned in Vidyarthi et al. (2015). Momentarily, the 96-well microtiter plates were coated overnight RT (25 \pm 2 °C) with morphine-BSA conjugate (1 mM, 100 μ l) in carbonate-bicarbonate buffer (pH 9.6). The plates were washed 3x with PBST (PBS 1M, Tween-20, 0.05%). Unsaturated sites of the wells were blocked with skimmed milk (5% in PBS 0.01M, pH 7.2, 150 μ l) for 2h at 37 °C. The plates were washed 3x with PBST. Different serum dilutions (0, 10, 100 and 1000) of the chronic morphine abusers and normal healthy controls in buffer (0.5% skimmed milk + PBST, 100 μ l) were added into the wells and incubated for 1 h at 37 °C. The plates were washed 3x with PBST, and anti-

human IgM+A+G-HRP (0.1 ng, 100 μ l) secondary Abs were added and incubated for 1 h at 37 °C. The plates were washed 5x with PBST and incubated with OPD for 20 min at 37 °C. The reaction was stopped using H₂SO₄ (7%, 50 μ l), and OD was measured at 492 nm using the Clariostar microplate reader (BMG Labtek, Ortenberg, Germany). BSA-coated wells were used as the negative control.

3.40 Demonstration of the level of anti-morphine Abs. The level of specificity of anti-morphine Abs was evaluated per the protocol mentioned by Kolekar S. et al. (2014). In short, different dilutions (0.001, 0.01, 0.1, 1) of morphine-BSA conjugates (1 μ M) were coated in separate wells of 96 well plates. Unsaturated sites of the wells were blocked with skimmed milk (5% in PBS 0.01M/pH 7.2, 150 μ l) for 2h at 37 °C. The serum samples of the chronic morphine abusers and normal healthy controls (100 μ l) were added into the wells and incubated for 1 h at 37 °C. The plates were washed 3x with PBST. Later, anti-human IgM+A+G-HRP (0.1 ng, 100 μ l) was added and incubated for 1 h at 37 °C. The plates were washed 5x with PBST and incubated with OPD (100 μ l) for 20 min at 37 °C. The reaction was stopped using H₂SO₄ (7%, 50 μ l), and OD was measured at 492 nm using the Clariostar microplate reader (BMG Labtek, Ortenberg, Germany).

3.41 Estimation of free morphine in the serum of chronic morphine users. The free and immune complexed morphine was estimated in the serum samples of the chronic morphine users and normal healthy controls. The free morphine was separated from the immune complexes (ICS) using the protocol described elsewhere (Chen et al., 2018). Briefly, PEG 6000 (20 μ M) in PBS (5 ml) was added to the serum of the chronic morphine users and healthy controls and incubated ON at 4 °C. The precipitate was centrifuged at 2,000 x g for 30 min at 4 °C, SN was discarded, and the pellet was washed with PEG 6000 (10 μ M) at 2,000 x g for 20 min at 4 °C. SNs were isolated, and precipitates were resuspended in pre-warmed PBS (2 ml) for 1 h at 37 °C. The concentration of morphine was estimated using a standard morphine [1-10 μ M/ml] curve by a Clariostar microplate reader (BMG Labtek, Ortenberg, Germany).

3.42 Neutralisation of morphine by anti-morphine Abs. The binding of anti-morphine Abs to morphine and its neutralisation efficiency was measured (Zhang Y. et al. (2016). Briefly, sera chronic morphine users and normal healthy controls were centrifuged for 30 min at 10,000 \times g

at 4 °C. Later, Tris-HCL (1M, pH 8.0, 1 ml) was added to the samples. With continuous stirring, saturated ammonium sulphate solution was added. The solution was incubated at 4 °C for 6 h with continuous stirring and centrifuged for 30 min at 10,000 × g. The SN was discarded, and the pellet was washed 2x with ammonium sulphate solution (50%). The pellet was dissolved in the buffer (PBS 10 mM, pH 7.4, 5 ml). It was dialysed and stored at -20 °C. The isolated Igs (10 µg/ml) were allowed to react with the exogenously added morphine (1 mM) ON at 37 °C. Later, it was dialysed 2X against PBS (2 ml) (0.01 M). The SN was collected and stored at -20 °C. The dialysate was collected, and the PEG precipitation method was used to quantify morphine-bound to the anti-morphine Abs (Meza-Carmen et al. 2012). Free morphine and morphine complexed with Abs were quantified using the standard curve of morphine using the Clariostar microplate reader.

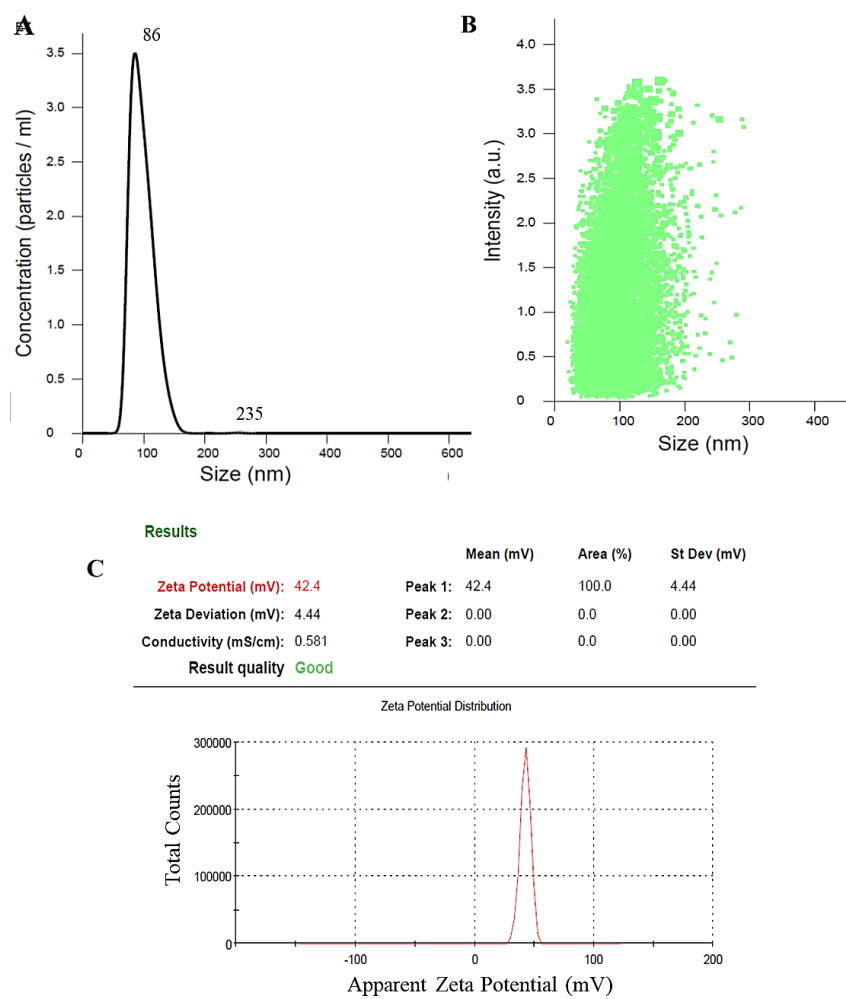
3.43 Isolation of RNA from the serum of chronic morphine users. Total RNA was isolated from the serum samples of all the chronic morphine users' patients and normal healthy controls, as mentioned elsewhere (Cheng G et al. (2008). Briefly, the frozen serum samples (400 µl) were thawed on ice, diluted with RNase-free H₂O (100 µl) and added with proteinase K (1 mg/ml). The samples were incubated at 37 °C for 20 min. Subsequently, the Tri-Reagent RT LS (Thermo-Fisher Scientific. Waltham, MA) (500 µl) was added to the tubes. The tubes were briefly inverted to homogenate and then transferred into microcentrifuge tubes (2 ml). The chloroform (200 µl) was added to the tubes, vortexed and centrifuged at 15,000 × g for 10 min at 4 °C. The upper transparent layer was transferred into a fresh tube, and isopropanol (100%, 500 µl) was added. The solution was incubated at 25±2 °C for 10 minutes and centrifuged for 20 minutes at 15,000 ×g at 4 °C. The pellet was collected and washed with ethanol (70%, 200 µl) and re-centrifuged at 10,000 × g for 10 min at 4 °C. The tubes were air-dried, and the pellets were dissolved with DEPC-treated water (50 µl). The purity of the isolated RNA was checked using the Nanodrop One/One C Micro volume UV-visible spectrophotometer (Thermo-Fisher Scientific. Waltham, MA) as per the standard operation protocol prescribed by the manufacturers.

3.44 Preparation of the cDNA. Per the manufacturer's instructions, the cDNA was prepared with a high-capacity reverse transcription kit (Thermo-Fisher Scientific, Waltham, MA). Briefly, the reaction master mix was prepared with RT buffer (10x, 2.0 µl), dNTPs Mix (25x,

100 mM, 0.8 μ l), RT Random Primers (10x, 2.0 μ l), reverse transcriptase (1.0 μ l), RNase inhibitor (1.0 μ l) and nuclease-free H₂O (3.2 μ l). Then RT master mix (2x, 10 μ l) was pipetted into the PCR tubes. Later, RNA (1 μ g) was diluted in DEPC-treated water (10 μ l) and pipetted into separate tubes. The tubes were sealed, and a quick spin was done to settle the contents and eliminate air bubbles. The tubes were loaded on the thermal cycler (Thermo-Fisher Scientific, Waltham, MA). The reaction was then carried out according to the manufacturer's instructions (Thermo-Fisher Scientific, Waltham, MA): step 1: temperature 25 °C, time 10 min; step 2: temperature 37 °C, time 120 mins; step 3: temperature 85 °C, time 5 mins; step 4: temperature 4 °C, time ∞ . Finally, the RT-qPCR was performed according to the program specified, step 0: 50 °C for 25 sec, step 1: 95 °C for 30 sec, step 2: 95 °C for 5 sec, step 3: 60 °C for 30 sec, step 4: 72 °C for 30 sec.

3.45 Statistical analysis. The statistical analysis was performed using the Two-Tailed test and One-way ANOVA's multiple comparisons tests. A two-tailed test is used to evaluate the data collected from the animals. It can be evaluated for positive and negative results, allowing a more comprehensive understanding of their responses. The One-way ANOVA's multiple comparison tests were used in the animal studies to determine if there was a statistically significant difference between the means of different groups within the study. This test allows researchers to look at the effect of multiple independent variables on a single dependent variable and then compare the means of the different groups to see if there is a significant difference. The data are represented as mean \pm SD unless and otherwise mentioned. * $p < 0.1$, ** $p < 0.01$, *** $p < 0.001$, **** $p < 0.0001$, ns = non-significant.

4.1. The *Mycobacterium tuberculosis* (Mtb) Acr1 protein nanoparticles (AN) coated with morphine and Pam3Cys exhibited polydispersity and positive zeta potentials. By examining the particle size distribution and zeta potential of the suspension, we aimed to gain important information regarding the physical and chemical properties of the morphine-Acr1-Pam3Cys nanoparticles vaccine (MAPNV) and control Acr1 nanoparticles (AN), such as charge, interactions with other particles, and binding potential. To investigate the size and charge distribution of nanoparticles, we have used particle size distribution and zeta potential. The particle size distribution analysis of the AN revealed a mean size of 86 ± 19.2 nm, with a concentration of 8.4×10^9 particles/ml (Fig. 1A). Additionally, the particle's dynamic light scattering analysis showed a polydispersity index of 0.2, indicating low polydispersity of the particles (Fig. 1B). The particles displayed a positive zeta potential charge of 42.4 mV (Fig. 1C).



The Nano-Tracking Analysis (NTA) of the MAPNV showed a mean particle diameter of 106.1 ± 23.9 nm (Fig. 1D), with a polydispersity index (PI) of 0.22 and a concentration of 2.0×10^4 particles/ml (Fig. 1E). Additionally, the charge on the particles was 37.3 mV (Fig. 1F). These results demonstrated that the particles had a low and a positive zeta potential charge.

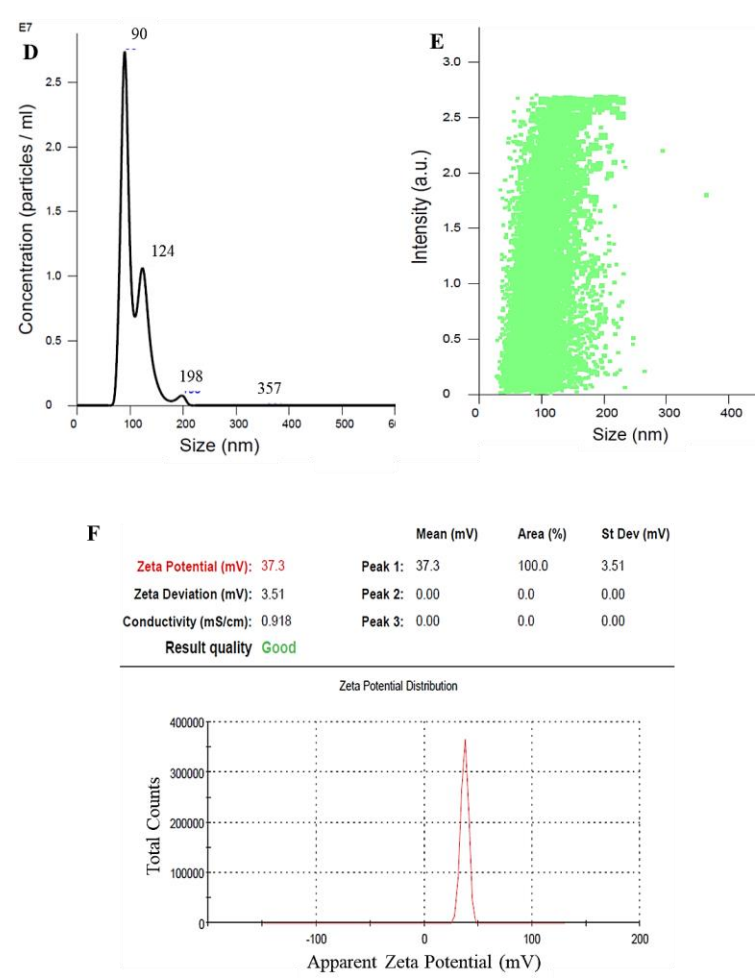


Figure 1. The particle size distribution and shape analysis of the *Mycobacterium tuberculosis* (*Mtb*) *Acr1* protein nanoparticles coated with morphine and Pam3Cys. *Acr1* nanoparticles (AN) (1 mg/ml) were synthesised and analysed using Nanosight NS300 for (A) size and concentration; (B) size versus intensity; (C) charge. The morphine-*Acr1*-Pam3Cys nanoparticle vaccine (MAPNV) was engineered using the *Acr1* protein of *Mtb* with morphine and Pam3Cys coated on the surface. The MAPNV (1 mg/ml) was analysed for (D) size and concentration; (E) size and intensity; (F) charge. The data shown are representative of 3 independent experiments.

4.2 *Particulation efficiency of Acr1 nanoparticles (AN)*. To evaluate the efficiency of the protocol to generate the optimum quantity of nanoparticles from the protein, the particulation efficiency of the nanoparticle formation was tested. The protein concentration of AN was 0.777 ± 0.047 mg/ml, while the protein content in the SNs was 0.089 ± 0.005 mg/ml and nanoparticulation efficiency was $77.7 \pm 4.7\%$. Thus indicating the high nanoparticulation efficiency of Acr1 nanoparticles (Fig. 2). These results demonstrated the suitability of Acr1 nanoparticles as a vaccine candidate.

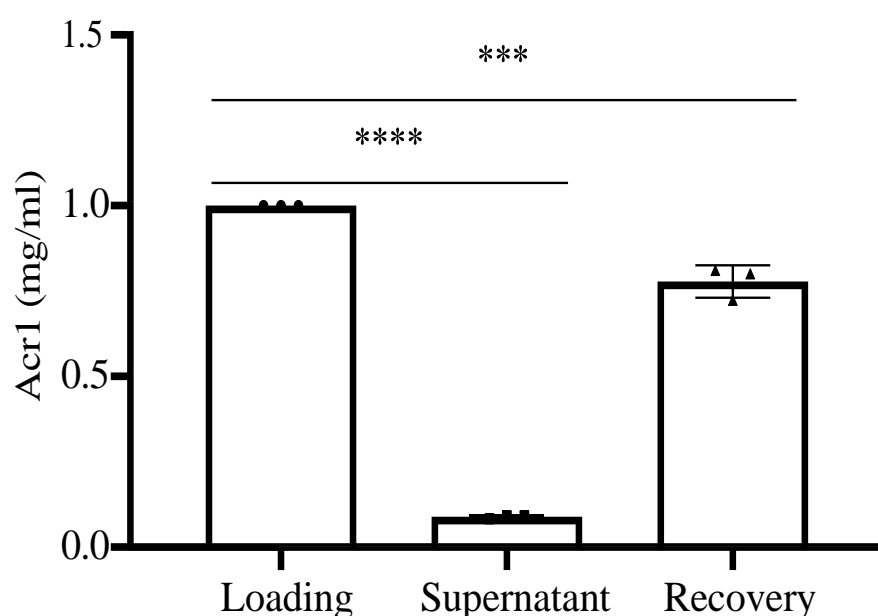


Figure 2. Particulation efficiency of Acr1 nanoparticles (AN). The ANs were checked for their particulation efficiency by the Bradford method. The bar graphs represent the total Acr1 protein in the nanoparticles (Loading), the free Acr1 protein after particulation (supernatant), and the particulation efficiency of AN (Recovery). The particulation efficiency was calculated using the formula: Particulation efficiency (%) = $\frac{\text{Acr1 concentration before particulation} - \text{Acr1 concentration in the supernatant}}{\text{Acr1 concentration before particulation}} \times 100$. The data are from 3 independent experiments. Each dot represents a single experiment. The Two-Tailed test was used for statistical analysis. The data (mg/ml) are represented as mean \pm SD. *** $p < 0.001$, **** $p < 0.0001$.

4.3 Scanning electron microscopy (SEM) showed that MAPNVs are highly ordered and crystalline with minimal aggregation. This investigation was done to understand the morphology of particles using scanning electron microscopy. This investigation was used to gain a detailed understanding of the various features of a particle, such as its size, shape, texture, and other related characteristics. To conduct this investigation, a scanning electron microscope was used to closely examine the particles at very high magnifications. The results of the SEM image analysis showed that the nanoparticles had a spherical shape with a smooth surface texture, highly distinguished and not aggregated. Additionally, the particles displayed a high degree of crystallinity, indicating that they were composed of ordered and crystalline structures. The analysis revealed that the AN (Fig. 3A) had a slight degree of aggregation, whereas the MAN (Fig. 3B) and MAPNV (Fig. 3C) particles were more distinctively segregated. These results demonstrated that MAPNV particles are highly ordered, crystalline structures with minimal aggregation.

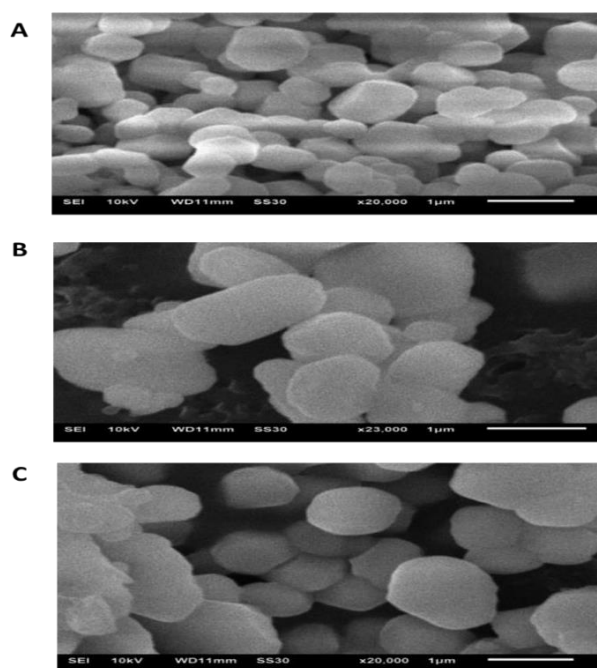


Figure 3. Scanning electron microscopy of the morphine-Acr1-Pam3Cys nanoparticle vaccine (MAPNV). The morphology of MAPNV was analysed by SEM. The images of particles of various sizes and shapes, with a smooth surface texture of (A) Acr1 nanoparticles, (B) morphine-Acr1 nanoparticles, (C) morphine-Acr1-Pam3Cys nanoparticles. The pictures were taken at 20000X magnification (scale: 1 μm). The data are representative of 3 independent experiments.

4.4 *The freeze-drying demonstrated a decrease in the MAPNV.* This experiment was conducted to investigate the effect of freeze-drying on the hydrodynamic size of the MAPNV. This investigation of redispersion ability was aimed at evaluating the efficacy of MAPNV to be redispersed in a given solution. This is important to determine its suitability for vaccine delivery. The results revealed that the size of the MAPNV was 151.3 ± 2.9 nm when synthesised (Fig. 4A) and 115.7 ± 3.0 nm after freeze-drying (Fig. 4B). This indicated a reduction in the size of MAPNV by $24.6 \pm 1.9\%$, suggesting that the nanoparticles had undergone redispersion. These findings demonstrated that freeze-drying had led to a decrease in particle size but not to the extent of aggregation, which is beneficial for vaccine efficiency.

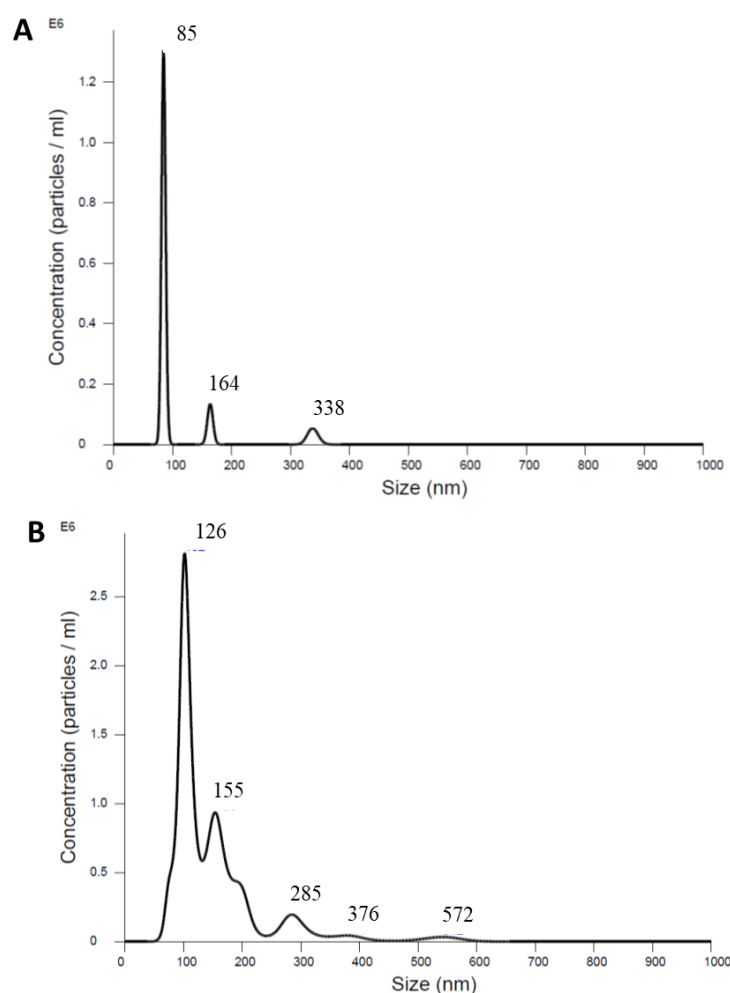


Figure 4. Impacts of freeze-drying on the hydrodynamic size of the MAPNV. The MAPNV was analysed for re-dispersion efficiency and hydrodynamic size using Nanosight NS300. The graph shows the size and concentration of the nanoparticles after (A) synthesis; (B) freeze-drying. The data are representative of 3 independent experiments.

4.5 Fourier transform infrared (FTIR) spectra of MAPNV. Fourier Transform Infrared (FTIR) spectroscopy was used to assess the physical and chemical properties of MAPNV. FTIR spectroscopy measures infrared light absorption or emission of a sample at different frequencies. This way, various functional groups of molecules in the sample are identified. By obtaining FTIR spectra of the MAPNV samples, we determined the presence of specific functional groups in the samples. The FTIR spectra of MAPNV (orange) and AN (blue) were collected and compared (Fig. 5). The absorbance of AN showed a broad peak at 1650 cm^{-1} , indicating the presence of an amide group. The transmittance of MAPNV showed two distinct peaks at 1664 cm^{-1} and 1620 cm^{-1} , denoting the presence of an amide group and a peptide bond, respectively. Additionally, an absorbance peak at 1415 cm^{-1} was observed, signifying the presence of a hydroxyl group in MAPNV (Fig. 5). The results suggested that the morphine and Pam3Cys were successfully conjugated on the surface of the MAPNV.

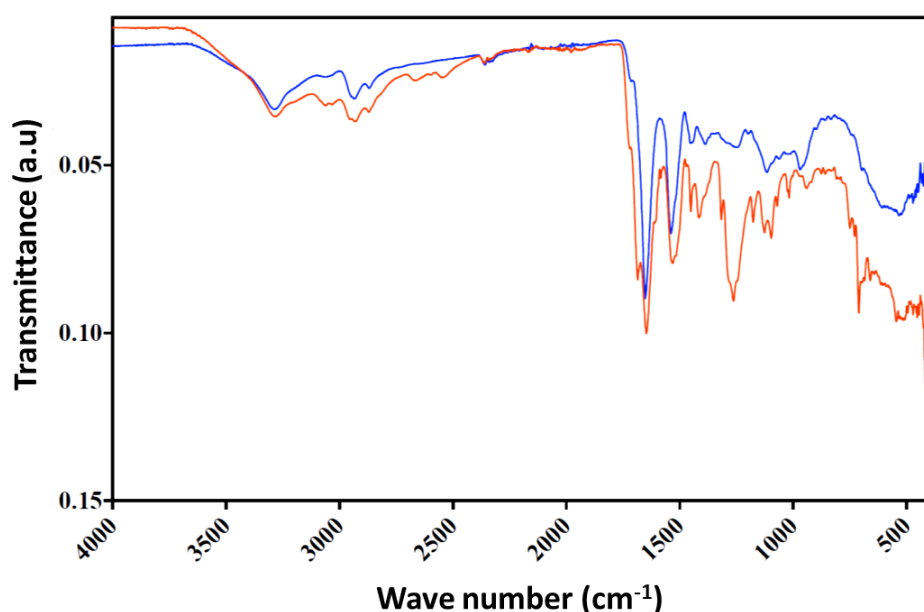


Figure 5. Fourier transform infrared (FTIR) spectra of MAPNV. The surface of the MAPNV was characterised by FTIR. The orange line depicts the surface interferogram of the MAPNV. The AN was taken as a control depicted in the blue line. The data shown are illustrative of 3 independent experiments.

4.6 The conjugation of morphine and Pam3Cys on the surface of MAPNV. This experiment was done to determine the coating of morphine and Pam3Cys onto the surface of MAPNV. By scanning the surface of the nanoparticles, we gain insight into specific characteristics of each sample, such as size, elemental composition, and surface topography. Results from surface spectral scans showed a shift from 320-350 nm and 450-550 nm, illustrating the successful conjugation of morphine and Pam3Cys to the MAPNV surface. Morphine is a hydrophobic molecule, and adding a hydrophobic moiety to the MAPNV's surface resulted in a change in the surface tension and a shift in the peak of the surface scan at 320-350 nm. The presence of the Pam3Cys molecule on the MAPNV surface increases the negative charge on the nanoparticle surface, resulting in a further surface scan peak shift at 450-550 nm (Fig. 6). These results suggested that the surface tension of the nanoparticle had changed, confirming the successful surface coating of morphine and Pam3Cys on the MAPNV.

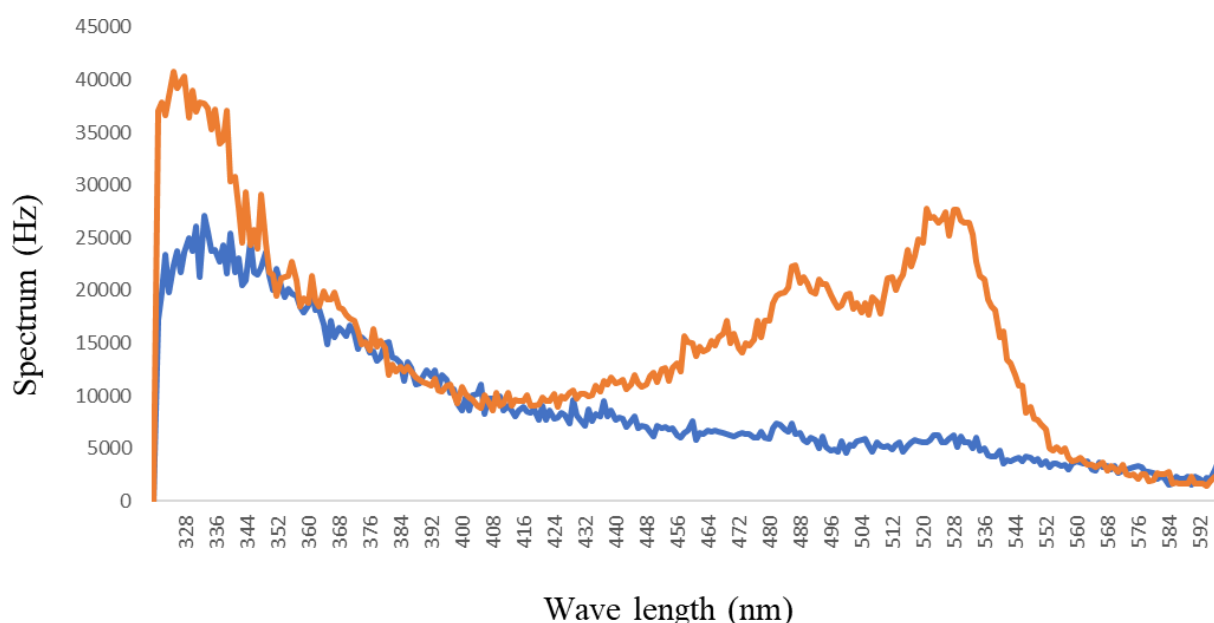


Figure 6. The demonstration of surface structure scan of MAPNV. The MAPNV was tested for its surface structure and characterised by spectral scan using the Clariostar UV-Visible spectrophotometer. The lines show the surface spectral scan of AN (blue) and MAPNV (orange) nanoparticles. AN was taken as a control. The data shown are representative of 3 independent experiments.

4.7 The concentration of morphine in the nanoparticles suggested effective conjugation of morphine on the surface of MAPNV. The experiment was conducted to determine the concentration of morphine in MAPNV. In this experiment, we tested the presence of morphine on the surface of MAPNV. Here we have used the spectro-photometer to quantify morphine. The content of morphine in the MAPNV (1.1 ± 0.012 mg/ml) was significantly ($p < 0.0001$) higher than negative control AN (0.04 ± 0.015 mg/ml), i.e., nanoparticles without morphine. The AN was taken as a control as it is the base for the MAPNV and do not have morphine on its surface. Besides suggesting the assay's specificity, the results also indicate the quantity of morphine in MAPNV (Fig. 7).

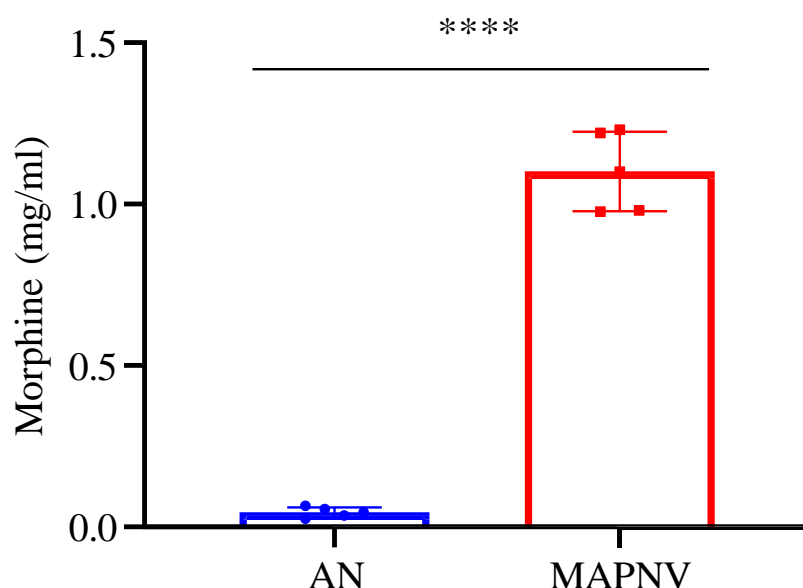
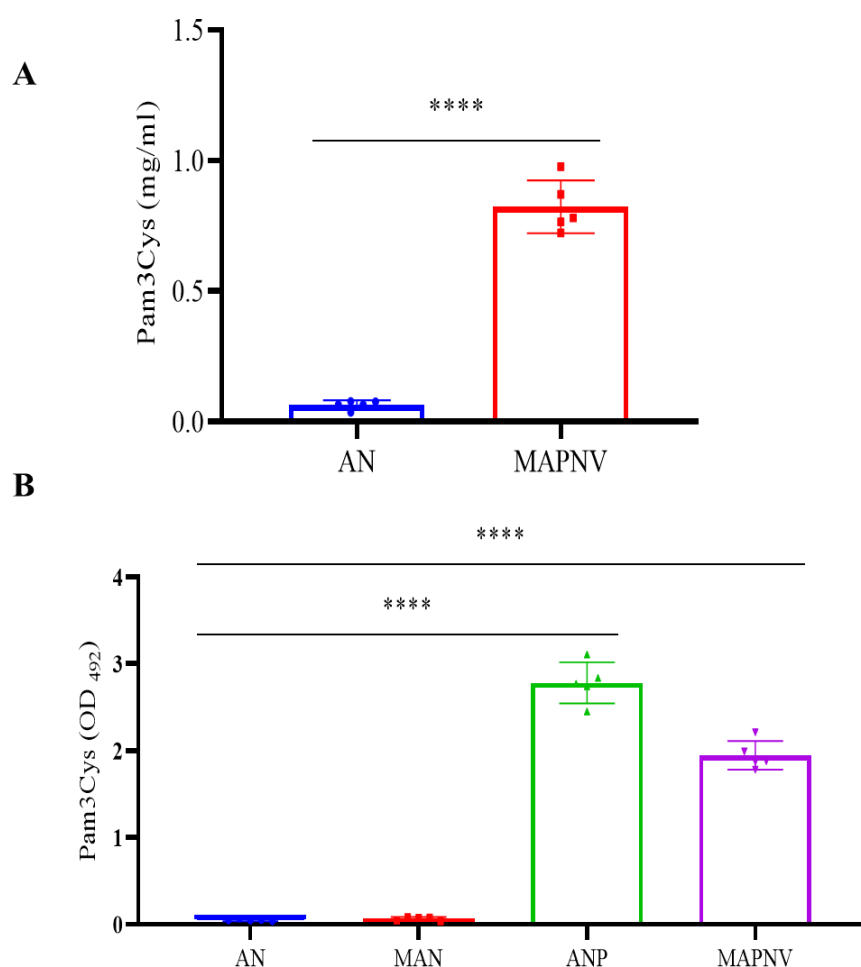


Figure 7. The estimation of the concentration of morphine in MAPNV. MAPNV (2×10^6 particles/ml) was tested for the presence of morphine by a standard curve of different concentrations of morphine. The red bar represents the amount of morphine coated on the surface of MAPNV. The AN was taken as a control and represented as a blue bar. The AN is the base variant for MAPNV, and morphine was coated on AN to formulate MAPNV. The data shown are from 5 independent experiments. Each dot indicates a single experiment. The results were analysed using a Two-Tailed test. The data (mg/ml) are represented as mean \pm SD. **** $p < 0.0001$.

4.8 The presence of Pam3Cys on the surface of MAPNV. We have investigated the presence of Pam3Cys on the surface of the MAPNV vaccine to quantify the amount of Pam3Cys coated on it. To accomplish this, a UV-visible spectrophotometer and colourimetric analysis were used to measure the adsorption of Pam3Cys onto the MAPNV nanoparticles. This technique provided a label-free measurement of the surface interaction, allowing for precisely determining the presence of Pam3Cys. The concentration of Pam3Cys (0.823 ± 0.1 mg/ml) in MAPNV was substantially greater ($p < 0.0001$) than the negative control AN (0.06 ± 0.17 mg/ml) that was without Pam3Cys (Fig. 8A). The results demonstrated the level of Pam3Cys in the MAPNV. Furthermore, biotinylated Pam3Cys was used to validate the presence of Pam3Cys on the surface of MAPNV. A significantly ($p < 0.0001$) higher absorbance (1.946 ± 0.16 nm) of MAPNV, as compared to the controls ANP (2.7 ± 0.23 nm), AN (0.04 ± 0.01 nm) and MAN (0.06 ± 0.02 nm), was noted (Fig. 8B). The results primary and secondary Abs used were taken as blank control to reduce cross reactivity. These results confirm the presence of Pam3Cys on the surface of MAPNV.



*Figure 8. The assessment of the presence of Pam3Cys on the surface of MAPNV. (A) The amount of Pam3Cys displayed on MAPNV (2×10^6 particles/ml) was estimated by a UV spectrometer. The red bar depicts the Pam3Cys coated on the surface of the MAPNV. The blue bar represents the control AN. The quantification of Pam3Cys was done using the standard curve of Pam3Cys by Absorbance spectrophotometry. (B) The coating of Pam3Cys on the surface of the MAPNV was evaluated using a colourimetric assay. The biotin-P3C was conjugated on the surface of the MAPNV. The bar graph shown in purple denotes the OD₄₉₂ values of the spectrophotometer after binding Pam3Cys with avidin-HRP. The Acr1 nanoparticles (AN), Morphine-Acr1 nanoparticles (MAN), and Acr1-P3Cys nanoparticles (APN) used as controls are denoted as blue, red and green bars, respectively. Each dot represented a single experiment. The results are from 5 independent experiments. The data were analysed through One-Way ANOVA. The data (OD₄₉₂) are represented as mean \pm SD. ****p<0.0001.*

4.9 *The binding of morphine on the surface of MAPNV.* This experiment was conducted to determine the effectiveness of coating morphine on the surface of MAPNV using anti-morphine Abs. The flow cytometric analysis revealed a considerable ($p < 0.0001$) binding ($67 \pm 6.5 \%$) of anti-morphine Abs on the surface of MAPNV than the control AN ($1.6 \pm 0.5 \%$) (Fig. 9A). Furthermore, we corroborated our flow cytometry results further by ELISA (Fig. 9B). The presence of morphine ($2.014 \pm 0.97 \text{ nm}$) in MAPNV was largely ($p < 0.0001$) detected by anti-morphine Abs on MAPNV, but not the controls AN (OD: $0.0614 \pm 0.01 \text{ nm}$) and ANP ($0.0668 \pm 0.08 \text{ nm}$), which were without morphine (Fig. 9B). The results primary and secondary Abs used were taken as blank control to reduce cross reactivity. These results confirmed the effective coating of morphine on the surface of MAPNV.

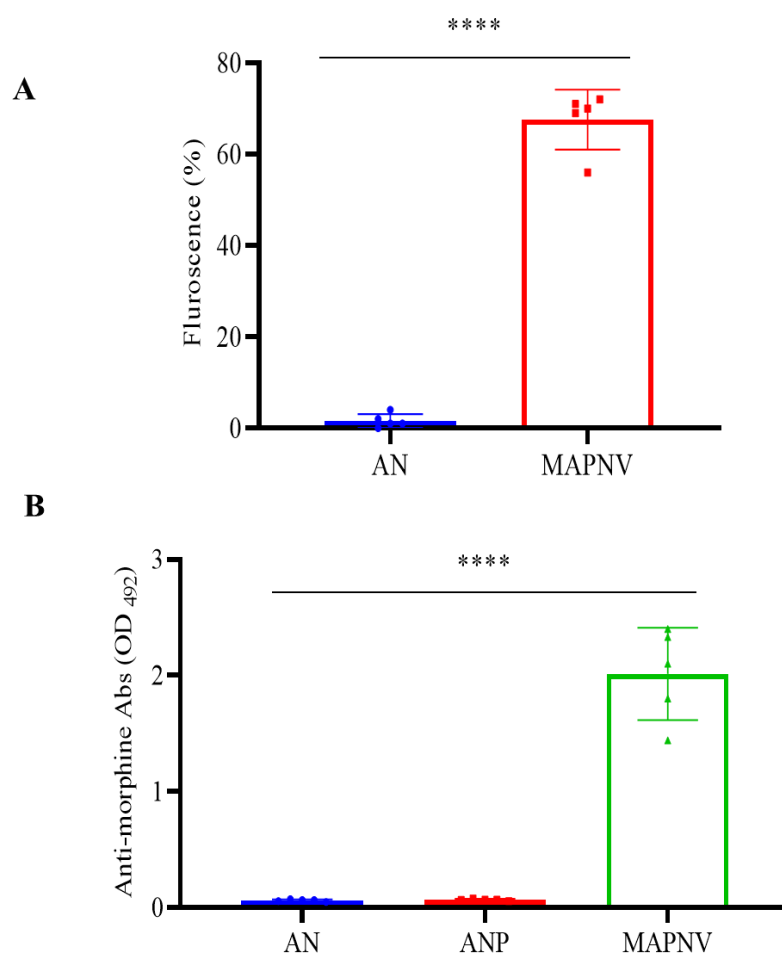


*Figure 9. The demonstration of the presence of morphine on the surface of MAPNV. (A) The presence of morphine expressed on the surface of the MAPNV was estimated by anti-morphine Abs using flow cytometry. The MAPNV (10×10^5) was incubated with anti-morphine Abs (ABM063) and secondary anti-mouse-Alexa fluor 488 and analysed by flow cytometer. The AN was taken as a control. (B) The presence of morphine on the surface of the MAPNV was estimated using anti-morphine Abs and secondary anti-mouse-HRP Abs through ELISA. The Acr1 nanoparticles (AN) and Acr1-P3C nanoparticles (ANP) were used as controls Each dot represents a single experiment. The data are from 5 independent experiments. The results were analysed through One-Way ANOVA. The data (OD₄₉₂) are represented as mean \pm SD. ****p<0.0001.*

4.10 *The hydrodynamic size of MAPNV was stable at 4 °C for 180 days.* This investigation was done to check the stability of the size of the MAPNV. We have used the dynamic light scattering technique to measure the size of the MAPNV. This technique relies on optical scattering of laser light from the nanoparticles to accurately measure their dimensions. The hydrodynamic size of the MAPNV remained almost stable, with a slight decrease in size. When stored for 180 days at 4 °C a size reduction from 180.6 ± 4.35 nm to 156 ± 3.06 (p<0.5), at -20 °C from 180.6 ± 4.35 nm to 128.6 ± 4.5 nm (p<0.01), freeze drying from 180.6 ± 4.35 nm to 115.3 ± 4.3 nm (p<0.001) and at room temperature (25 ± 2 °C) from 180.6 ± 4.35 nm to 54.04 ± 4.35 nm (p<0.0001) (Fig. 10A). These results suggest that the hydrodynamic size of the nanoparticles was most stable at 4 °C, followed by -20 °C, freeze-dried, and RT (25 ± 2 °C) (Fig. 10B). Further, we noted not much difference in the stability of MAPNV, when stored for 180 days at either day 0 or days 180 days, as revealed in the spectrum (Fig. 10C). Furthermore, the Dynamic Light Scattering (DLS) measurements showed the mean particle size of the MAPNV 95.56 ± 2.67 nm, which was significantly (p<0.0001) stable across pH 4-9 (Fig. 10D). The mean size of the MAPNV at pH 7 was 102.66 ± 0.5 nm; at pH 4 was 86.66 ± 5.77 nm, and at pH 9 was 92.73 ± 2.05 nm. The UV-Visible spectrophotometer analyses confirmed that the surface cross-linking of the MAPNV was more stable at pH 7 than either pH 4 or pH 9 (Fig. 10E), indicating the stability of MAPNV at physiological pH 7.

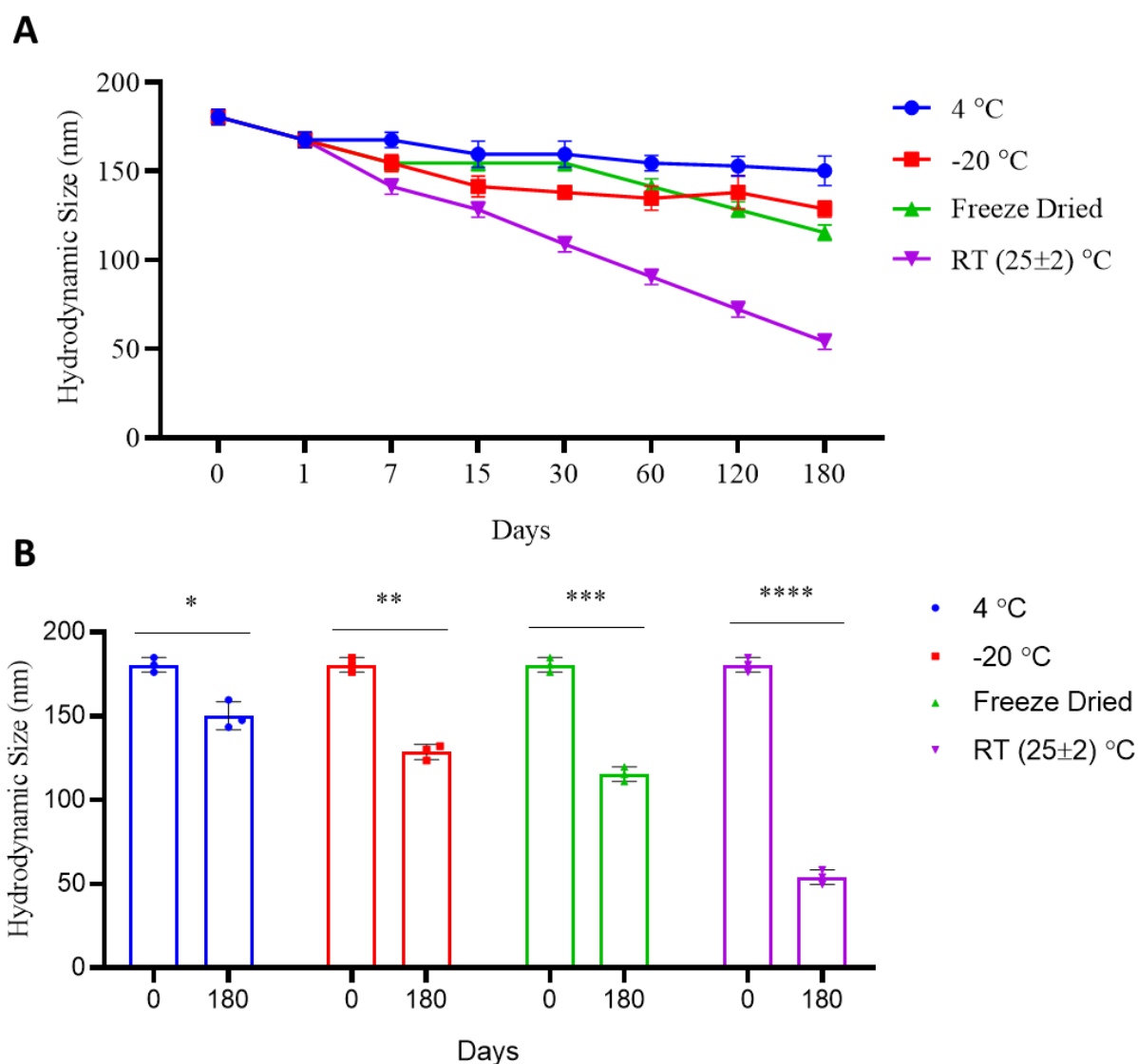


Figure 10A-B. Hydrodynamic size stability of MAPNV over time. The stability of the MAPNV was evaluated by measuring the hydrodynamic size of the nanoparticles through dynamic light scattering (DLS). (A) The line diagram represents the size of the MAPNV at different time intervals (0-180 days) and storage conditions, viz 4 °C (blue), -20 °C (red), freeze-dried (green), and RT (25 ±2 °C (purple). (B) The bar graph shows the comparative hydrodynamic size analysis of the MAPNV on day 0 and day 180 at different storage conditions. Each dot represented a single experiment. The data shown are from 5 independent experiments. The results were analysed by ordinary One-Way ANOVA. The data (nm) are shown as mean ± SD. * p<0.5; **p<0.01; ***p<0.001; ****p<0.0001.

C

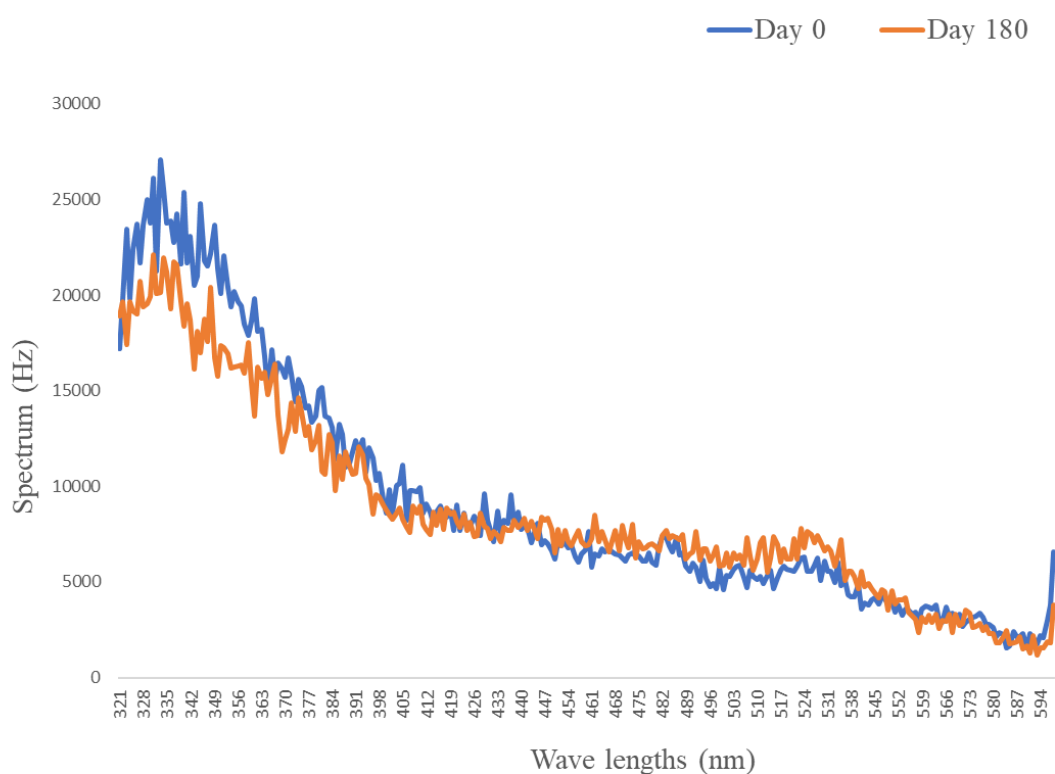


Figure 10C. MAPNV shows stability up to 180 days. The stability of the MAPNV was tested for surface scan analysis by a spectrophotometer at 4 °C for 180 days. The line graph shows the spectral scan with a wavelength range of 321-594 nm. The blue line indicates the surface scan of the MAPNV on day 0, and the orange line for day 180 when stored at 4°C. The data are representative of three independent experiments.

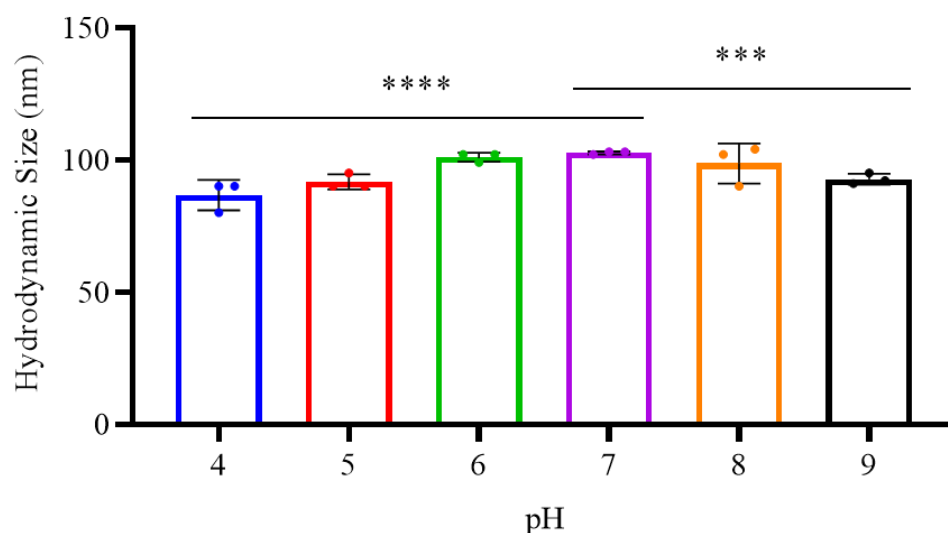
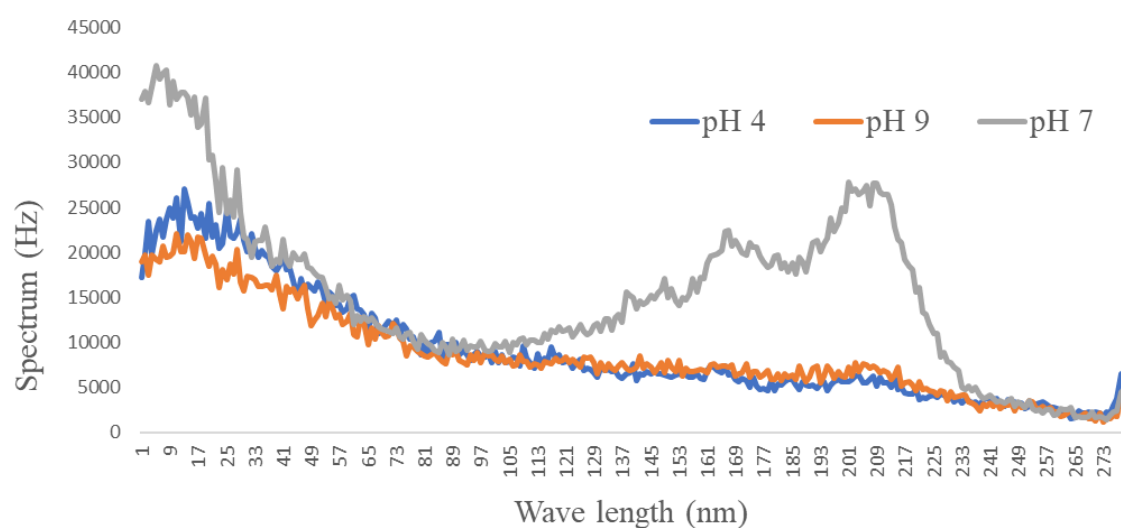
D**E**

Figure 10D-E. Stability of MAPNV at different pH. The strength of the MAPNV was tested at various pH. (D) The bar graph shows the hydrodynamic size of the vaccine stored at diverse pH. (E) The line graphs illustrate the surface spectral scan analysis of the nanoparticles at pH 4 (acidic) and pH 9 (basic). The pH 7 (neutral) condition was taken as a control. The data shown are from 3 independent experiments. Each dot represented a single experiment. The results were analysed using the ordinary One-Way ANOVA. The data are represented as mean \pm SD. *** $p < 0.001$; **** $p < 0.0001$.

4.11 *The detection of morphine in the morphine-BSA conjugate by immunoblotting.* The presence of morphine in a morphine-BSA conjugate was examined by immunoblotting. Immunoblotting was chosen because it is a highly sensitive and accurate detection method capable of detecting small amounts of antigens in a complex mixture. The results of this investigation could potentially be used to elucidate the potential benefits of this particular conjugate as a delivery system for morphine. The SDS-PAGE image stained with Coomassie blue showed the presence of m.wt. markers (lane 1), BSA (lane 2) and morphine-BSA (lane 3) (Fig. 11A). The immunoblot analysis of the morphine-BSA protein conjugate but not the control BSA protein showed a single band at ~68 kDa when probed with anti-morphine Abs (Fig. 11B). The detection of morphine in the conjugate provides evidence of morphine linked to BSA.

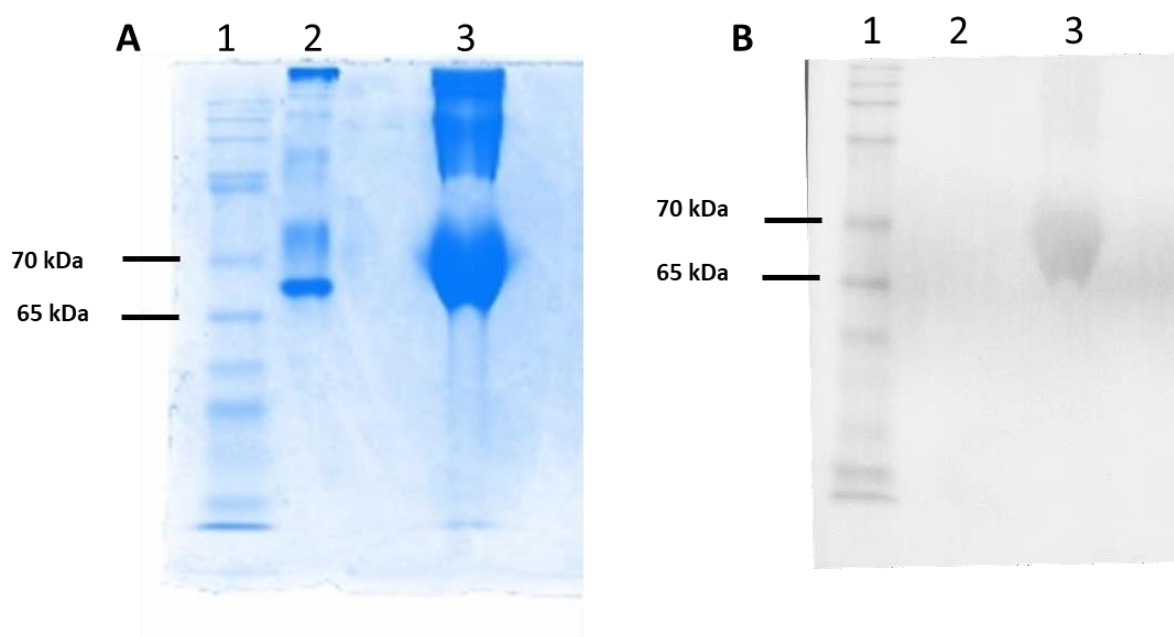


Figure 11. The detection of morphine in morphine-BSA conjugate by immunoblotting. The conjugation of morphine with the carrier protein BSA was confirmed by Western blotting. The images show the (A) SDS-PAGE gel stained with a Coomassie blue stain for carrier protein in the conjugate. Lane 1: m.wt. markers, lane 2: BSA, lane 3: morphine-BSA. (B) Immunoblot of the conjugate showing the presence of morphine when probed with anti-morphine Abs. Lane 1: m.wt. markers, lane 2: BSA stained with anti-morphine Abs, lane 3: morphine-BSA probed with anti-morphine Abs. The data are representative of 3 experiments.

4.12 *MAPNV is not cytotoxic for the cells.* This experiment was done to determine cytotoxicity of MAPNV on the cells. The nanoparticles were incubated with L929 cells for a predetermined period of time. The effect of the nanoparticles was evaluated by measuring cell viability. We observed negligible cytotoxicity of MAPNV on L929 cells at doses up to 20 µg/ml for 24 h (ns), 48 h (ns) and 72 h ($p < 0.5$) (Fig. 12A, B). However, at a dose of 50 µg/ml for 24 h ($p < 0.01$), 48 h ($p < 0.01$) and 72 h ($p < 0.001$), significant cytotoxicity was noticed (Fig. 12C). The results suggested that MAPNV is not toxic for the cells at a dose of 20 µg/ml.

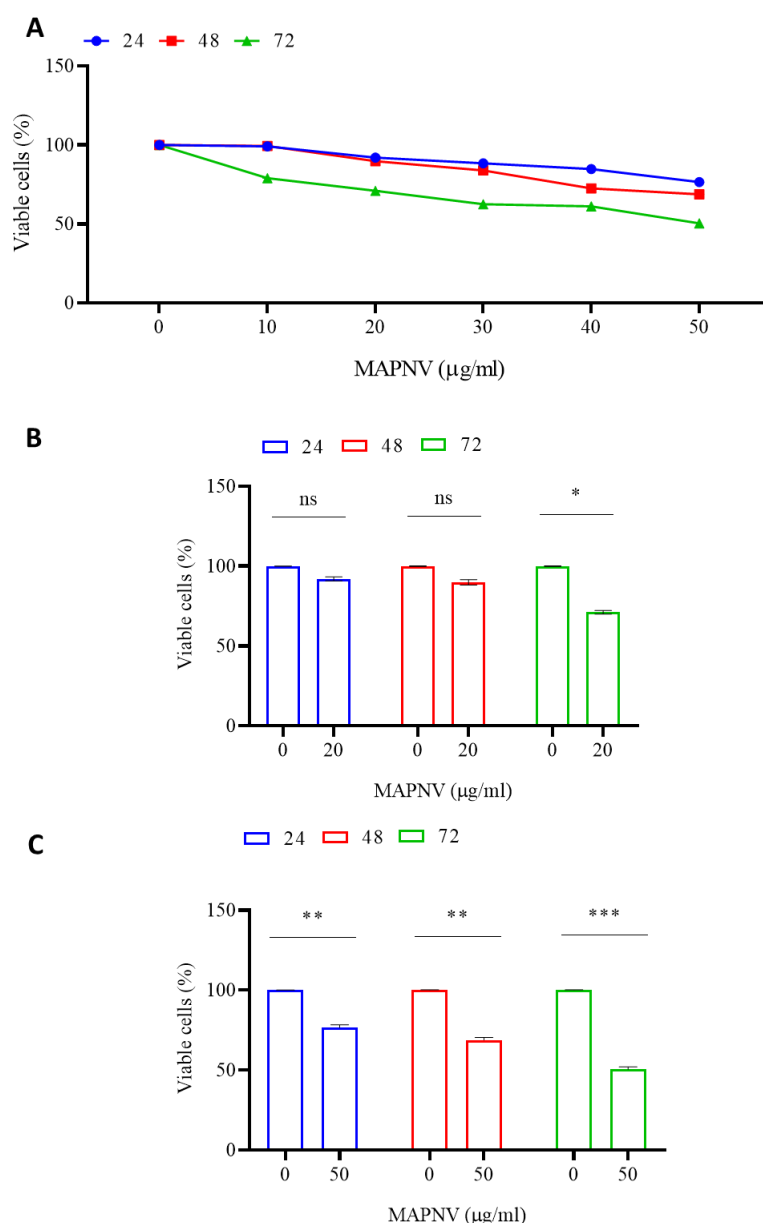
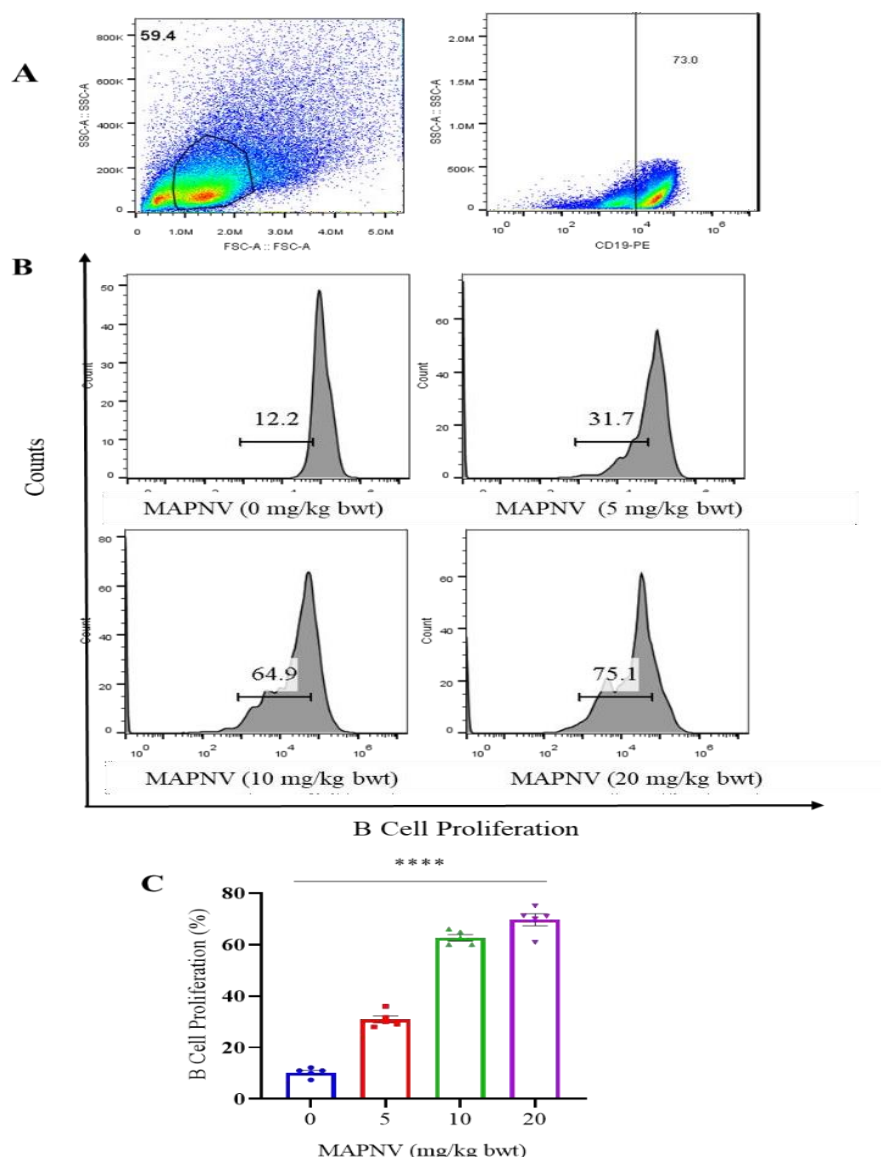


Figure 12. MAPNV is not cytotoxic for the cells. The MAPNV was evaluated for its toxicity on L929 cells. (A) The line diagram suggests the cells incubated with varying concentrations of MAPNV (0-50 µg/ml) for different time intervals. (B) Bar diagrams signify the comparative analysis of per cent of viable L929 cells after treatment with MAPNV (0-20 µg/ml) for 24h, 48h and 72h. (C) Bar diagrams indicate the relative analysis of per cent of viable L929 cells after treatment with MAPNV (0-50 µg/ml) for 24h, 48h and 72h. The results are from 5 independent experiments. The statistical analysis was performed by the ordinary One-Way ANOVA. The data (%) are expressed as mean \pm SD. * $p < 0.05$; ** $p < 0.01$; *** $p < 0.001$; ns = non-significant.

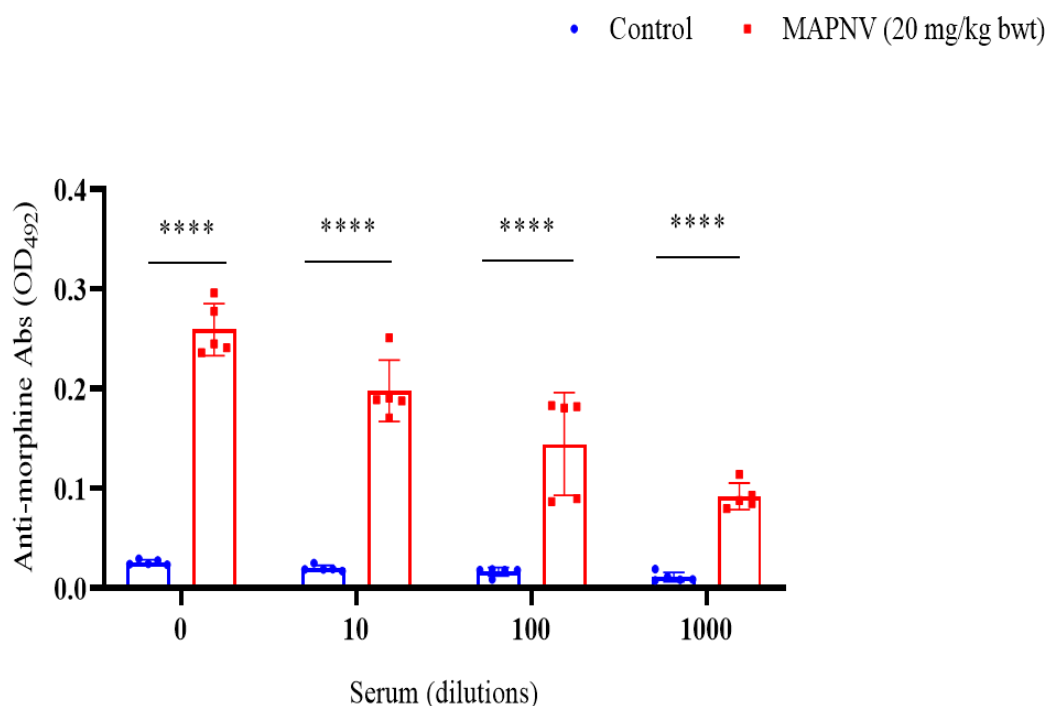
4.13 *MAPNV has self-adjuvant properties and stimulates B cells to release anti-morphine Abs that clears the morphine from the brain and blood.* In this study, we investigated the potential of the vaccine MAPNV to effectively clear morphine from the brain and blood by stimulating B cells to produce anti-morphine antibodies. We evaluated the self-adjuvant properties of the vaccine by inducing the production of anti-morphine antibodies in the absence of an exogenous adjuvant. Mice vaccinated with MAPNV showed an expansion of B cells in a dose-dependent manner ($p < 0.0001$), as compared to the unvaccinated control group (Fig. 13A-C). Further, an enhancement ($p < 0.0001$) in the level of anti-morphine Abs was detected in the serum of the MAPNV-vaccinated animals. The response was observed in a dose-dependent manner (Fig. 13D-E). The subtype of anti-morphine Abs was predominantly IgG ($p < 0.0001$) and, to a lesser extent, IgM ($p < 0.001$) (Fig. 13F). Furthermore, a substantial decline in the level of morphine in the serum ($p < 0.0001$) and brain ($p < 0.0001$) of the mice was noticed (Fig. 13G, H). It may be deduced from these results that MAPNV stimulated the secretion of anti-morphine Abs that could successfully clear morphine from the brain and blood.

MAPNV displays on its surface Pam3Cys, a TLR-2 ligand, which has adjuvant properties. Consequently, we immunised mice with MAPNV supplemented with adjuvant alum to prove MAPNV self-adjuvanting properties. We could not detect any change in the production of anti-morphine Abs or proliferation of CD19⁺ B cells with MAPNV+alum against MAPNV (Fig. 13F, 13I-K). Furthermore, we examined the pool of CD19⁺ morphine reactive B cells using morphine-FITC and PE-anti-CD19 Abs. We noticed an insignificant change in the percentage of CD19⁺ morphine reactive B cells obtained from groups administered with MAPNV versus MAPNV + alum (Fig. 13L-N).

The gating strategies of B cells are depicted in figures 13A, I, and L. Overall, these results document that MAPNV does not require any exogenous adjuvant and has sufficient intrinsic adjuvant properties to activate B cells to secrete anti-morphine Abs to clear the morphine from the body of the vaccinated mice. The ELISA results in primary and secondary Abs used were taken as blank control to reduce cross-reactivity



*Figure 13A-C. MAPNV induces the proliferation of morphine-reactive B cells in the vaccinated mice. The mice were immunised with MAPNV (0-20 mg/kg bwt) on day 0 and day 7. Twelve days post initial vaccination; the animals were sacrificed, splenocytes were isolated, labelled with cell proliferation dyes, and *in vitro* challenged with MAPNV for 72 h. Flow cytometry graphs (A) denote the gating strategy for CD19⁺ B cells and (B) CFSE dye-dilution assay for CD19⁺ B cells (anti-CD19-PE Abs). The bar graphs (C) show the mean CD19⁺ B cell proliferation. The flow-cytometry histogram and bar diagrams are from 3 independent experiments. Each dot represents one animal. The Two-Tailed test was performed for the statistical analysis. The data (%) are expressed as mean \pm SD. **** $p < 0.0001$.*

D

*Figure 13D. The anti-morphine Abs exhibit dose responsiveness with serum dilutions. The mice were immunised with the MAPNV (20 mg/kg bwt) on days 0 and 7. Later, they were continuously administered morphine (10 mg/kg bwt) from days 12 to 45. On day 46, the mice were bled, serum was isolated and anti-morphine Abs were estimated by ELISA. Microtiter plates were coated with morphine-KLH (0.01 μ M). Later, serum (0, 10, 100, 1000 dilutions), secondary anti-mouse-HRP Abs and OPD were added, and the colour developed was measured by ELISA reader at OD₄₉₂. Regular steps of incubations and washings were followed at each stage. The data are from 3 independent experiments. Each dot represents one animal. The statistical analysis was performed by a One-Way ANOVA. Data (OD₄₉₂) are denoted as mean \pm SD, ****p<0.001.*

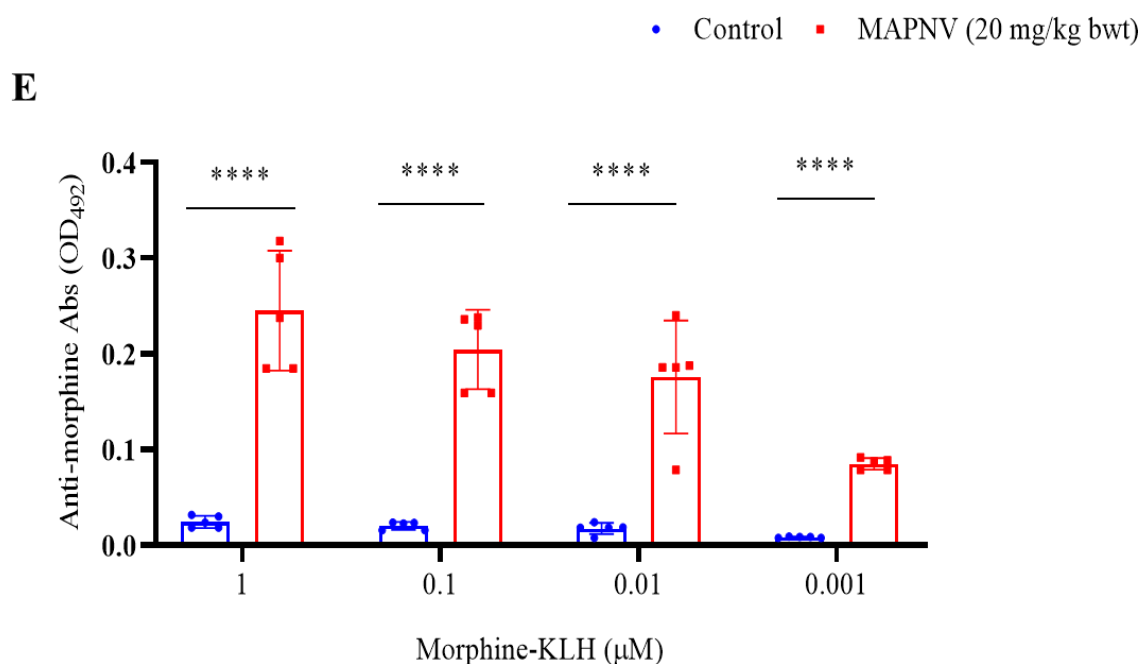


Figure 13E. MAPNV elicit anti-morphine Abs production in immunized animals. The mice were injected MAPNV (20 mg/kg bwt) on days 0 and 7. Later, they were continuously administered morphine (10 mg/kg bwt) from days 12 to 45. On day 46, the mice were bled, sera were isolated and anti-morphine Abs were estimated by ELISA. Different concentrations of morphine-KLH (0.001-1 μM) were coated in the microtiter plates. Later, 100 μl of serum (1:10 dilution), secondary anti-mouse-HRP Abs and OPD were added, and ELISA reader measured the colour developed at OD₄₉₂. Regular steps of incubations and washings were followed at each phase. The data are from 3 independent experiments. Each dot represents one animal. The statistical analysis was performed by a One-Way ANOVA test. Data (OD₄₉₂) are denoted as mean ± SD. ****p<0.0001.

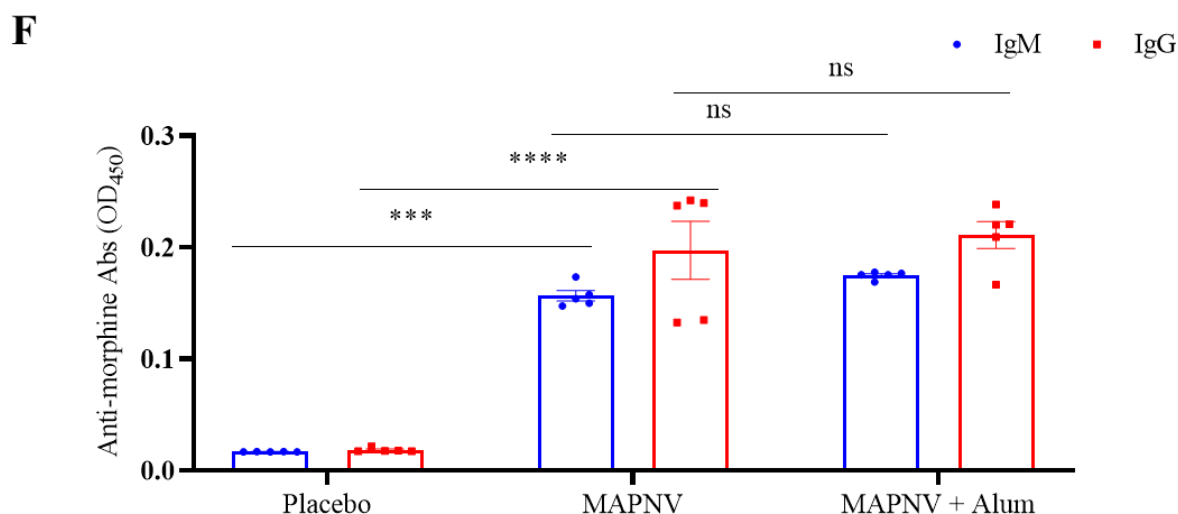


Figure 13F. MAPNV induces primarily IgG-subtype of anti-morphine Abs. The mice were immunised with the MAPNV (20 mg/kg bwt) on days 0 and 7. Later, morphine (10 mg/kg bwt) was administered from days 12 to 45. On day 46, the mice were bled, serum was isolated, and the level of IgM anti-morphine Abs and IgG anti-morphine Abs were estimated by ELISA. The animals inoculated with placebo (PBS), MAN and MAPV + alum was taken as controls. The data are from 3 independent experiments. Each dot represents one animal. The data (OD₄₅₀) analysed by One-Way ANOVA are represented as mean \pm SD. ns=non-significant, ****p<0.0001, ns= non-significant.

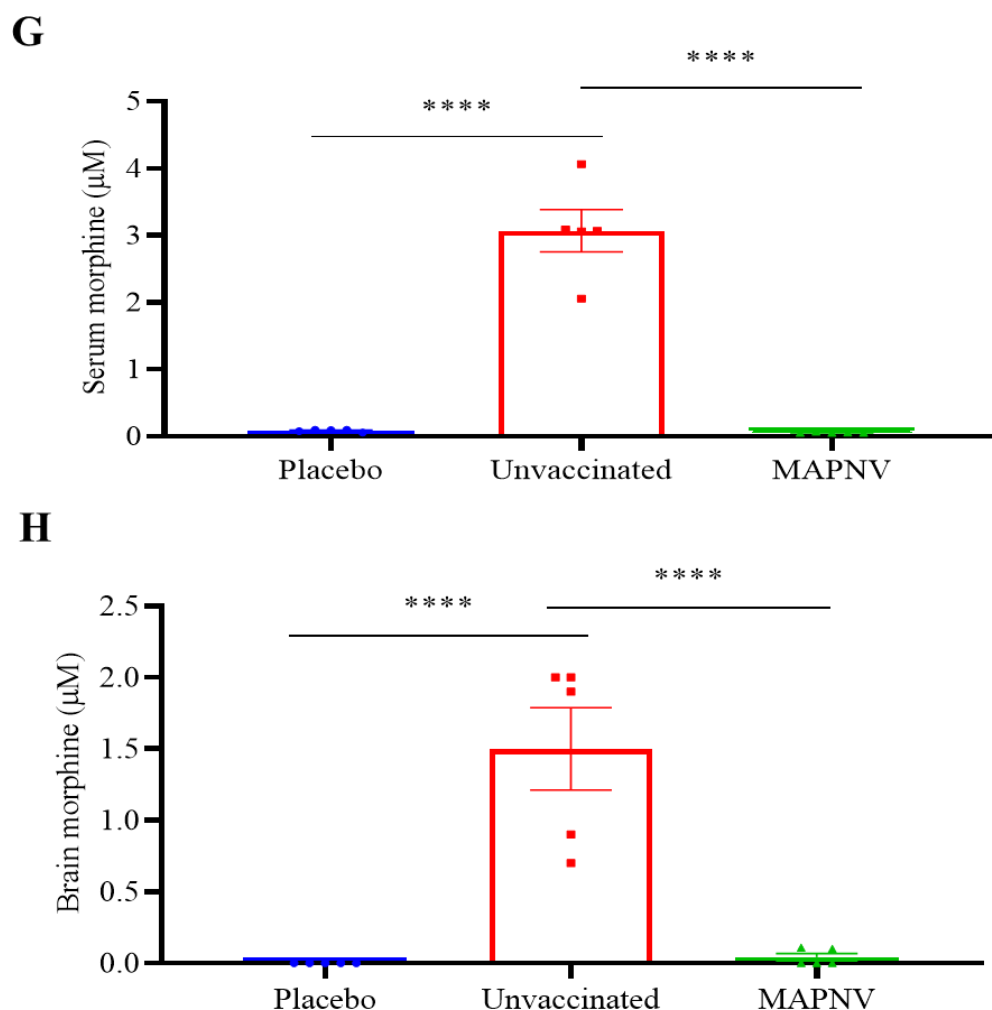


Figure 13G-H. MAPNV substantively clears morphine from the blood and brain of immunized animals. The mice were immunised with the MAPNV (20 mg/kg bwt) on days 0 and 7. Later, morphine (10 mg/kg bwt) was administered from days 12 to 45. On day 46, the mice were sacrificed. The level of morphine in the blood and brain was measured by a UV-visible spectrophotometer. The bar diagrams represent the morphine in the (G) serum; (H) brain. The control groups were inoculated with placebo (PBS) and morphine (Unvaccinated). The data are from 3 independent experiments. Each dot represents one animal. The data (µM) analysed by One-Way ANOVA are denoted as mean \pm SD. ****p<0.0001.

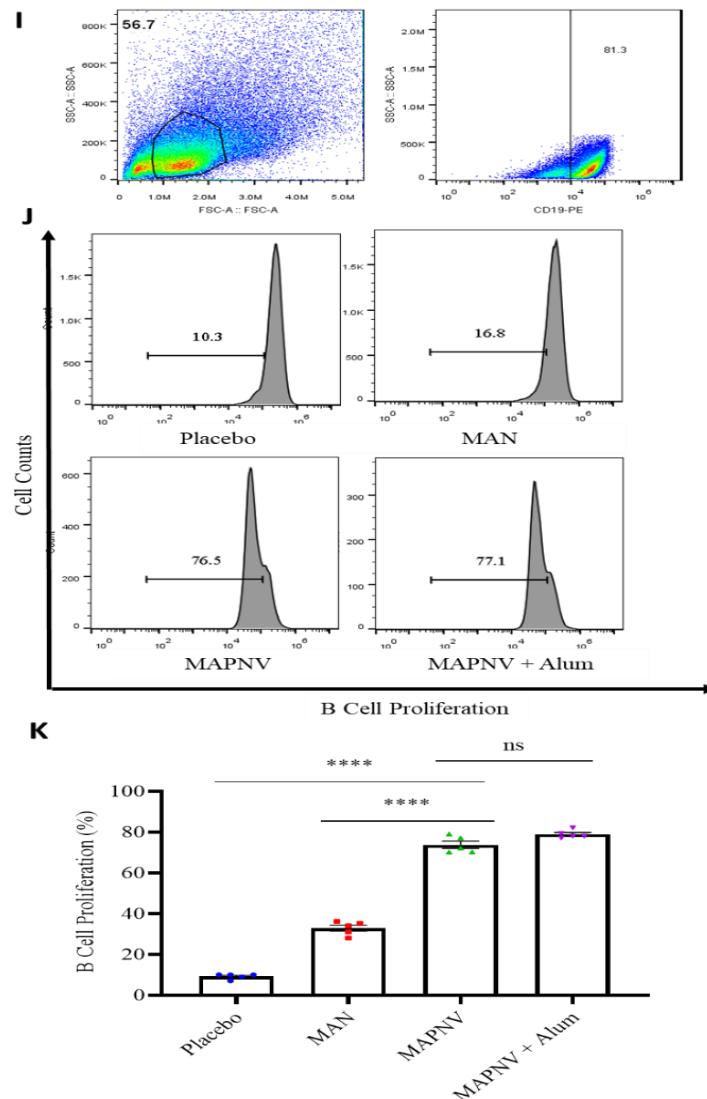


Figure 13I-K. MAPNV exhibits optimum self-adjuvanting characteristics, and supplementing with alum does not improve its efficiency in proliferating B cells. The mice were immunised with the MAPNV (20 mg/kg bwt) and MAPNV (20 mg/kg bwt) + alum on days 0 and 7. Later, morphine (10 mg/kg bwt) was administered from days 12 to 45. On day 46, the mice were sacrificed. The splenocytes were isolated, labelled with CFSE and cultured with MAPNV (20 µg/ml) for 72 h. The graph represents the gating strategies for (I) CD19⁺ B cells (anti-CD19-PE). The flow cytometry histograms and their descriptive bar diagrams signify the proliferation of (J) CD19⁺ B cells. The animals inoculated with placebo (PBS), MAN, and MAPNV + alum was taken as controls. The data are from 3 independent experiments. Each dot represents one animal. The statistical analysis was done using One-Way ANOVA. Data (%) are denoted as mean \pm SD. **** $p < 0.0001$, ns= non-significant.

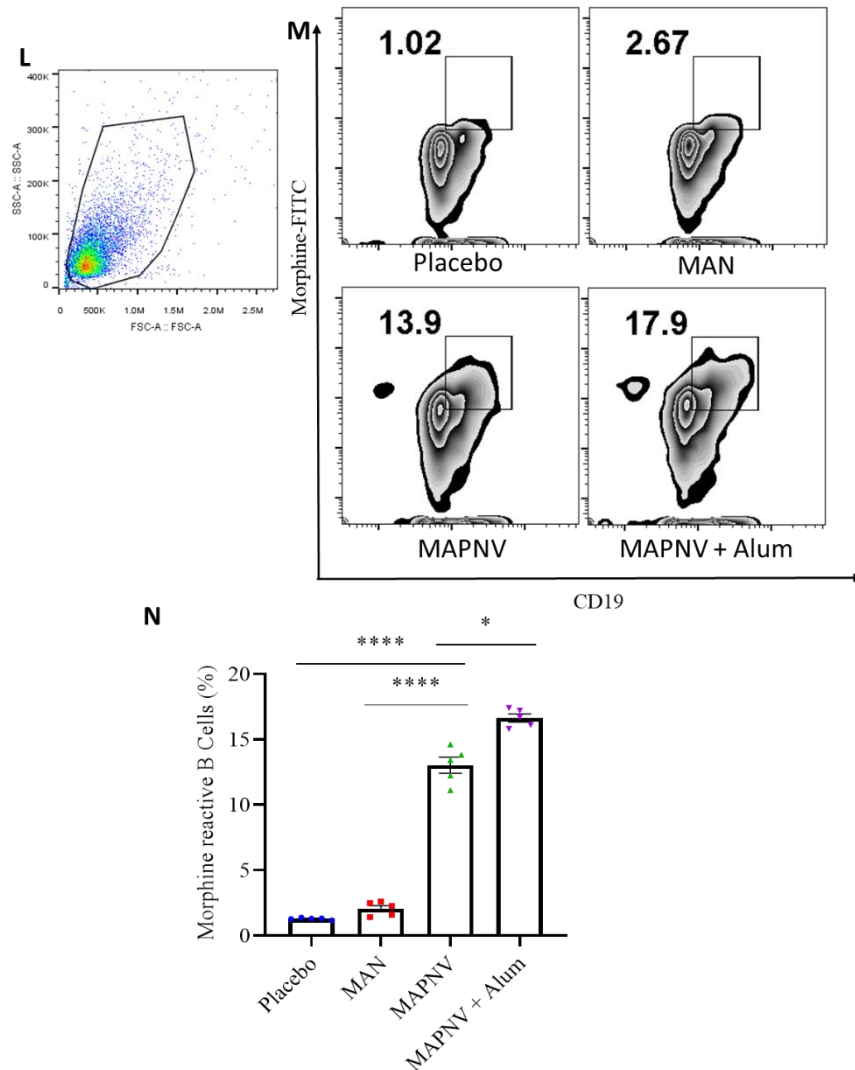
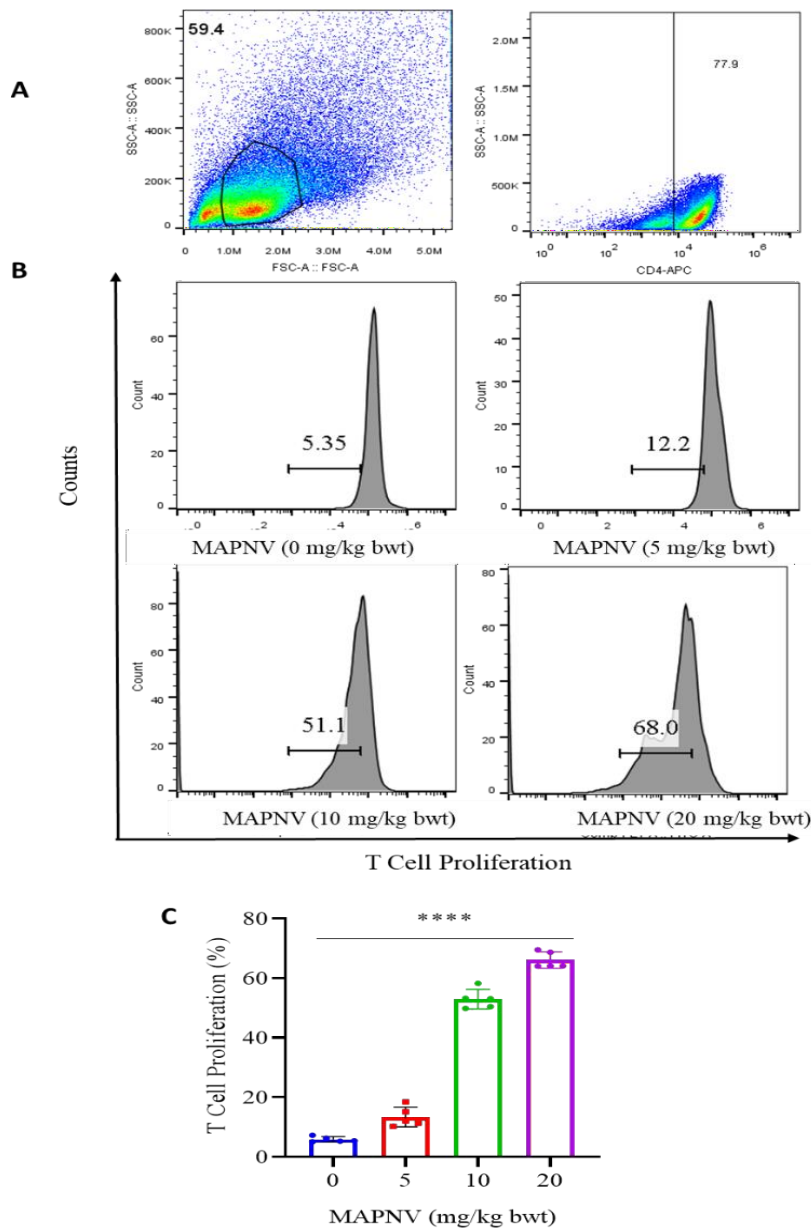


Figure 13L-N. MAPNV expands the pool of morphine-reactive B cells in vaccinated animals. The mice were immunised with the MAPNV (20 mg/kg bwt) on days 0 and 7. Later, morphine (10 mg/kg bwt) was administered from days 12 to 45. On day 46, the mice were sacrificed. The splenocytes were isolated and challenged *in vitro* with MAPNV (10 μ g/ml) for 72 h. Next, the cells were incubated with morphine-FITC for 4 h and anti-CD19 Abs (anti-CD19-PE) and analysed through flow cytometry for the presence of morphine-reactive B cells. (L) Gating of CD19⁺ B cells. (M-N) The contour plots and bar diagram depict the percentage of CD19⁺ morphine-reactive B cells. The animals inoculated with placebo (PBS), MAN and MAPNV + alum were taken as controls. The data are from 3 independent experiments. Each dot represents one mouse. The statistical analysis was performed using a One-Way ANOVA test. The data (%) are represented as mean \pm SD. **p<0.01; ****p<0.0001, ns = non-significant.

4.14 *Immunization with MAPNV does not require any exogenous adjuvant and induces optimum proliferation, differentiation and generation of CD4 T cells memory cells.* This study sought to evaluate the ability of an adjuvant-free vaccine utilizing MAPNV to induce proliferation, differentiation, and generation of CD4 T cell memory cells. To address this, the study compared the immune responses to an adjuvant-free MAPNV vaccine in mice to those of mice receiving an adjuvanted vaccine and control mice. The animals were administered MAPNV as mentioned in Fig. 13. We observed the proliferation ($p < 0.0001$) of the Acr1-specific CD4⁺ T cell in a dose-dependent fashion (Fig. 14A-C), as compared to the PBS (placebo) control group. Further, vaccination with MAPNV showed a substantially higher yield of (i) TNF- α ($p < 0.0001$), (ii) IL-4 ($p < 0.0001$), (iii) IL-6 ($p < 0.0001$), and (iv) IFN- γ ($p < 0.0001$) compared to the control placebo group (Fig. 14D), suggesting the presence of both Th1 cells and Th2 cells. Furthermore, MAPNV induced a significantly higher ($p < 0.0001$) generation of CD44^{hi}CD62^{hi} memory CD4 T cells, as compared to placebo (PBS) (Fig. 14E-G).

Like B cells, we could not notice any augmentation in the proliferation, differentiation or memory CD4 T cell generation of CD4 T cells in the group administered with MAPNV+ alum compared to MAPNV (Fig. 14H-J). These results support that MAPNV has enough adjuvant properties to evoke the activation of CD4 T cells. However, significant ($p < 0.001$) change was perceived in the MAPNV versus control MAN (without Pam3Cys) groups. The gating strategies of CD4 T cells are depicted in the figures (Fig. 14A, E, H). The CD4 T cell results validate the B cells data that MAPNV has self-adjuvanting properties and does not need any extrinsic adjuvant.



*Figure 14A-C. MAPNV induce the proliferation of Acr1-specific T cells in vaccinated mice. The mice were immunised with MAPNV (0-20 mg/kg bwt) on day 0 and day 7. Twelve days post initial vaccination; the animals were sacrificed, splenocytes were isolated, labelled with cell proliferation dyes, and *in vitro* challenged with MAPNV for 72 h. Flow cytometry graphs (A) denote the gating strategy for CD4⁺ T cells. The proliferation was assessed by (B) CFSE dye-dilution assay for CD4 T cells with anti-CD4-APC Abs). The bar graphs (C) show the mean CD4⁺ T cell proliferation. The flow-cytometry histogram and bar diagrams are from 3 independent experiments. Each dot represents one mouse. The Two-Tailed test was performed for the statistical analysis. The data (%) are expressed as mean \pm SD. **** p <0.0001.*

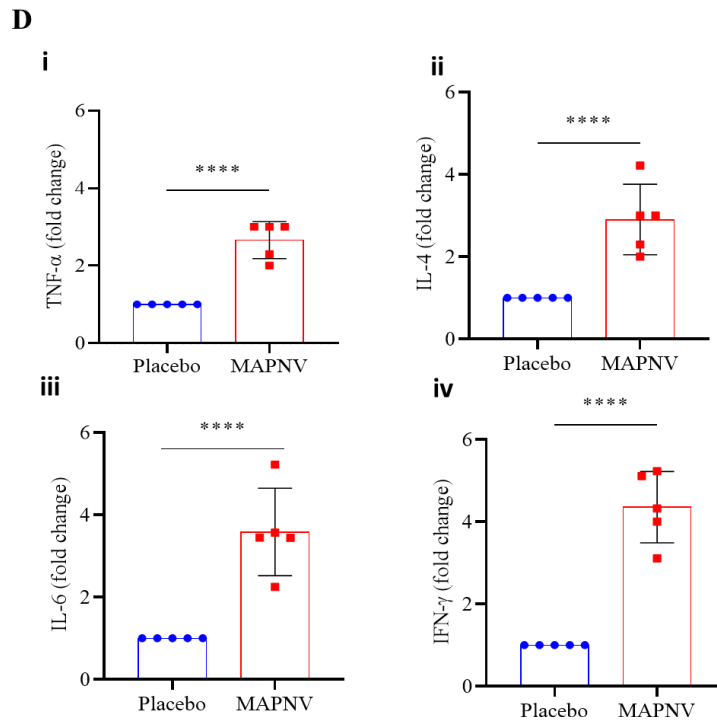
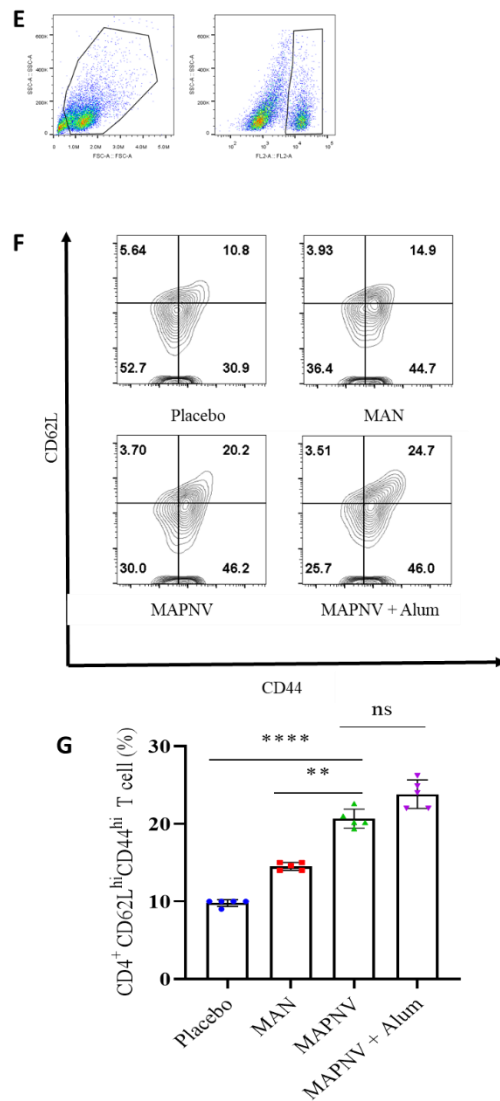


Figure 14D. MAPNV induces the production of pro-inflammatory cytokines in immunized mice. The mice were immunised with the MAPNV (20 mg/kg bwt) on days 0 and 7. Later, RNA was isolated from the splenocytes, and RT-qPCR was performed to monitor the expression of (i) TNF- α ; (ii) IL-4; (iii) IL-6; (iv) IFN- γ . The PBS (placebo) group was taken as a control. The results are from five independent experiments, and each dot represents one animal. The data (fold change) analysed by a One-Way ANOVA are denoted as mean \pm SD. **** $p < 0.0001$.



*Figure 14E-G. The MAPNV induces the generation of memory T cells in vaccinated animals. The mice were immunised with the MAPNV (20 mg/kg bwt) on days 0 and 7. Later, morphine (10 mg/kg bwt) was administered from days 12 to 45. On day 46, the mice were sacrificed. The splenocytes were isolated, labelled with efluor and in vitro challenged with MAPNV (20 µg/ml) for 72 h. (E) The graph represents the gating strategies for CD4⁺ T cells. (F-G) The flow cytometry histograms and their expressive bar diagrams suggest the expression of central memory CD4⁺ T cell markers CD44^{hi}CD62L^{hi}. The animals injected with placebo (PBS), MAN and MAPNV + alum was taken as controls. The results are from 3 independent experiments. Each dot indicates one mouse. The statistical analysis was performed using a One-Way ANOVA test. The data (%) are represented as mean ± SD. **p<0.01, ***p<0.001, ns=non-significant.*

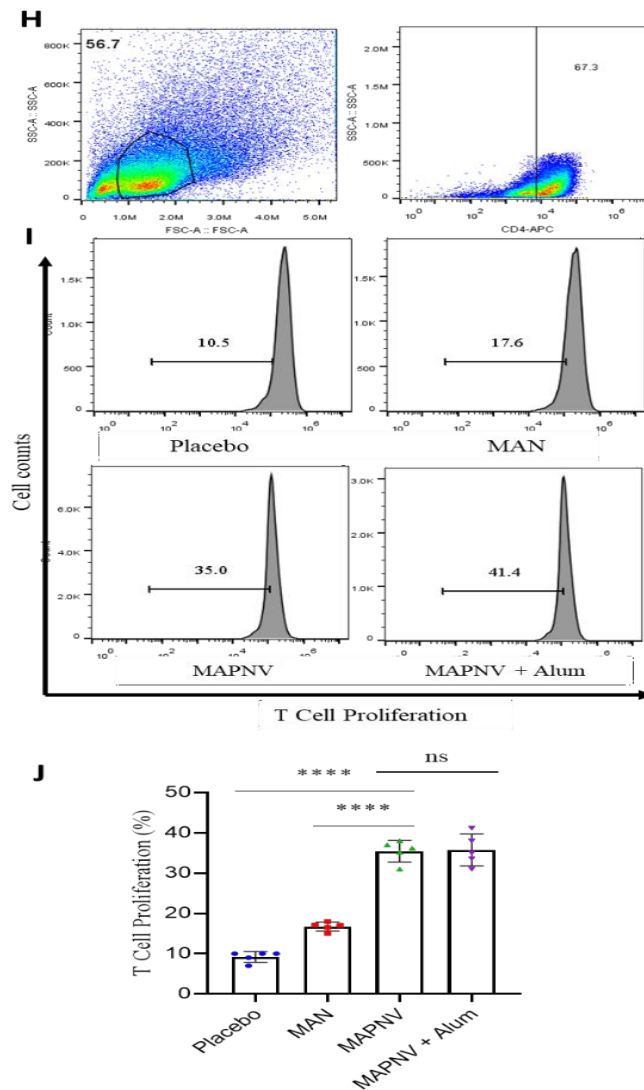


Figure 14H-J. MAPNV exhibits optimum self-adjuvanting characteristics, and supplementing with alum does not improve its efficiency in proliferating T cells. The mice were immunised with the MAPNV (20 mg/kg bwt) and MAPNV (20 mg/kg bwt) + alum on days 0 and 7. Later, morphine (10 mg/kg bwt) was administered from days 12 to 45. On day 46, the mice were sacrificed. The splenocytes were isolated, labelled with CFSE and cultured with MAPNV (20 µg/ml) for 72 h. The graph represents the gating strategies for (H) CD4⁺ T cells. The flow cytometry histograms and their descriptive bar diagrams signify the proliferation of (I-J) CD4⁺ T cells by CFSE dye-dilution assay. The animals inoculated with placebo (PBS), MAN, and MAPNV + alum was taken as controls. The results are from 3 independent experiments. Each dot represents one animal. The statistical analysis was done using One-Way ANOVA. Data (%) are denoted as mean ± SD. ****p<0.0001, ns= non-significant.

4.15 MAPNV effectively activated macrophage function suppressed due to regular exposure to morphine. This study was done to investigate if MAPNV can potentially reduce the inhibition of macrophage function caused by regular exposure to morphine. We noticed that macrophages were successfully activated by MAPNV, as evidenced by increased ($p < 0.0001$) uptake of MAPNV-FITC (Fig. 15A-C). This experiment proved that the macrophages avidly phagocytosed MAPNV and presented it to CD4 T cells (Fig. 13D, E).

The macrophage function is suppressed in people regularly administering morphine (Eisenstein et al., 2019; Liang et al., 2016). Therefore, we were curious to check whether the MAPNV can activate macrophages whose functionality is suppressed by morphine. Accordingly, we exposed macrophages to morphine (10 $\mu\text{g/ml}$) for 48 h. After that, it was incubated with MAPNV labelled with FITC (20 $\mu\text{g/ml}$) for 4 h. The control cells were cultured with FITC tagged AN and MAN. We observed no change in the uptake of MAPNV by macrophages either exposed or not to morphine (Fig. 15D, E). In contrast, remarkably lesser endocytosis was observed in the case of controls AN ($p < 0.0001$) and MAN ($p < 0.0001$). Furthermore, much higher ($p < 0.0001$) uptake of MAPNV was observed in the macrophages compared to control AN and MAN. These results infer that phagocytosis of MAPNV by macrophages is not impaired on exposure to morphine. Further, the uptake of MAPNV was substantially greater than AN or MAN due to the presence of Pam3Cys, which binds to TLR-2 and delivers a series of signalling events responsible for the activation of the cells.

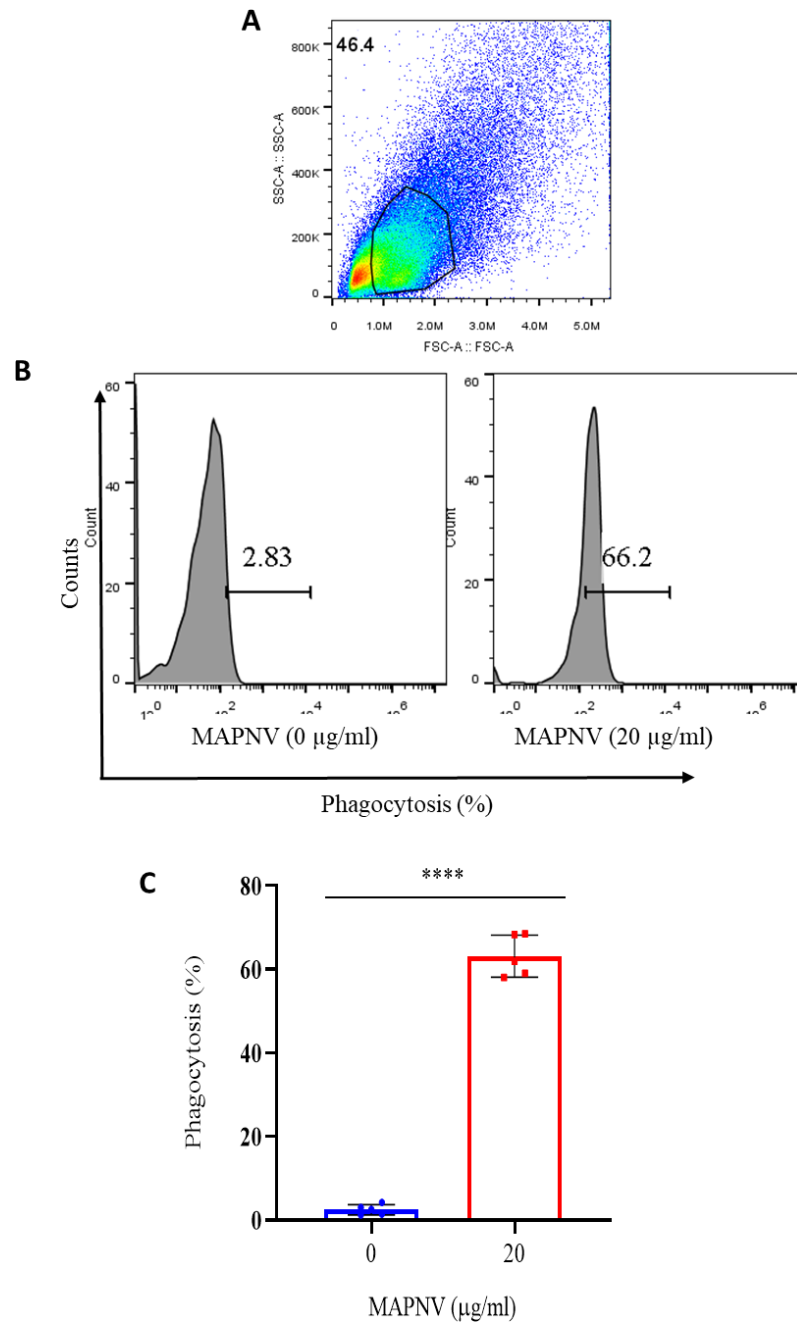
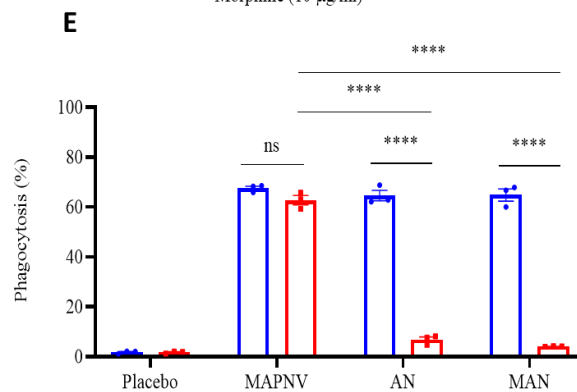
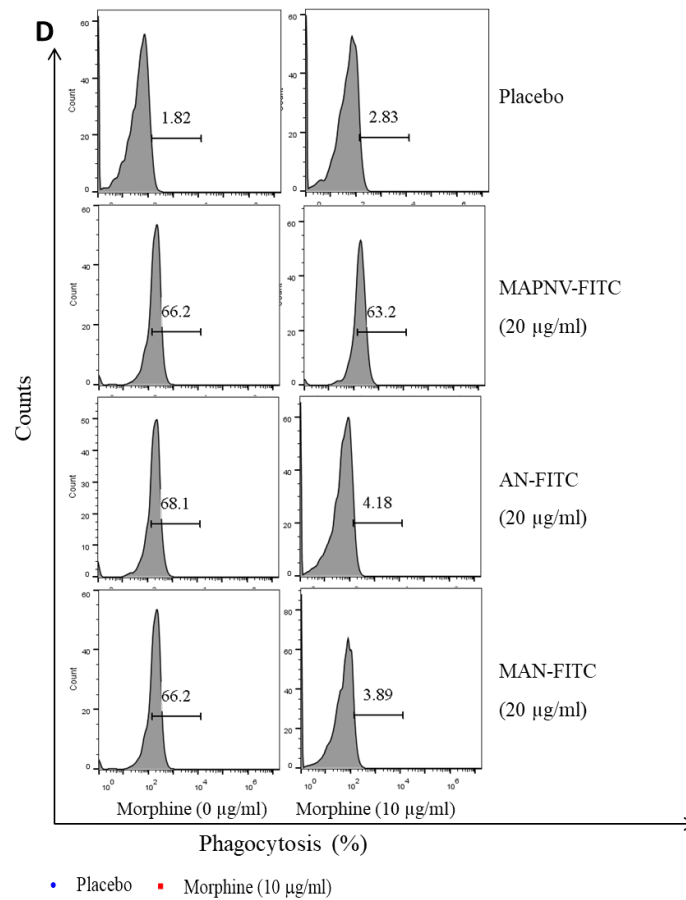
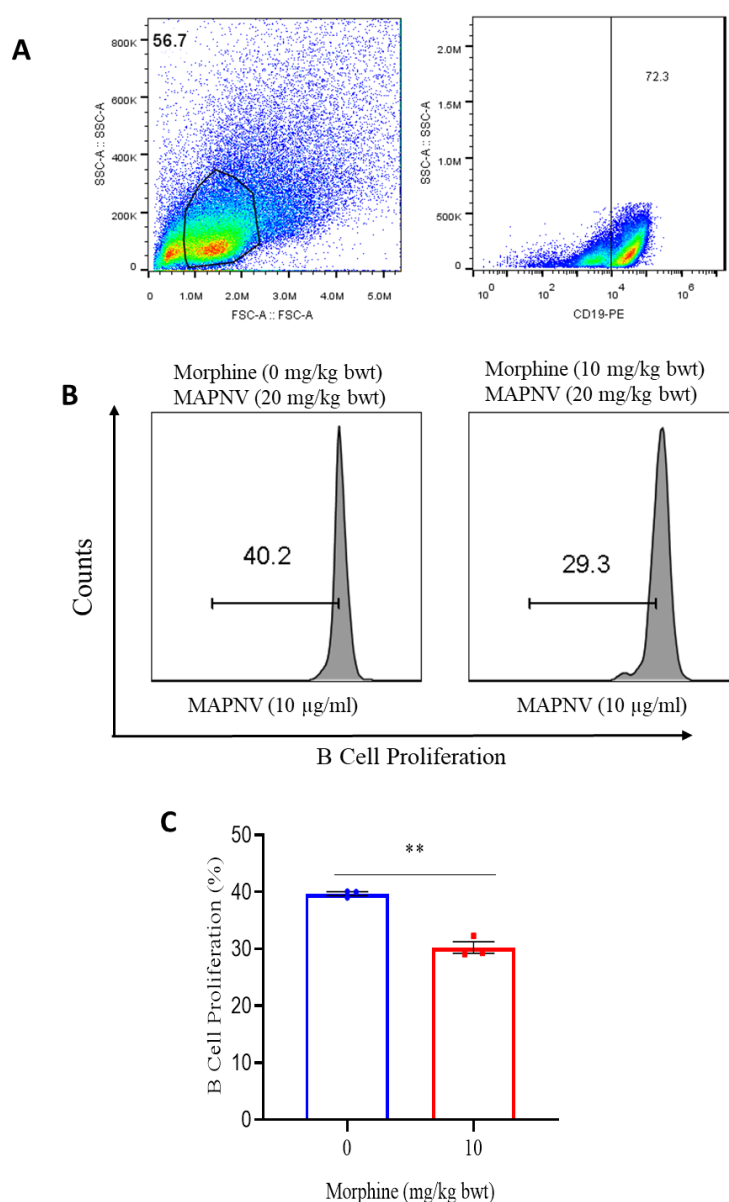


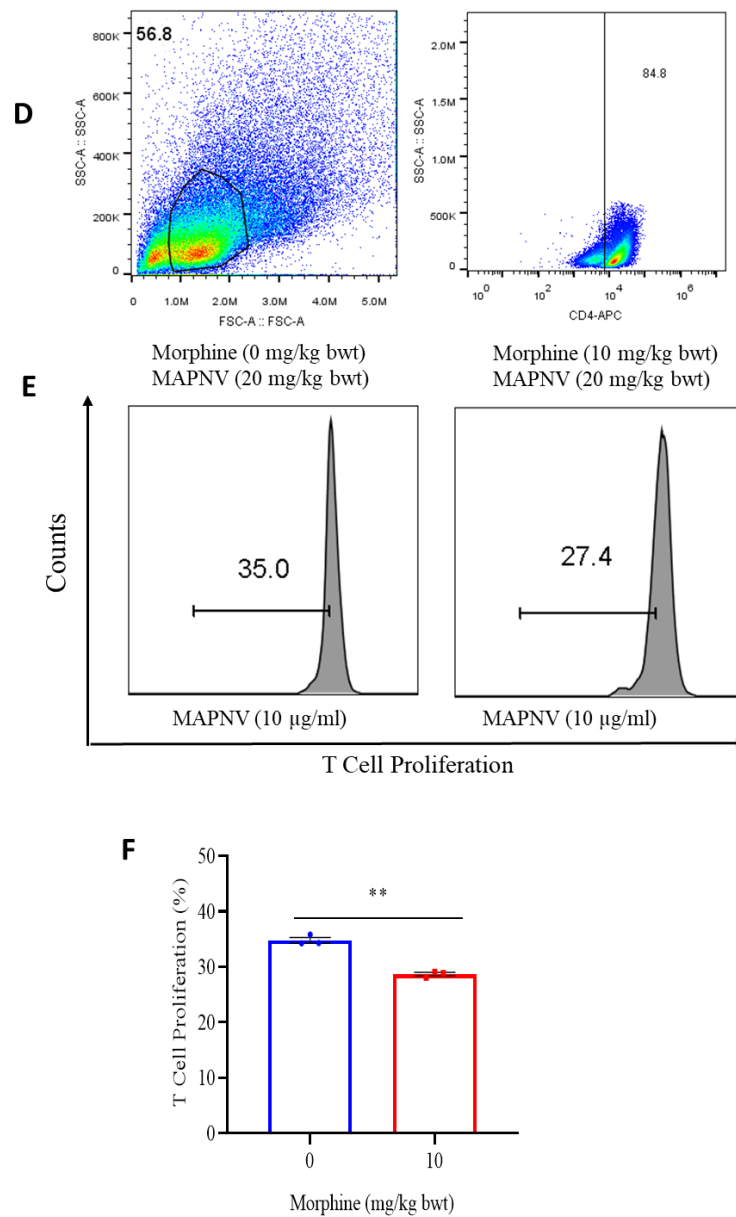
Figure 15A-C. Phagocytosis of MAPNV by macrophages. Macrophages (RAW 264.7) were incubated with MAPNV-FITC (20 µg/ml) for 4h and analysed by flow cytometry for phagocytosis. Flow cytometry data represents the (A) Gating strategy; (B) Histogram signifies phagocytosis of MAPNV. (C) The bar diagram designates the ingestion of MAPNV-FITC by the macrophages. The data are from 3 independent experiments. Each dot represents one animal. The statistical analysis was performed by a Two-Tailed test. The data (%) are shown as mean \pm SD. **** $p < 0.0001$.



*Figure 15D-E. Macrophages suppressed by morphine exposure were activated by MAPNV. Macrophages (RAW 264.7) were treated with morphine (0-10 µg/ml) for 48h. Later, these macrophages were incubated with MAPNV-FITC (20 µg/ml) for 4h. (D) The flow histograms (E) bar diagrams show the uptake of MAPNV-FITC by morphine-treated macrophages. The AN-FITC, MAN-FITC and placebo (PBS) groups were taken as controls. The data are from three independent experiments. Each dot represents one experiment. The data (%) analysed by Two-Tailed tests are expressed as mean \pm SD. **** $p < 0.0001$, ns= non-significant.*

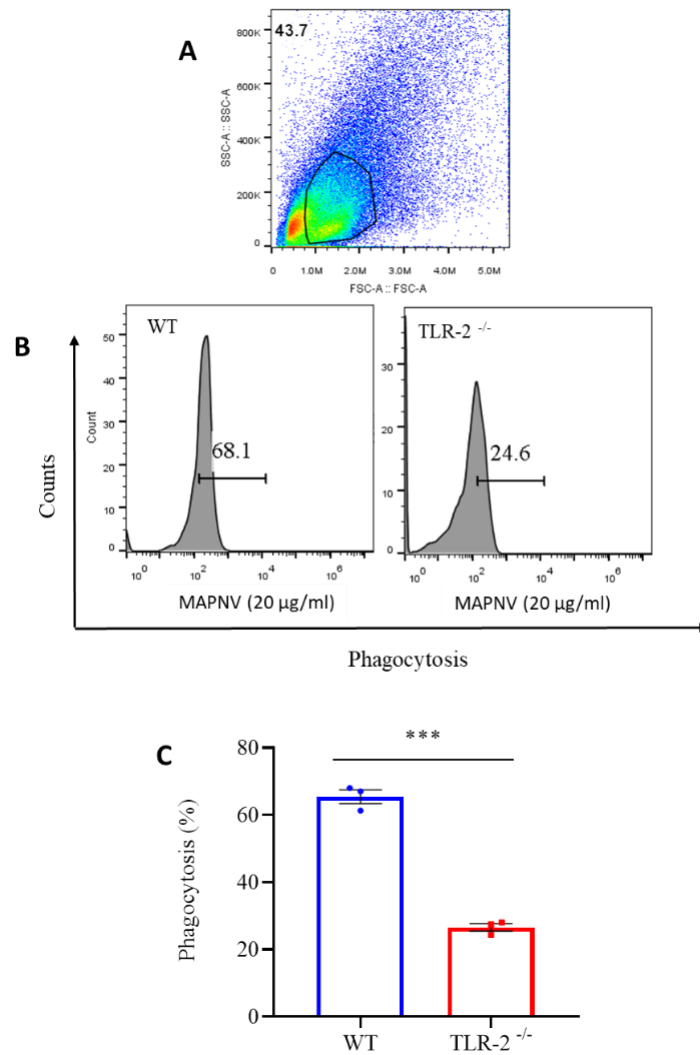
4.16 MAPNV induced the activation of B cells and T cells in the mice exposed to morphine. Drug addicts are constantly exposed to SOA, suppressing their immunity (Friedman et al., 2003). Therefore, we wanted to examine the efficacy of MAPNV in animals exposed to morphine. The mice were inoculated with morphine (10 mg/kg bwt) for 7 days before MAPNV vaccination. We noticed a significant ($p < 0.001$) proliferation of morphine-reactive B cells (Fig. 16 A-C). Likewise, we noted substantial ($p < 0.001$) proliferation of Acr1-specific CD4⁺ T cells (Fig. 16 D-F). We have also shown gating strategies for B cells (Fig. 16A) and CD4 T cells (Fig. 16D). It may be concluded that prior exposure of animals with morphine does not interfere in the performance of the MAPNV to activate B cells and CD4 T cells.

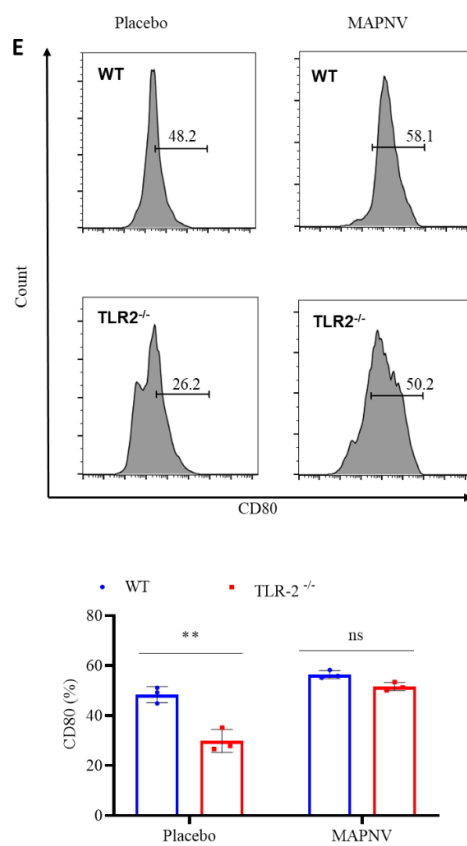
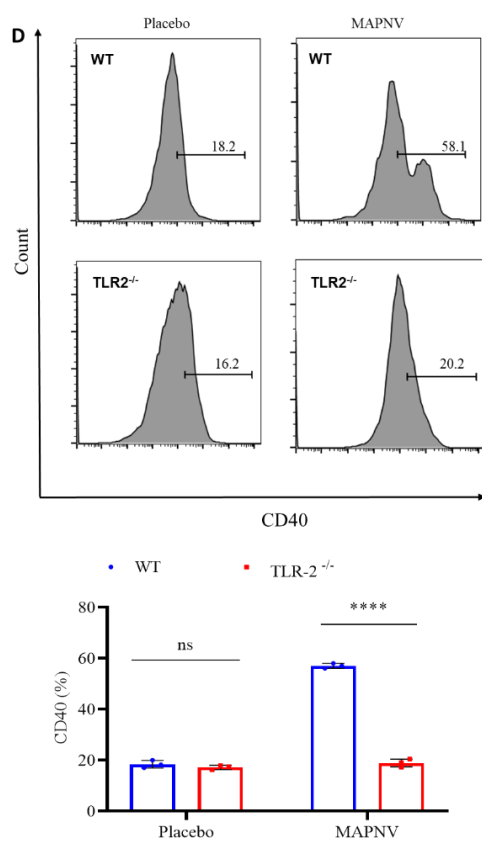




*Figure 16. Prior exposure of mice to morphine does not influence the efficacy of MAPNV to activate B and T cells. The mice were exposed to morphine (10 mg/kg bwt) for 7 days. Later, they were inoculated with MAPNV (20 mg/kg bwt). The flow cytometry graphs (A) and (D) show the gating strategies. The histograms denote the proliferation of CFSE-labelled (B) CD19⁺ B cells and (E) CD4⁺ T cells. The bar diagrams represent the (C) mean B cells proliferation (F) mean T cell proliferation. The data are from 3 independent experiments. Each dot represents one animal. The results were analysed through a Two-Tailed test. The data (%) are expressed as mean \pm SD. ***p<0.001.*

4.17 *DC endocytose MAPNV predominantly through the TLR-2 pathway.* The MAPNV expresses on its surface Pam3Cys, a ligand of TLR-2. Therefore, we wanted to investigate whether MAPNV is endocytosed mainly by the TLR-2 pathway. DCs generated from the TLR-2^{-/-} and wild-type mice were incubated with FITC labelled MAPNV and monitored for endocytosis. The DCs of the TLR-2^{-/-} mice showed a significant ($p < 0.001$) decrease in the endocytosis of MAPNV, as compared to wild-type DCs (Fig. 17 A-C). The gating strategy is shown in Fig. 16A. Further, we observed down-regulation in the expression of CD40 ($p < 0.0001$) and CD86 ($p < 0.05$) on the TLR-2^{-/-} DCs than the wild-type DCs (Fig. 17D, E). No change was noticed in the CD80 (Fig. 17F). These experiments signify that MAPNV is endocytosed primarily through the TLR-2 pathway.





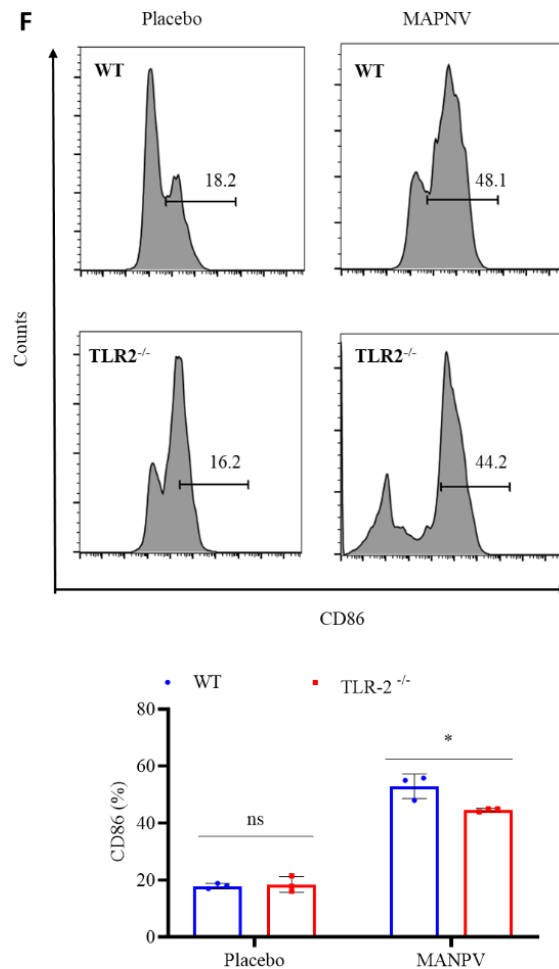


*Figure 17. Exposures of MAPNV to DCs of WT but not TLR-2^{-/-} mice show upregulation of CD40 costimulatory molecule. The DCs generated from TLR-2^{-/-} and wild-type C57BL/6 mice were incubated with MAPNV-FITC and monitored for phagocytosis by flow cytometry. (A) Dot plot show gating. (B, C) histogram and its bar diagram illustrated the mean phagocytosis of MAPNV-FITC. The flow histograms and their bar diagrams show the expression of (D) CD40; (E) CD80; (F) CD86. The data are from 3 independent experiments. Each dot represents one animal. The statistical analysis was performed through the Two-Tailed test. The data (%) are expressed as mean \pm SD. ** $p < 0.01$, *** $p < 0.001$, **** $p < 0.0001$, ns=non-significant.*

4.18 *MAPNV vaccination downregulates the expression of OPRM and dopamine genes.* In this study, we investigated how MAPNV vaccination affects the expression of OPRM and dopamine genes. Morphine causes the brain to release dopamine, the feel-good neurotransmitter. This ignites the reward system, encouraging repeated use of morphine by causing cravings. To do this, we used a mouse model and assessed gene expression using quantitative RT-PCR. We observed that the MAPNV-vaccinated mice, on exposure to morphine, significantly ($p < 0.0001$) downregulated the expression of OPRM and dopamine receptors gene, as compared to the unvaccinated groups (Fig. 18A-B). Therefore, suggesting the effectiveness of MAPNV in blocking the binding of morphine to OPRM and dopamine receptors. This will intensely reduce the influence of morphine.

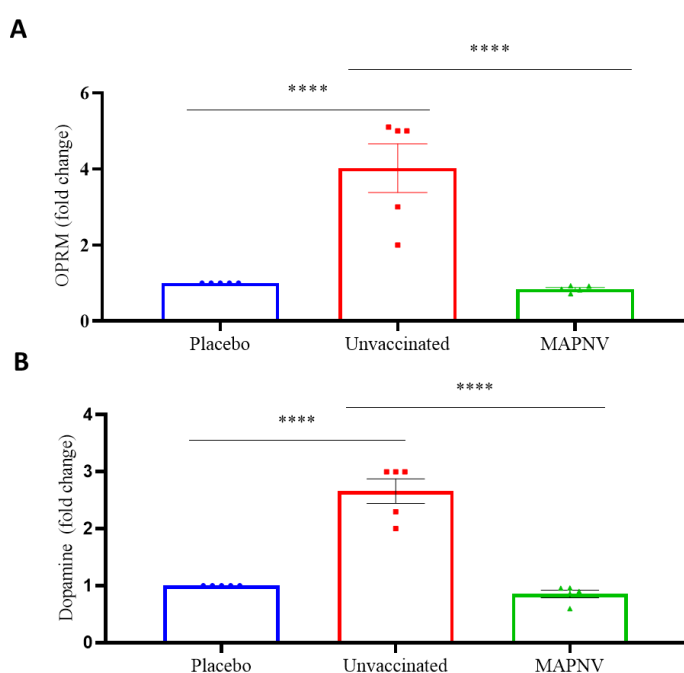
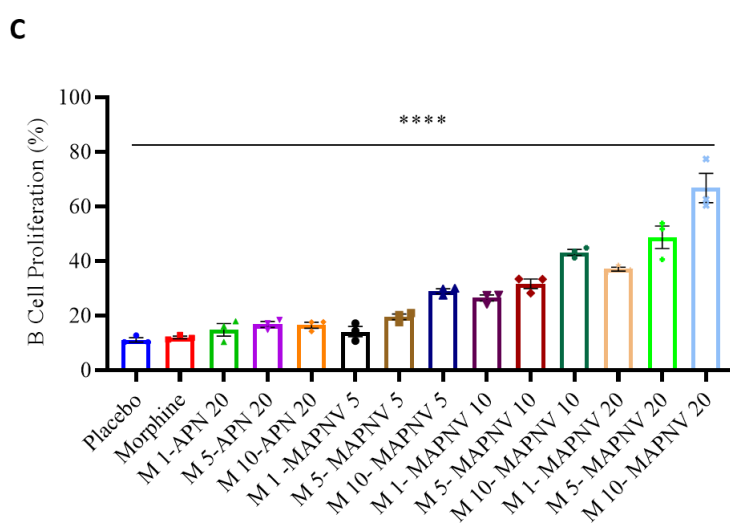
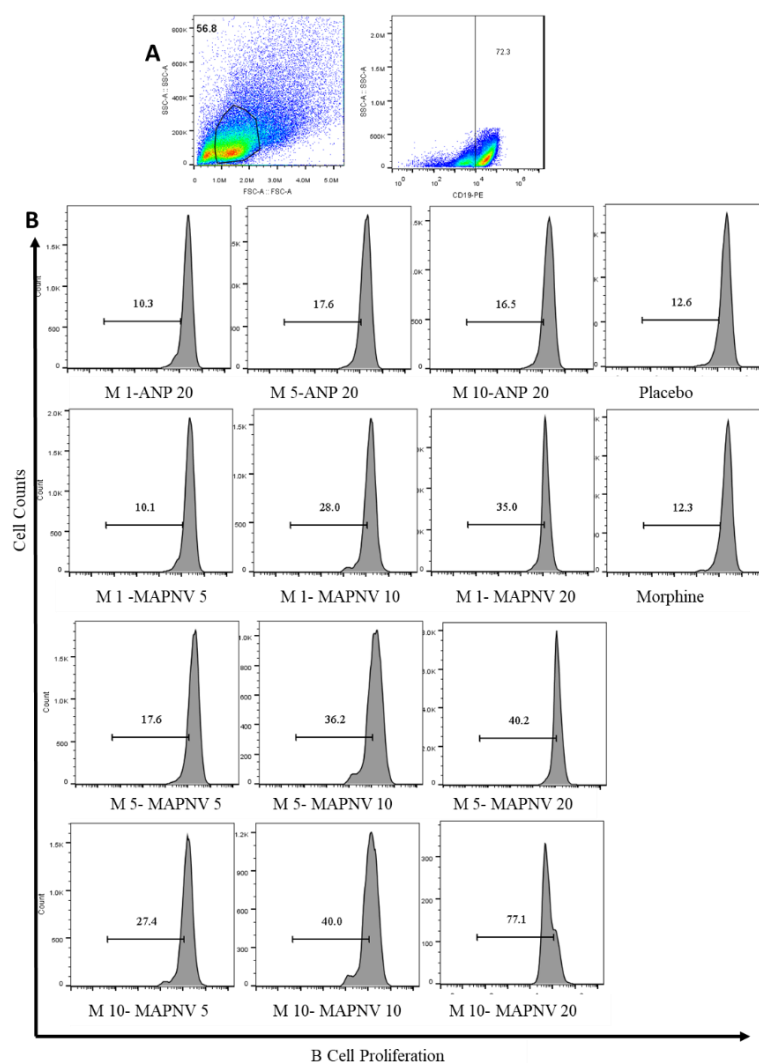
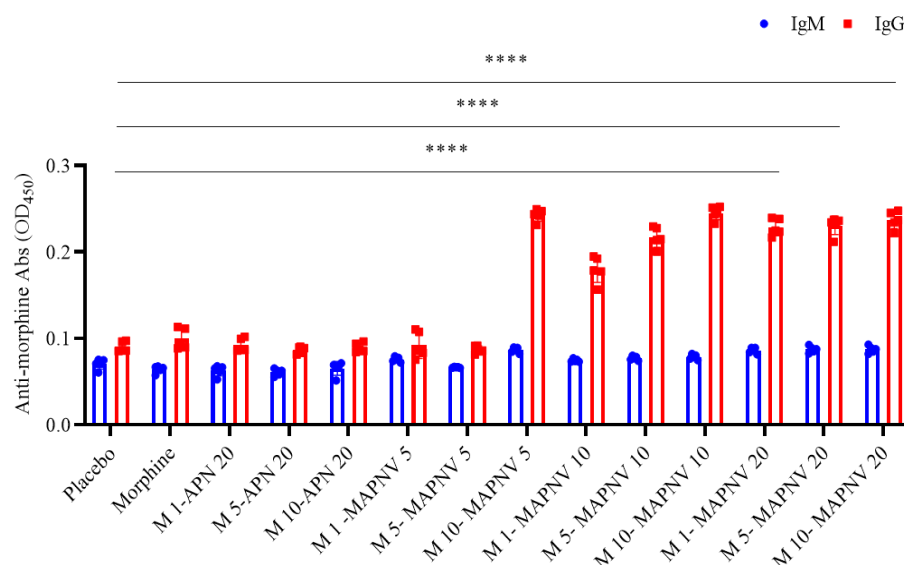


Figure 18. MAPNV inoculation downregulates the expression of addiction-associated OPRM and dopamine genes. The mice were immunised with the MAPNV (20 mg/kg bwt) on days 0 and 7. Later, they were exposed to morphine (10 mg/kg bwt) from days 12 to 45. On day 46, the mice were sacrificed. The RNA was isolated from the brains, and RT-qPCR was performed to examine the expression of (A) OPRM (B) dopamine. The unvaccinated control groups were either administered PBS (placebo) or morphine. The results are from 5 independent experiments. Each dot represents one animal. The data were analysed by One-Way ANOVA. Data (fold change) are denoted as mean \pm SD. **** $p < 0.0001$.

4.19 *MAPNV exhibited therapeutic efficacy and induced the proliferation of B cells and secretion of anti-morphine Abs that neutralised morphine in the blood and brain.* After establishing the prophylactic potential of the vaccine, we next examined its therapeutic efficiency in animals intoxicated with different doses of morphine. This study was performed to investigate the therapeutic potential of MAPNV for treating addiction. Specifically, we examined whether MAPNV could induce B cell proliferation and the secretion of anti-morphine antibodies that neutralise morphine in the blood and brain. To evaluate the efficacy of MAPNV, a laboratory mouse model was used to quantify the therapeutic effects of MAPNV on morphine addiction. Later, the mice were injected with various doses of MAPNV. We observed noteworthy ($p < 0.0001$) proliferation of B cells with 20 mg/kg bwt of MAPNV, even though the mice had prior exposure to 10 mg/kg bwt of morphine (Fig. 19A-C). Further, a significantly ($p < 0.0001$) elevated level of anti-morphine Abs in the serum of MAPNV-vaccinated groups were identified compared to the controls inoculated with placebo (PBS) or morphine (Fig. 19D). The subtypes of anti-morphine Abs were mainly of IgG but not IgM. Furthermore, anti-morphine Abs efficiently cleared the morphine from the serum ($p < 0.0001$) and brain ($p < 0.0001$) (Fig. 19E, F) of the MAPNV (20 mg/kg bwt) immunised mice, compared to the unvaccinated group. The response was observed in a dose-dependent manner. These results demonstrated the therapeutic potential of MAPNV in generating anti-morphine Abs, which exhibited the capacity to clear the morphine from the blood and brain.



D



*Figure 19A-D. MAPNV induces B cell proliferation and generates mainly IgG anti-morphine Abs upon exposure to morphine in immunised mice. The animals were injected with morphine (1, 5, 10 mg/kg bwt) from days 0 to 21. Different groups were vaccinated with MAPNV (5, 10, 20 mg/kg bwt) on days 16 and 18. On day 22, the mice were sacrificed, and splenocytes were labelled with CFSE and cultured *in vitro* with MAPNV (10 µg/ml) for 72h. The cells were examined for the proliferation of B cells through flow cytometry. The dot plots represent the gating strategies of (A) CD19⁺ B cells. Placebo: PBS, Morphine: mice inoculated with morphine (10 mg/kg bwt) for 21 days; M1-APN20: mice inoculated with morphine (1 mg/kg bwt) for 21 days and injected APN (20 mg/kg bwt); M5-APN20: mice inoculated with morphine (5 mg/kg bwt) for 21 days and injected APN (20 mg/kg bwt); M10-APN20: mice inoculated with morphine (10 mg/kg bwt) for 21 days and injected APN (20 mg/kg bwt); M1-MAPNV5: mice inoculated with morphine (1 mg/kg bwt) for 21 days and injected MAPNV (5 mg/kg bwt); M1-MAPNV10: mice inoculated with morphine (1 mg/kg bwt) for 21 days and injected MAPNV (10 mg/kg bwt); M1-MAPNV20: mice inoculated with morphine (1 mg/kg bwt) for 21 days and injected MAPNV (20 mg/kg bwt); M5-MAPNV5: mice inoculated with morphine (5 mg/kg bwt) for 21 days and injected MAPNV (5 mg/kg bwt); M5-MAPNV10: mice inoculated with morphine (5 mg/kg bwt) for 21 days and injected MAPNV (10 mg/kg bwt); M5-MAPNV20: mice inoculated with morphine (5 mg/kg bwt) for 21 days and injected MAPNV (20 mg/kg bwt); M10-MAPNV5: mice inoculated with morphine (10 mg/kg bwt) for*

[illegible]

Figure 19E-F. MAPNV clears morphine from the serum and brain. The animals were injected with morphine (1, 5, 10 mg/kg bwt) from days 0 to 21. Different groups were vaccinated on days 16 and 18 with MAPNV (5, 10, 20 mg/kg bwt). On day 22, the mice were sacrificed, and morphine in the (A) blood (B) brain was estimated using a UV-visible spectrophotometer. The

placebo (PBS), morphine (10 mg/kg bwt), and APN (20 mg/kg bwt) treated groups were used as controls. Placebo: PBS, Morphine: mice inoculated with morphine (10 mg/kg bwt) for 21 days; M1-APN20: mice inoculated with morphine (1 mg/kg bwt) for 21 days and injected APN (20 mg/kg bwt); M5-APN20: mice inoculated with morphine (5 mg/kg bwt) for 21 days and injected APN (20 mg/kg bwt); M10-APN20: mice inoculated with morphine (10 mg/kg bwt) for 21 days and injected APN (20 mg/kg bwt); M1-MAPNV5: mice inoculated with morphine (1 mg/kg bwt) for 21 days and injected MAPNV (5 mg/kg bwt); M1-MAPNV10: mice inoculated with morphine (1 mg/kg bwt) for 21 days and injected MAPNV (10 mg/kg bwt); M1-MAPNV20: mice inoculated with morphine (1 mg/kg bwt) for 21 days and injected MAPNV (20 mg/kg bwt); M5-MAPNV5: mice inoculated with morphine (5 mg/kg bwt) for 21 days and injected MAPNV (5 mg/kg bwt); M5-MAPNV10: mice inoculated with morphine (5 mg/kg bwt) for 21 days and injected MAPNV (10 mg/kg bwt); M5-MAPNV20: mice inoculated with morphine (5 mg/kg bwt) for 21 days and injected MAPNV (20 mg/kg bwt); M10-MAPNV5: mice inoculated with morphine (10 mg/kg bwt) for 21 days and injected MAPNV (5 mg/kg bwt); M10-MAPNV10: mice inoculated with morphine (10 mg/kg bwt) for 21 days and injected MAPNV (10 mg/kg bwt); M10-MAPNV20: mice inoculated with morphine (10 mg/kg bwt) for 21 days and injected MAPNV (20 mg/kg bwt). Each dot represents one animal. The data (μ M) analysed by One-Way ANOVA are expressed as mean \pm SD. *** $p < 0.001$, **** $p < 0.0001$.

4.20 MAPNV exhibited therapeutic efficacy and induced the proliferation, differentiation and generation of memory CD4 T cells. This study was conducted to examine the therapeutic efficacy of MAPNV nanoparticles in inducing the proliferation, differentiation, and generation of memory CD4 T cells. This research was conducted in order to better understand how in therapeutic mice model the MAPNV nano-vaccine works. The study utilized in vivo mouse models to assess the therapeutic efficacy of the nanoparticles. The animals were vaccinated, as mentioned in the case of B cell proliferation (Fig. 19). A significantly higher level ($p<0.0001$) of Acr1-specific CD4⁺ T cell proliferation was noted in the mice immunised with MAPNV (Fig. 20A-C). Further, we observed the augmented level of TNF- α ($p<0.0001$), IL-4 ($p<0.0001$), IL-6 ($p<0.0001$), and IFN- γ ($p<0.0001$), compared to the control placebo (PBS) group (Fig. 20D). These results indicated the presence of both Th1 cells and Th2 cells.

Furthermore, CD4⁺ T cells expressed significantly ($p<0.0001$) higher upregulation of CD44^{hi}/CD62L^{hi} markers. Thus, specifying the generation of central memory CD4⁺ T cells (Fig. 20E-G). The results suggested that MAPNV can work as a therapeutic and prophylactic vaccine. Therefore, it can help in treating patients suffering from substance abuse disorder.

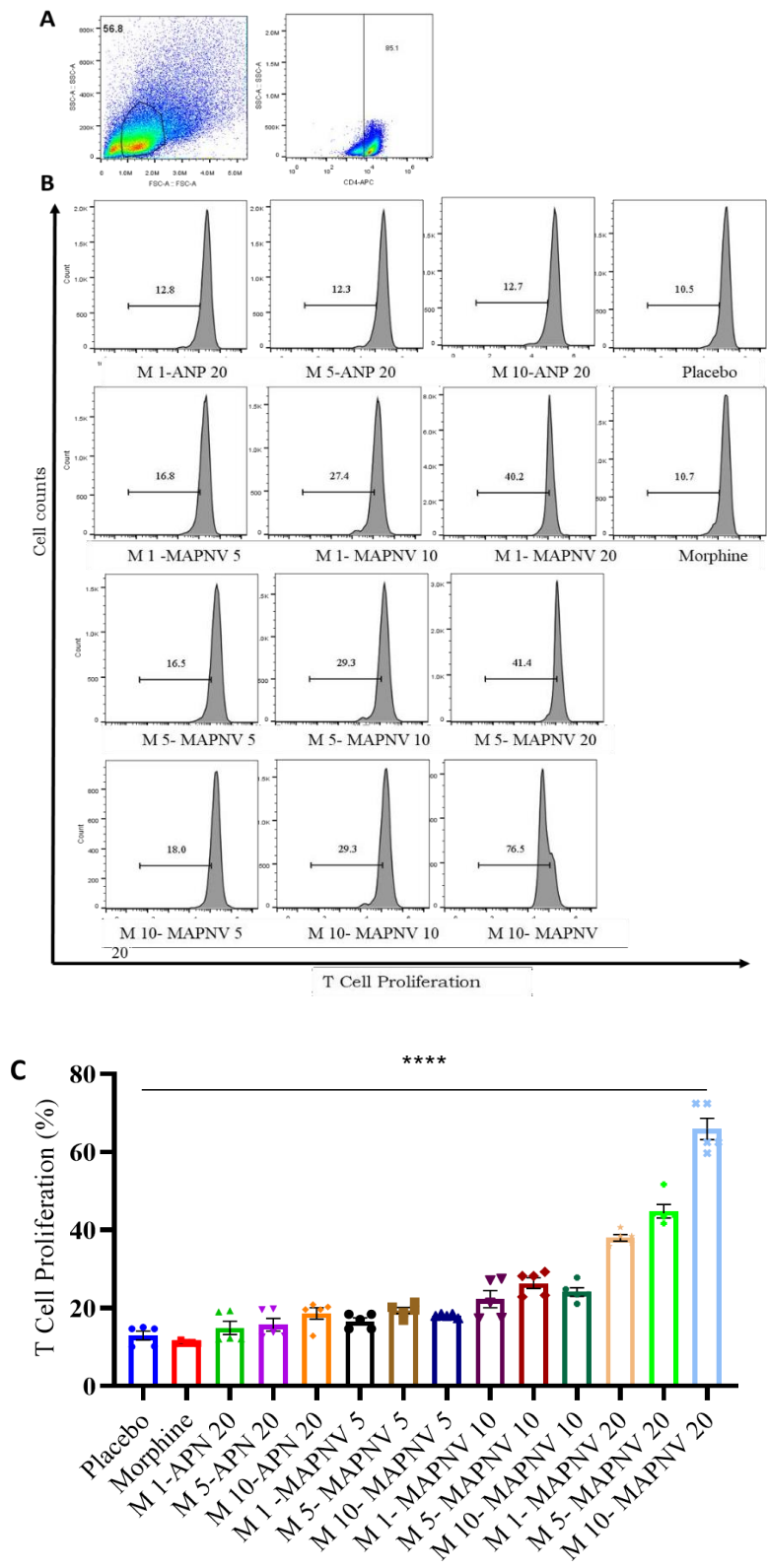


Figure 20A-C. Immunotherapy with MAPNV induces the proliferation of CD4 T cells in mice exposed to morphine. The animals were injected with morphine (1, 5, 10 mg/kg bwt) from days 0 to 21. Different groups were vaccinated with MAPNV (5, 10, 20 mg/kg bwt) on days 16 and 18. On day 22, the mice were sacrificed, and splenocytes were labelled with CFSE and cultured *in vitro* with MAPNV (10 µg/ml) for 72h. The cells were examined for the proliferation of CD4 T cells by CFSE dye-dilution assay through flow cytometry. The dot plots represent the gating strategies of (A) CD4⁺ T cells. Placebo: PBS, Morphine: mice inoculated with morphine (10 mg/kg bwt) for 21 days; M1-APN20: mice inoculated with morphine (1 mg/kg bwt) for 21 days and injected APN (20 mg/kg bwt); M5-APN20: mice inoculated with morphine (5 mg/kg bwt) for 21 days and injected APN (20 mg/kg bwt); M10-APN20: mice inoculated with morphine (10 mg/kg bwt) for 21 days and injected APN (20 mg/kg bwt); M1-MAPNV5: mice inoculated with morphine (1 mg/kg bwt) for 21 days and injected MAPNV (5 mg/kg bwt); M1-MAPNV10: mice inoculated with morphine (1 mg/kg bwt) for 21 days and injected MAPNV (10 mg/kg bwt); M1-MAPNV20: mice inoculated with morphine (1 mg/kg bwt) for 21 days and injected MAPNV (20 mg/kg bwt); M5-MAPNV5: mice inoculated with morphine (5 mg/kg bwt) for 21 days and injected MAPNV (5 mg/kg bwt); M5-MAPNV10: mice inoculated with morphine (5 mg/kg bwt) for 21 days and injected MAPNV (10 mg/kg bwt); M5-MAPNV20: mice inoculated with morphine (5 mg/kg bwt) for 21 days and injected MAPNV (20 mg/kg bwt); M10-MAPNV5: mice inoculated with morphine (10 mg/kg bwt) for 21 days and injected MAPNV (5 mg/kg bwt); M10-MAPNV10: mice inoculated with morphine (10 mg/kg bwt) for 21 days and injected MAPNV (10 mg/kg bwt); M10-MAPNV20: mice inoculated with morphine (10 mg/kg bwt) for 21 days and injected MAPNV (20 mg/kg bwt). The histogram and bar diagrams illustrate the proliferation of (B, C) CD4⁺ T cells. The placebo (PBS), morphine (10 mg/kg bwt), and APN (20 mg/kg bwt) treated groups were taken as control. Each dot represents one animal. The data (%) analysed by One-Way ANOVA are represented as mean ± SD. ****p<0.0001.

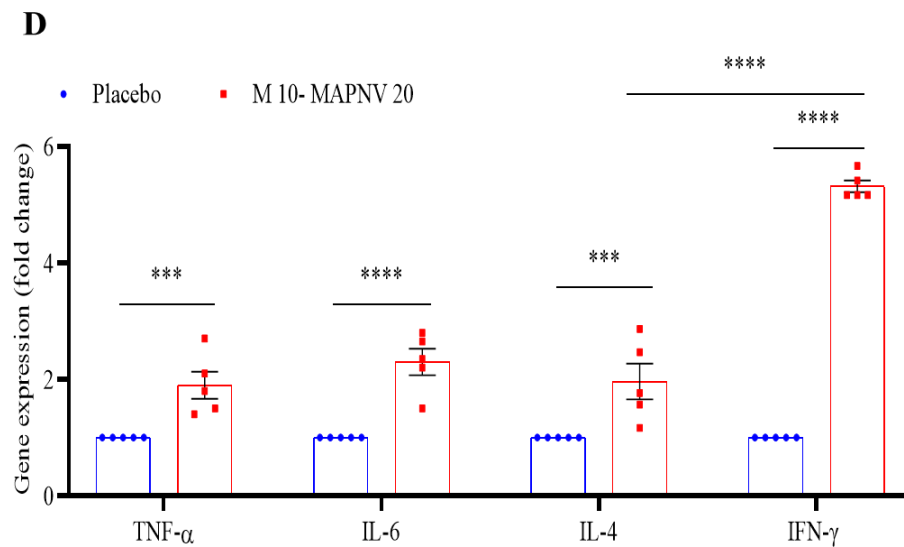


Figure 20D. MAPNV induces the production of pro-inflammatory cytokines. The animals were injected with morphine (10 mg/kg bwt) from days 0 to 21. On days 16 and 18, mice were vaccinated with MAPNV (20 mg/kg bwt). On day 22, the mice were sacrificed. The RNA was isolated from splenocytes, and RT-qPCR was performed to quantify cytokines. The placebo (PBS) group was taken as a control. Each dot represents one animal. The data (fold change) analysed by One-Way ANOVA are represented as mean \pm SD. *** $p < 0.001$, **** $p < 0.0001$. Placebo: PBS; M10-MAPNV20: mice inoculated with morphine (10 mg/kg bwt) for 21 days and injected MAPNV (20 mg/kg bwt).

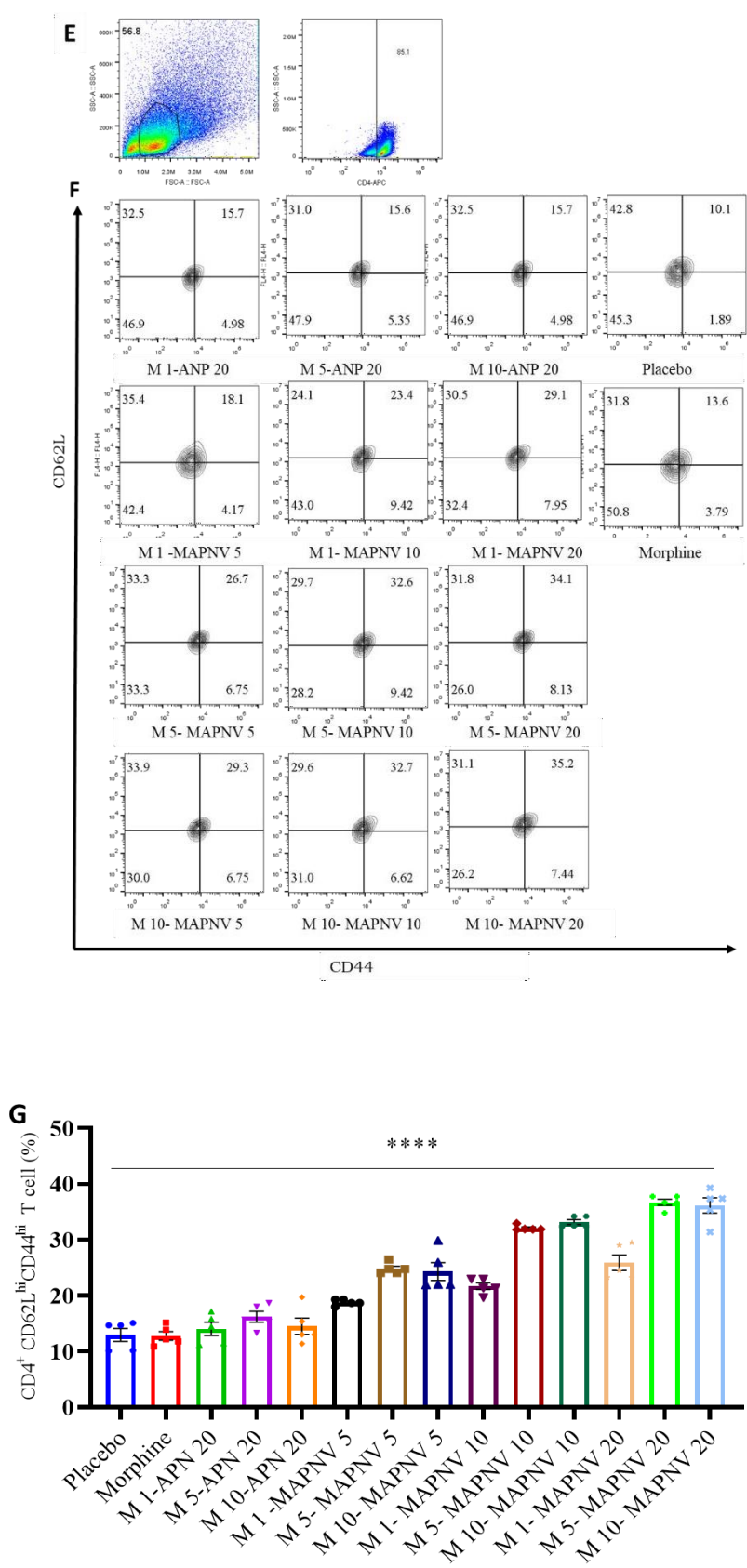


Figure 20E-G. MAPNV induces the generation of memory CD4 T cells in mice exposed to morphine. The animals were injected with morphine (1, 5, 10 mg/kg bwt) from days 0 to 21. Different groups were vaccinated on days 16 and 18 with MAPNV (5, 10, 20 mg/kg bwt). On day 22, the mice were sacrificed, and splenocytes were cultured with MAPNV (10 µg/ml) for 72h. The cells were examined for the expression of central memory CD4 T cell markers CD44^{hi}CD62L^{hi}. The dot plots represent the gating strategies of (E) CD4⁺ T cells. (F, G) The histogram and bar diagrams illustrate the expression of CD44^{hi} and CD62L^{hi} on CD4⁺ T cells. The placebo (PBS), morphine (10 mg/kg bwt), and APN (20 mg/kg bwt) treated groups were used as controls. Placebo: PBS, Morphine: mice inoculated with morphine (10 mg/kg bwt) for 21 days; M1-APN20: mice inoculated with morphine (1 mg/kg bwt) for 21 days and injected APN (20 mg/kg bwt); M5-APN20: mice inoculated with morphine (5 mg/kg bwt) for 21 days and injected APN (20 mg/kg bwt); M10-APN20: mice inoculated with morphine (10 mg/kg bwt) for 21 days and injected APN (20 mg/kg bwt); M1-MAPNV5: mice inoculated with morphine (1 mg/kg bwt) for 21 days and injected MAPNV (5 mg/kg bwt); M1-MAPNV10: mice inoculated with morphine (1 mg/kg bwt) for 21 days and injected MAPNV (10 mg/kg bwt); M1-MAPNV20: mice inoculated with morphine (1 mg/kg bwt) for 21 days and injected MAPNV (20 mg/kg bwt); M5-MAPNV5: mice inoculated with morphine (5 mg/kg bwt) for 21 days and injected MAPNV (5 mg/kg bwt); M5-MAPNV10: mice inoculated with morphine (5 mg/kg bwt) for 21 days and injected MAPNV (10 mg/kg bwt); M5-MAPNV20: mice inoculated with morphine (5 mg/kg bwt) for 21 days and injected MAPNV (20 mg/kg bwt); M10-MAPNV5: mice inoculated with morphine (10 mg/kg bwt) for 21 days and injected MAPNV (5 mg/kg bwt); M10-MAPNV10: mice inoculated with morphine (10 mg/kg bwt) for 21 days and injected MAPNV (10 mg/kg bwt); M10-MAPNV20: mice inoculated with morphine (10 mg/kg bwt) for 21 days and injected MAPNV (20 mg/kg bwt). Each dot represents one animal. The data (%) analysed by One-Way ANOVA are expressed as mean ± SD. ****p<0.0001.

4.21 *Immunotherapy with MAPNV downregulates the expression of addiction-associated OPRM and dopamine genes.* The effect of immunotherapy with MAPNV on the expression of addiction-associated genes related to OPRM and dopamine was examined to examine the therapeutic efficacy of the vaccine better. To achieve this, gene expression levels in placebo and MAPNV vaccinated were measured using quantitative real-time PCR. The animals exposed to morphine were later treated with MAPNV. As observed in the case of prophylactic vaccination, similar results were noticed in the downregulation of the expression of both OPRM and dopamine genes on changing the MAPNV immunisation strategy to a therapeutic approach (Fig. 21A, B). These results demonstrated that MAPNV effectively reduced ($p < 0.0001$) the expression of addiction-associated genes and, therefore, can be used as a therapeutic agent to treat people inflicted with addiction.

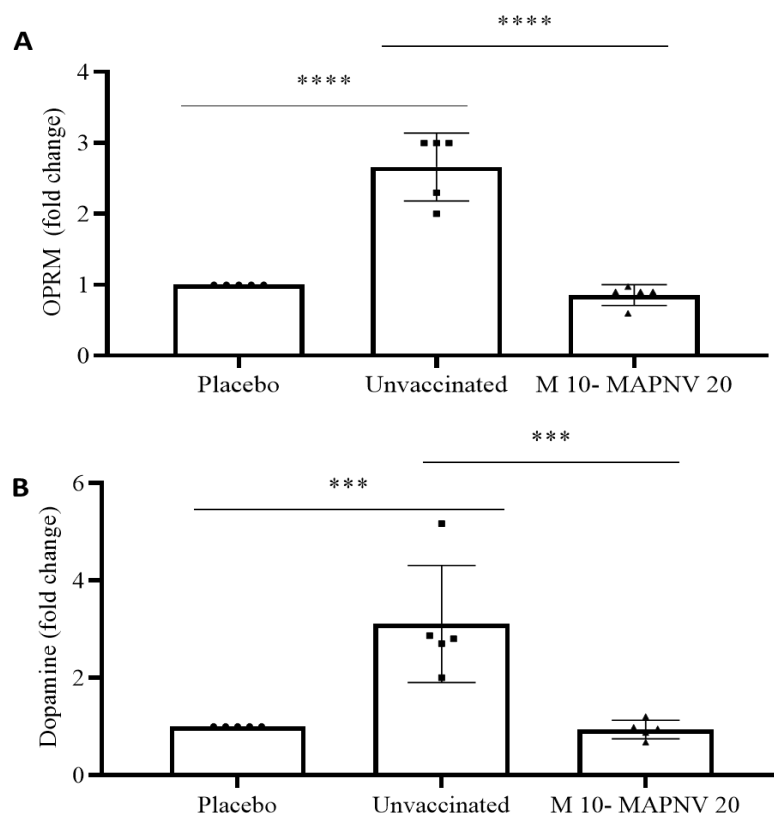
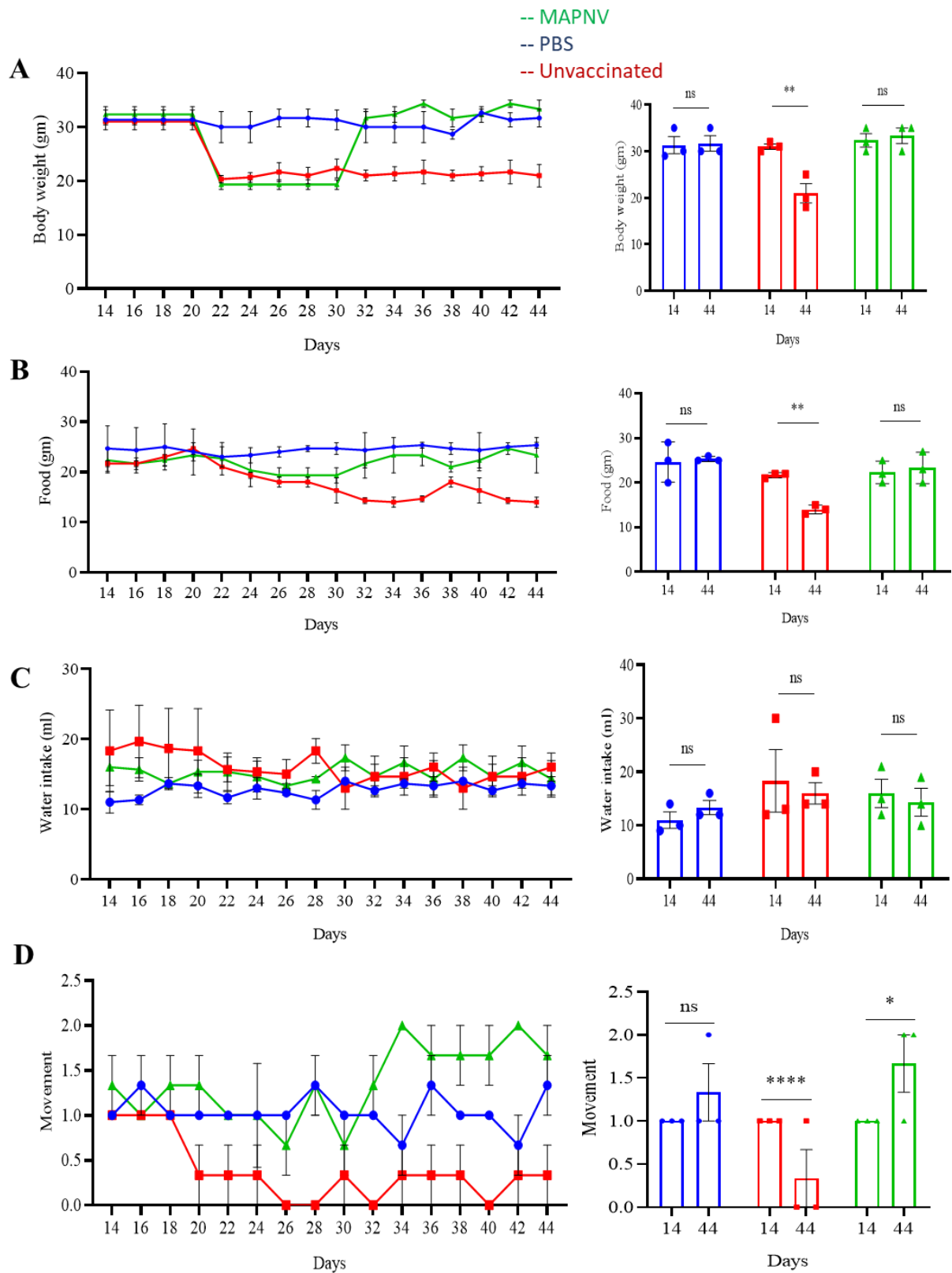


Figure 21. Immunotherapy with MAPNV downregulates the expression of addiction-associated genes OPRM and dopamine. The animals were injected with morphine (10 mg/kg bwt) from days 0 to 21. On days 16 and 18, mice were vaccinated with MAPNV (20 mg/kg bwt). On day 22, the mice were sacrificed. The RNA was isolated from splenocytes, and RT-qPCR was performed to quantify (A) OPRM and (B) dopamine genes. The placebo group was taken as a control. Placebo: PBS, Morphine: mice inoculated with morphine (10 mg/kg bwt) for 21 days; M10-MAPNV20: mice inoculated with morphine (10 mg/kg bwt) for 21 days and injected MAPNV (20 mg/kg bwt). Each dot represents one animal. The data were analysed by One-Way ANOVA. The data (fold change) are expressed as mean \pm SD. *** $p < 0.001$, **** $p < 0.0001$.

4.22 MAPNV-vaccinated mice on exposure to morphine do not show a change in their behaviour. The study was done to investigate whether exposure to morphine would change the behaviour of mice vaccinated with MAPNV to determine whether the vaccine could protect them from the effects of morphine. To answer this question, an experiment was conducted in which vaccinated and non-vaccinated mice were exposed to morphine and their behaviour was observed and compared. The animals inoculated with MAPNV did not change their body weight, food and water intake, or dark-seeking behaviour (Fig. 22A-C, F). Further, the MAPNV-vaccinated animals showed an active state towards movements ($p<0.05$) and sensitivity to heat ($p<0.0001$) (Fig. 22D, E). Significantly, the behaviour of the vaccinated animals was not changed with the exposure to morphine (Fig. 22A-C, F). This suggests the efficacy of MAPNV in neutralising the influence of morphine on the behaviour of the animals. The placebo group did not show a difference in their behaviours.



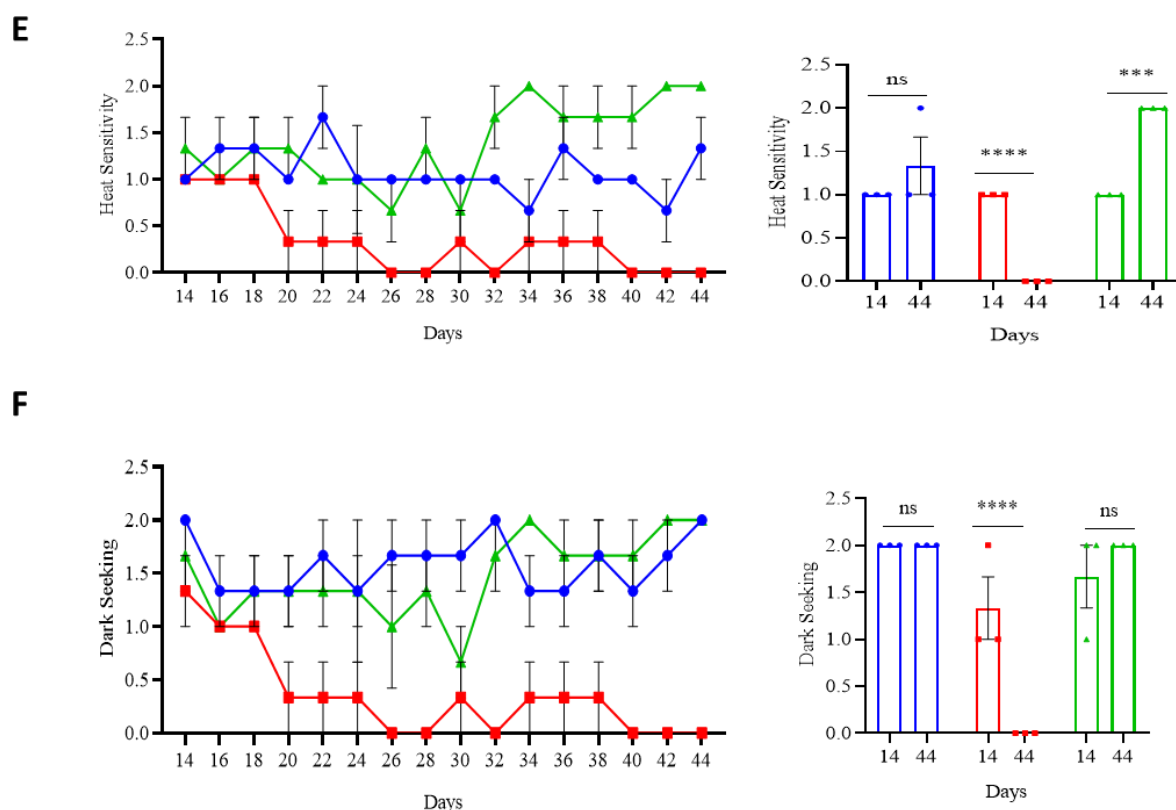
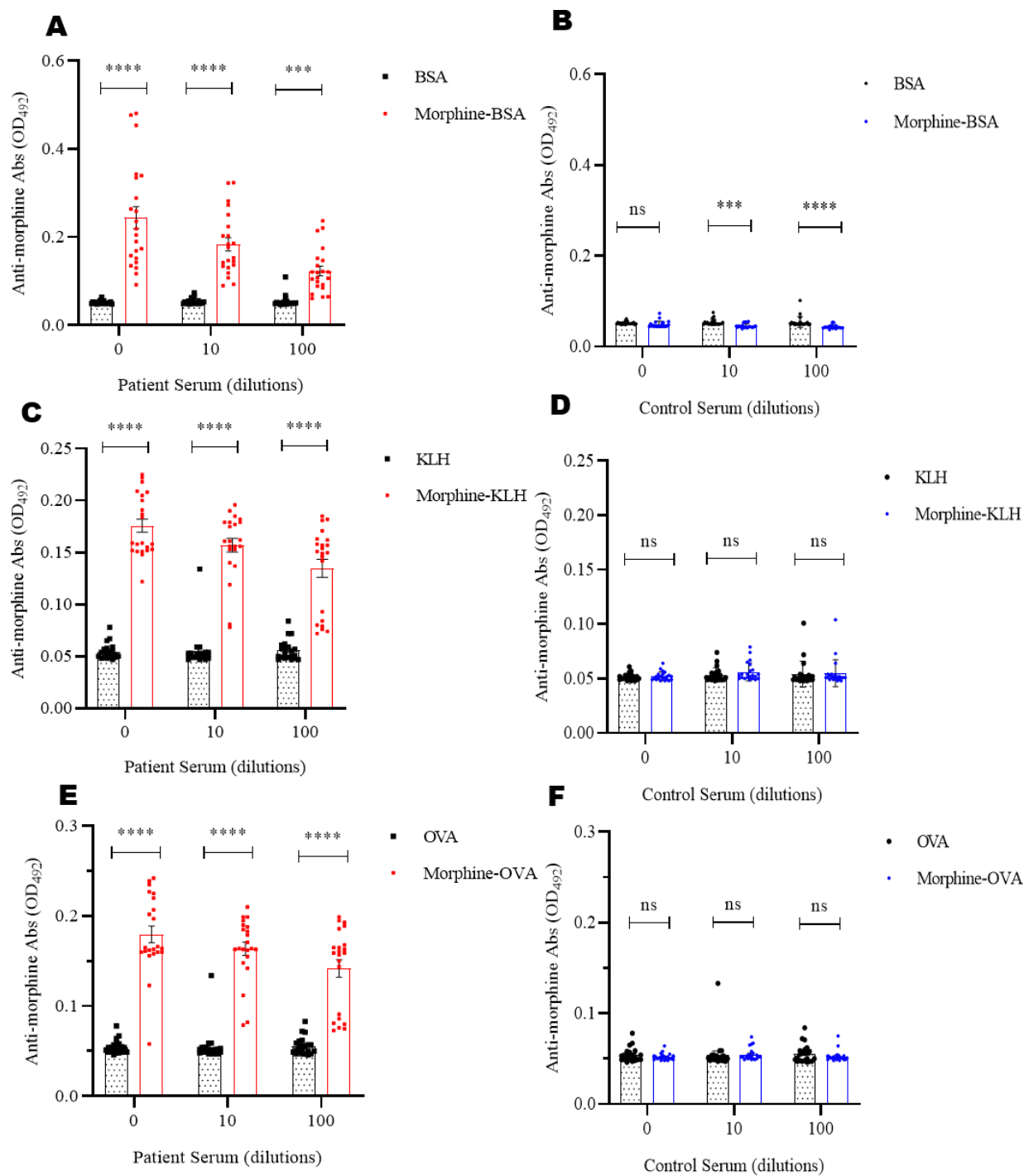


Figure 22. No change in the behaviour of the MAPNV-inoculated animals was observed on exposure to morphine. The mice were injected MAPNV (20 mg/kg bwt) on days 0 and 7. The control groups were injected with PBS (placebo). Later, they were exposed to morphine (10 mg/kg bwt) from day 12 to 44. morphine (10 mg/kg bwt). An uninjected group was also kept as a control. The behavioural changes in the animals were recorded on every alternate day for (A) body weight, (B) food intake, (C) water intake, (D) movements, (E) heat sensitivity, (F) dark seeking. The line diagram denotes the days-wise behavioural differences, and the bar graphs represent the comparison in the behaviour before (day 14) and after morphine exposure (day 44). The movement was represented as 0: no, 1: minimal, and 2: active. The heat sensitivity was represented as 0: no, 1: minimal, and 2: maximum. The dark seeking was represented as 0: no, 1: minimal, and 2: active. Each dot represents one animal. The data are from three independent experiments. The data were analysed by Two-Way ANOVA. The data are expressed as mean \pm SEM. * $p < 0.05$, *** $p < 0.01$, **** $p < 0.0001$, ns=non-significant.

4.23 *The presence of anti-morphine Abs in the serum of patients with Opioid Use Disorder (OUD).* This study aimed to investigate the presence of anti-morphine Abs in the serum of patients with Opioid Use Disorder to understand the underlying generation of anti-morphine Abs. We utilised the ELISA method to measure the concentrations of anti-morphine Abs. The patients with OUD took morphine for a prolonged period with a median dependency of 5.5 years. The serum of all the 22 patients with OUD showed the presence of anti-morphine Abs, compared to healthy controls with no history of morphine consumption (Fig. 23A-F). To ensure the specificity and rule out any possibility of cross-reactivity of the anti-morphine Abs with the carrier protein BSA in the morphine-BSA conjugate, we tested the serum using morphine-KLH and morphine-ovalbumin (OVA) conjugates. No anti-morphine Abs were detected against the carrier proteins BSA, KLH and OVA alone (Fig. 23A, C, E). Furthermore, no anti-morphine Abs were noticed in the serum of the healthy controls (Fig. 23B, D, F). Additionally, we coated different concentrations of morphine-BSA (0.001-1.0 μM) and accordingly observed dose-dependent responsiveness in the level of anti-morphine Abs (Fig. 23G). Different levels of anti-morphine Abs were found in the serum of OUD, which was significantly ($p < 0.0001$) higher in the patients with OUD than in healthy controls (Fig. 23H). Consequently, establishing the specificity of the presence of anti-morphine Abs in the serum of the patients with OUD. We observed a predominance of IgG anti-morphine Abs over the IgM and IgA subtypes (Fig. 23I), signifying the long-term persistence of the Abs. IgG stays in the blood longer and has higher neutralising power.



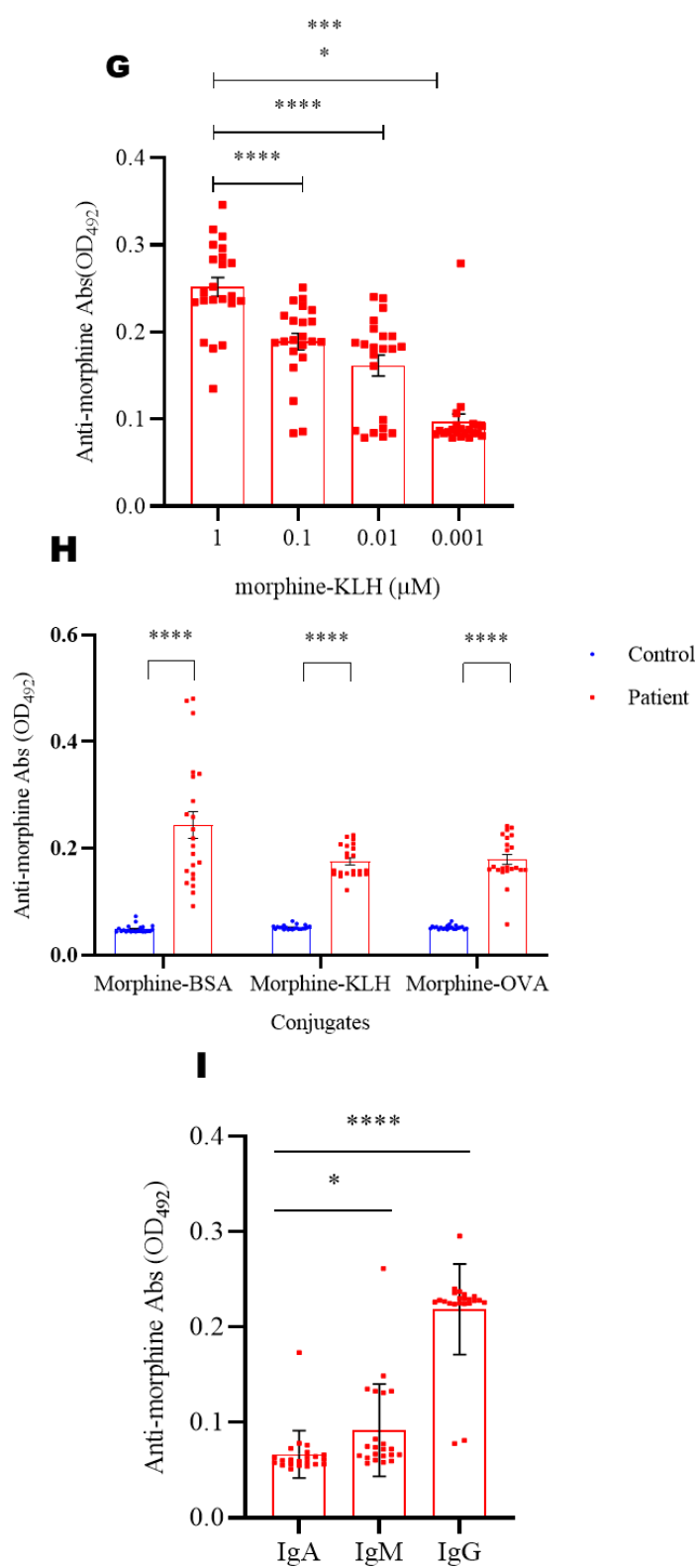


Figure 23. Demonstration of anti-morphine Abs in the serum of Opioid Use Disorder (OUD) patients. The investigation examined the presence of anti-morphine Abs in the serum of OUD patients. The purpose of this investigation was to understand the potential role that these Abs play in OUD. An enzyme-linked immunosorbent assay (ELISA) was performed on serum samples collected from OUD patients to determine the presence of anti-morphine Abs. The anti-morphine Abs were estimated in the serum of (A, C, E) OUD patients and (B, D, F) normal healthy controls. The specificity of the anti-morphine Abs was established using morphine conjugated to different carrier proteins (A, B) morphine-BSA; (C, D) morphine-KLH; (E, F) morphine-OVA. (G) The ELISA plates were coated with various concentrations of morphine-KLH (0.001-1 μ M) to monitor the dose-dependent response of anti-morphine Abs. (H) The overall specificity of anti-morphine Abs was monitored with different carrier protein-morphine conjugates. (I) The presence of IgG, IgA and IgM subclass of anti-morphine Abs was assessed by ELISA. The unconjugated carrier proteins BSA, KLH, and OVA were used as controls. The Abs was quantified using different serum dilutions (1: 0, 10, 100). The data shown as mean \pm SEM (OD₄₉₂) are of OUD patients (22 Nos) and healthy controls (22 Nos). Each dot represents a single individual. The data (OD₄₉₂) analysed by One-Way ANOVA are represented as mean \pm SD. *p<0.5, **p<0.01, ***p<0.001, ****p<0.0001. ns: non-significant.

4.24 *Free and immune-complexed morphine was present in the serum of the patients with OUD.* This study investigated the presence and levels of free and immune-complexed morphine in the serum of patients with Opioid Use Disorder (OUD). This investigation aimed to gain insight into the potential therapeutic benefits of immune-complexed morphine in these patients. To conduct this investigation, serum samples were collected from the patients with OUD and analysed for free and immune-complexed morphine using ELISA assays. The patients with OUD took morphine at 30-300 µg/day. We noticed a significantly ($p < 0.0001$) higher level of free morphine in the serum of the patients with OUD. Further, morphine was found in the form of immune complexes. However, it was at a much lower concentration than the free morphine. No morphine was detected in the serum of healthy controls (Fig. 24A-B). The presence of morphine in the immune complexes is another proof of anti-morphine Abs presence.

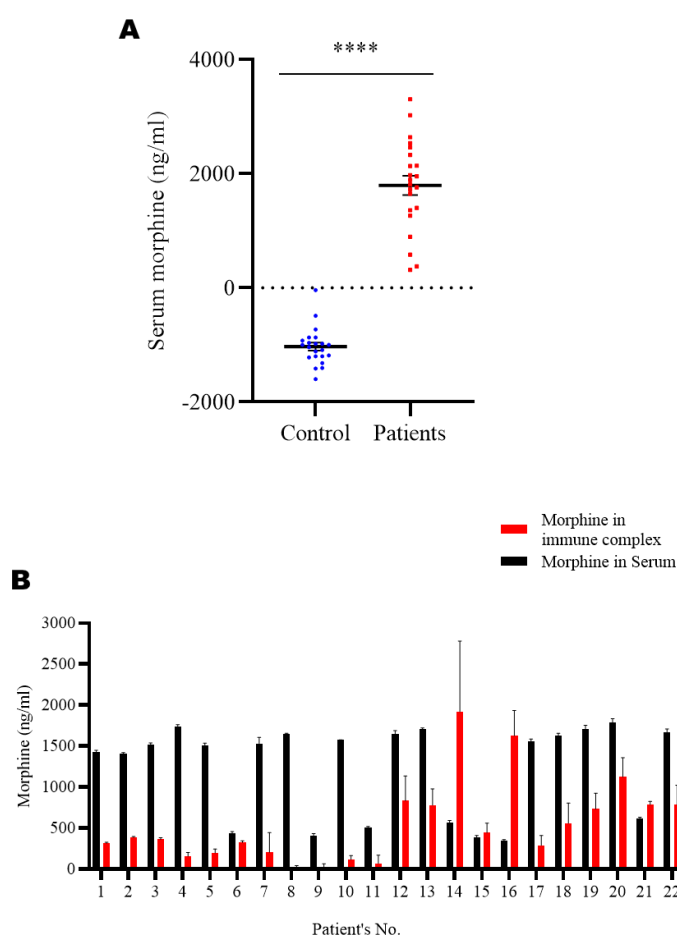


Figure 24. The presence of morphine in the serum of the OUD patients. (A) The morphine was estimated in the serum of the OUD patients and normal healthy controls by UV-visible spectrophotometry. Each dot represents a single individual. (B) The morphine in the immune complexes (ICs) of morphine-anti-morphine Abs was released and measured. Each dot denotes one individual. The data (mean \pm SD) shown are of OUD patients (22 Nos) and healthy controls (22 Nos). Statistical analysis was performed through the Two-Tailed test. ****p<0.0001.

4.25 Anti-morphine Abs binds morphine. Here, we determined the ability of anti-morphine antibodies to bind morphine. This was studied to gain insight into the development of therapeutics that could potentially counteract the physiological effects of morphine. We observed that the equal quantity of anti-morphine Abs of different patients with OUD showed diverse binding affinities for morphine, as evidenced by the presence of the free versus complexed morphine. However, the majority of the samples showed high to moderate binding to the exogenously added morphine, whereas some to a lesser extent (OUD patients ID No. 4, 14, 19, 20, 22), when compared to the positive control having standard anti-morphine Abs (Fig. 25A, B). Further, no correlation was noticed between the binding efficiency of the anti-morphine Abs and their titre (Fig. 25C). This indicates that the neutralising ability of the Abs plays a fundamental role in clearing the morphine and not the magnitude of the titre.

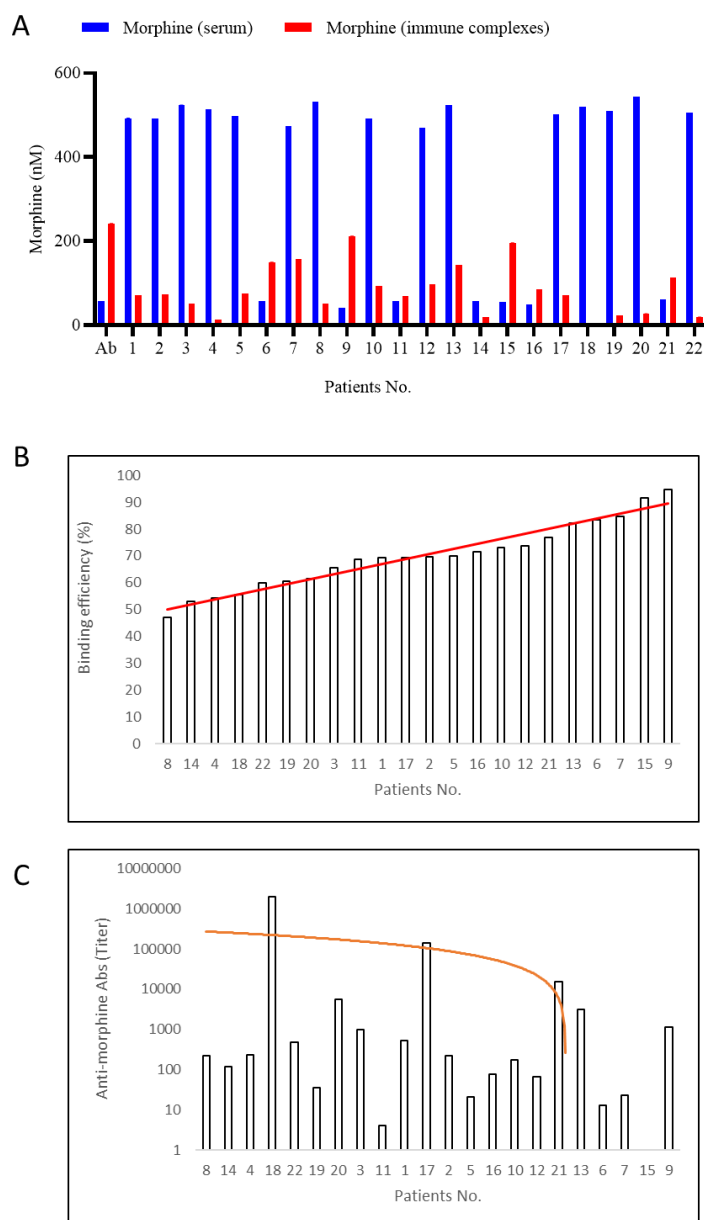


Figure 25. The binding efficiency of anti-morphine Abs to morphine. The IgG (10 μ g) isolated from the serum of the OUD patients was incubated with (A) morphine (1 mM). The binding of anti-morphine Abs (10 μ g) to morphine was calculated using a standard plot of different concentrations of morphine (0.05, 0.1, 0.25, 0.5, 1, 2.5, 5 M). (B) The bar diagram reveals the binding efficiency (%) of the serum anti-morphine Abs to morphine. The red line denotes the cumulative analysis of morphine binding to the serum of OUD patients. (C) The bar diagrams depict the titre of anti-morphine Abs, and the orange line shows the trend of binding of serum anti-morphine Abs to morphine. The data shown are of 22 OUD patients.

4.26 Morphine supports the expression of FoxP-3. This study investigated the differences in FoxP-3, iNOS and IL-6 expression levels between patients with Opioid Use Disorder (OUD) and healthy individuals. It was conducted to understand better the immunological effects of chronic opioid exposure on the body. The expression levels were assessed with a series of qPCR assays. The patients with OUD exhibited significantly ($p < 0.001$) higher expression of FoxP-3, as compared to healthy controls (Fig. 26A). In contrast, a lower level of iNOS and IL-6 was observed (Fig. 26B, C). The FoxP-3 is a transcription factor of Tregs. Tregs are responsible for the immunosuppression of both iNOS and IL-6 pro-inflammatory responses. The results suggest that people are inflicted with immunosuppression on regular intake of morphine.

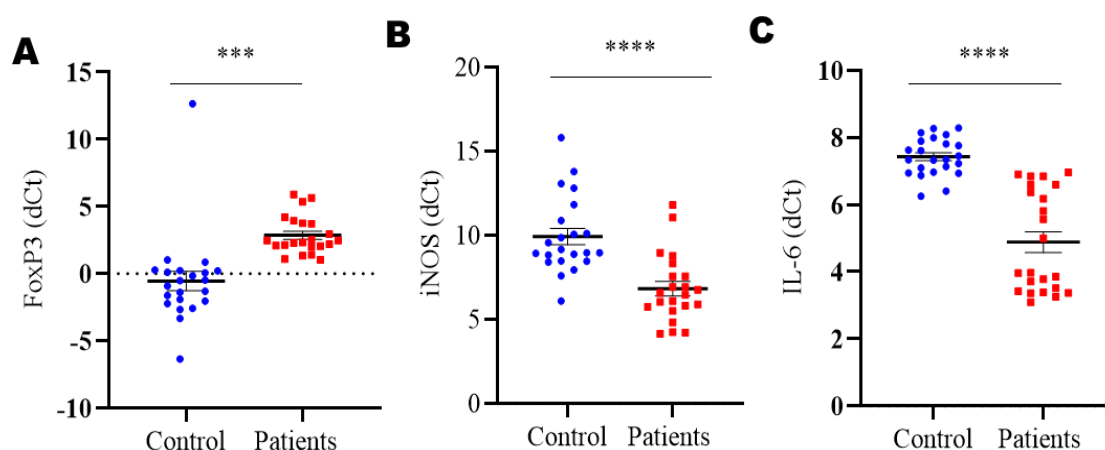


Figure 26. The presence of FoxP-3, iNOS and IL-6 in the OUD patients versus healthy controls. The RNA was isolated from the blood of the OUD patients and healthy controls. The anti-inflammatory (A) FoxP3 and pro-inflammatory (B) iNOS; (C) IL-6 molecules were estimated by RT-qPCR. Each dot represents the data (mean \pm SD) of OUD patients (22 Nos) and normal healthy controls (22 Nos). The data were analysed through a Two-Tailed paired T-Test and expressed as dCt values. * $p < 0.05$, ** $p < 0.01$, **** $p < 0.0001$.

4.27 *The patients with OUD showed a weaker generation of Abs against the Acr1 protein of Mtb.* In this study, we investigated the susceptibility of opioid use disorder (OUD) patients to infections, particularly tuberculosis (TB). We hypothesised that OUD patients in TB-endemic regions might have a weakened immune system, so we measured the levels of FoxP3 and anti-Acr1 antibodies in serum samples from OUD patients and healthy controls. We observed that the patients with OUD showed a higher level of FoxP3, which makes them susceptible to opportunistic infections, particularly *Mtb* in TB-endemic regions. The serum samples from the patients with OUD were analysed for antibodies against the latency-associated protein Acr1, which is secreted by *Mtb* during the latent phase of TB. The patients with OUD exhibited significantly ($p < 0.0001$) reduced levels of anti-Acr1 Abs, as compared to the healthy controls (Fig. 27A-C). We found significantly reduced levels of anti-Acr1 antibodies in OUD patients, suggesting that they had impaired immunity. The results suggest that OUD patients have suppressed immunity.

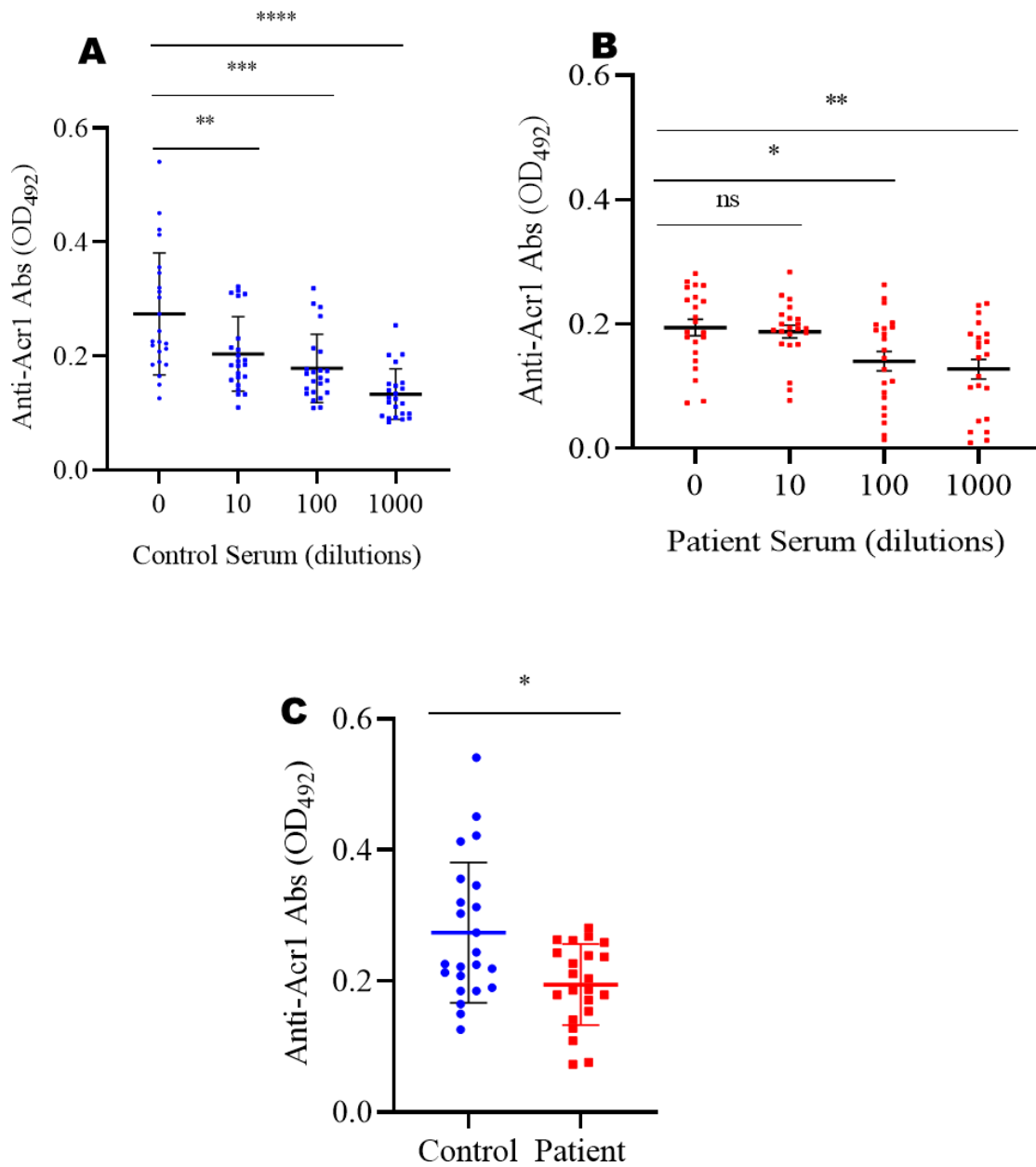


Figure 27. OUD patients exhibit lower levels of Abs against the Acr1 antigen of *Mtb*. The presence of anti-Acr1 Abs was estimated in the serum (dilutions 1, 10, 100, 1000) of the (A) normal healthy controls (22 Nos) and (B) OUD patients (22 Nos) by ELISA. (C) A comparative analysis of the level of anti-Acr1 Abs in the serum of normal healthy controls and patients was performed. Each dot represents a single individual. The data were analysed through a Two-Tailed paired T-Test. The data (OD₄₉₂) are represented as mean \pm SD. * $p < 0.5$, ** $p < 0.01$, *** $p < 0.001$, **** $p < 0.0001$, ns: non-significant.

Drug addiction is a growing problem that affects individuals of all ages and is spreading globally (*National Institute on Drug Abuse, 2020; UNODC, 2020*). It is a recurring chronic condition that harms individuals and can potentially destroy families and communities. Those struggling with addiction often experience numerous negative consequences, including declining physical health, social isolation, financial difficulties, and legal troubles. Additionally, addiction can lead to fatal overdoses (*National Institute on Drug Abuse, 2018*). While there are various treatment options available for drug addiction, such as counselling, medication-assisted therapy, and support groups, a definitive cure has yet to be found (*National Institute on Drug Abuse, 2020; American Academy of Addiction Psychiatry, 2020; National Institute of Health, 2020; National Institute on Alcohol Abuse and Alcoholism, 2020*). Opioid substitution therapy (OST), which involves using the agonist buprenorphine, is used to treat patients. However, it still requires exposure to opioids and maintains a dependence on these substances (*Rehm, 2010*). Despite the lack of effective treatments, there is still a demand for opioids due to their ability to induce feelings of euphoria and pleasure. As a result, the scientific community faces an urgent need and a significant challenge to develop innovative therapeutic strategies and radically change the current approach.

The incidence of tuberculosis (TB) among drug addicts is typically higher compared to the general population. Drug addiction can weaken the immune system, making individuals more vulnerable to TB infection or the reactivation of latent TB. Furthermore, sharing needles and drug paraphernalia can directly contribute to the transmission of TB (*Guichard et al., 2015; Parantainen et al., 2011; Fernandes et al., 2017*). It is of utmost importance to prevent and control TB among drug addicts. Vaccines have successfully eradicated numerous debilitating diseases such as smallpox, polio, measles, diphtheria, pertussis, and tetanus (*Orenstein et al., 2003*). Therefore, there exists significant potential for vaccines to address drug dependence. Developing a vaccine against drug addiction assumes paramount importance due to its status as a significant global public health concern. Such a vaccine would stimulate an immune response to a specific drug by generating antibodies that bind to it and impede its passage into the brain. By obstructing the drug's effects, the vaccine could diminish cravings and reduce the risk of relapse. This would prove particularly advantageous for individuals endeavouring to overcome addiction to opioids, morphine, cocaine, or other challenging-to-treat substances. Consequently, vaccines against addiction offer a promising avenue towards

eradicating the affliction of drug addiction while simultaneously promoting an individual's path to sobriety.

Another advantage of our vaccine MAPNV over the others is that it is based on nanotechnology. Nanoparticles play a pivotal role in vaccine development, offering numerous benefits such as targeted delivery, controlled release, adjuvant properties, stability and protection, and versatility in the formulation. These qualities promise to enhance vaccine effectiveness, improve patient compliance, and expand vaccine accessibility, ultimately contributing to global healthcare efforts (*Harris et al., 2017; Asmal et al., 2020*). Nanoparticles have emerged as crucial components in vaccine development, demonstrating the immense potential to improve their efficacy through various mechanisms. The targeted delivery of antigens using nanoparticles ensures precise and efficient antigen presentation to specific cells or tissues, enhancing the immune response (*Chymkowitch et al., 2018; Meenakshi et al., 2014; Jiang et al., 2019*). Moreover, nanoparticles can mimic pathogen features, triggering immune recognition and generating a robust immune reaction. This property aids in eliciting a strong and durable immune response (*Zeng et al., 2017; De Gregorio et al., 2015; Li et al., 2013*)

Nanoparticles also contribute to the stability and protection of vaccine antigens, safeguarding them against degradation during storage and transportation (*Willem et al., 2017; Steve et al., 2009; Wei et al., 2017; Paul et al., 2009*). By improving antigen stability, nanoparticles ensure that vaccines remain effective and potent for extended periods. Nanoparticles can be engineered to facilitate the controlled release of antigens, resulting in sustained antigen presentation and prolonged immune stimulation. This controlled release mechanism can enhance immune responses and reduce vaccine doses (*Hogervorst et al., 2013; Diebolder et al., 2016; Bhandari et al., 2016*). The versatility of nanoparticles in vaccine formulation allows for incorporating multiple antigens or combination vaccines within a single nanoparticle system. This approach simplifies vaccine administration and enhances patient compliance (*Sung et al., 2008; Wang et al., 2018; Sharquie et al., 2019*). Notably, the development of MAPNV has demonstrated favourable characteristics, including enhanced stability and sustained release of antigens, making it a suitable vaccine candidate (*Patnaik et al., 2015; Albukhari et al., 2019*).

Nanoparticle-based vaccines offer non-invasive delivery through inhalation or oral administration routes, eliminating the need for injections. This feature enhances vaccine

accessibility, particularly in resource-limited settings, and improves patient acceptance (Damond *et al.*, 2019; Pinto *et al.*, 2018; Rajkumar *et al.*, 2012). Additionally, nanoparticles can be designed to target specific cells like DCs, B cells or tissues, further enhancing the immune response and overall vaccine effectiveness. The presence of Pam3Cys and morphine on the surface of MAPNV aids in the targeted delivery of both the antigen and adjuvant to morphine-specific B cells. Thus, stimulating them to process and present Acr1 to T cells to help B cells further differentiate between secreting high-affinity anti-morphine Abs. Pam3Cys will also help target MAPNV to DCs, the only immune system cells that activate naïve T cells.

Based on the information above, we have developed a novel chimeric vaccine MAPNV consisting of Acr1 nanoparticles expressing morphine and Pam3Cys on their surface. Mice vaccinated with MAPNV yielded several significant findings: 1] proliferation and differentiation of morphine-specific B cells; 2] induction of high levels of anti-morphine antibodies, which effectively cleared morphine from the blood and brain of the animals; 3] proliferation and differentiation of Acr1-reactive CD4 T cells; 4] expansion of both Th1 cell and Th2 cell populations; 5] generation and persistence of memory CD4 T cells and memory B cells; 6] macrophages exhibited an enhanced endocytic property, primarily through the TLR-2 pathway; 7] MAPNV demonstrated self-adjuvant properties, and the addition of an adjuvant did not improve its ability to activate B cells and CD4 T cells; 8] prior-exposure to morphine did not interfere with the efficacy of MAPNV; 9] the expression of addiction-associated OPRM and dopamine genes were downregulated; 10] MAPNV showed efficacy not only as a prophylactic vaccine but also as a therapeutic option.

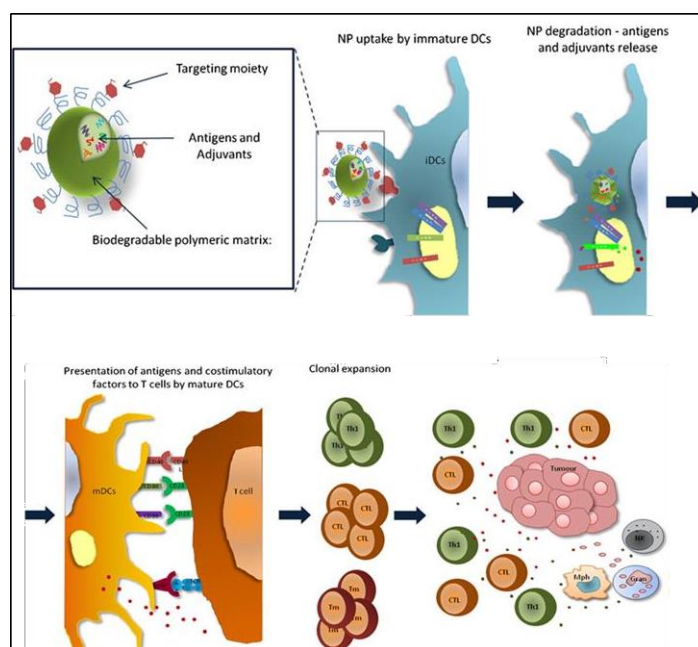
We synthesised nanoparticles using the Acr1 protein from *Mycobacterium tuberculosis* (*Mtb*). Acr1 is a 16 kDa antigen of *Mtb* and is also known as Ag85B or antigen 85B. It is a potential target for therapeutic intervention against *Mtb*, the etiological agent of tuberculosis (TB). It is a well-studied protein and one of the promising vaccine candidates for TB. Acr1 is a significant component of the cell wall of *Mtb* and plays a critical role in the pathogenesis of TB. Several studies have investigated the immunogenicity and protective efficacy of Acr1 as a vaccine antigen against TB. Preclinical studies in animal models and early-stage clinical trials have shown promising results, indicating that Acr1 can induce potent immune responses and provide protective immunity against *Mtb* infection (Aagaard *et al.*, 2011). Further, Acr1 has been used as a component of viral vector-based vaccines, such as adenoviruses and modified vaccinia

Ankara (MVA). These vaccines deliver the Acr1 antigen to the immune system, triggering a robust immune response. Several preclinical studies have demonstrated the immunogenicity and protective efficacy of Acr1 (*Kaufmann et al., 2014; Smaill et al., 2013*). Furthermore, the Acr1 antigen is endowed with immunodominant CD4 T cell and CD8 T cell epitopes that elicit an enduring immune response and protection against *Mtb* (*Cooper et al., 2016; Sullivan et al., 2020*). Many studies have demonstrated that Acr1 is essential for producing antimicrobial lipids, such as Lys-phosphatidylcholine, for killing *Mtb* (*Amir et al., 2017; Mubin et al., 2018*). In addition, Acr1 is involved in the production of anti-inflammatory lipids, such as lysophosphatidic acid, which are essential for maintaining the cell's homeostasis in response to *Mtb* (*Bayne et al., 1990; Mustafa et al., 2010*). Moreover, Acr1-specific antibodies were induced after immunisation with the Acr1 protein, indicating that it is a potent immunogen against *Mtb* (*Fritsche et al., 2014*).

Although several vaccines against substance abuse (SoA) have been developed, none have been successful due to limited efficacy, variable immune responses, and lack of specificity (*Mattingly et al., 2018; Kornfield et al., 2012; Piderman et al., 2017; Finch et al., 2015*). These vaccines did not universally benefit all individuals struggling with drug addiction, as the effectiveness varied from person to person, leading to inconsistent outcomes in reducing drug use and preventing relapse. The varied immune responses to the vaccines resulted in different levels of antibody production. While some individuals produced sufficient antibodies to neutralise the drug's effects, others showed a weaker response, diminishing the vaccine's effectiveness (*Cahill et al., 2020; Dalrymple et al., 2016; Waight et al., 2013*). Furthermore, these vaccines did not exclusively target the desired drug of addiction and failed to generate antibodies that efficiently bound to and neutralised the influence of SoA (*McIndoe et al., 2016; Randel et al., 2017; Wightman et al., 2017*). Some of these vaccines provided only temporary or short-term protection against the drug's effects, requiring multiple boosters to maintain efficacy over time. This can pose challenges regarding patient compliance and healthcare delivery, as regular follow-up and administration are necessary (*Weiner et al., 2001; Hurgaonkar et al., 2011*). The limitations associated with developing these vaccines mainly stemmed from the conventional synthesis process and the concept of hapten carrier conjugation. Further, these vaccines lacked inherent adjuvants and had to be supplemented with exogenous adjuvants, resulting in insufficient activation of B and T cells,

which are crucial for producing high-affinity antibodies. Additionally, the vaccines lacked a targeted delivery system.

With careful consideration of the limitations associated with previous vaccines, we have developed a vaccine against morphine that addresses these weaknesses. Our approach involves conjugating Pam3Cys and morphine onto the surface of Acr1 nanoparticles. Pam3Cys serves as a ligand for TLR-2 and possesses adjuvant properties. It is abundantly expressed on the surface of dendritic cells (DCs), allowing the vaccine to specifically target antigen-presenting cells (APCs) such as DCs, B cells, and macrophages. The MAPNV vaccine activates and differentiates morphine-reactive B cells by interacting with the displayed morphine and Pam3Cys on the surface. Consequently, providing morphine-specific B cells with the necessary signals is required for their optimum proliferation and differentiation. Additionally, this B cell will present Acr1 to T cells. Thus inducing their activation and differentiation and helping morphine-specific B cells. Hence, the advantage of our vaccine over others lies in its ability to simultaneously provide adjuvanticity through TLR-2 to the morphine-specific B cells that recognise morphine.



and presentation inside the DCs. Peptides loaded on MHCs are then presented to naïve T cells to elicit immune responses (Figure adapted) (*Silva et al., 2013*).

In contrast, mixing an adjuvant with the vaccine conjugate would predominantly be recognised by B cells without coming into direct contact with the adjuvant, reducing the chances of activating a larger population of morphine-reactive B cells.

The novelty of our vaccine also lies in its targeting of dendritic cells (DCs). DCs are significant in initiating, activating, and regulating the adaptive immune response (*Gowthaman 2011*). DCs present antigens to T cells and B cells, leading to their activation and differentiation into effector cells. Additionally, DCs secrete cytokines that stimulate B-cell differentiation into antibody-secreting plasma cells (*Al-Garawi et al., 2015*). Furthermore, DCs assist B cells undergoing somatic hypermutation, which results in the generation of B cells producing antibodies with higher affinity (*Risso & Vicari, 2009*).

Our chimeric vaccine offers a distinct advantage over the previous ones by protecting against morphine addiction and TB infection. To achieve this, we utilised Acr1 nanoparticles conjugated with morphine, ensuring easy accessibility for binding to morphine-reactive B cell receptors (*Cooper et al., 2015*). The presence of morphine on the surface of MAPNV enables recognition by morphine-reactive B cells, facilitating their binding to the vaccine. Additionally, Pam3Cys, functioning as an adjuvant, is crucial in eliciting an immune response against morphine. What sets our vaccine apart is the dual functionality of Pam3Cys. It serves as both an adjuvant and a targeted delivery source. Pam3Cys is a ligand for TLR-2, a receptor abundantly expressed on DCs, macrophages, and B cells (*Nguyen, 2016*). This unique property allows Pam3Cys to act as an adjuvant, enhancing the immune response while specifically targeting MAPNV to DCs and B cells. The immune response triggered by Pam3Cys leads to high-affinity anti-morphine antibodies (*Summers et al., 2006; Zhang et al., 2004; Marina et al., 2020*), effectively neutralising the influence of morphine. By incorporating these features into our chimeric vaccine, we have developed a system that addresses morphine addiction and TB infection (*Reynolds et al., 2015; Vongsa et al., 2019*), offering a comprehensive approach to combatting these challenges.

In the immune system, dendritic cells (DCs) are the only antigen-presenting cells (APCs) capable of activating naïve T cells, effectively initiating the body's immune response against foreign pathogens. As a result, understanding the role of DCs in immune defence is of utmost

importance for developing more effective immunological treatments (Willard-Mack *et al.*, 2015). By satisfying the requirements for a suitable vaccine against morphine addiction and TB, MAPNV is expected to stimulate an optimal immune response, effectively combating morphine addiction and *Mtb* infection.

We demonstrated that macrophages and DCs could efficiently phagocytose MAPNV. Phagocytosis of MAPNV by macrophages is crucial as it triggers an immune response that activates T cells. Additionally, macrophages significantly release various cytokines, such as TNF- α , IFN- γ , IL-6, etc., which mediate an inflammatory response (Rivas *et al.*, 2006). This recruitment of immune system cells, including B cells and T cells, helps clear the foreign material. We observed that MAPNV could overcome morphine-induced immunosuppression and activate phagocytosis of MAPNV by macrophages. This finding is supported by previous studies showing morphine's ability to inhibit the expression of proinflammatory cytokines TNF- α , IL-6, IL-1 β , IFN- γ , etc., by macrophages (Liu *et al.*, 2013). Furthermore, morphine can reduce the expression of toll-like receptors (TLRs) and other pattern recognition receptors (PRRs), which are crucial for macrophage and other APC activation (Li *et al.*, 2016). Further, we observed efficient phagocytosis of MAPNV by DCs through TLR-2 signalling pathways. DCs carry antigens from various body sites to the secondary lymphoid organs to prime naive T cells (Bachmann *et al.*, 2010; Reddy *et al.*, 2007; Swartz *et al.*, 1996). This finding aligns with previous studies suggesting that TLR-2 is a crucial receptor for recognising and internalising specific antigens (Das *et al.*, 2022; Kolekar *et al.*, 2014; Zhang *et al.*, 2016). Moreover, TLR-2 plays a vital role in generating long-lasting protection against various pathogens, including *Mycobacterium tuberculosis*, *Staphylococcus aureus*, *Listeria monocytogenes*, etc. (Bishu *et al.*, 2012; Carmen *et al.*, 2012). Additionally, the expression of CD40 on dendritic cells (DCs) is essential for TLR-2 pathways to enable phagocytosis. TLR-2^{-/-} animals showed reduced CD40 expression, indicating that TLR-2 pathways facilitate the phagocytosis of MAPNV.

The unique self-adjuvant property of MAPNV makes it a promising vaccine candidate. This advancement is crucial in vaccine development, as mixing adjuvants often leads to an inconsistent immune response (Zitelli *et al.*, 2018). Remarkably, mice vaccinated with MAPNV demonstrated activation, proliferation, and differentiation of morphine-specific B cells and Acr1-reactive CD4 T cells. The B cells secreted high-affinity anti-morphine

antibodies that effectively bound to morphine, clearing it from the brain and blood of the vaccinated animals. The presence of memory B cells persisted, indicated by the predominance of IgG subtype anti-morphine antibodies that lasted more than 45 days after immunisation. This suggests the ability of MAPNV to elicit a lasting effect, a vital feature of a successful vaccine.

Notably, the vaccine's potency remained unaffected by the prior exposure of animals to morphine, as it successfully enhanced the production of anti-morphine antibodies. The vaccinated animals demonstrated optimal proliferation of CD4 T cells, with a predominant presence of Th1 and Th2 cells based on the expression of IFN- γ and IL-4, respectively. Furthermore, the CD4 T cells exhibited increased levels of CD44 and CD62L, indicative of generating a central memory phenotype. These findings suggest the potential development of Acr1-reactive Th1 cells, which are crucial for protecting against TB (*Hanafusa et al., 2020; Lai et al., 2020*). Further, Th2 cells will provide help to B cells to secrete Abs. Thus, it can be inferred that the prior exposure of mice to morphine does not impact the proliferation of CD4 T cells like B cells (*Naor et al., 2015; Zheng et al., 2015; Krawczyk et al., 2010*). This underscores the effectiveness of MAPNV in efficiently activating and differentiating both cell types to counteract the effects of morphine.

To explore the adjuvant properties of Pam3Cys in MAPNV and the potential need for additional adjuvants, we administered MAPNV supplemented with alum to immunise mice. Interestingly, no improvement in vaccine efficacy was observed with alum, as there were no changes in the proliferation and differentiation of morphine-specific B cells and Acr1-reactive CD4 T cells. This finding emphasises the self-adjuvant nature of our vaccine. Thus giving it a distinct advantage of delivering the adjuvant signal directly to the B cells that recognise morphine.

In addition to effectively clearing morphine from the blood and brain of vaccinated mice, we observed a significant downregulation in the expression of opioid receptor μ (OPRM) and dopamine receptors in the brain. This observation holds excellent significance as OPRM and dopamine receptors play pivotal roles in drug addiction, particularly in the brain's reward pathway and the reinforcing effects of drugs. The involvement of dopamine and OPRM in the brain's reward and pleasure pathways is well-documented (*Beyder et al., 2008; Duman et al., 2012; Boutrel et al., 2005; Toll-Wang, 2008*). Their crucial roles in drug addiction stem

from the ability to reinforce drug-seeking behaviour. Drugs such as morphine, cocaine, amphetamines, and others elevate dopamine levels in the brain, resulting in intense pleasure and euphoria. This surge in dopamine and OPRM strengthens the association between drug use and reward, creating a powerful incentive for continued drug-seeking behaviour (*Ostojic et al., 2015; Lynskey et al., 2007*). The finding of downregulated OPRM and dopamine receptors in the brain following vaccination highlights a significant achievement of MAPNV as a potentially prosperous future vaccine.

Noteworthy, MAPNV showcased effective prophylactic characteristics and remarkable therapeutic capabilities. This was evident as the vaccinated animals generated an optimal immune response against morphine, effectively safeguarding them from its influence upon subsequent morphine exposure. Moreover, in the case of mice that were previously exposed to morphine, the administration of MAPNV commendably countered its effects. These findings highlight the dual functionality of MAPNV, acting as both a protective measure against substance abuse and a viable therapeutic intervention.

This comprehensive investigation highlights the pivotal role of MAPNV in safeguarding individuals from the perils of morphine addiction and TB infection through the induction of robust and effective immunity mediated by CD4 T cells and B cells. Furthermore, high-affinity anti-morphine antibodies signify their capacity to avidly bind and efficiently eliminate morphine from the body, prohibiting it from exerting its effects by binding to opioid receptors. The impact of morphine was further diminished through the downregulation of OPRM and dopamine receptors. Additionally, MAPNV demonstrates the potential to provide enduring protection against future encounters with morphine and TB due to the presence of Acr1-reactive memory CD4 T cells and morphine-specific B cells. The tremendous prospects of MAPNV as a prophylactic and therapeutic vaccine in mitigating the perils of morphine addiction and TB infection are compelling.

Morphine and its derivative, heroin, are widely abused by adolescents worldwide, as reported in the World Drug Report-2022. Morphine use disorder has devastating consequences, as it not only leads to psychological impairments but also disrupts the functioning of immune cells such as macrophages, dendritic cells, T cells, and B cells. Additionally, it hampers the production of reactive oxygen intermediates, cytokines, and chemokines, thereby increasing susceptibility to diseases such as tuberculosis (TB), typhoid, AIDS, and STDs.

Various drugs, such as rifampicin, isoniazid, and dapsone, can potentially bind to body proteins during prolonged treatment, rendering them immunogenic and evoking the production of antibodies against them (*Pai et al., 2018; Sajeed et al., 2019; Manalo et al., 2011; Winter et al., 2014*). These Abs can interact with the drug molecules and neutralise their effects. Similarly, in the case of patients with Opioid Use Disorder (OUD) who continuously consume morphine over an extended period, morphine can bind to body proteins. As a result, there is a likelihood that a morphine-protein conjugate may trigger an Ab response and generate anti-morphine Abs. In our study, we examined the presence of anti-morphine Abs in the serum of patients with OUD who were chronically exposed to morphine, and we made the following significant observations: 1) the presence of anti-morphine Abs; 2) the presence of free morphine as well as morphine in the form of immune complexes (ICs); 3) the anti-morphine Abs predominantly were of the IgG subtype, with lower levels of IgM and IgA; 4) the anti-morphine Abs effectively bound to exogenously added morphine; 5) higher levels of FoxP-3, a transcription factor associated with regulatory T cells (Tregs), and lower concentrations of iNOS and IL-6; 6) a decrease in the magnitude of the immune response against the Acr1 antigen of *Mycobacterium tuberculosis* (*Mtb*).

The anti-morphine Abs detected in our study displayed specificity towards morphine, regardless of the type of carrier proteins involved. No binding was observed with carrier proteins, and no anti-morphine Abs was detected in the serum of healthy controls. The predominance of the IgG subtype suggests the prolonged persistence of these Abs in the serum. Furthermore, their ability to bind exogenously added morphine indicates their continuous ability to clear morphine from the bloodstream. Notably, there was no correlation between the binding of anti-morphine Abs and their titers, as the binding is determined by the affinity of the Abs to the antigen, not the concentration of the Abs.

Patients with OUD are known to have compromised immunity. Our findings revealed elevated levels of FoxP3, indicating an increase in Tregs. At the same time, there was no noticeable change in IL-17, a cytokine produced by Th17 cells. Further, we observed a decrease in the levels of iNOS and IL-6. Tregs suppress the host immune response, whereas iNOS, IL-6, and IL-17 play essential roles in defending against pathogens by generating pro-inflammatory responses. These results suggest that patients with OUD exposed to morphine have suppressed immunity. This was further supported by the fact that patients with OUD exhibited a

diminished immune response against the Acr1 protein of *Mtb*. It is worth noting that individuals with OUD are more susceptible to *Mtb*.

This study suggests that long-term exposure to morphine results in the binding of morphine to body proteins, making it antigenic and prompting an Ab response. Anti-morphine Abs formed may bind morphine and clear it from the blood before influencing the physiology of patients with OUD. Anti-morphine Abs have been demonstrated to remove morphine from the blood of experimental animals before it could alter their behaviour (*Janda et al., 2015; Ali et al., 2015; Sack et al., 2013*). Generating vaccines against morphine may be a prudent prophylactic and therapeutic strategy to combat the morphine menace efficiently.

Drug addiction is a chronic mental illness that affects millions of individuals worldwide. It is caused by the use of drugs of abuse, which provide pleasure or relaxation to a person, often leading to cravings and continued drug use despite harmful consequences. Opioid substitution therapy (OST) is a medication-assisted treatment (MAT) used to reduce and manage opioid addiction. It is designed to replace illicit opioids with prescription opioid substitutes, such as buprenorphine and naloxone, which have fewer side effects and are less likely to cause a "high" for the user. However, opioid substitution therapy is not a perfect solution. Some individuals struggle to adhere to the treatment plan and do not benefit from the prescribed medication. There is also a risk of relapse, as the same behaviours associated with addiction may still be present since the underlying causes of addiction are not addressed. Moreover, adverse effects of naloxone include cardiovascular problems, brain tissue rupture, and neurological disorders. Additionally, research has linked opioid abuse to an increased risk of *Mycobacterium tuberculosis* (*Mtb*) infection, which can lead to tuberculosis (TB).

Vaccines have successfully eradicated deadly diseases like poliomyelitis, measles, and smallpox, indicating their potential to mitigate the adverse effects of opioids and thus making them a viable treatment option. Vaccines may offer a permanent solution to eliminate opioid abuse.

Considering the aforementioned facts, we skilfully designed a unique vaccine against morphine addiction and TB infection. Morphine and Pam3Cys were conjugated on the surface of nanoparticles synthesised of Acr1 protein (MAPNV). Morphine will be recognised by the B cells. Pam3Cys (TLR-2 ligand) will deliver an adjuvant signal, and Acr1 reactive T cells will help morphine-specific B cells activate and secrete anti-morphine Abs. Acr1 is an immunodominant antigen of *Mtb* that can be used as a vaccine.

The animals vaccinated with MAPNV demonstrated promoted the activation of morphine-specific B cells and Acr1-reactive CD4 T cells. Further, anti-morphine Abs successfully neutralised the presence of morphine in the blood and brain. The expression of OPRM and dopamine genes was downregulated, indicating the obstruction in the binding of morphine to these receptors. Interestingly, prior exposure of animals to morphine did not interfere with the vaccine's efficacy in generating high-affinity anti-morphine Abs. Furthermore, supplementing MAPNV with adjuvant alum failed to enhance the vaccine's potency. Thus, suggesting the self-adjuvanting MAPNV property of the vaccine.

The study proposes that the MAPNV offers a viable alternative to current OST medications and could represent a significant breakthrough in reducing the consequences of opioid addiction while concurrently protecting against TB. In essence, MAPNV shows promising prospects in protecting against morphine obsession.

Abdallah, A.M., Hill-Cawthorne, G.A., Otto, T.D., Coll, F., Guerra-Assuncao, J.A., Gao, G., Naeem, R., Ansari, H., Malas, T.B., Adroub, S.A., et al. (2015). Genomic expression catalogue of a global collection of BCG vaccine strains show evidence for highly diverged metabolic and cell-wall adaptations. *Scientific reports* 5, 15443.

Abraham, E. (1992). Intranasal immunization with bacterial polysaccharide containing liposomes enhances antigen-specific pulmonary secretory antibody response. *Vaccine* 10, 461-468.

Agrewala, J.N., and Wilkinson, R.J. (1999). Influence of HLA-DR on the phenotype of CD4+ T lymphocytes specific for an epitope of the 16-kDa alpha-crystallin antigen of *Mycobacterium tuberculosis*. *European journal of immunology* 29, 1753-1761.

Aguilar, J.C., and Rodriguez, E.G. (2007). Vaccine adjuvants revisited. *Vaccine* 25, 3752-3762.

Aguilo, N., Alvarez-Arguedas, S., Uranga, S., Marinova, D., Monzon, M., Badiola, J., and Martin, C. (2016). Pulmonary but Not Subcutaneous Delivery of BCG Vaccine Confers Protection to Tuberculosis-Susceptible Mice by an Interleukin 17-Dependent Mechanism. *The Journal of infectious diseases* 213, 831-839.

Ajdary, M., Moosavi, M.A., Rahmati, M., Falahati, M., Mahboubi, M., Mandegary, A., Jangjoo, S., Mohammadinejad, R., and Varma, R.S. (2018). Health Concerns of Various Nanoparticles: A Review of Their in Vitro and in Vivo Toxicity. *Nanomaterials* 8.

Ali, O.A., Huebsch, N., Cao, L., Dranoff, G., and Mooney, D.J. (2009). Infection-mimicking materials to program dendritic cells in situ. *Nature materials* 8, 151-158.

Alving, C.R., Richards, R.L., Moss, J., Alving, L.I., Clements, J.D., Shiba, T., Kotani, S., Wirtz, R.A., and Hockmeyer, W.T. (1986). Effectiveness of liposomes as potential carriers of vaccines: applications to cholera toxin and human malaria sporozoite antigen. *Vaccine* 4, 166-172.

Amir, M., Aqdas, M., Nadeem, S., Siddiqui, K.F., Khan, N., Sheikh, J.A., and Agrewala, J.N. (2017). Diametric Role of the Latency-Associated Protein Acr1 of *Mycobacterium tuberculosis* in Modulating the Functionality of Pre- and Post-maturational Stages of Dendritic Cells. *Frontiers in immunology* 8, 624.

Andersen, P., and Doherty, T.M. (2005). The success and failure of BCG - implications for a novel tuberculosis vaccine. *Nature reviews Microbiology* 3, 656-662.

Anwar, M.A., Shah, M., Kim, J., and Choi, S. (2019). Recent clinical trends in Toll-like receptor targeting therapeutics. *Medicinal research reviews* 39, 1053-1090.

Appelberg, R., Castro, A.G., Pedrosa, J., and Minoprio, P. (1994). Role of interleukin-6 in the induction of protective T cells during mycobacterial infections in mice. *Immunology* 82, 361-364.

Aronson, N.E., Santosham, M., Comstock, G.W., Howard, R.S., Moulton, L.H., Rhoades, E.R., and Harrison, L.H. (2004). Long-term efficacy of BCG vaccine in American Indians and Alaska Natives: A 60-year follow-up study. *Jama* 291, 2086-2091.

Asli, A., Brouillette, E., Ster, C., Ghinet, M.G., Brzezinski, R., Lacasse, P., Jacques, M., and Malouin, F. (2017). Antibiofilm and antibacterial effects of specific chitosan molecules on *Staphylococcus aureus* isolates associated with bovine mastitis. *PloS one* 12, e0176988.

Bachmann, M.F., and Jennings, G.T. (2010). Vaccine delivery: a matter of size, geometry, kinetics and molecular patterns. *Nature reviews Immunology* 10, 787-796.

Bakhru, P., Sirisaengtaksin, N., Soudani, E., Mukherjee, S., Khan, A., and Jagannath, C. (2014). BCG vaccine mediated reduction in the MHC-II expression of macrophages and dendritic cells is reversed by activation of Toll-like receptors 7 and 9. *Cellular immunology* 287, 53-61.

Bal, S.M., Hortensius, S., Ding, Z., Jiskoot, W., and Bouwstra, J.A. (2011). Co-encapsulation of antigen and Toll-like receptor ligand in cationic liposomes affects the quality of the immune response in mice after intradermal vaccination. *Vaccine* 29, 1045-1052.

Bancroft, G.J., Collins, H.L., Sigola, L.B., and Cross, C.E. (1994). Modulation of murine macrophage behavior in vivo and in vitro. *Methods in cell biology* 45, 129-146.

Banik, B.L., Fattahi, P., and Brown, J.L. (2016). Polymeric nanoparticles: the future of nanomedicine. *Wiley interdisciplinary reviews Nanomedicine and nanobiotechnology* 8, 271-299.

Barrenschee, M., Lex, D., and Uhlig, S. (2010). Effects of the TLR2 agonists MALP-2 and Pam3Cys in isolated mouse lungs. *PLoS One* 5, e13889.

Bi, Y., Xu, Q., Su, L., Xu, J., Liu, Z., Yang, Y., Tang, H., Li, Y., and Fan, M. (2019). The Combinations Chitosan-Pam3CSK4 and Chitosan-Monophosphoryl Lipid A: Promising Immune-Enhancing Adjuvants for Anticaries Vaccine PAC. *Infection and immunity* 87.

Bielinska, A.U., Janczak, K.W., Landers, J.J., Makidon, P., Sower, L.E., Peterson, J.W., and Baker, J.R., Jr. (2007). Mucosal immunization with a novel nanoemulsion-based recombinant anthrax protective antigen vaccine protects against *Bacillus anthracis* spore challenge. *Infection and immunity* 75, 4020-4029.

Biering-Sorensen, S., Jensen, K.J., Aamand, S.H., Blok, B., Andersen, A., Monteiro, I., Netea, M.G., Aaby, P., Benn, C.S., and Haslov, K.R. (2015). Variation of growth in the production of the BCG vaccine and the association with the immune response. An observational study within a randomised trial. *Vaccine* 33, 2056-2065.

Black, G.F., Weir, R.E., Floyd, S., Bliss, L., Warndorff, D.K., Crampin, A.C., Ngwira, B., Sichali, L., Nazareth, B., Blackwell, J.M., et al. (2002). BCG-induced increase in interferon-gamma response to mycobacterial antigens and efficacy of BCG vaccination in Malawi and the UK: two randomised controlled studies. *Lancet* 359, 1393-1401.

Bold, T.D., and Ernst, J.D. (2009). Who benefits from granulomas, mycobacteria or host? *Cell* 136, 17-19.

Braverman, J., and Stanley, S.A. (2017). Nitric Oxide Modulates Macrophage Responses to *Mycobacterium tuberculosis* Infection through Activation of HIF-1alpha and Repression of NF-kappaB. *Journal of immunology* 199, 1805-1816.

Cambau, E., and Drancourt, M. (2014). Steps towards the discovery of *Mycobacterium tuberculosis* by Robert Koch, 1882. *Clinical microbiology and infection : the official publication of the European Society of Clinical Microbiology and Infectious Diseases* 20, 196-201.

Carroll, E.C., Jin, L., Mori, A., Munoz-Wolf, N., Oleszycka, E., Moran, H.B.T., Mansouri, S., McEntee, C.P., Lambe, E., Agger, E.M., et al. (2016). The Vaccine Adjuvant Chitosan Promotes Cellular Immunity via DNA Sensor cGAS-STING-Dependent Induction of Type I Interferons. *Immunity* 44, 597-608.

Carroll, E.C., Jin, L., Mori, A., Munoz-Wolf, N., Oleszycka, E., Moran, H.B.T., Mansouri, S., McEntee, C.P., Lambe, E., Agger, E.M., et al. (2016). The Vaccine Adjuvant Chitosan Promotes Cellular Immunity via DNA Sensor cGAS-STING-Dependent Induction of Type I Interferons. *Immunity* 44, 597-608.

Casanova, J.L., and Abel, L. (2002). Genetic dissection of immunity to mycobacteria: the human model. *Annu Rev Immunol* 20.

Cervantes, J.L. (2017). MyD88 in *Mycobacterium tuberculosis* infection. *Medical microbiology and immunology* 206, 187-193.

Chackerian, A.A., Alt, J.M., Perera, T.V., Dascher, C.C., and Behar, S.M. (2002). Dissemination of *Mycobacterium tuberculosis* is influenced by host factors and precedes the initiation of T-cell immunity. *Infection and immunity* 70, 4501-4509.

Chen, L., Xu, M., Wang, Z.Y., Chen, B.W., Du, W.X., Su, C., Shen, X.B., Zhao, A.H., Dong, N., Wang, Y.J., et al. (2010). The development and preliminary evaluation of a new *Mycobacterium tuberculosis* vaccine comprising Ag85b, HspX and CFP-10:ESAT-6 fusion protein with CpG DNA and aluminum hydroxide adjuvants. *FEMS immunology and medical microbiology* 59, 42-52.

Colacurcio, D.J., and Nixon, R.A. (2016). Disorders of lysosomal acidification-The emerging role of v-ATPase in aging and neurodegenerative disease. *Ageing research reviews* 32, 75-88.

CHAPTER 7

BIBLIOGRAPHY

Cooper, A.M. (2009). Cell-mediated immune responses in tuberculosis. *Annual review of immunology* 27, 393-422.

Cooper, A.M., and Khader, S.A. (2008). The role of cytokines in the initiation, expansion, and control of cellular immunity to tuberculosis. *Immunological reviews* 226, 191-204.

Cooper, A.M., Dalton, D.K., Stewart, T.A., Griffin, J.P., Russell, D.G., and Orme, I.M. (1993). Disseminated tuberculosis in interferon gamma gene-disrupted mice. *The Journal of experimental medicine* 178, 2243-2247.

Cooper, A.M., Kipnis, A., Turner, J., Magram, J., Ferrante, J., and Orme, I.M. (2002). Mice lacking bioactive IL-12 can generate protective, antigen-specific cellular responses to mycobacterial infection only if the IL-12 p40 subunit is present. *Journal of immunology* 168, 1322-1327.

Cooper, A.M., Magram, J., Ferrante, J., and Orme, I.M. (1997). Interleukin 12 (IL-12) is crucial to the development of protective immunity in mice intravenously infected with mycobacterium tuberculosis. *The Journal of experimental medicine* 186, 39-45.

Cooper, A.M., Roberts, A.D., Rhoades, E.R., Callahan, J.E., Getzy, D.M., and Orme, I.M. (1995). The role of interleukin-12 in acquired immunity to *Mycobacterium tuberculosis* infection. *Immunology* 84, 423-432.

Covian, C., Fernandez-Fierro, A., Retamal-Diaz, A., Diaz, F.E., Vasquez, A.E., Lay, M.K., Riedel, C.A., Gonzalez, P.A., Bueno, S.M., and Kalergis, A.M. (2019). BCG-Induced Cross-Protection and Development of Trained Immunity: Implication for Vaccine Design. *Frontiers in immunology* 10, 2806.

da Costa, A.C., Nogueira, S.V., Kipnis, A., and Junqueira-Kipnis, A.P. (2014). Recombinant BCG: Innovations on an Old Vaccine. Scope of BCG Strains and Strategies to Improve Long-Lasting Memory. *Frontiers in immunology* 5, 152.

Danhier, F., Ansorena, E., Silva, J.M., Coco, R., Le Breton, A., and Preat, V. (2012). PLGA-based nanoparticles: an overview of biomedical applications. *Journal of controlled release : official journal of the Controlled Release Society* 161, 505-522.

Das, I., Padhi, A., Mukherjee, S., Dash, D.P., Kar, S., and Sonawane, A. (2017). Biocompatible chitosan nanoparticles as an efficient delivery vehicle for Mycobacterium tuberculosis lipids to induce potent cytokines and antibody response through activation of gammadelta T cells in mice. *Nanotechnology* 28, 165101.

DeFrates, K., Markiewicz, T., Gallo, P., Rack, A., Weyhmiller, A., Jarmusik, B., and Hu, X. (2018). Protein Polymer-Based Nanoparticles: Fabrication and Medical Applications. *International journal of molecular sciences* 19.

Demoulins, T., Bassi, I., Thomann-Harwood, L., Jandus, C., Kaeuper, P., Simon, H.U., von Gunten, S., and McCullough, K.C. (2013). Alginate-coated chitosan nanogel capacity to modulate the effect of TLR ligands on blood dendritic cells. *Nanomedicine : nanotechnology, biology, and medicine* 9, 806-817.

DesJardin, L.E., Kaufman, T.M., Potts, B., Kutzbach, B., Yi, H., and Schlesinger, L.S. (2002). Mycobacterium tuberculosis-infected human macrophages exhibit enhanced cellular adhesion with increased expression of LFA-1 and ICAM-1 and reduced expression and/or function of complement receptors, FcγRII and the mannose receptor. *Microbiology* 148, 3161-3171.

Dockrell, H.M., and Smith, S.G. (2017). What Have We Learnt about BCG Vaccination in the Last 20 Years? *Frontiers in immunology* 8, 1134.

Domingo-Gonzalez, R., Prince, O., Cooper, A., and Khader, S.A. (2016). Cytokines and Chemokines in *Mycobacterium tuberculosis* Infection. *Microbiology spectrum* 4.

Dudek, A.M., Martin, S., Garg, A.D., and Agostinis, P. (2013). Immature, Semi-Mature, and Fully Mature Dendritic Cells: Toward a DC-Cancer Cells Interface That Augments Anticancer Immunity. *Front Immunol* 4, 438.

Duggan, J.M., You, D., Cleaver, J.O., Larson, D.T., Garza, R.J., Guzman Pruneda, F.A., Tuvim, M.J., Zhang, J., Dickey, B.F., and Evans, S.E. (2011). Synergistic interactions of TLR2/6 and TLR9 induce a high level of resistance to lung infection in mice. *Journal of immunology* 186, 5916-5926.

Eisen, H.N., Hou, X.H., Shen, C., Wang, K., Tanguturi, V.K., Smith, C., Kozyrsky, K., Nambiar, L., McKinley, C.A., Chen, J., et al. (2012). Promiscuous binding of extracellular peptides to cell surface class I MHC protein. *Proceedings of the National Academy of Sciences of the United States of America* 109, 4580-4585.

Feng, C.G., Jankovic, D., Kullberg, M., Cheever, A., Scanga, C.A., Hieny, S., Caspar, P., Yap, G.S., and Sher, A. (2005). Maintenance of pulmonary Th1 effector function in chronic tuberculosis requires persistent IL-12 production. *Journal of immunology* 174, 4185-4192.

Feng, G., Jiang, Q., Xia, M., Lu, Y., Qiu, W., Zhao, D., Lu, L., Peng, G., and Wang, Y. (2013). Enhanced immune response and protective effects of nano-chitosan-based DNA vaccine encoding T cell epitopes of Esat-6 and FL against *Mycobacterium tuberculosis* infection. *PloS one* 8, e61135.

Flynn, J.L., Chan, J., Triebold, K.J., Dalton, D.K., Stewart, T.A., and Bloom, B.R. (1993). An essential role for interferon gamma in resistance to *Mycobacterium tuberculosis* infection. *The Journal of experimental medicine* 178, 2249-2254.

Foged, C., Brodin, B., Frokjaer, S., and Sundblad, A. (2005). Particle size and surface charge affect particle uptake by human dendritic cells in an in vitro model. *International journal of pharmaceutics* 298, 315-322.

Foroozandeh, P., and Aziz, A.A. (2018). Insight into Cellular Uptake and Intracellular Trafficking of Nanoparticles. *Nanoscale research letters* 13, 339.

Fortsch, D., Rollinghoff, M., and Stenger, S. (2000). IL-10 converts human dendritic cells into macrophage-like cells with increased antibacterial activity against virulent *Mycobacterium tuberculosis*. *Journal of immunology* 165, 978-987.

Fremond, C.M., Yermeev, V., Nicolle, D.M., Jacobs, M., Quesniaux, V.F., and Ryffel, B. (2004). Fatal *Mycobacterium tuberculosis* infection despite adaptive immune response in the absence of MyD88. *The Journal of clinical investigation* 114, 1790-1799.

Frohlich, E. (2013). Cellular targets and mechanisms in the cytotoxic action of non-biodegradable engineered nanoparticles. *Current drug metabolism* 14, 976-988.

Fromen, C.A., Robbins, G.R., Shen, T.W., Kai, M.P., Ting, J.P., and DeSimone, J.M. (2015). Controlled analysis of nanoparticle charge on mucosal and systemic antibody responses following pulmonary immunization. *Proceedings of the National Academy of Sciences of the United States of America* 112, 488-493.

Fujiwara, M., Kawasaki, M., Hariguchi, N., Liu, Y., and Matsumoto, M. (2018). Mechanisms of resistance to delamanid, a drug for *Mycobacterium tuberculosis*. *Tuberculosis* 108, 186-194.

Getts, D.R., Shea, L.D., Miller, S.D., and King, N.J. (2015). Harnessing nanoparticles for immune modulation. *Trends in immunology* 36, 419-427.

Goldinger, S.M., Dummer, R., Baumgaertner, P., Mihic-Probst, D., Schwarz, K., Hammann-Haenni, A., Willers, J., Geldhof, C., Prior, J.O., Kundig, T.M., et al. (2012). Nano-particle vaccination combined with TLR-7 and -9 ligands triggers memory and effector CD8(+) T-cell responses in melanoma patients. *European journal of immunology* 42, 3049-3061.

Gopal, R., Monin, L., Slight, S., Uche, U., Blanchard, E., Fallert Junecko, B.A., Ramos-Payan, R., Stallings, C.L., Reinhart, T.A., Kolls, J.K., et al. (2014). Unexpected role for IL-17 in protective immunity against hypervirulent *Mycobacterium tuberculosis* HN878 infection. *PLoS pathogens* 10, e1004099.

Gopal, R., Rangel-Moreno, J., Slight, S., Lin, Y., Nawar, H.F., Fallert Junecko, B.A., Reinhart, T.A., Kolls, J., Randall, T.D., Connell, T.D., et al. (2013). Interleukin-17-dependent CXCL13 mediates mucosal vaccine-induced immunity against tuberculosis. *Mucosal immunology* 6, 972-984.

Gopalakrishnan, A., and Salgame, P. (2016). Toll-like receptor 2 in host defense against *Mycobacterium tuberculosis*: to be or not to be-that is the question. *Current opinion in immunology* 42, 76-82.

Gowthaman, U., and Agrewala, J.N. (2008). In silico tools for predicting peptides binding to HLA-class II molecules: more confusion than conclusion. *Journal of proteome research* 7, 154-163.

Gowthaman, U., and Agrewala, J.N. (2009). In silico methods for predicting T-cell epitopes: Dr Jekyll or Mr Hyde? Expert review of proteomics 6, 527-537.

Gowthaman, U., Rai, P.K., Khan, N., Jackson, D.C., and Agrewala, J.N. (2012). Lipidated promiscuous peptides vaccine for tuberculosis-endemic regions. Trends in molecular medicine 18, 607-614.

Gowthaman, U., Rai, P.K., Zeng, W., Jackson, D.C., and Agrewala, J.N. (2013). Lipidated promiscuous peptide augments the expression of MHC-II molecules on dendritic cells and activates T cells. The Indian journal of medical research 138, 744-748.

Gowthaman, U., Singh, V., Zeng, W., Jain, S., Siddiqui, K.F., Chodiseti, S.B., Gurram, R.K., Parihar, P., Gupta, P., Gupta, U.D., et al. (2011). Promiscuous peptide of 16 kDa antigen linked to Pam2Cys protects against Mycobacterium tuberculosis by evoking enduring memory T-cell response. The Journal of infectious diseases 204, 1328-1338.

Gowthaman, U., Singh, V., Zeng, W., Jain, S., Siddiqui, K.F., Chodiseti, S.B., Gurram, R.K., Parihar, P., Gupta, P., Gupta, U.D., et al. (2011). Promiscuous peptide of 16 kDa antigen linked to Pam2Cys protects against Mycobacterium tuberculosis by evoking enduring memory T-cell response. The Journal of infectious diseases 204, 1328-1338.

Grabnar, P.A., and Kristl, J. (2011). The manufacturing techniques of drug-loaded polymeric nanoparticles from preformed polymers. Journal of microencapsulation 28, 323-335.

Green, A.M., Difazio, R., and Flynn, J.L. (2013). IFN-gamma from CD4 T cells is essential for host survival and enhances CD8 T cell function during *Mycobacterium tuberculosis* infection. *Journal of immunology* 190, 270-277.

Green, L.C., Wagner, D.A., Glogowski, J., Skipper, P.L., Wishnok, J.S., and Tannenbaum, S.R. (1982). Analysis of nitrate, nitrite, and [15N]nitrate in biological fluids. *Analytical biochemistry* 126, 131-138.

Greenfield, E.A. (2020). *Standard Immunization of Mice, Rats, and Hamsters*. Cold Spring Harbor protocols 2020, 100297.

Griffiths, K.L., Ahmed, M., Das, S., Gopal, R., Horne, W., Connell, T.D., Moynihan, K.D., Kolls, J.K., Irvine, D.J., Artyomov, M.N., et al. (2016). Targeting dendritic cells to accelerate T-cell activation overcomes a bottleneck in tuberculosis vaccine efficacy. *Nature communications* 7, 13894.

Han, J., Zhao, D., Li, D., Wang, X., Jin, Z., and Zhao, K. (2018). Polymer-Based Nanomaterials and Applications for Vaccines and Drugs. *Polymers* 10.

Hanekom, W.A., Mendillo, M., Manca, C., Haslett, P.A., Siddiqui, M.R., Barry, C., 3rd, and Kaplan, G. (2003). *Mycobacterium tuberculosis* inhibits maturation of human monocyte-derived dendritic cells in vitro. *The Journal of infectious diseases* 188, 257-266.

Harding, C.V., and Boom, W.H. (2010). Regulation of antigen presentation by *Mycobacterium tuberculosis*: a role for Toll-like receptors. *Nature reviews Microbiology* 8, 296-307.

CHAPTER 7

BIBLIOGRAPHY

Henderson, R.A., Watkins, S.C., and Flynn, J.L. (1997). Activation of human dendritic cells following infection with *Mycobacterium tuberculosis*. *Journal of immunology* 159, 635-643.

Herzenberg, L.A., Tokuhiya, T., and Herzenberg, L.A. (1980). Carrier-priming leads to hapten-specific suppression. *Nature* 285, 664-667.

Heuking, S., Rothen-Rutishauser, B., Raemy, D.O., Gehr, P., and Borchard, G. (2013). Fate of TLR-1/TLR-2 agonist functionalised pDNA nanoparticles upon deposition at the human bronchial epithelium in vitro. *Journal of nanobiotechnology* 11, 29.

Highton, A.J., Kojarunchitt, T., Girardin, A., Hook, S., and Kemp, R.A. (2015). Chitosan hydrogel vaccine generates protective CD8 T cell memory against mouse melanoma. *Immunology and cell biology* 93, 634-640.

Ho, P., Wei, X., and Seah, G.T. (2010). Regulatory T cells induced by *Mycobacterium chelonae* sensitization influence murine responses to bacille Calmette-Guerin. *Journal of leukocyte biology* 88, 1073-1080.

Houben, R.M., and Dodd, P.J. (2016). The Global Burden of Latent Tuberculosis Infection: A Re-estimation Using Mathematical Modelling. *PLoS medicine* 13, e1002152.

Hulten, K., El-Zimaity, H.M., Karttunen, T.J., Almashhrawi, A., Schwartz, M.R., Graham, D.Y., and El-Zaatari, F.A. (2001). Detection of *Mycobacterium avium* subspecies paratuberculosis in Crohn's diseased tissues by in situ hybridization. *The American journal of gastroenterology* 96, 1529-1535.

Hunsawong, T., Sunintaboon, P., Warit, S., Thaisomboonsuk, B., Jarman, R.G., Yoon, I.K., Ubol, S., and Fernandez, S. (2015). Immunogenic Properties of a BCG Adjuvanted Chitosan Nanoparticle-Based Dengue Vaccine in Human Dendritic Cells. *PLoS neglected tropical diseases* 9, e0003958.

Hurt, R. (2004). Tuberculosis sanatorium regimen in the 1940s: a patient's personal diary. *Journal of the Royal Society of Medicine* 97, 350-353.

Husain, A.A., Daginawala, H.F., Singh, L., and Kashyap, R.S. (2016). Current perspective in tuberculosis vaccine development for high TB endemic regions. *Tuberculosis* 98, 149-158.

Itoh, T., and Celis, E. (2005). Transcutaneous immunization with cytotoxic T-cell peptide epitopes provides effective antitumor immunity in mice. *Journal of immunotherapy* 28, 430-437.

Jackson, D.C., Lau, Y.F., Le, T., Suhrbier, A., Deliyannis, G., Cheers, C., Smith, C., Zeng, W., and Brown, L.E. (2004). A totally synthetic vaccine of generic structure that targets Toll-like receptor 2 on dendritic cells and promotes antibody or cytotoxic T cell responses. *Proceedings of the National Academy of Sciences of the United States of America* 101, 15440-15445.

Jackson, D.C., Lau, Y.F., Le, T., Suhrbier, A., Deliyannis, G., Cheers, C., Smith, C., Zeng, W., and Brown, L.E. (2004). A totally synthetic vaccine of generic structure that targets Toll-like receptor 2 on dendritic cells and promotes antibody or cytotoxic T cell responses. *Proceedings of the National Academy of Sciences of the United States of America* 101, 15440-15445.

Jia, J., Zhang, Y., Xin, Y., Jiang, C., Yan, B., and Zhai, S. (2018). Interactions Between Nanoparticles and Dendritic Cells: From the Perspective of Cancer Immunotherapy. *Frontiers in oncology* 8, 404.

Jin, M.S., Kim, S.E., Heo, J.Y., Lee, M.E., Kim, H.M., Paik, S.G., Lee, H., and Lee, J.O. (2007). Crystal structure of the TLR1-TLR2 heterodimer induced by binding of a tri-acylated lipopeptide. *Cell* 130, 1071-1082.

Jung, S.N., Kang, S.K., Yeo, G.H., Li, H.Y., Jiang, T., Nah, J.W., Bok, J.D., Cho, C.S., and Choi, Y.J. (2015). Targeted delivery of vaccine to dendritic cells by chitosan nanoparticles conjugated with a targeting peptide ligand selected by phage display technique. *Macromolecular bioscience* 15, 395-404.

Kaumaya, P.T., Kobs-Conrad, S., Seo, Y.H., Lee, H., VanBuskirk, A.M., Feng, N., Sheridan, J.F., and Stevens, V. (1993). Peptide vaccines incorporating a 'promiscuous' T-cell epitope bypass certain haplotype restricted immune responses and provide broad spectrum immunogenicity. *Journal of molecular recognition : JMR* 6, 81-94.

Kennaway, C.K., Benesch, J.L., Gohlke, U., Wang, L., Robinson, C.V., Orlova, E.V., Saibil, H.R., and Keep, N.H. (2005). Dodecameric structure of the small heat shock protein Acr1 from *Mycobacterium tuberculosis*. *The Journal of biological chemistry* 280, 33419-33425.

Khader, S.A., and Cooper, A.M. (2008). IL-23 and IL-17 in tuberculosis. *Cytokine* 41, 79-83.

Khader, S.A., Bell, G.K., Pearl, J.E., Fountain, J.J., Rangel-Moreno, J., Cilley, G.E., Shen, F., Eaton, S.M., Gaffen, S.L., Swain, S.L., et al. (2007). IL-23 and IL-17 in the establishment of protective pulmonary CD4⁺ T cell responses after vaccination and during *Mycobacterium tuberculosis* challenge. *Nature immunology* 8, 369-377.

Khader, S.A., Partida-Sanchez, S., Bell, G., Jelley-Gibbs, D.M., Swain, S., Pearl, J.E., Ghilardi, N., Desauvage, F.J., Lund, F.E., and Cooper, A.M. (2006). Interleukin 12p40 is required for dendritic cell migration and T cell priming after *Mycobacterium tuberculosis* infection. *The Journal of experimental medicine* 203, 1805-1815.

Khan, S., Weterings, J.J., Britten, C.M., de Jong, A.R., Graafland, D., Melief, C.J., van der Burg, S.H., van der Marel, G., Overkleeft, H.S., Filippov, D.V., et al. (2009). Chirality of TLR-2 ligand Pam3CysSK4 in fully synthetic peptide conjugates critically influences the induction of specific CD8⁺ T-cells. *Molecular immunology* 46, 1084-1091.

Koppolu, B., and Zaharoff, D.A. (2013). The effect of antigen encapsulation in chitosan particles on uptake, activation and presentation by antigen presenting cells. *Biomaterials* 34, 2359-2369.

Kuhn, D.A., Vanhecke, D., Michen, B., Blank, F., Gehr, P., Petri-Fink, A., and Rothen-Rutishauser, B. (2014). Different endocytotic uptake mechanisms for nanoparticles in epithelial cells and macrophages. *Beilstein journal of nanotechnology* 5, 1625-1636.

Land, W.G. (2018). Antigen Uptake, Processing, and Presentation by Dendritic Cells. In *Damage-Associated Molecular Patterns in Human Diseases: Volume 1: Injury-Induced Innate Immune Responses* (Cham: Springer International Publishing), pp. 723-748.

Leal, I.S., Smedegard, B., Andersen, P., and Appelberg, R. (1999). Interleukin-6 and interleukin-12 participate in induction of a type 1 protective T-cell response during vaccination with a tuberculosis subunit vaccine. *Infection and immunity* 67, 5747-5754.

Lerner, T.R., Borel, S., and Gutierrez, M.G. (2015). The innate immune response in human tuberculosis. *Cellular microbiology* 17, 1277-1285.

Li, Q., Yu, H., Zhang, Y., Wang, B., Jiang, W., Da, Z., Xian, Q., Wang, Y., Liu, X., and Zhu, B. (2011). Immunogenicity and protective efficacy of a fusion protein vaccine consisting of

antigen Ag85B and HspX against Mycobacterium tuberculosis infection in mice. Scandinavian journal of immunology 73, 568-576.

Li, W., Joshi, M.D., Singhania, S., Ramsey, K.H., and Murthy, A.K. (2014). Peptide Vaccine: Progress and Challenges. Vaccines 2, 515-536.

Li, W., Joshi, M.D., Singhania, S., Ramsey, K.H., and Murthy, A.K. (2014). Peptide Vaccine: Progress and Challenges. Vaccines 2, 515-536.

Li, Y., Sun, F., and Zhang, W. (2019). Bedaquiline and delamanid in the treatment of multidrug-resistant tuberculosis: Promising but challenging. Drug development research 80, 98-105.

Lin, H.H., Zhang, G.L., Tongchusak, S., Reinherz, E.L., and Brusic, V. (2008). Evaluation of MHC-II peptide binding prediction servers: applications for vaccine research. BMC bioinformatics 9 Suppl 12, S22.

Lin, P.L., Plessner, H.L., Voitenok, N.N., and Flynn, J.L. (2007). Tumor necrosis factor and tuberculosis. The journal of investigative dermatology Symposium proceedings 12, 22-25.

Lombardi, V., Van Overtvelt, L., Horiot, S., Moussu, H., Chabre, H., Louise, A., Balazuc, A.M., Mascarell, L., and Moingeon, P. (2008). Toll-like receptor 2 agonist Pam3CSK4 enhances the induction of antigen-specific tolerance via the sublingual route. Clinical and experimental allergy : journal of the British Society for Allergy and Clinical Immunology 38, 1819-1829.

Lombardi, V., Van Overtvelt, L., Horiot, S., Moussu, H., Chabre, H., Louise, A., Balazuc, A.M., Mascarell, L., and Moingeon, P. (2008). Toll-like receptor 2 agonist Pam3CSK4 enhances the induction of antigen-specific tolerance via the sublingual route. *Clinical and experimental allergy : journal of the British Society for Allergy and Clinical Immunology* 38, 1819-1829.

Lu, J.M., Wang, X., Marin-Muller, C., Wang, H., Lin, P.H., Yao, Q., and Chen, C. (2009). Current advances in research and clinical applications of PLGA-based nanotechnology. *Expert review of molecular diagnostics* 9, 325-341.

Luca, S., and Mihaescu, T. (2013). History of BCG Vaccine. *Maedica* 8, 53-58.

Lung, P., Yang, J., and Li, Q. (2020). Nanoparticle formulated vaccines: opportunities and challenges. *Nanoscale* 12, 5746-5763.

Lutz, M.B., Kukutsch, N., Ogilvie, A.L., Rossner, S., Koch, F., Romani, N., and Schuler, G. (1999). An advanced culture method for generating large quantities of highly pure dendritic cells from mouse bone marrow. *Journal of immunological methods* 223, 77-92.

Lyadova, I.V., and Panteleev, A.V. (2015). Th1 and Th17 Cells in Tuberculosis: Protection, Pathology, and Biomarkers. *Mediators of inflammation* 2015, 854507.

Lynn, G.M., Laga, R., Darrah, P.A., Ishizuka, A.S., Balaci, A.J., Dulcey, A.E., Pechar, M., Pola, R., Gerner, M.Y., Yamamoto, A., et al. (2015). In vivo characterization of the physicochemical properties of polymer-linked TLR agonists that enhance vaccine immunogenicity. *Nature biotechnology* 33, 1201-1210.

Made, V., Els-Heindl, S., and Beck-Sickinger, A.G. (2014). Automated solid-phase peptide synthesis to obtain therapeutic peptides. *Beilstein journal of organic chemistry* 10, 1197-1212.

Makidon, P.E., Knowlton, J., Groom, J.V., 2nd, Blanco, L.P., LiPuma, J.J., Bielinska, A.U., and Baker, J.R., Jr. (2010). Induction of immune response to the 17 kDa OMPA *Burkholderia cenocepacia* polypeptide and protection against pulmonary infection in mice after nasal vaccination with an OMP nanoemulsion-based vaccine. *Medical microbiology and immunology* 199, 81-92.

Manish, M., Rahi, A., Kaur, M., Bhatnagar, R., and Singh, S. (2013). A single-dose PLGA encapsulated protective antigen domain 4 nanoformulation protects mice against *Bacillus anthracis* spore challenge. *PloS one* 8, e61885.

Manolova, V., Flace, A., Bauer, M., Schwarz, K., Saudan, P., and Bachmann, M.F. (2008). Nanoparticles target distinct dendritic cell populations according to their size. *European journal of immunology* 38, 1404-1413.

Marino, S., Pawar, S., Fuller, C.L., Reinhart, T.A., Flynn, J.L., and Kirschner, D.E. (2004). Dendritic cell trafficking and antigen presentation in the human immune response to *Mycobacterium tuberculosis*. *Journal of immunology* 173, 494-506.

Martinez, A.N., Mehra, S., and Kaushal, D. (2013). Role of interleukin 6 in innate immunity to *Mycobacterium tuberculosis* infection. *The Journal of infectious diseases* 207, 1253-1261.

Martirosyan, A., and Schneider, Y.J. (2014). Engineered nanomaterials in food: implications for food safety and consumer health. *International journal of environmental research and public health* 11, 5720-5750.

Mendez-Samperio, P. (2018). Development of tuberculosis vaccines in clinical trials: Current status. *Scandinavian journal of immunology* 88, e12710.

Mishra, B.B., Lovewell, R.R., Olive, A.J., Zhang, G., Wang, W., Eugenin, E., Smith, C.M., Phuah, J.Y., Long, J.E., Dubuke, M.L., et al. (2017). Nitric oxide prevents a pathogen-permissive granulocytic inflammation during tuberculosis. *Nature microbiology* 2, 17072.

Miyake, K. (2007). Innate immune sensing of pathogens and danger signals by cell surface Toll-like receptors. *Seminars in immunology* 19, 3-10.

Mohammed, M.A., Syeda, J.T.M., Wasan, K.M., and Wasan, E.K. (2017). An Overview of Chitosan Nanoparticles and Its Application in Non-Parenteral Drug Delivery. *Pharmaceutics* 9.

Mohammed, M.A., Syeda, J.T.M., Wasan, K.M., and Wasan, E.K. (2017). An Overview of Chitosan Nanoparticles and Its Application in Non-Parenteral Drug Delivery. *Pharmaceutics* 9.

Monin, L., Griffiths, K.L., Slight, S., Lin, Y., Rangel-Moreno, J., and Khader, S.A. (2015). Immune requirements for protective Th17 recall responses to *Mycobacterium tuberculosis* challenge. *Mucosal immunology* 8, 1099-1109.

Mora, A.L., and Tam, J.P. (1998). Controlled lipidation and encapsulation of peptides as a useful approach to mucosal immunizations. *Journal of immunology* 161, 3616-3623.

Mubin, N., Pahari, S., Owais, M., and Zubair, S. (2018). Mycobacterium tuberculosis host cell interaction: Role of latency associated protein Acr-1 in differential modulation of macrophages. *PloS one* 13, e0206459.

Murray, J.F., Schraufnagel, D.E., and Hopewell, P.C. (2015). Treatment of Tuberculosis. A Historical Perspective. *Annals of the American Thoracic Society* 12, 1749-1759.

Narayanan, P.R. (2006). Influence of sex, age & nontuberculous infection at intake on the efficacy of BCG: re-analysis of 15-year data from a double-blind randomized control trial in South India. *The Indian journal of medical research* 123, 119-124.

Negi, S., Pahari, S., Das, D.K., Khan, N., and Agrewala, J.N. (2019). Curdlan Limits Mycobacterium tuberculosis Survival Through STAT-1 Regulated Nitric Oxide Production. *Frontiers in microbiology* 10, 1173.

Nguipdop-Djomo, P., Heldal, E., Rodrigues, L.C., Abubakar, I., and Mangtani, P. (2016). Duration of BCG protection against tuberculosis and change in effectiveness with time since vaccination in Norway: a retrospective population-based cohort study. *The Lancet Infectious diseases* 16, 219-226.

Nguyen, T.V.A., Anthony, R.M., Banuls, A.L., Nguyen, T.V.A., Vu, D.H., and Alffenaar, J.C. (2018). Bedaquiline Resistance: Its Emergence, Mechanism, and Prevention. *Clinical infectious diseases* : an official publication of the Infectious Diseases Society of America 66, 1625-1630.

Niikura, K., Matsunaga, T., Suzuki, T., Kobayashi, S., Yamaguchi, H., Orba, Y., Kawaguchi, A., Hasegawa, H., Kajino, K., Ninomiya, T., et al. (2013). Gold nanoparticles as a vaccine

platform: influence of size and shape on immunological responses in vitro and in vivo. *ACS nano* 7, 3926-3938.

Oliveira-Nascimento, L., Massari, P., and Wetzler, L.M. (2012). The Role of TLR2 in Infection and Immunity. *Frontiers in immunology* 3, 79.

Ong, C.W., Elkington, P.T., and Friedland, J.S. (2014). Tuberculosis, pulmonary cavitation, and matrix metalloproteinases. *American journal of respiratory and critical care medicine* 190, 9-18.

Pahari, S., Chatterjee, D., Negi, S., Kaur, J., Singh, B., and Agrewala, J.N. (2017). Morbid Sequences Suggest Molecular Mimicry between Microbial Peptides and Self-Antigens: A Possibility of Inciting Autoimmunity. *Frontiers in microbiology* 8, 1938.

Pati, R., Shevtsov, M., and Sonawane, A. (2018). Nanoparticle Vaccines Against Infectious Diseases. *Frontiers in immunology* 9, 2224.

Purcell, A.W., McCluskey, J., and Rossjohn, J. (2007). More than one reason to rethink the use of peptides in vaccine design. *Nature reviews Drug discovery* 6, 404-414.

Qian, C., Yang, L.J., and Cui, H. (2020). Recent Advances in Nanotechnology for Dendritic Cell-Based Immunotherapy. *Frontiers in pharmacology* 11, 960.

Qie, Y., Yuan, H., von Roemeling, C.A., Chen, Y., Liu, X., Shih, K.D., Knight, J.A., Tun, H.W., Wharen, R.E., Jiang, W., et al. (2016). Surface modification of nanoparticles enables selective evasion of phagocytic clearance by distinct macrophage phenotypes. *Scientific reports* 6, 26269.

Queval, C.J., Brosch, R., and Simeone, R. (2017). The Macrophage: A Disputed Fortress in the Battle against *Mycobacterium tuberculosis*. *Frontiers in microbiology* 8, 2284.

Rai, P.K., Chodisetti, S.B., Maurya, S.K., Nadeem, S., Zeng, W., Janmeja, A.K., Jackson, D.C., and Agrewala, J.N. (2018). A lipidated bi-epitope vaccine comprising of MHC-I and MHC-II binder peptides elicits protective CD4 T cell and CD8 T cell immunity against *Mycobacterium tuberculosis*. *Journal of translational medicine* 16, 279.

Rai, P.K., Chodisetti, S.B., Zeng, W., Nadeem, S., Maurya, S.K., Pahari, S., Janmeja, A.K., Jackson, D.C., and Agrewala, J.N. (2017). A lipidated peptide of *Mycobacterium tuberculosis* resuscitates the protective efficacy of BCG vaccine by evoking memory T cell immunity. *Journal of translational medicine* 15, 201.

Rai, P.K., Chodisetti, S.B., Zeng, W., Nadeem, S., Maurya, S.K., Pahari, S., Janmeja, A.K., Jackson, D.C., and Agrewala, J.N. (2017). A lipidated peptide of *Mycobacterium tuberculosis* resuscitates the protective efficacy of BCG vaccine by evoking memory T cell immunity. *Journal of translational medicine* 15, 201.

Renu, S., Han, Y., Dhakal, S., Lakshmanappa, Y.S., Ghimire, S., Feliciano-Ruiz, N., Senapati, S., Narasimhan, B., Selvaraj, R., and Renukaradhya, G.J. (2020). Chitosan-adjuvanted *Salmonella* subunit nanoparticle vaccine for poultry delivered through drinking water and feed. *Carbohydr Polym* 243, 116434.

Riedel, D.D., and Kaufmann, S.H. (1997). Chemokine secretion by human polymorphonuclear granulocytes after stimulation with *Mycobacterium tuberculosis* and lipoarabinomannan. *Infection and immunity* 65, 4620-4623.

Riteau, N., and Sher, A. (2016). Chitosan: An Adjuvant with an Unanticipated STING. *Immunity* 44, 522-524.

Ritz, N., and Curtis, N. (2009). Mapping the global use of different BCG vaccine strains. *Tuberculosis* 89, 248-251.

Roach, D.R., Bean, A.G., Demangel, C., France, M.P., Briscoe, H., and Britton, W.J. (2002). TNF regulates chemokine induction essential for cell recruitment, granuloma formation, and clearance of mycobacterial infection. *J Immunol* 168, 4620-4627.

Romagnoli, A., Etna, M.P., Giacomini, E., Pardini, M., Remoli, M.E., Corazzari, M., Falasca, L., Goletti, D., Gafa, V., Simeone, R., et al. (2012). ESX-1 dependent impairment of autophagic flux by *Mycobacterium tuberculosis* in human dendritic cells. *Autophagy* 8, 1357-1370.

Rozot, V., Vigano, S., Mazza-Stalder, J., Idrizi, E., Day, C.L., Perreau, M., Lazor-Blanchet, C., Petruccioli, E., Hanekom, W., Goletti, D., et al. (2013). *Mycobacterium tuberculosis*-specific CD8⁺ T cells are functionally and phenotypically different between latent infection and active disease. *European journal of immunology* 43, 1568-1577.

Russell, D.G. (2007). Who puts the tubercle in tuberculosis? *Nature reviews Microbiology* 5, 39-47.

Russell, D.G., Cardona, P.J., Kim, M.J., Allain, S., and Altare, F. (2009). Foamy macrophages and the progression of the human tuberculosis granuloma. *Nature immunology* 10, 943-948.

Sakai, S., Mayer-Barber, K.D., and Barber, D.L. (2014). Defining features of protective CD4 T cell responses to *Mycobacterium tuberculosis*. *Current opinion in immunology* 29, 137-142.

Salgame, P. (2011). MMPs in tuberculosis: granuloma creators and tissue destroyers. *The Journal of clinical investigation* 121, 1686-1688.

Schenten, D., and Medzhitov, R. (2011). The control of adaptive immune responses by the innate immune system. *Advances in immunology* 109, 87-124.

Schmidt, S.T., Khadke, S., Korsholm, K.S., Perrie, Y., Rades, T., Andersen, P., Foged, C., and Christensen, D. (2016). The administration route is decisive for the ability of the vaccine adjuvant CAF09 to induce antigen-specific CD8(+) T-cell responses: The immunological consequences of the biodistribution profile. *Journal of controlled release : official journal of the Controlled Release Society* 239, 107-117.

Schrager, L.K., Harris, R.C., and Vekemans, J. (2018). Research and development of new tuberculosis vaccines: a review. *F1000Research* 7, 1732.

Schromm, A.B., Howe, J., Ulmer, A.J., Wiesmuller, K.H., Seyberth, T., Jung, G., Rossle, M., Koch, M.H., Gutschmann, T., and Brandenburg, K. (2007). Physicochemical and biological analysis of synthetic bacterial lipopeptides: validity of the concept of endotoxic conformation. *The Journal of biological chemistry* 282, 11030-11037.

Sendide, K., Deghmane, A.E., Pechkovsky, D., Av-Gay, Y., Talal, A., and Hmama, Z. (2005). *Mycobacterium bovis* BCG attenuates surface expression of mature class II molecules through IL-10-dependent inhibition of cathepsin S. *Journal of immunology* 175, 5324-5332.

Shams, H., Wizel, B., Weis, S.E., Samten, B., and Barnes, P.F. (2001). Contribution of CD8(+) T cells to gamma interferon production in human tuberculosis. *Infection and immunity* 69, 3497-3501.

Shastri, V.P. (2003). Non-degradable biocompatible polymers in medicine: past, present and future. *Current pharmaceutical biotechnology* 4, 331-337.

Shen, H., and Chen, Z.W. (2018). The crucial roles of Th17-related cytokines/signal pathways in *M. tuberculosis* infection. *Cellular & molecular immunology* 15, 216-225.

Shen, H., and Chen, Z.W. (2018). The crucial roles of Th17-related cytokines/signal pathways in *M. tuberculosis* infection. *Cellular & molecular immunology* 15, 216-225.

Shi, C., Chen, L., Chen, Z., Zhang, Y., Zhou, Z., Lu, J., Fu, R., Wang, C., Fang, Z., and Fan, X. (2010). Enhanced protection against tuberculosis by vaccination with recombinant BCG over-expressing HspX protein. *Vaccine* 28, 5237-5244.

Shi, G.N., Zhang, C.N., Xu, R., Niu, J.F., Song, H.J., Zhang, X.Y., Wang, W.W., Wang, Y.M., Li, C., Wei, X.Q., et al. (2017). Enhanced antitumor immunity by targeting dendritic cells with tumor cell lysate-loaded chitosan nanoparticles vaccine. *Biomaterials* 113, 191-202.

Shinnick, T.M., and Good, R.C. (1994). Mycobacterial taxonomy. *European journal of clinical microbiology & infectious diseases* : official publication of the European Society of Clinical Microbiology 13, 884-901.

Shukla, R., Bansal, V., Chaudhary, M., Basu, A., Bhonde, R.R., and Sastry, M. (2005). Biocompatibility of gold nanoparticles and their endocytotic fate inside the cellular

compartment: a microscopic overview. *Langmuir : the ACS journal of surfaces and colloids* 21, 10644-10654.

Siddiqui, K.F., Amir, M., and Agrewala, J.N. (2011). Understanding the biology of 16 kDa antigen of *Mycobacterium tuberculosis*: scope in diagnosis, vaccine design and therapy. *Critical reviews in microbiology* 37, 349-357.

Siddiqui, K.F., Amir, M., Gurram, R.K., Khan, N., Arora, A., Rajagopal, K., and Agrewala, J.N. (2014). Latency-associated protein Acr1 impairs dendritic cell maturation and functionality: a possible mechanism of immune evasion by *Mycobacterium tuberculosis*. *The Journal of infectious diseases* 209, 1436-1445.

Siddiqui, K.F., Amir, M., Khan, N., Rama Krishna, G., Sheikh, J.A., Rajagopal, K., and Agrewala, J.N. (2015). Prime-boost vaccination strategy with bacillus Calmette-Guerin (BCG) and liposomized alpha-crystalline protein 1 reinvigorates BCG potency. *Clinical and experimental immunology* 181, 286-296.

Silva, J.M., Videira, M., Gaspar, R., Preat, V., and Florindo, H.F. (2013). Immune system targeting by biodegradable nanoparticles for cancer vaccines. *Journal of controlled release : official journal of the Controlled Release Society* 168, 179-199.

Skwarczynski, M., and Toth, I. (2016). Peptide-based synthetic vaccines. *Chemical science* 7, 842-854.

Smith, D.M., Simon, J.K., and Baker, J.R., Jr. (2013). Applications of nanotechnology for immunology. *Nature reviews Immunology* 13, 592-605.

CHAPTER 7

BIBLIOGRAPHY

Spratt, J.M., Britton, W.J., and Triccas, J.A. (2010). In vivo persistence and protective efficacy of the bacille Calmette Guerin vaccine overexpressing the HspX latency antigen. *Bioengineered bugs* 1, 61-65.

Steinhagen, F., Kinjo, T., Bode, C., and Klinman, D.M. (2011). TLR-based immune adjuvants. *Vaccine* 29, 3341-3355.

Steller, M.A., Gurski, K.J., Murakami, M., Daniel, R.W., Shah, K.V., Celis, E., Sette, A., Trimble, E.L., Park, R.C., and Marincola, F.M. (1998). Cell-mediated immunological responses in cervical and vaginal cancer patients immunized with a lipidated epitope of human papillomavirus type 16 E7. *Clinical cancer research : an official journal of the American Association for Cancer Research* 4, 2103-2109.

Sterne, J.A., Rodrigues, L.C., and Guedes, I.N. (1998). Does the efficacy of BCG decline with time since vaccination? *The international journal of tuberculosis and lung disease : the official journal of the International Union against Tuberculosis and Lung Disease* 2, 200-207.

Sturgill-Koszycki, S., Schlesinger, P.H., Chakraborty, P., Haddix, P.L., Collins, H.L., Fok, A.K., Allen, R.D., Gluck, S.L., Heuser, J., and Russell, D.G. (1994). Lack of acidification in *Mycobacterium* phagosomes produced by exclusion of the vesicular proton-ATPase. *Science* 263, 678-681.

Tait, D.R., Hatherill, M., Van Der Meeren, O., Ginsberg, A.M., Van Brakel, E., Salaun, B., Scriba, T.J., Akite, E.J., Ayles, H.M., Bollaerts, A., et al. (2019). Final Analysis of a Trial of M72/AS01E Vaccine to Prevent Tuberculosis. *The New England journal of medicine* 381, 2429-2439.

Taylor, J.L., Hattle, J.M., Dreitz, S.A., Troudt, J.M., Izzo, L.S., Basaraba, R.J., Orme, I.M., Matrisian, L.M., and Izzo, A.A. (2006). Role for matrix metalloproteinase 9 in granuloma formation during pulmonary *Mycobacterium tuberculosis* infection. *Infection and immunity* 74, 6135-6144.

Tengood, J.E., Levy, R.J., and Stachelek, S.J. (2016). The use of CD47-modified biomaterials to mitigate the immune response. *Experimental biology and medicine* 241, 1033-1041.

Thiele, L., Merkle, H.P., and Walter, E. (2003). Phagocytosis and phagosomal fate of surface-modified microparticles in dendritic cells and macrophages. *Pharmaceutical research* 20, 221-228.

Tian, F., Clift, M.J., Casey, A., Del Pino, P., Pelaz, B., Conde, J., Byrne, H.J., Rothen-Rutishauser, B., Estrada, G., de la Fuente, J.M., et al. (2015). Investigating the role of shape on the biological impact of gold nanoparticles in vitro. *Nanomedicine (Lond)* 10, 2643-2657.

Tobin, D.M., Vary, J.C., Jr., Ray, J.P., Walsh, G.S., Dunstan, S.J., Bang, N.D., Hagge, D.A., Khadge, S., King, M.C., Hawn, T.R., et al. (2010). The *lta4h* locus modulates susceptibility to mycobacterial infection in zebrafish and humans. *Cell* 140, 717-730.

Trombetta, E.S., Ebersold, M., Garrett, W., Pypaert, M., and Mellman, I. (2003). Activation of lysosomal function during dendritic cell maturation. *Science* 299, 1400-1403.

Tsolmongyn, B., Koide, N., Jambalmaniin, U., Odkhuu, E., Naiki, Y., Komatsu, T., Yoshida, T., and Yokochi, T. (2013). A Toll-like receptor 2 ligand, Pam3CSK4, augments interferon-gamma-induced nitric oxide production via a physical association between MyD88 and interferon-gamma receptor in vascular endothelial cells. *Immunology* 140, 352-361.

Tsolmongyn, B., Koide, N., Jambalganiin, U., Odkhuu, E., Naiki, Y., Komatsu, T., Yoshida, T., and Yokochi, T. (2013). A Toll-like receptor 2 ligand, Pam3CSK4, augments interferon-gamma-induced nitric oxide production via a physical association between MyD88 and interferon-gamma receptor in vascular endothelial cells. *Immunology* 140, 352-361.

van der Wel, N., Hava, D., Houben, D., Fluitsma, D., van Zon, M., Pierson, J., Brenner, M., and Peters, P.J. (2007). *M. tuberculosis* and *M. leprae* translocate from the phagolysosome to the cytosol in myeloid cells. *Cell* 129, 1287-1298.

Velasquez, L.N., Stuve, P., Gentilini, M.V., Swallow, M., Bartel, J., Lycke, N.Y., Barkan, D., Martina, M., Lujan, H.D., Kalay, H., et al. (2018). Targeting Mycobacterium tuberculosis Antigens to Dendritic Cells via the DC-Specific-ICAM3-Grabbing-Nonintegrin Receptor Induces Strong T-Helper 1 Immune Responses. *Frontiers in immunology* 9, 471.

Volkman, H.E., Pozos, T.C., Zheng, J., Davis, J.M., Rawls, J.F., and Ramakrishnan, L. (2010). Tuberculous granuloma induction via interaction of a bacterial secreted protein with host epithelium. *Science* 327, 466-469.

Wang, S., Guo, L., Liu, D., Liu, W., and Wu, Y. (2016a). HLA^{sup}E: an integrated database of HLA supertype-specific epitopes to aid in the development of vaccines with broad coverage of the human population. *BMC immunology* 17, 17.

Wang, Y., Li, P., Truong-Dinh Tran, T., Zhang, J., and Kong, L. (2016b). Manufacturing Techniques and Surface Engineering of Polymer Based Nanoparticles for Targeted Drug Delivery to Cancer. *Nanomaterials* 6.

Wong, S.H., Santambrogio, L., and Strominger, J.L. (2004). Caspases and nitric oxide broadly regulate dendritic cell maturation and surface expression of class II MHC proteins. *Proceedings of the National Academy of Sciences of the United States of America* 101, 17783-17788.

Woodworth, J.S., Wu, Y., and Behar, S.M. (2008). Mycobacterium tuberculosis-specific CD8+ T cells require perforin to kill target cells and provide protection in vivo. *Journal of immunology* 181, 8595-8603.

Wu, S., Wang, M.G., Wang, Y., and He, J.Q. (2019). Polymorphisms of cytokine genes and tuberculosis in two independent studies. *Scientific reports* 9, 2507.

Zeng, W., Jackson, D.C., and Rose, K. (1996). Synthesis of a new template with a built-in adjuvant and its use in constructing peptide vaccine candidates through polyoxime chemistry. *Journal of peptide science : an official publication of the European Peptide Society* 2, 66-72.

Zeng, W., Jackson, D.C., Murray, J., Rose, K., and Brown, L.E. (2000). Totally synthetic lipid-containing polyoxime peptide constructs are potent immunogens. *Vaccine* 18, 1031-1039.

Zeng, W., Jackson, D.C., Murray, J., Rose, K., and Brown, L.E. (2000). Totally synthetic lipid-containing polyoxime peptide constructs are potent immunogens. *Vaccine* 18, 1031-1039.

Zhao, W., Wu, W., and Xu, X. (2007). Oral vaccination with liposome-encapsulated recombinant fusion peptide of urease B epitope and cholera toxin B subunit affords prophylactic and therapeutic effects against *H. pylori* infection in BALB/c mice. *Vaccine* 25, 7664-7673.

Zielinska, A., Carreiro, F., Oliveira, A.M., Neves, A., Pires, B., Venkatesh, D.N., Durazzo, A., Lucarini, M., Eder, P., Silva, A.M., et al. (2020). Polymeric Nanoparticles: Production, Characterization, Toxicology and Ecotoxicology. *Molecules* 25.

Zodpey, S.P. (2004). The BCG controversy: a reappraisal of the protective effect against tuberculosis and leprosy. *Indian journal of public health* 48, 70-77.

Zom, G.G., Khan, S., Filippov, D.V., and Ossendorp, F. (2012). TLR ligand-peptide conjugate vaccines: toward clinical application. *Advances in immunology* 114, 177-201.

Zom, G.G., Khan, S., Filippov, D.V., and Ossendorp, F. (2012). TLR ligand-peptide conjugate vaccines: toward clinical application. *Advances in immunology* 114, 177-201.

Zom, G.G., Willems, M., Khan, S., van der Sluis, T.C., Kleinovink, J.W., Camps, M.G.M., van der Marel, G.A., Filippov, D.V., Melief, C.J.M., and Ossendorp, F. (2018). Novel TLR2-binding adjuvant induces enhanced T cell responses and tumor eradication. *Journal for immunotherapy of cancer* 6, 146.

Zom, G.G., Willems, M., Khan, S., van der Sluis, T.C., Kleinovink, J.W., Camps, M.G.M., van der Marel, G.A., Filippov, D.V., Melief, C.J.M., and Ossendorp, F. (2018). Novel TLR2-binding adjuvant induces enhanced T cell responses and tumor eradication. *Journal for immunotherapy of cancer* 6, 146.



Sidhanta Nanda

Department of Biomedical Engineering,
Indian Institute of Technology (IIT)
Ropar, Punjab, India

CONTACT

PHONE: +91-7325821621, 7504032848

EMAIL:

sidhantananda23@gmail.com
sidhantananda.gsa@gmail.com

RESEARCH SKILLS

Immunoblotting, nanoparticle based vaccine, HPLC, Akta pure and Aktaadvant, SEM, TEM, FTIR, XRD, Confocal microscopy, Fluorescence microscopy, Mammalian cell cultures, anti-cancer drug discovery, Hypoxia generation, feed batch production of monoclonal antibodies, clonal propagation and selection in mAb, stem cell culture and maintenance, bio-conjugation, microbial culture, ELISA, RIA, Elispot, Immuno diffusion, Flowcytometry, Cell sorting, immunofluorescence, immunocytochemistry, immunohistochemistry, Animal handling (mice, rat, rabbit, zebrafish), anti-narcotics vaccines, cytokine profiling and pathways delineation.

RESEARCH INTERESTS

- Development of immuno-therapeutics
- Cell based and Immune-modulation approach to treat cancer and other diseases
- Molecular signaling and investigating Bregs and Tregs in lymphomas and autoimmune diseases

EDUCATION

- **Ph. D (2018 – Thesis Submitted, Defense expected in June 2023)**
Immunology laboratory, Department of Biomedical Engineering, Indian Institute of Technology Ropar, India
Thesis title: Induction of the activation of immunity against opioid narcotics drug and *Mtb* by a chimeric vaccine.
Ph. D supervisor: Prof. Javed N Agrewala, PhD
- **M. Sc in Biotechnology (2017)**
North Orissa University, India
Dissertation title: Biotechnological potential of some soil bacteria from Simlipal Biosphere Reserve, India
Supervisor: Prof. HN Thatoi, PhD
- **B. Sc in Biotechnology (2015)**
Utkal University, India
Dissertation title: Importance of microbiology in Dairy
Supervisor: Dr. B Pati, PhD

RESEARCH EXPERIENCE

- Project Assistant II [Feb 2018-July 2018]
- Employer: CSIR-IMTECH, Chandigarh, Govt of India
- Supervisor: Dr. DK Sahoo, Chief Scientist

RESEARCH SUPERVISION

- Master thesis : 5
- Project assistant : 3
- Interns : 5

RESEARCH SUPERVISION

- Teaching assistance for 600 level courses
- Tutorials for 100 level courses

ADMINISTRATIVE ROLE

- Ph. D representative for two years
- Snehita buddy for two years

AWARDS AND NATIONAL LEVEL QUALIFYING EXAMS

1. Selected for poster presentation in **Nature's conference; Next Gen Immunology 2020, Israel**
2. **DST Inspire Fellow (2018-2023), Govt of India**
3. **University Gold Medal (2017), North Orissa University**
4. JNU-Combined Entrance Examination for Biotechnology for Master's in biotechnology
5. Best student award 2017, North Orissa University

PUBLICATIONS

1. Deepjyoti Kumar Das#, Mohammad Adeel Zafar#, **Sidhanta Nanda**#, Sanpreet Singh, Taruna Lamba, Hilal Bashir, Pargat Singh, Sudeep Kumar Maurya, Sajid Nadeem, Sharvan Sehrawat, Vijayender Bhalla, Javed Naim Agrewala, targeting dendritic cells with TLR-2 ligand-coated nanoparticles loaded with Mycobacterium tuberculosis epitope induce anti-tuberculosis immunity, *Journal of Biological Chemistry*, 2022, 102596. (Equal contributions).
2. Leena Arora; Debarun Patra, Soumyajit Roy, **Sidhanta Nanda**, Navneet Singh, Anita Verma, Anuradha Chakraborti, Suman Dasgupta, Durba Pal; Hypoxia-induced miR-210 expression in non-small cell lung cancer potentiates tumor development by regulating CCL2 mediated monocyte infiltration" by; *Molecular Oncology*. Manuscript ID MOLONC-21-1077.
3. KN Mihooliya, J Nandal, A Kumari, **S Nanda**, H Verma, DK Sahoo; Studies on efficient production of a novel L-asparaginase by a newly isolated *Pseudomonas resinovorans* IGS-131 and its heterologous expression in *Escherichia coli*; *3 Biotech*. 2020 Apr; 10(4):148.
4. Gurpreet Kaur, Sanpreet Singh, **Sidhanta Nanda**, Mohammad Adeel Zafar, Junaidid Ahmad Malik, Mohammad Umar Arshi, Taruna Lamba, Javed Naim Agrewala; Fiction and facts about BCG imparting trained immunity against COVID-19, *Vaccines*, Manuscript ID: vaccines-1759599.
5. Arnab Chowdhury, Saurav Chatterjee, Apoorv Kushwaha, **Sidhanta Nanda**, T. J. Dhillip Kumar, and Anupam Bandyopadhyay; Sulfonil Diazaborine 'Click' Chemistry Enables Rapid and Efficient Bioorthogonal Labeling; *Chem. Eur. J.* 2023, e202300393, 10.1002/chem.202300393.
6. **Sidhanta Nanda**, Mohammad Adeel Zafar, Sanpreet Singh, Ritika Gautam, Abhishek Ghosh, Debasish Basu, Javed N Agrewala; Chronic administration of morphine provokes the generation of anti-morphine antibodies and immunosuppression in individuals with opioid use disorder. *BMC Immunology* (Under Review)
7. Kritika Pasricha, Shivank Prajapati, **Sidhanta Nanda**, Taruna Lamba, Mohammad Adeel Zafar, Nitesh M Tripathi, Anupam Bandyopadhyay, Javed Naim Agrewala, Cross-reactive T cell and B cell epitopes of mycobacteria and SARS-CoV-2: a possible reason for a higher rate of protection of TB-endemic population against COVID-19. *Journal of Translational Medicine* (Under Review).
8. Jonaid Ahmad Malik, **Sidhanta Nanda**, Mohammad Adeel Zafar, Sharvan Sehrawat, Javed N Agrewala; Influence of chronic administration of morphine and its withdrawal on the behavior of zebrafish, *Journal of Biosciences* (In-press)

CONFERENCES

1. **Presented paper entitled** "Induction of the Activation of Immunity against Opioids and *Mycobacterium tuberculosis* by a Chimeric Vaccine" at **Nature's Next Gen Immunology 2020**, Weizmann Institute of Science, Israel
2. **Poster presentation** at National Seminar on Biotechnology for Sustainable Utilization of Bioresources (BSUB-2018)
3. **Poster presentation** at UK-India International workshop on "Advance Biomaterials and Biosensors (ABB-2018)" by British Council and Newton Bhaba fund
4. **Poster presentation** at IMMUNOCON-2022, the annual meeting of the Indian Immunology Society
5. Delivered an **invited lecture** on "Next Gen sequencing" in SPARC Indo-US International Immunology workshop
6. Attended Pan-IIT Research Conclave conference and **presented a poster**

REFERENCES

1. Prof. Javed N Agrewala, Professor, Department of Biomedical Engineering, Indian Institute of Technology Ropar, Rupnagar, Punjab, India. Email ID: jagrewala@iitrpr.ac.in, jagrewala@gmail.com; Contact number: +919417869408
2. Dr. Srivatsava Naidu, Assistant Professor, Department of Biomedical Engineering, Indian Institute of Technology Ropar, Rupnagar, Punjab, India. Email ID: srivatsava.naidu@iitrpr.ac.in; Contact number: +918968531467
3. Dr. Yashveer Singh, Associate Professor, Department of Chemistry, Indian Institute of Technology Ropar, Rupnagar, Punjab, India. Email ID: yash@iitrpr.ac.in; Contact number: +919779668895
4. Dr Amit Jaiswal, Associate Professor, School of Biosciences and Bioengineering, Indian Institute of Technology Mandi, Kamand, Mandi-175075, Himachal Pradesh, India, Email: j.amit@iitmandi.ac.in, Tel: 01905-267-154